PUNCHING SHEAR RESISTANCE OF REINFORCED CONCRETE FLAT SLABS

A thesis submitted to The University of Manchester for the degree of Doctor of Philosophy in the Faculty of Engineering and Physical Sciences

2014

SHAHRAM DEROGAR

SCHOOL OF MECHANICAL, AEROSPACE AND CIVIL ENGINEERING

CONTENT

WORD COUNT: 52764

LIST OF FIGURES

LIST OF TABLES

The University of Manchester
Shahram Derogar
Doctor of Philosophy
Punching Shear Resistance of Reinforced Concrete Flat Slabs
2014

ABSTRACT

In spite of considerable amount of research on flat plate structures, understanding the brittle and catastrophic punching shear failure is still somewhat incomplete. The thesis focuses on the punching shear behaviour of interior flat slab-column connections under gravity loading. A Comprehensive literature review has shown that although there are several different mechanical models available to calculate punching shear capacity, they are not only complex and difficult to apply in engineering practice but also are not precise. Code provisions such as ACI 318-08 (2008), Eurocode 2-2004, CEB-FIP Model Code 1990 and BS 8118-1997 are all based on empirical equations which were developed using limited experiments from the literature. Therefore, the precision of punching shear capacity prediction using the code equations are questionable. Previous researches assessed the accuracy of the code provisions only by comparing with their limited set of experiments. In this thesis, the author has constructed a large database using 549 punching shear experiments from the literature and concluded that to assess the code provisions in a much more rigorous manner, it is essential to evaluate the effect of the key parameters that affect the punching shear capacity of flat slab-column connections using this database. This study has shown that BS 8110 (1997) predicts punching shear capacity with high accuracy while ACI 318-08 (2008) underestimates the punching shear capacity for slabs with low flexural reinforcement. Lenton Steel Fortress (LSF) type of shear reinforcement has a better anchorage behaviour compared to stirrups. However, experiments with this type of shear reinforcement are very limited. In order to gain an insight of the behaviour of slab-column connections under gravity loading, two series of experiments were conducted in this study: 72 pullout tests using LSF strips and 3 real scale slab-column connections. LSF strips have been shown to have enhanced anchorage behaviour and the use of LSF type shear reinforcement has resulted in an increase of 67% punching shear capacity and 152% in deformation capacity. In addition to the experiments, numerical modelling was carried out to further investigate the behaviour of flat slab-column connections. It is also concluded that Finite Element analyses using ABAQUS is capable of predicting the behaviour of such connections with sufficient accuracy. Using the validated numerical models, a parametric study was carried out to investigate the effect of parameters such as column dimensions, slab depths, top and bottom reinforcement ratios and shear reinforcement area on the punching shear capacity of the flat slab-column connections. A development of a simplified shear model was achieved by Bayesian Neural Network (NN) using the parameters previously determined from the comprehensive databases and numerical analyses. The simplified shear model that was developed by the author predicts punching shear capacity with high accuracy.

DECLARATION

No portion of the work referred to in the thesis has been submitted in support of an application for another degree or qualification of this or any other university or other institute of learning.

COPYRIGHT STATEMENT

i The author of this thesis (including any appendices and/or schedules to this thesis) owns any copyright in it (the "Copyright") and she has given The University of Manchester the right to use such Copyright for any administrative, promotional, educational and/or teaching purposes.

ii Copies of this thesis, either in full or in extracts, may be made only in accordance with the regulations of the John Rylands University Library of Manchester. Details of these regulations may be obtained from the Librarian. This page must form part if any such copies made.

iii The ownership of any patents, designs, trade marks and any and all other intellectual property rights except for the Copyright (the "Intellectual Property Rights") and any reproductions of copyright works, for example graphs and tables ("Reproductions"), which may be described in this thesis, may not be owned by the author and may be owned by third parties. Such Intellectual Property Rights and Reproductions cannot and must not be made available for use without the prior written permission of the owner(s) of the relevant Intellectual Property Rights and/or Reproductions.

iv Further information on the conditions under which disclosure, publication and exploitation of this thesis, the Copyright and any Intellectual Property Rights and/or Reproductions described in it may take place is available from the Head of School of Mechanical, Aerospace and Civil Engineering.

To my parents Khatun and Eissa…

ACKNOWLEDGEMENTS

First of all, I would like to thank to my supervisor Dr Parthasarathi Mandal for his guidance, support and constructive criticisms. I acknowledge his invaluable supervision and his patience especially in the write up period of this study. I would also like to express my profound gratitude to my supervisor especially for his support at difficult times during the course of the study.

Very special thanks go to Prof. Thomas Michelitsch for his great companionship and for his continual support. I greatly acknowledge all the advice and suggestions he has kindly offered not only for the successful completion of the thesis but also on the personal level.

I would also like to thank Osimen Iruansi for his great criticism and useful directions on the development of Bayesian Neural Network. The support from all colleagues (past and present) of Room of F1 at the University of Manchester has also been appreciated.

I would like to thank to my family for their continuous patience and support. The completion of this thesis would not been possible without their love and faith. Special thanks go to my brothers and sisters for their moral support and encouragements.

Last but not least, I would like to thank my loving wife Ceren Ince who has supported me at every stage of this study. Her love, patience and support have become the light for the study.

NOTATION

Latin letters

a = the side length of the slab

A_v = the area of the shear reinforcement within a distance s

A_{sw} = the area of one perimeter of shear reinforcement

A_{sw} = the area of one perimeter of shear reinforcement around the column

b = the perimeter of the loading area

b_o = the shear perimeter

b_p = the critical perimeter located 1.5d away from the column face

β = the diameter of the circular column

c = the side length of the square column

c_a = the displacement correction

d = the effective depth of the slab

d_{avg} = the average effective depth of the slab

dD = the dowel forces

D_u = the displacement at ultimate load

D_y = the displacement at yielding

E_D = the error function

E_s = the elastic modulus of the steel

E_w = the degree of regularisation

f = the linear or nonlinear activation function

f^1 = the activation function at the hidden nodes

f^2 = the activation function at the output nodes

f_{ave} = the average pullout stress

f_{bo} = the compressive strength under biaxial loading of concrete

f_c = cylinder concrete strength

f'_c = the concrete compressive strength

f'_{c1} = the concrete compressive strength of cubes after pull out tests

$f'_{c,cube,\ 100}$ = the compressive strength of cubes (100/100/100 mm)

$f'_{c,cube,\ 150}$ = the compressive strength of cubes (150/150/150 mm)

$f'_{c,cyl,100,300}$ = the compressive strength of cylinders ($\phi = 100\,\text{mm}$, h=300 mm)

$f'_{c,cyl,150,300}$ = the compressive strength of cylinder ($\phi = 150\,\text{mm}$, h=300 mm)

f_{ck} = the characteristic concrete compressive cylinder strength

f_{co} = the uniaxial compressive strength of concrete

f_{ct} = the splitting tensile strength

f_{ctm} = the mean tensile strength

f_{cu} = the characteristic concrete cube strength

F_{cr} = the inclined bearing force

F_{ct} = forces in the concrete (vertical component of the concrete tensile forces)

F_{dow} = the dowel contribution of the flexural reinforcement

f_{max} = the maximum pullout stress

F_{max} = the maximum pullout load

F_{pun} = the punching load of a slab

F_{sr} = the radial net force

F_{st} = forces in the steel

F_{sw} = the vertical component of the force in the studs, stirrups or bent up bars

f_t = the steel yield strength (axial tensile stress in the reinforcing bar)

f_u = the ultimate load

f_y = the yield strength of flexural reinforcement

f_{yv} = the characteristic strength of shear reinforcement

f_{ywd} = the design yield of shear reinforcement

$f_{ywd,ef}$ = the effective design strength of shear reinforcement

G = the adequate plastic potential function

G_f = the material parameter describing the amount of energy required to open a unit area of a crack

h = the slab depth

h_1 = the hooks length in longer direction of the pullout specimen

h_2 = the hooks length in shorter direction of the pullout specimen

H = the hessian matrix

I_1 = the first stress invariant

I_a = the internal force

I_b = the new internal force

J_2 = the second invariant of the stress deviator

K_a = the new structure stiffness

l_1 = the span between supports

l_s = the dimension of the slab specimen

L = the characteristic element length

m = the total number of parameters in the network

n_c = the stress concentration factor

p = the equivalent pressure

$\bar{p}$ = the hydrostatic pressure stress

P = the external load

P_u = the ultimate load

q = the equivalent deviatoric pressure

$\bar{q}$ = the Mises equivalent effective stress

r_o = the diameter of the column

r_1 = corresponds to 1/10 of the effective depth

r_2 = the radius extends up to the flexural reinforcing bars

R = the function described by the ANN (Chapter 7)

R = the bending radius

R_a = the unbalance force vector

R_b = the residual

s = the spacing of the shear reinforcement in a direction parallel to longitudinal reinforcement

s_r = the radial spacing of perimeters of shear reinforcement

t = the nominal thickness

t' = the actual thickness

u = the control perimeter for circular and rectangular loaded areas

u_a = the current structure

u_0 = the opening of crack at which the concrete tensile strength becomes zero

u_1 = the control perimeter at a distance of 2d from the column face

U = the energy absorption capacity

V_a = the resistance provided by the aggregate interlock

V_{ACI} = the calculated punching shear strength according to the ACI 318-08

V_{BS8110} = the calculated punching shear strength according to the BS 8110 (1997)

V_c = the vertical component of the concrete resistance provided in the compression zone

V_{cal} = the calculated punching shear capacity of the slab

$V_{CEB\ FIP}$ = the calculated punching shear strength according to the CEB FIP Model 1990 (1991)

V_d = the resistance provided by the dowel action

V_{EC2} = the calculated punching shear strength according to the EC2 (2004)

V_{flex} = the flexural capacity based on the yield line analysis

V_f = the flexural strength of the slab

V_{max} = the maximum shear capacity of the slab

V_n = the nominal shear strength

V_{pred} = the predicted punching shear strength

$V_{Rd,c}$ = the nominal punching shear design strength

$V_{Rd,cs}$ = the design value of the punching shear resistance of the slab with punching shear reinforcement

V_s = the shear reinforcement provided by the shear reinforcement

V_{test} = the measured punching shear strength of the slab

V_u = the punching shear capacity

V_ε = the punching load at critical tangential concrete strain

V_σ = the punching shear load

v_c = the maximum design shear stress

v_u = the shear stress

w = the "flat" length or the tail length

x = the height of the compression zone at flexure in the tangential direction at punching failure

x = the input for a two-layer network

x_i = the original value of the dataset

$(x_i)_n$ = the normalised value of the dataset

x_{mean} = the mean of the parameter under normalization

X = the depth of the compression zone

y = the depth of the radial compression zone

y = the output for a two-layer network

y_i = the original value of the dataset

$(y)_{max}$ = the maximum values of the parameters under normalisation

$(y)_{min}$ = the minimum values of the parameters under normalisation

$(y_i)_n$ = the normalised value of the dataset

z = moment arm

Greek Letters

α = the angle between the shear reinforcement and the plane of the slab

$\alpha\chi_{pu}$ = the height of the equivalent rectangular stress block

β = the aspect ratio

β_c = the ratio of longer to shorter dimensions of the loaded area

ε = the eccentricity that defines the rate at which the plastic potential function approached the asymptote

ε = the strain tensor

ε_u = the ultimate tensile strain

$\dot{\varepsilon}^p$ = the plastic incremental deformation

$\breve{\varepsilon}^{pl}$ = the effective plastic strain

$\breve{\varepsilon}_c^{pl}$ = the effective compression plastic strain

ε_{cpu} = the tangential concrete strain

σ = the hydrostatic compressive stress

σ_c = the concrete compressive stress

σ_i = the standard deviation

$\overline{\sigma}_{max}$ = the algebraically maximum eigenvalue

$\overline{\sigma}_c(\bar{\varepsilon}_c^p)$ = the effective compressive cohesion stress

σ_s = the uniaxial stress of concrete in compression

$\overline{\sigma}_t(\bar{\varepsilon}_t^p)$ = the effective tension cohesion stress

σ_1 = the slip inside the concrete cube

σ_2 = the overall slip along the bar

θ = the inclined crack angle

η = analytical relation represents the influence of radius of column on punching crack initiation

μ = the regularisation coefficient

μ_{MP} = the optimal regularisation coefficient

ξ = the size effect

φ_s = the diameter of the corresponding bars crossing the punching crack

$\dot{\kappa}$ = the positive scalar hardening parameter

Ψ = the dilation angle

ρ = the average reinforcement ratio

ρ_{Bot} = the average bottom reinforcement ratio

ρ_{Top} = the average top reinforcement ratio

ρ_{x} = the reinforcement ratio in *x* direction

ρ_{y} = the reinforcement ratio in *y* direction

ω_{c} = the crack opening

ω_{MP} = the optimum weight parameters

Chapter 1
INTRODUCTION

1.1 Introduction

One of the most common concrete floor systems is the flat slab. A flat slab structural system consists of a slab of uniform thickness supported directly on columns without any beams, an example of this is shown in Figure 1.1. Flat slab structural systems, in the absence of downstand beams allow lower building heights and greater ease of service routing that provides greater architectural flexibility compared with other concrete floor systems. This also provides constructional benefits with easier formwork, resulting in reduced construction time.

Figure 1.1: Typical flat plate structure, Tabriz-Iran.

These architectural and constructional benefits can come at some cost structurally that relates to the absence of structural hierarchy. Flat plates are prone to punching failure, which is a failure within the slab, at, or near to, its interface with the columns. This

failure mode is caused by the high shear loads at these locations and is excarebated by any inunbalance in the moment between slabs and columns.

Punching shear failure is a sudden, brittle failure of the slab-column connection that is catastrophic. Following failure, the column is pushed through the slab and a considerable portion of slab is also being pushed during this event. A section through a slab-column connection is shown in Figure 1.2. The failure sequence tends to be: - firstly flexural cracks are observed at the top surface of the slab, as the cracking moment per unit width is reached around the loading area.

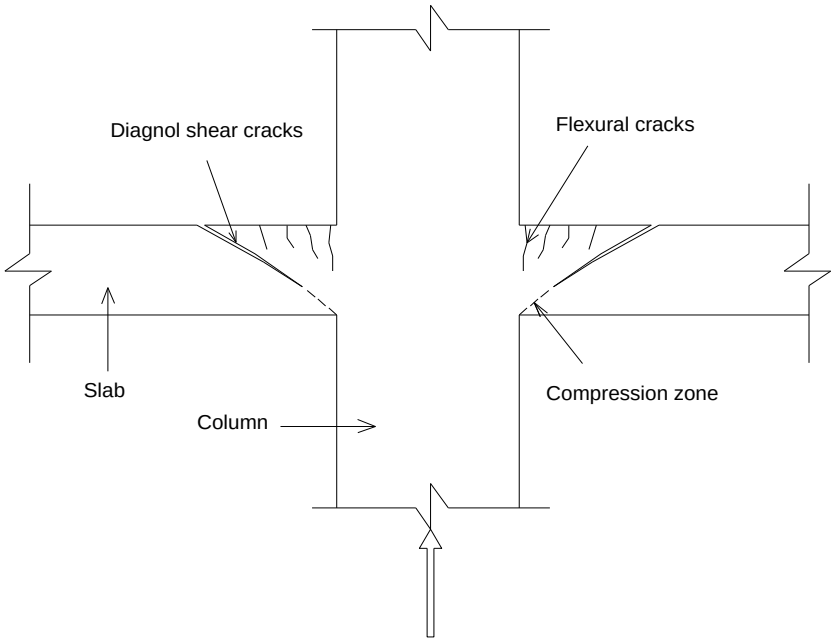

Figure 1.2: Punching Shear Failure Mechanism.

At 60-70% of the ultimate load, an inclined shear crack begins to develop. This inclined shear crack makes an angle of 20 to 35° with the tension face of the slab. The 3-dimensional geometry of this inclined crack is a truncated cone for circular columns and a similarly truncated pyramid for rectangular columns. Once the inclined crack has developed, shear force is carried by friction in the compression zone and aggregate interlock along the surface of the inclined crack. At this stage, the connection is still stable meaning that the connection can be loaded and unloaded without changing its load carrying capacity.

As further load is applied, the longitudinal reinforcement starts to yield. This starts at the face of the connection and then propagates towards the span as the load is increased.

This propagation of yielding is dependent on the reinforcement ratio. As the width of the inclined crack increases aggregate interlock becomes less effective in carrying load resulting in more load being carried by dowel action.

At collapse load the inclined crack penetrates into the compression zone, at which point brittle failure occurs without warning (CEB-FIP 2001).

1.2 Problem Statement

Punching shear failure is all too frequently a factor in flat slab failures. This is undoubtedly due to its brittle nature giving little warning of incipient failure. That these failures occur, also suggests that not only do we have little warning of overstress, but that we are not able to accurately predict failure loads.

The code provision for punching shear capacity was developed empirically, based on nonlinear regression analysis from limited databases. This has resulted in poor assessment of the code provisions. Therefore, there is a need to construct a bigger database that would assess the code equations in a more realistic manner.

Improving the ductility of this failure mode is possible with the use of reinforcement. This has clear safety benefits in terms of giving better advance warning of impending failure and to allow locallised failures not to propagate disproportionately. A relatively new reinforcement technique the Lenton Steel Fortress (LSF) shear reinforcement provides better anchorage compared to stirrups and thus is perceived to produce good ductility. LSF also increases the effective depth of the flexural reinforcement, and is light and easy to place. However, there is limited resreach on LSF and thus a detailed research in this field was vital to improve our understanding.

There is limited published work on the numerical modelling of such systems and therefore, implementing a numerical approach to simulate the performance of flat slab-column connections is essential. A detailed parametric study has been performed to gain a better understanding of the parameters that significantly affects the punching shear capacity both numerically and experimentally.

Limited work using an Artificial Neural Network (ANN) has shown to promise, and to predict punching shear capacity with a higher accuracy than other analytical methods.

Hence it is recommended that this approach should be employed and developed further for the accurate prediction of the punching shear capacity.

1.3 Objectives of the thesis:

- To gain an in-depth understanding of the underlying mechanisms and the fundamental reasons for punching shear failure in flat slabs-column connections, by way of a detailed literature review.
- Previous researchers conducted experiments to predict the behavior of flat slab-column connections. However, the comparison of these experiments with the code equations only provide limited conclusions as they were modelled, loaded and tested differently for differing purposes. Therefore, a detailed database needed to be constructed utilising existing experiments that have been reported in studies on punching shear. This would allow a more accurate comparison of the code equations with the test data.
- Research on the use of Lenton Steel Fortress (LSF) shear reinforcement is limited. The major problem with the punching shear experiments with LSF shear reinforcement is that the slabs were designed with low flexural capacity and this resulted in a slight increase in flexural rather than shear capacity of the slabs. This has resulted in a growing need to carry out more experiments, using LSF shear reinforcement, on flat slab-column connections and therefore three real scale experiments with higher flexural reinforcement were designed and tested.
- Besides the experiments, numerical models using Finite Element Analysis (FEA) can be an effective tool in order to further enhance the understanding of the punching shear behaviour of flat slab-column connections.
- An investigation of the major parameters that affect the prediction of the shear strength of interior slab-column connections with and without shear reinforcement is to be performed by carrying out a detailed numerical parametric study.
- Despite years of intensive research, the accuracy and rationality of punching shear equations could not be improved adequately to the point where an internationally accepted model that predicts the punching shear capacity of flat

slab-column connection could be developed. Although not sufficiently accurate, the available models in the literature such as Shehata (1990), Kinnunen and Nylander (1961), Theodorakopoulas and Swamy (2002) and Broms (1990) are too complex to implement in design codes without further simplifications. Therefore, an alternative approach was sought, and the development of a simple shear model using Artificial Neural Network (ANN) that predicts punching shear capacity with improved accuracy is crucial.

1.4 Layout of the Thesis:

This thesis consists of 8 chapters. Chapter 1 is an introduction, providing definitions, scope of investigations, its objectives and its layout.

Chapter 2 comprises of a comprehensive focused literature review. It then goes on to review estabilished and more recent shear reinforcement types such as stirrups and bent-up bars, shear studs and thin plate stirrups. The slab-column connections subjected to gravity loading are discussed in detail and the available mechanical models of slab-column connections are reported and discussed. Standards such as ACI 318-08 (2008), Eurocode 2-2004, CEB-FIP model code 1990 and BS 8118-1997 are studied in detail and the precision of these standards in calculating the punching shear capacity of slab-column connections is discussed. Finite element analysis (FEA) of the behaviour of flat slab-column connections is reviewed and different element types are discussed.

Chapter 3 presents the database, constructed by the author, based on 549 experiments from the literature on punching shear. The distribution of the parameters on the database of punching shear is also studied, and the database has been used to evaluate the existing punching shear design code provisions. A parametric study using the aforementioned database is carried out.

Chapter 4 presents the results of two series of experiments- pullout and punching shear experiments using Lenton Steel Fortress (LSF) stirrups. This looks at Material characteristics, specimen classification and instrumentation, test set-up and configuration. Experimental results such as load deformation, energy absorption capacity, test observations, strain measurements in the shear reinforcement are also discussed.

Chapter 5 focuses on the numerical modelling of flat slab-column connections and begins with a review of the constitutive material models available for finite element analyses of concrete along with a description of the uniaxial and biaxial behaviour of concrete in order to assess how this is implemented in models based on concrete damage plasticity theory. The nonlinear Newton-Raphson technique is discussed along with the resultant issues of numerical instability and their solutions. Slab modelling techniques and element types are then reported and discussed. Sensitivity analysis to find appropriate model parameters is carried out and described. Finally, the experiments on slab-column connections reported in Chapter 4 and experiments carried out by Li (1997) are analysed using Finite Element modelling. The numerical results are compared with the experimental results and observations on the load deformation, stress-strain behaviour and crack pattern are reported.

Chapter 6 presents series of parametric studies conducted on the validated models which were previously discussed in Chapter 5. This allows an assessment on the sensitivity of certain parameters such as column dimensions, slab depths, top and bottom reinforcement ratios, shear reinforcement areas, etc. to be carried out with the intention of gaining an understanding of how slab-column connections behave under gravity load.

Chapter 7 describes the development of the Bayesian Neural Network model to predict the punching shear. This chapter begins with an introduction to the Artificial Neural Network and the Integration of a Bayesian Framework. The experimental database reported in Chapter 3 is employed in order to develop a Bayesian Neural Network (NN) model that predicts punching shear capacity of flat slab-column connections.

Chapter 8 sets out the conclusions of the thesis and provides suggestions for areas of future research.

Chapter 2

LITERATURE REVIEW

2.1 Introduction

The problem of punching shear of reinforced concrete slabs subjected to concentrated loads and lateral forces has received attention over several decades (fib Bulletin No. 12, 2001). Failure of flat-plate structures initiated by punching failure, including those of the Sampoong Department Store occurred in 1995 or Bullocks department in 1994 indicated that two way shear strength of slab-column connections and the mechanics of punching shear failure have not been well understood (see Figure 2.1).

Sampoong departmental collapse, South Korea (after Gardner *et al*., 2002).

Punching shear failures in Bullock's Department- 1994 Northridge earthquake (after Mitchell *et al*., 1995).

Figure 2.1: Punching shear failures

The purpose of this chapter is to briefly summarize the major contributions of earlier researchers to the understanding of the problem of punching failure. Therefore punching shear problems and solutions are reviewed first. The mechanical models available to predict the punching shear strength of the slab-column connections under gravity loading are discussed. Code Provisions such as ACI 318-08 (2008), EC 2 (2004), CEB-

FIP Model Code 1990 (1991) and BS 8110 (1997) are reported in detail and are used to assess the precision in calculating the punching shear strength of the slab-column connections. Finite Element Modelling is utilised later in this document to aid the understanding of the behaviour of slab-column connections and thus element types, constitutive material models and example of FE analysis of the slabs are reported in detail.

2.2 Problems and solutions to Punching Shear

2.2.1 Punching shear failure

Punching shear failure is a local brittle failure of the slab-column connection. Following failure, the column together with a portion of the slab is pushed through the slab. Flexural cracks are observed as soon as the cracking moment per unit width is reached around the loading area. An inclined shear crack develops at about 60% to 70% of the ultimate load (Menetrey, 1996). The inclined crack is in the form of a truncated cone or pyramid for circular and rectangular columns respectively.

2.2.2 Solutions to the punching problems

Punching shear failure is brittle and catastrophic. Preventing such a brittle failure can be achieved in several ways:

1. Increasing the area of concrete resisting shear stresses. This can be achieved by increasing the slab thickness around the columns by providing a drop panel or an inverted cone (capital) as shown in Figure 2.2.
2. Using high strength concrete. Using higher compressive strength concrete leads to higher tensile strength, which is of great import in shear resistance.
3. Increasing shear strength by placing shear reinforcement around the column.

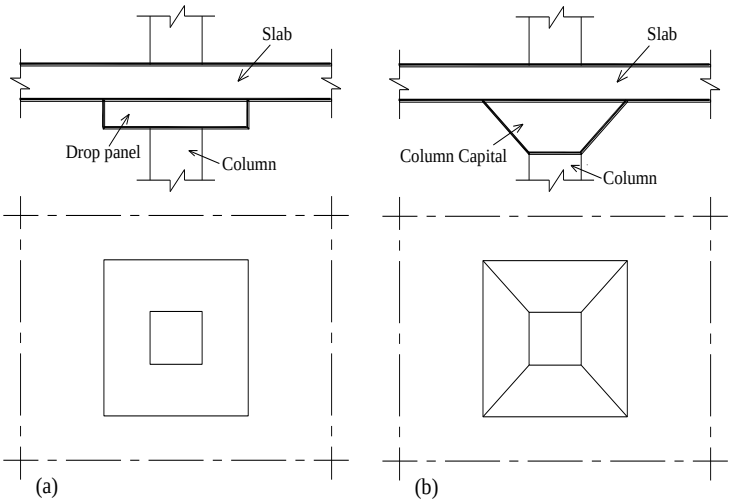

Figure 2.2: Type of shear reinforcement (a) Drop panels (b) Column Capital.

The above methods can effectively increase the punching shear strength. Megally (1998) conducted experiments on slabs strengthened with shear capitals, drop panels and shear studs. The author concluded that all methods increased the punching shear strength of the slabs, but only properly anchored shear reinforcement created ductile connections. The use of higher compressive strength concrete in slabs increased the punching shear strength but not the ductility of the connections (Marzouk and Hussein (1991)). The importance of the ductility of the slab-column connections is evident when deformations beyond the yielding of flexural reinforcement are needed. If the connection continues to deform beyond the steel yielding (*e.g.* in an earthquake), the concrete in the connection continues to crack, which results in reduction in shear strength. Ultimately this can result in the punching failure at large inelastic deformations. The use of shear reinforcement in slab-column connections can increase strength and ductility by changing the mode of failure from punching to flexure and is the preferred solution in seismic regions.

2.2.2.1 Shear reinforcement

The aim of all types of shear reinforcement is to increase shear capacity and add ductility to the post-peak load behaviour of slab-column connections (Polak *et al*., 2005). Strength and ductility as well as ability and ease of placing the shear reinforcement in the crowded slab-column zone and economic consideration play

critical roles in choosing the reinforcement type (Polak *et al*., 2005). Shear reinforcements can be classified into the following categories:

1. reinforcing bars formed into stirrups and bent bars

2. headed reinforcement, Shear studs

3. thin plate stirrups called Lenton Steel Fortress (LSF) reinforcement

4. e.g. Structural Steel Sections called Shearheads, UFO (cone shaped steel device)

Stirrups and Bent-up Bars

The use of stirrups in the form of bent-up bars, single or multiple leg or closed stirrups is permitted in the design standards as shown in Figure 2.3; however, conventional stirrups have several practical problems. The use of stirrups as shear reinforcement was investigated in the past by Hawkins (1974), Chana and Desai (1992), Beutel and Hegger (2002), Oliveira *et al*., (2000) and Broms (2000). Bent-up shear reinforcement was first investigated by Graf in 1938 (Cited in Xin Li 1997 PhD thesis). Bent-up reinforcements are not favoured in earthquake regions since they show very little increase in ductility (Megali, 1998). The use of bent-up reinforcement complicates both fabrication and construction and is not commonly used in practice.

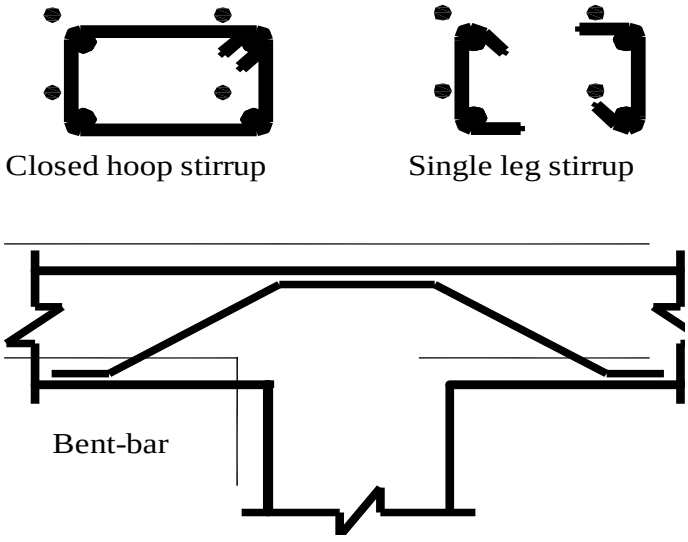

Figure 2.3: Stirrups and Bent-up shear reinforcement.

The failure mode of a stirrup is controlled by concrete crushing under the bend therefore stirrup bars typically develop about 70% of yield strength at failure. It has also been reported that significant slip occurs at the corners of the stirrups which causes the vertical legs of the shear reinforcement to be less effective. Moreover, the corners of the stirrups can significantly reduce the effective height of the shear reinforcement leg.

Shear studs

Stud shear reinforcement was first tested in Calgary by Mokhtar *et al*., (1985). They proposed the use of preassembled units of shear stud rails (SSR) as shear reinforcement. Shear Stud Rail (SSR) reinforcement is shown in Figure 2.4. SSR relies on mechanical anchorage of the heads at both ends of the stem, or a mechanical weld at one end and a head at the other end. The stem is normally welded to a steel strip. The steel strip keeps the SSR in place during casting. The development of the full yield strength of the reinforcement bar was found to be achieved when the head of the stirrup is about ten times the stem cross-sectional area. The use of Stud shear reinforcement has been investigated by many researchers; Megally and Ghali (1994), Megally and Ghali (2000), Gomez and Regan (1999), Regan (2000), Robertson *et al*., (2002), Kang and Wallace (2005).

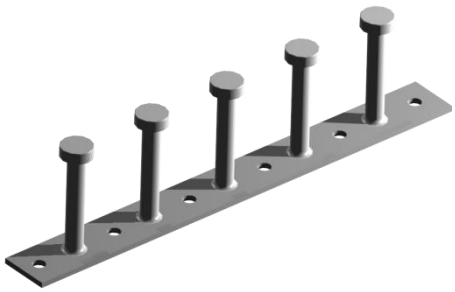

Figure 2.4: Shear Stud Rail (SSR) reinforcement.

Though the stud shear reinforcement is the preferred option of structural engineers, the high cost of stud shear reinforcement and potential interference problems with slab reinforcement necessitates the evaluation of potentially more cost-effective and less

intrusive reinforcement solutions. One such solution will be represented by thin plate stirrups in the following.

Thin Plate Stirrups

A new thin plate stirrup called Shear Band reinforcement was conceived at the University of Sheffield for the first time (Li, 1997). This reinforcement is now in the market and called Lenton Steel Fortress (LSF). It is made up of a thin steel strip of high strength and high ductility as shown in Figure 2.5. There are several advantages of using LSF shear reinforcement such as increase in the effective depth of flexural reinforcement due to small thickness of LSF; easy handling due to the light weight of reinforcement (only man-handling); easy placement on top of the flexural reinforcement and good anchorage.

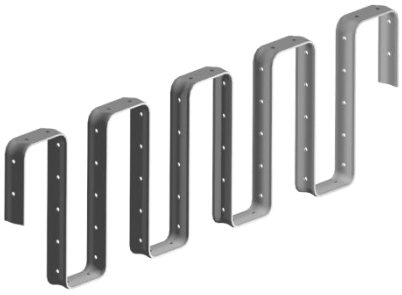

Figure 2.5: Thin plate stirrups (Lenton Steel Fortress).

Li (1997) assessed the effectiveness of the shear band reinforcement and conducted eight experiments on interior slab-column connections. One experiment was carried out without shear reinforcement as a control specimen and the other 7 specimens were prepared using LSF shear reinforcement. The result of this study indicated strongly that the brittle punching failure could be prevented by using LSF shear reinforcement and the ductility of the connection could also be increased. Soon after, Ioannou (2001) conducted another 5 experiments on slabs with different pattern of holes in the slab, to assess the effectiveness of LSF shear reinforcement. These experiments confirmed the increase in both punching shear capacity and deformation.

Shearhead reinforcement (Figure 2.6 (a)) was one of the first proposed types of shear reinforcement for concrete plates. Though the use of shearhead reinforcement increases

both strength and ductility of the connection, there are difficulties in placing the shearhead amoung the flexural reinforcement especially for thin slabs. Alander (2000) proposed new reinforcing system called UFO punching preventer. This consists of a cone-shaped steel device that is placed in the slab around the column, crossing the shear crack as shown in Figure 2.6.

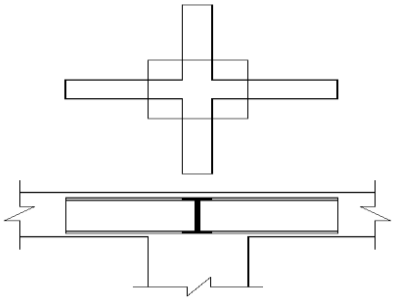

(a)

(b)

Figure 2.6: Types of shear reinforcement, a) Shearhead (I section) reinforcement. b) The UFO punching preventer (Alander, 2000).

2.3 Slab-Column Connections subjected to gravity loading only

A large amount of experimental and analytical research has been carried out since the 1950s to understand the punching shear resistance of slab-column connections. Two main state-of-the-art documents, "Punching Shear in Reinforced Concrete" (Shear Reinforcement for Slabs; ACI-ASCE-421 1999) and "Punching of Structural Concrete Slabs" (CEB-FIP 2001) have been published on shear in concrete slabs in the last three decades. Repetition of the discussions in these documents is not the intention of this section; important points in these reports are highlighted, however, as they relate to this study.

2.3.1 Mechanical Models

A number of different types of models for punching are described below. They are presented in chronological order and are key models that either influenced code provisions or address new aspects of behavior of flat plates.

2.3.1.1 Moe (1961)

Moe (1961) carried out 41 experiments that were subjected to pure shear loading on interior slab-column connections. The experimental results led Moe to propose an expression that could predict the load carrying capacity of slab-column connections as given in Equation 2.1:

$$\frac{V_u}{bd} = \frac{15(1-0.075\frac{r}{d})}{1+\frac{5.25bc\sqrt{f_c'}}{V_{flex}}} \qquad [N/mm^2] \qquad (2.1)$$

where V_{flex} is the flexural capacity based on yield line analysis, b is the perimeter of the loading area, c is the side length of the square column, d is the effective depth of the slab and f_c' is the concrete compressive strength.

It should be noted that Equation 2.1 involves interaction between the flexural and shear strength of the slab. The main conclusions from Moe's work were:

1. Punching shear failure is related to tensile failure of concrete and $\sqrt{f_c'}$ was used to predict the punching shear capacity for the first time.
2. Shear strength of concrete slabs acting in two-way action is higher than that of one-way members.
3. The interaction between flexural and shear strength of two-way slabs can be incorporated in the shear strength expressions.

Later, in 1962, Equation 2.1 was further simplified for design purposes by ACI Committee 326. This was achieved by setting the ratio of shear to flexural capacity equal to one in order to ensure flexural distress prior to the shear failure. The following expression (given in Equation 2.2) was then obtained (cited in the CEB FIP Bulletin 12, 2001):

$$\frac{V_u}{bd} = (9.75 - 1.125\frac{c}{d})\sqrt{f_c'} \qquad [N/mm^2] \qquad (2.2)$$

It is worth noting that Equation 2.2 becomes negative in the case of large values of c/d. In order to overcome this problem, Equation 2.2 was then modified by ACI Committee

326 by using the lower bound of test results from Moe and others. This led to Equation 2.3:

$$\frac{V_u}{bd} = 4(1+\frac{c}{d})\sqrt{f_c'} \qquad [\text{N/mm}^2] \qquad (2.3)$$

They also proposed a critical section located $d/2$ away from the column face at which to check for shear for design purposes.

2.3.1.2 Kinnunen and Nylander (1960)

Based on 61 tests on circular slabs supported on circular columns, Kinnunen and Nylander (1960) proposed the first mechanical model to estimate the punching shear capacity of slabs in the vicinity of columns (cited by CEB-FIP Model 1990 (1991)). The main variables in the tests were the type and amount of reinforcement and the column diameter. The most important observations from these tests were that the slab portion outside the shear crack acted as a rigid body rotating around the root of the shear crack as shown in Figure 2.7.

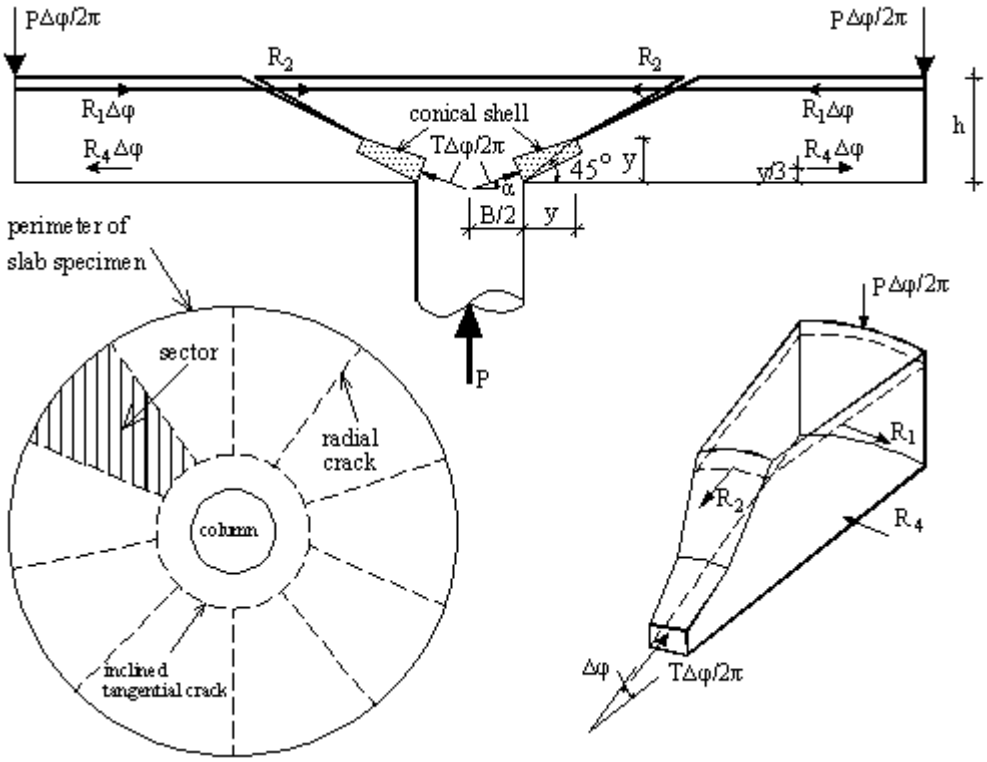

Figure 2.7: Mechanical model of Kinnunen and Nylander (adopted from fib bulletin No. 12, 2001).

The model assumed that each segmental slab is supported on the conical shell between the column and the root of the shear crack. In this model, failure is assumed to occur when the tangential compressive deformation in the concrete on the bottom surface of the slab under the root of the shear crack reached a critical value. This critical value was found to be a function of the ratio of column size to the slab depth and was determined from the test data. The load carrying capacity was computed using an iterative procedure by assuming an initial value of compression zone, *y*, and considering equations of equilibrium in the radial and tangential directions as well as failure criteria. The disadvantage of the model is its complexity, since the depth of compression zone is calculated by iteration. The failure criterion, based simply on strain, is controversial, other researchers (Shehata and Regan, 1989; Broms, 1990) proposed modifications which are described below.

2.3.1.3 Broms (1990)

The failure criterion in the model proposed by Kinnunen and Nylander (1961) was modified by Broms (1990). The modification involved the use of a tangential strain limit, taken as the strain inducing microcracking in the compression zone, and a limiting stress in a conical shell under biaxial compressive stress, as shown in Figure 2.8.

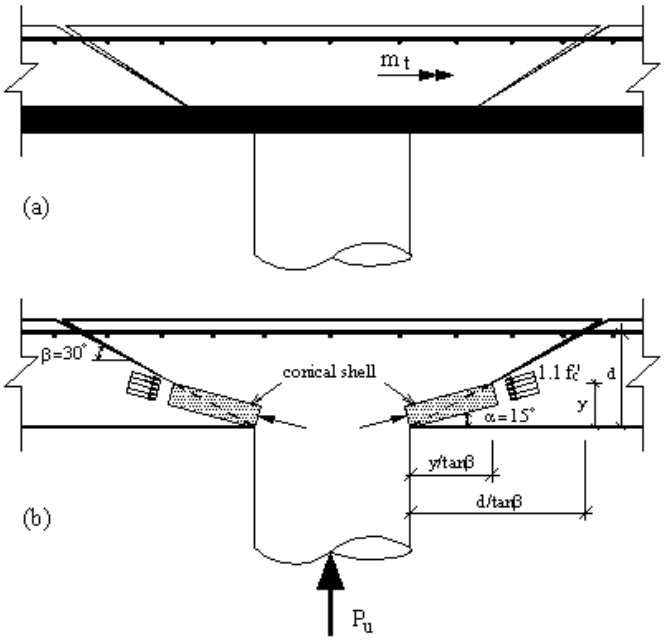

Figure 2.8: Broms model: (a) High tangential compression strain failure mechanism (b) High radial compression stress failure mechanism (adapted from Broms, 1990).

Equation 2.4 was derived by Broms (1990) on the basis of experimental tests performed on cylinders 150mm × 300mm loaded in uniaxial compression. This expresses tangential concrete strain as a function of concrete strength and depth of compression zone:

$$\varepsilon_{\mathrm{cpu}} = 0.0008\left(\frac{150}{\alpha\chi_{\mathrm{pu}}} \times \frac{25}{f_{\mathrm{c}}^{'}}\right)^{1/3} \tag{2.4}$$

Where 150 is the diameter of the cylinder specimens (mm), $\alpha\chi_{\mathrm{pu}}$ is the height of the equivalent rectangular stress block (mm), $f_{\mathrm{c}}^{'}$ is the concrete compressive strength (MPa).

The punching load corresponding to the limiting tangential strain, V_{ε}, was computed based on linear elastic bending moments of a circular slab loaded around the periphery and on the bilinear section properties of concrete and steel. In order to account for possible yielding of the reinforcement, calculations were carried out as a function of reinforcement ratio.

When the compression stress in a conical shell (of a constant thickness and inclination of 15°) reached the critical value of $1.1f_{\mathrm{c}}^{'}$ at the root of the inclined crack, punching failure was assumed to occur in the radial direction (Figure 2.8 b). Equation 2.5 defines the punching shear load, V_{σ}, which is calculated from the equilibrium of forces in the vertical direction incorporating a size effect factor $(150/0.5y)^{1/3}$:

$$V_{\sigma} = \left[\pi\left(B + \frac{2y}{\tan 30^{\circ}}\right)\frac{y\sin 15^{\circ}}{\sin 30^{\circ}}(1{,}1f_{\mathrm{c}}^{'})\left(\frac{150}{0.5y}\right)^{1/3}\right]\sin 15^{\circ} \qquad \text{[kN]} \tag{2.5}$$

where B is the diameter of the circular column and y is the depth of the radial compression zone.

The governing punching load is taken as the smallest of the capacities V_{ε} and V_{σ}. Based on the model proposed by Broms (1990), it was assumed that punching failure occurred at the root of the inclined crack in a compression-shear failure mode. Broms recognized the importance of size effect and showed that the size effect is a function of concrete compressive strength. This was further extended for rectangular slab-column connections by using an equivalent circular column approach.

2.3.1.4 Modified model by Shehata

Shehata and Regan (1989) proposed a mechanical model on punching capacity of slab-column connections. This model was based on the observations from experiments carried out on slab-column connections conducted by the authors as well as numerical analysis. Based on the observed crack pattern of test specimens, Shehata and Regan (1989) divided the slab into rigid radial segments that rotate around a centre of rotation (CR) located at the column face and at the level of the neutral axis. This is shown in Figure 2.9. This model was too complex to be adopted by current codes and therefore, Shehata (1990) proposed a simpler model. Only the simplified model Shehata (1990) is described in this section as this can be easily used in practice. Figure 2.9 shows a radial segment of the slab of the sectorial angle $\Delta\varphi$ bounded by two radial crack planes and an inclined crack surface.

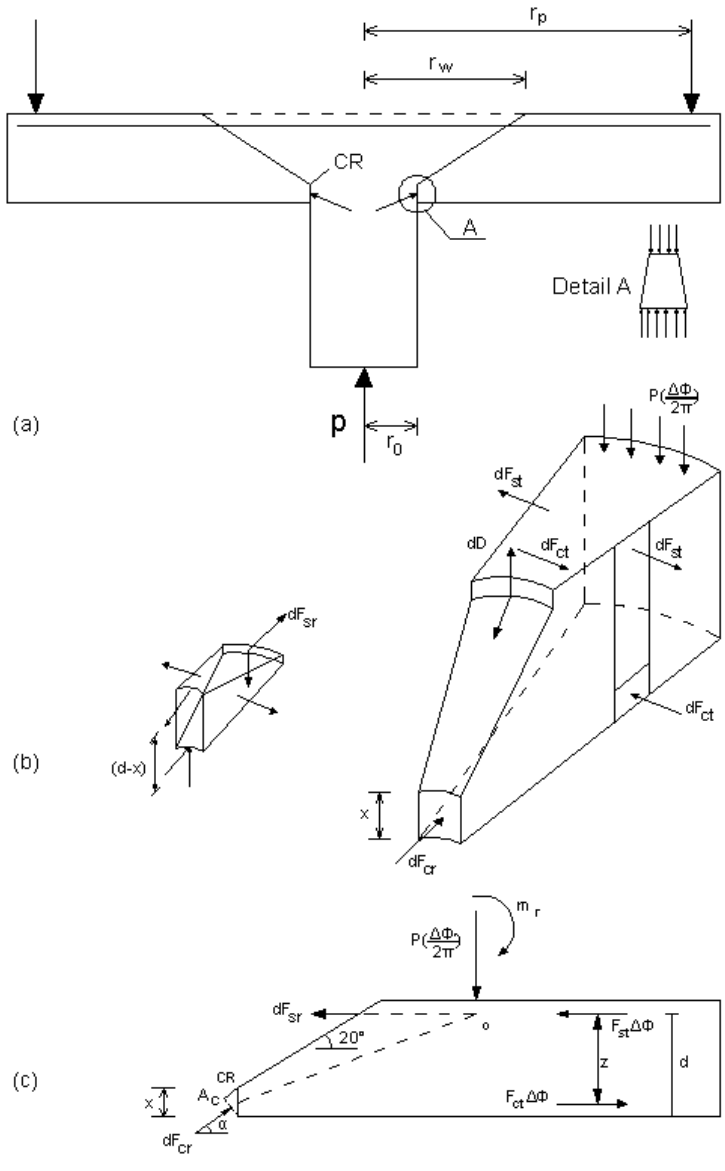

Figure 2.9: Model Used for Punching Analysis: (a) Stress Concentration Region; (b) Forces Acting on Segment; (c) Forces Acting on Segment in Radial Plane (after Shehata, 1990).

The forces involved in the analysis of each radial segment of the slabs are:

- The external load $P(\Delta\varphi / 2\pi)$, at a distance $r = r_p$;
- Resultant tangential forces in the steel $(F_{st}.\Delta\phi)$ due to slab deformation;
- Resultant tangential forces in the concrete $(F_{ct}.\Delta\phi)$ due to slab deformation;
- The inclined bearing force (dF_{CR}) in the concrete at the face of column;
- Dowel forces, dD, on the steel cutting across the inclined crack. The dowel forces are ignored since yielding of reinforcement is assumed;
- Radial forces in the steel crossing the inclined crack, dF_{sr}.

Shehata (1990) classified three critical states at which the frontal part of the radial segment fails to sustain the force at the column face:

1. If the angle α of the compressive force reaches 20°, the associated principle tensile stresses would exceed the concrete tensile strain and cause splitting of the concrete.
2. If the average radial strain on the compressed face reaches a value of 0.0035 in the plastic length starting from the column face.
3. If the tangential strain of the compressed face reaches 0.0035 at a distance x from the column face, there is a tangential crushing of the concrete.

In order to define the ultimate capacity of the connection, four equilibrium conditions in a radial plane are considered.

$$\Sigma H^{\text{tangential}}: \qquad F_{st}.\Delta\phi = F_{ct}.\Delta\phi$$

$$\Sigma V: \qquad P(\frac{\Delta\phi}{2\pi}) = dF_{cr}.\sin 10^{\circ}$$

$$\Sigma H^{\text{radial}}: \qquad dF_{sr} = dF_{ct}.\cos 10^{\circ}$$

$$\Sigma M^{O}: \qquad m_r = F_{ct}.\Delta\phi.z = F_{st}.\Delta\phi.z$$

Consequently, the punching capacity of the connection can be calculated from Equation 2.6:

$$P = 2\pi r_0 x n_c f_c \tan 10^\circ \qquad \text{[kN]} \qquad (2.6)$$

Experiments carried out by Shehata and Regan (1989) (cited in Shehata, 1990) considered the size effect on punching shear. Shehata proposed the size effect as $\sqrt[3]{\frac{500}{d}}$ where d is in mm. Therefore, the estimated punching load may be calculated as shown in Equation 2.7:

$$P = 2\pi r_0 x n_c f_c \tan 10^\circ \sqrt[3]{\left(\frac{500}{d}\right)} \qquad \text{[kN]} \qquad (2.7)$$

Where r_0 is the diameter of column in mm, n_c is stress concentration factor that expresses the concrete strength under a multiaxial state of stress that can be calculated by Equation 2.8.

$$n_c = 1.4\sqrt{\left(\frac{2d}{r_0}\right)} \geq 1.25 \qquad (2.8)$$

where f_c is the cylinder strength of concrete (MPa), x is the height of compression zone at flexure in the tangential direction when punching failure occurs.

2.3.1.5 Menetrey (1996)

Menetrey (1996) proposed an analytical model to compute the punching shear strength of reinforced concrete slab-column connections. The model was derived from experimental results and from numerical simulations using finite element analysis (FEA). The punching capacity was calculated by integrating the tensile resistance of concrete and reinforcements in the vertical direction along the punching crack (Figure 2.10).

The punching load of a slab is calculated using Equation 2.9:

$$F_{pun} = F_{ct} + F_{dow} + F_{sw} \qquad \text{[N]} \qquad (2.9)$$

Where F_{ct} is the vertical component of the concrete tensile force (N), F_{dow} is the dowel contribution of the flexural reinforcement (N), F_{sw} is the vertical component of the force in the studs, stirrups or bent up bars which are well anchored (N).

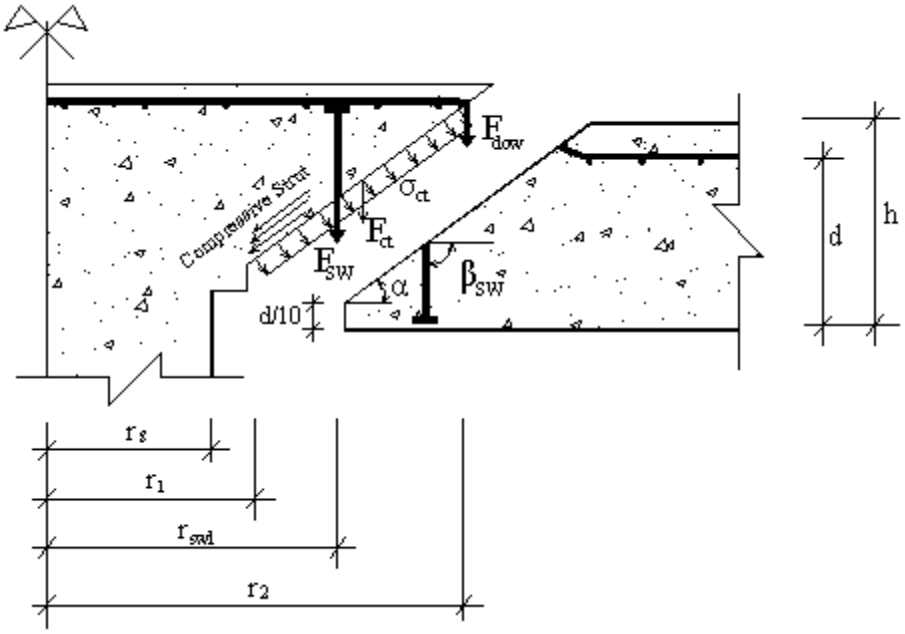

Figure 2.10: Representation of the punching shear capacity of a general reinforced slab (after Menetrey, 2002).

Based on nonlinear finite element simulations, Menetrey derived Equation 2.10 to compute F_{ct} which is a function of the reinforcement ratio (ρ), concrete tensile strength (f_{ct}), size effect (η and μ) and radii of punching crack (r_1 and r_2) (Equation 2.10):

$$F_{ct} = \pi(r_1 + r_2)s\, f_{ct}^{2/3} \xi \eta \mu \qquad \text{[kN]} \qquad (2.10)$$

Menetrey then computed the shear force which can be transferred by flexural reinforcing bars crossing the punching crack by adopting the approach proposed by the CEB-FIP model code 1990 (1991). The dowel force, F_{dow}, is then calculated by Equation 2.11 for the summation of all bars crossing the crack.

$$F_{dow} = \frac{1}{2} \sum^{bars} \phi_s^2 \sqrt{f_c f_t (1 - \zeta^2)} \sin\alpha \qquad \text{[kN]} \qquad (2.11)$$

where ϕ_s is the diameter of the corresponding bars crossing the punching crack, f_t is the steel yield strength, f_c is the concrete compressive strength.

A parabolic interaction is assumed between the axial force and the dowel force in the reinforce bar. This parabolic interaction is expressed with the term $(1-\zeta^2)$ where $\zeta = \frac{\sigma_s}{f_t}$ and f_t is the axial tensile stress in the reinforcing bar.

The contribution of shear reinforcement was computed by taking the vertical component of the yield force in the stirrups.

2.3.1.6 Theodorakopoulos and Swamy (2002)

In 2002, a simple engineering model was proposed by Theodorakopoulos and Swamy to predict the punching shear capacity of slab-column connections without shear reinforcement. This was done by analysing the equilibrium conditions of the free-body diagram model. This model considered the free-body diagram around the slab-column connection area at the stage when an inclined crack had formed and its propagation was prevented by the compression zone. The punching shear failure surface considered by Theodorakopoulos and Swamy, (2002) is shown in Figure 2.11. According to this study, the failure is assumed to take place when splitting failure occurs along lines AA' and BB' in the compression zone.

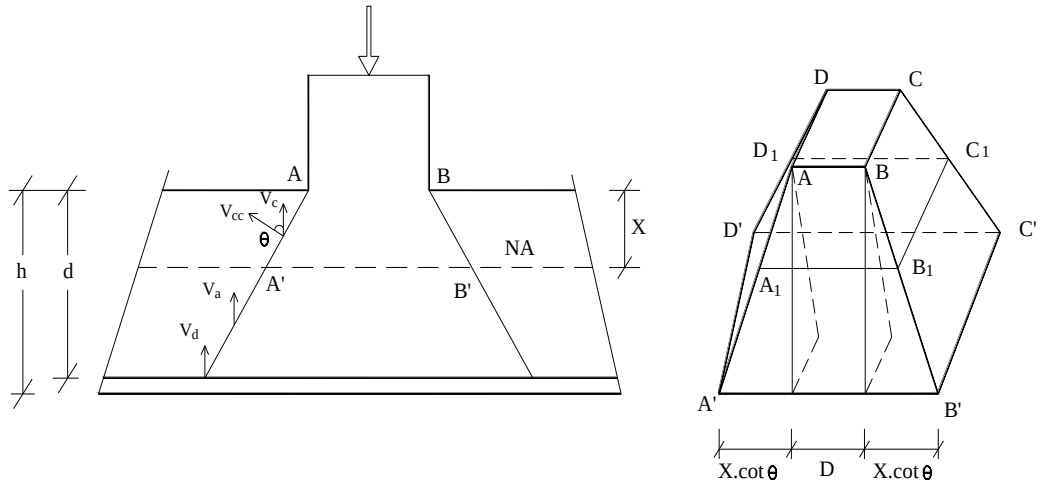

Figure 2.11: Punching shear model (Theodorakopouos and Swamy 2002).

The total shear resistance of a slab-column connection without shear reinforcement was computed as follows (Equation 2.12):

$$V_u = V_c + V_a + V_d \qquad \text{[kN]} \qquad (2.12)$$

where V_u is the punching shear capacity, V_c is vertical component of the concrete resistance provided in the compression zone, V_a and V_d are the resistances provided by the aggregate interlock and dowel action respectively.

The aggregate interlock force is activated only after the formation of the inclined crack. However, because of the large separation of the crack faces ($V_a = 0$) the model neglects this effect.

Where dowel action was expected to occur, Theodorakopouos and Swamy (2002) assumed that the dowel action was proportional to the length of the crack location. The British Standard's control perimeter (1.5*d* from column face) was used to combine the terms V_c and V_d and this is given in Equation 2.13:

$$V_c = b_p X \cot\theta \, f_{ct} \qquad \text{[N]} \qquad (2.13)$$

where b_p is the critical perimeter located 1.5*d* away from the column face, X is the depth of the compression zone, θ is the assumed inclined crack angle (30°), and f_{ct} is the splitting tensile strength taken as $0.27 f_c'^{2/3}$ (MPa).

2.3.1.7 Discussions of mechanical models

There is no accepted theoretical model for the treatment of punching shear strength of slabs with and without shear reinforcement. However, theoretical models are determined considering: the equilibrium; assumed constitutive laws, material strength and failure criteria; and compatibility.

Normally, equilibrium and the relation to the loads and sections are considered to be in the linear elastic region of the material behaviour only but the theoretical models considered these criteria to punching shear failure problem.

Most models contain empirical aspects or parameters such as assuming the geometry of failure surface or using simplified constitutive material laws or simplified failure

criteria. However, it should be accepted that mechanical models need further efford for the analysis and for the definition of the different parameters which are involved.

Although Kinnunen and Nylander model is the first mechanical model which determines the shear capacity of slab in the vicinity of column and visualized the flow of force, due to its complication in calculation and simple failure criterion it is not used in practice. Nevertheless Kinnunen and Nylander model was modified by others (e.g. Shehata and Regan, 1989; Broms, 1990).

2.3.2 Codes of Practice

The approaches adopted to calculate the punching shear capacity of slab-column connections by three of the most widely used standards are discussed in the following.

2.3.2.1 ACI 318-08 (2008)

The ACI code requires that the factored shear force, V_u, at a critical section, should be greater than the nominal shear strength, V_n. The nominal shear strength is the sum of shear strength provided by the concrete, V_c, and the shear strength provided by the shear reinforcement, V_s. The equation for slabs without shear reinforcement is shown in Equation 2.14:

$$V_u \leq \Phi V_c \tag{2.14}$$

where $\Phi = 0.85$. The nominal shear strength provided by the concrete for a slab without shear reinforcement, V_c, is given by the smallest of the values obtained from Equations 2.15, 2.16 and 2.17:

$$V_c = \frac{1}{12} \times (2 + \frac{4}{\beta_c}) \sqrt{f'_c} b_o d, \quad \text{[N]} \tag{2.15}$$

$$V_c = \frac{1}{12} \times (2 + \frac{\alpha_s \times d}{b_o}) \sqrt{f'_c} b_o d, \quad \text{[N]} \tag{2.16}$$

$$V_c = \frac{1}{3} \sqrt{f'_c} b_o d, \quad \text{[N]} \tag{2.17}$$

Where V_c is the punching shear strength, $f_c^{'}$ is the specified concrete cylinder strength (MPa), α_s is 40 for interior columns, β_c is the ratio of longer to shorter dimension of the loaded area, b_o is the shear perimeter and is equal to $\pi(c+d)$ for interior circular columns, and is equal to $\Sigma c+4d$ for interior rectangular columns. (Figure 2.12).

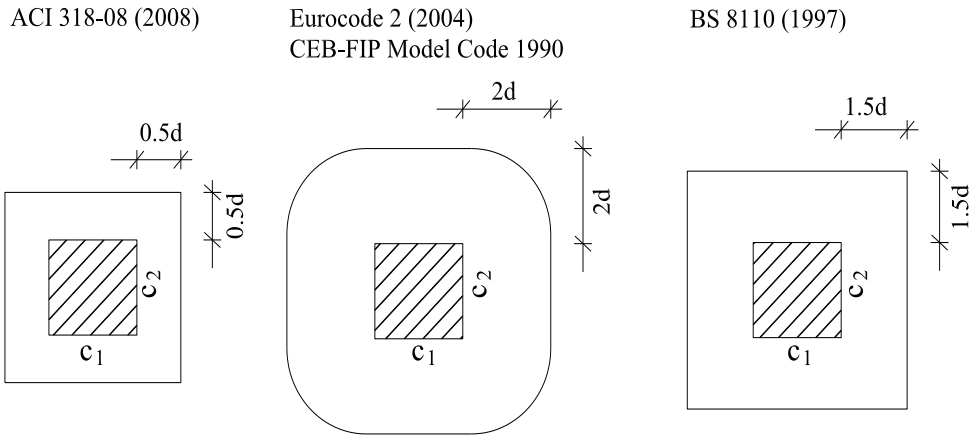

Figure 2.12: Critical shear section for slabs without shear reinforcement (ACI 318-08, 1997; Eurocode 2, 2004; CEB-FIP Model Code, 1990; BS 8110, 1997).

The use of shear reinforcement in the form of bars or wires or single- or multiple leg stirrups is permitted for slabs with an effective depth, *d*, greater than or equal to 152.4 mm (6 inch). The punching shear capacity of slabs reinforced in shear with stirrups is calculated in accordance to Equation 2.18:

$$V_u \leq \Phi V_n \qquad \text{[N]}$$

(2.18)

$$V_n = V_c + V_s \leq \frac{1}{2}\sqrt{f'_c}\, b_o d \qquad \text{[N]} \qquad (2.19)$$

where $\Phi = 0.85$, is the strength reduction factor for shear. V_c in Equation 2.19 shall not be taken greater than $\frac{1}{6}\sqrt{f_c'}\, b_o d$ and the contribution provided by shear reinforcement is calculated by:

$$V_s = \frac{A_v\ f_y d}{s} \qquad \text{[N]} \qquad (2.20)$$

where A_v is the area of the shear reinforcement within a distance s in mm^2, s is the spacing of the shear reinforcement in a direction parallel to longitudinal reinforcement in mm and d is the effective depth in mm.

The use of Stud rail shear reinforcement was introduced in ACI 318 in 2008. Equation 2.18 is also used to calculate the punching shear capacity of slabs reinforced with stud rails. However, the nominal shear strength, V_n, is limited to $0.67\sqrt{f_c'}b_o d$ and V_c should not be taken greater than $0.25\sqrt{f_c'}.b_o.d$.

2.3.2.2 Eurocode 2-2004 & CEB-FIP Model code 1990:

The Eurocode 2-2004 provisions are similar to those of CEB-FIP Model Code 1990 with a control perimeter $2d$ from the loaded area and this perimeter should be constructed so as to minimise its length (see Figure 2.12). The nominal punching shear design strength, $V_{Rd,c}$, of an interior slab-column connection can be calculated as

$$V_{Rd,c} = 0.18 \times \xi \times (100 \times \rho \times f_{ck})^{1/3} \times u_1 \times d \qquad \text{[N]} \qquad (2.21)$$

where, f_{ck} is the characteristic concrete cylinder strength (MPa); ρ is the flexural reinforcement ratio, $\rho = \sqrt{\rho_x \times \rho_y}$; ξ is the size effect, $\xi = (1 + \sqrt{200/d})$, d in mm.

Eurocode 2-2004 limits the size effect to 2 and reinforcement ratio, ρ, to 0.02. Where shear reinforcement is required the nominal punching shear design strength should be calculated in accordance with Equation (2.22):

$$V_{Rd,c} = 0.75V_{Rd,c} + 1.5\frac{d}{s_r}A_{sw} f_{ywd,ef} \frac{1}{u_1 d}\sin\alpha \qquad \text{[N]} \qquad (2.22)$$

where A_{sw} is the area of one perimeter of shear reinforcement around the column (mm^2), s_r is the radial spacing of perimeters of shear reinforcement (mm), $f_{ywd,ef}$ is the effective design strength of the punching shear reinforcement, and is given in Equation 2.23:

$$f_{ywd,ef} = 250 + 0.25d \le f_{ywd} \qquad \text{[MPa]} \qquad (2.23)$$

where d is the mean of the effective depths in the orthogonal directions (mm) and α is the angle between the shear reinforcement and the plane of the slab.

2.3.2.3 BS 8110-1997

The British Standard, BS 8110-1997, uses a rectangular control perimeter 1.5d from the loaded area for both circular and rectangular loaded areas (Figure 2.12).

$$v_c = 0.79 \times (100\rho)^{1/3} \times (f_{cu}/25)^{1/3} \times (400/d)^{1/4} \quad (2.24)$$

where f_{cu} is characteristic concrete cube strength ($f_{cu} \leq 40$ MPa), $u = 4(c + 3d)$ is control perimeter for circular and rectangular loaded areas in mm, the size effect $(400/d)^{0.25} \geq 1$, $\rho = (\rho_x + \rho_y)/2 < 0.03$ and flexural reinforcement ratio is calculated for the width equal to $c + 3d$.

The maximum design shear stress, v_c, should not exceed $0.8\sqrt{f_{cu}}$ or 5N/mm^2. Shear reinforcement is required when V is greater than V_c but $< 2V_c$. Shear reinforcement is required according to Equations 2.25 and 2.26:

For $V \leq 1.6V_c$ $$\Sigma A_{sv} \sin\alpha \geq \frac{(V - V_c)}{0.95 f_{yv}} \quad (2.25)$$

And for $1.6V_c < V \leq 2.0V_c$ $$\Sigma A_{sv} \sin\alpha \geq \frac{5(0.7V - V_c)}{0.87 f_{yv}} \quad (2.26)$$

where f_{yv} is the characteristic strength of the shear reinforcement, A_{sv} is the area of the shear reinforcement in mm^2 and α is the angle between the shear reinforcement and the plane of the slab.

The shear reinforcement should be distributed evenly around the zone on at least two perimeters within 1.5d from the column. Shear reinforcement can only be used when the thickness of the slab is equal to 200 mm or more.

2.3.2.4 Discussion of Codes:

In ACI 318-08 (2008), Eurocode 2 (2004), CEB-FIP model code 1990 and BS 8110 (1997), punching shear capacity calculations are based on a critical perimeter, which is

located between 0.5 and 2d from the face of the column. BS 8110, Eurocode2-2004 and CEB-FIP Model code consider the effect of flexural reinforcement and size effect on the punching capacity of the connection. However, the effect of flexural reinforcement and size effect are slightly different in BS 8110 and Eurocode 2-2004. Figure 2.13 compares the shape of different size effect expressions from three codes. In order to compare the size effect parameter in codes, the author has normalised the size effect factor to a value of 1 when the average effective depth is 200 mm. The size effect factor in BS 8110 does not decrease beyond an average effective depth of 400 mm. ACI considers only the concrete strength.

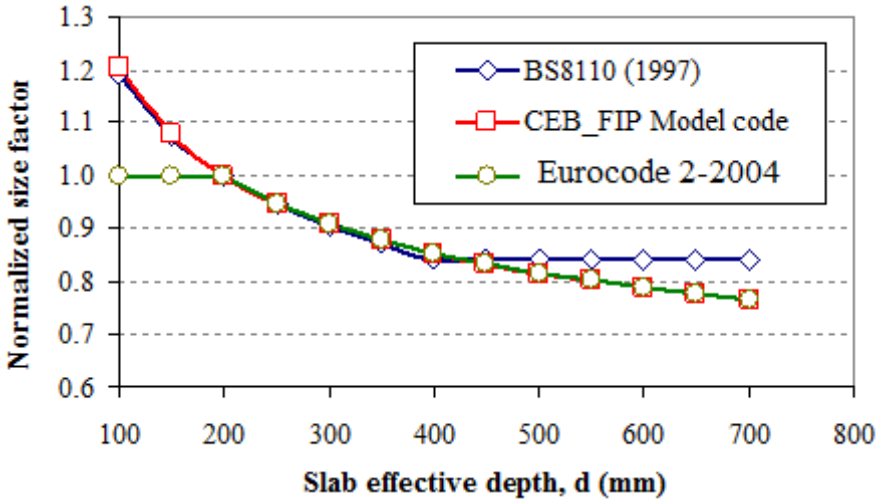

Figure 2.13: Size effect factors normalized to the average effective depth of 200 mm.

The amount of shear reinforcement varies widely between codes. The stress in shear reinforcement is limited only in Eurocode 2. BS 8110 (1997) and Eurocode 2 (2004) specify that shear reinforcement should be distributed evenly around at least two perimeters, while the ACI adopts cross line shear reinforcement. ACI 318-08 requires that the stress on the critical section at $d/2$ from the outermost shear reinforcement be less than the one way shear resistance of concrete ($0.17\sqrt{f_c'}b_o d$). This gives a higher shear reinforced zone compared to other codes.

To demonstrate the difference in design of shear reinforcement according to different building standards, an interior slab-column connection was designed by the author according to ACI 318-08, BS 8110 (1997), EC2 (2004) and CEB-FIP MC90 (1991) building codes by utilizing stud rail shear reinforcement. The connection is transferring

V only with no moment as shown in Figure 2.14 (a). Design data are: dead load is 8.5 kPa; live load is 4.5 kPa; flat plate span length in the two orthogonal directions is 7300 mm; square column dimension is 400 mm; slab thickness is 230 mm; effective depth, *d* is 194 mm; flexural reinforcement ratio is 0.8 %; concrete cylinder strength is 30 MPa; yield strength of flexural reinforcement is 400 MPa and yield strength of stud rail shear reinforcement is 330 MPa. Figures 2.14 (b) to 2.14 (e) show the arrangement of stud rail shear reinforcement for the design connection required by the above mentioned codes.

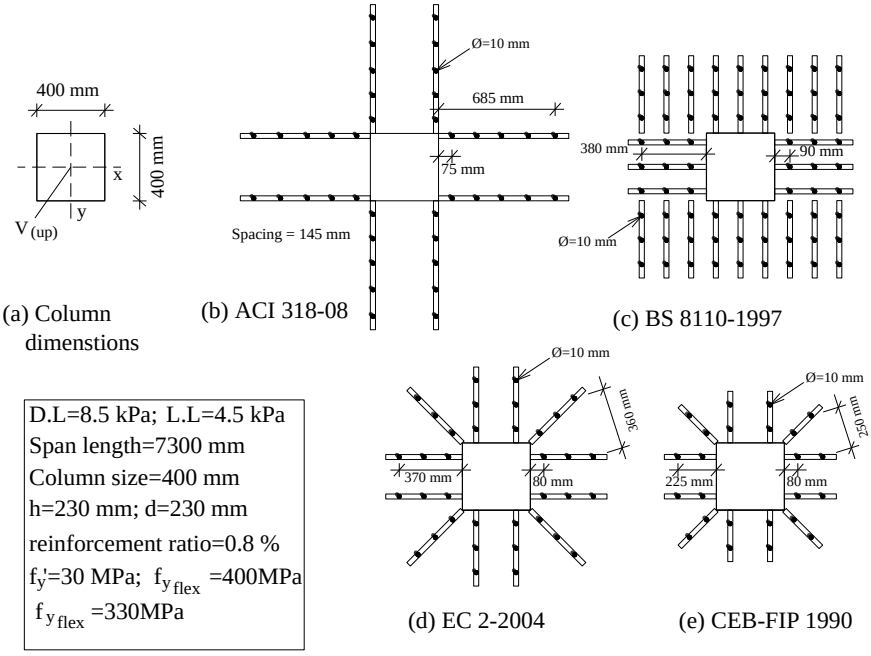

Figure 2.14: Design example.

As expected, the extension of shear reinforced zone is relatively small when the design is in accordance with CEB-FIP Model Code, Eurocode 2-2004 and BS 8110-1997.

2.3.3 *Finite Element Analysis*

Finite element simulations are increasingly becoming an important tool for the analysis and behaviour prediction of reinforced concrete structures. However, the work on numerical modelling punching shear in RC slab-column connections is limited. This section will deal with element types and constitutive material models.

2.3.3.1 Element Types

Studies utilising axisymmetric elements: Menetrey (1994), 3D continuum elements (bricks): Marzouk and Jiang (1996); Staller (2000); Beutel *et al*., (2000); Bhatt and Lim (2000) and shell elements: Marzouk and Chen (1993); Li (1997); Polak (1998a) and Ioannou (2001) are reported in the literature.

Axisymmetric Elements

Axisymmetric elements can only be used to simulate circular slabs with rotationally symmetric boundary conditions. However, slabs with orthogonal reinforcement which are generally used in practice can not be modelled easily using 2D axisymmetric elements.

Shell Elements

Due to the relatively small number of degrees of freedom per node of shell elements, the majority of researchers (e.g. Marzouk and Chen (1993), Li (1997), Polak (1998) and Ioannou (2001)) simulate flat slabs using layered shell elements. Shell elements are composed of a series of through-thickness layers, each assumed to be in the state of plane stress (Cervera *et al*., 1987). Since shear stresses are accounted elastically in shell elements and cracks are only calculated from plane stresses, simple shell elements, arranged in one plane, are not able to model shear failures. For this reason, Polak (1998) developed a shell element which is based on layered, degenerate shell elements incorporating a formulation for transverse shear. Marzouk and Chen (1994), Li (1997), Ioannou (2001) and Tian (2007) used shell elements from ABAQUS (ABAQUS User's Manual 2008), a general purpose FE software. Marzouk and Chen (1993) simulated high-strength flat slabs and their model did not show the ability to predict punching shear failure. Li (1997) reported convergence problems in his simulations of slabs with orthogonal reinforcement. Ioannou (2001) simulated slabs with and without holes and confirmed that the FE analysis with ABAQUS gives fairly accurate load-deflection curves and stiffness in both the pre and post cracking stages up to 75% of the ultimate load of solid slab (PSSG, Li (1997)). From the work available in the literature and the nature of the shell elements, it can be concluded that shell elements can be used to predict the overall deformational behaviour of flat slabs, but can not predict the punching shear failure.

Solid Elements

The inadequacies of shell elements reveal the importance of the use of 3-D solid elements (brick elements) for the simulation of punching shear in solid slabs. However, Polak (1998) argues that brick elements are not suitable for simulating structures as a whole since they introduce too many degrees of freedom and use too much computer space and time. There is limited work on simulating RC slabs with 3-D elements as reported in the state-of-the-art publication by CEB-FIP on "International Workshop on Punching Shear Capacity of RC Slabs" (Staller (2000), Beutel *et al*., (2000), Ožbolt *et al*., (2000)). The key to the successful use of solid elements for flat slabs is the existence of an appropriate constitutive material model that can deal well with shear.

2.3.3.2 Constitutive material models

To achieve an accurate prediction of the response of reinforced concrete structures, a reasonable material model is of importance that adequately reproduces the physical characteristics of the concrete response and produces reasonably good results (Marzouk and Chen, 1993). Although many constitutive material models have been developed over the last three decades (Cervenka *et al*., 2008), the analyses of reinforced concrete flat slabs has not improved much due to the lack of appropriate description of the concrete material properties (Gonzalez-Vidosa *et al*., 1987). The existing material models are classified in two categories: (1) micro models and (2) Macro models, such as plasticity, plasticity damage, continuum damage mechanics and microplane model (Ožbolt *et al*., 2000). In micro models the structure of the material is modelled at the micro level and the interaction between the micro components is described by means of relatively simple laws.

The fundamental disadvantages of the micro models is the enormous numerical effort required for analysis and being not readily available in FE programs such as ABAQUS. Plasticity and Plasticity damage models are available constitutive laws for concrete in the more advanced FE softwares (*e.g.* ABAQUS). A disadvantage of the plasticity-based approach compared to plasticity damage approach is that the stiffness degradation due to progressive damage is not modelled (ABAQUS Manual, 2008). However, the degradation of the elastic stiffness does not seem to cause major errors in simulating of slabs under monotonic loading (fib bulletin no. 12, 2001).

Damage zones (crack) can be modelled using the smeared crack approach or the discrete crack approach. In the discrete crack approach, the cracks are represented by fixed geometrical patterns. However, this method proved cumbersome and often required redefinition of mesh during the analysis (fib bulletin no. 12, 2001). In the smeared crack approach, the cracks are smeared over a continuum concrete element and are generated in a non-predefined direction, without the need of mesh redefinition. However, due to the strain softening nature of concrete, the results of smeared analysis may depend significantly of the mesh size (fib bulletin no.12, 2001).

In the case of highly non-linear systems which are sensitive to convergence problems, numerical solving algorithms should be used to establish a proper material model (ABAQUS User's Manual, 2008).

To summarize, it was shown that to have an accurate simulation in FE analysis, there is demand on properly (a) choosing the appropriate element to simulate the structure, (b) appropriate encoding of the material properties of the structure in the material model and (c) constructing a rigorous numerical algorithm for the iterative solution of the non-linear problem. In the following, a review on finite element applications on slabs without and with shear reinforcement is given.

2.3.3.3 Examples of FE analysis of slabs

Ožbolt, Vocke and Eligehausen (2000)

Ožbolt *et al*., (2000) used one experiment from Beutel *et al*., 2000 to make comparison with their FE analysis. They used non-linear finite element program, MASA, which was developed by Ozbolt, (1998) (cited by Ožbolt *et al*., 2000). The program was based on the microplane material model and a smeared crack approach. The microplane model describes the material behaviour on planes of various orientations within the material, in terms of uniaxial stress-strain relations in both the normal and shear directions (Ožbolt *et al*., 2000). To assure mesh independency of the results the constitutive law was related to the element size.

The slab was modelled with 8-noded solid elements and the steel reinforcement with discrete 2-noded bar elements connected to the concrete elements at the nodes. The steel was represented by uniaxial ideally elasto-plastic stress-strain relationship. The authors claimed that they obtained a numerical representation of the punching cone as shown in

Figure 2.15 (a) with a contour plot of the maximal principal strains. However, with regards to the load deformation of the slab along the length, shown in Figure 2.15(b), it can be concluded that the model is not representative of the kinematic status of shear deformations when the punching shear is happening. Figure 2.15 (b) indicates that the FE and experimental vertical displacement do not compare well.

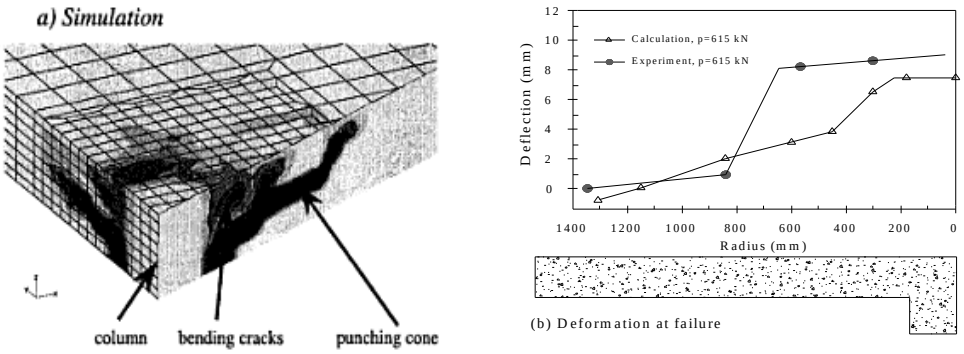

Figure 2.15: Numerical representation of punching surface (Ožbolt *et al*., 2000).

Figure 2.16 compares the load deflection curves from both analytical and experimental results which also confirm that the kinematics of failure were not simulated accurately. However, the authors concluded a good overall agreement between FE and test values for the load-deflection curve, with identical elastic stiffness and good approximation of the peak load as shown in Figure 2.16. The authors also reported that in the cracking stage, the FE response shows a higher stiffness. They also reported convergence problem in the post-peak load stage.

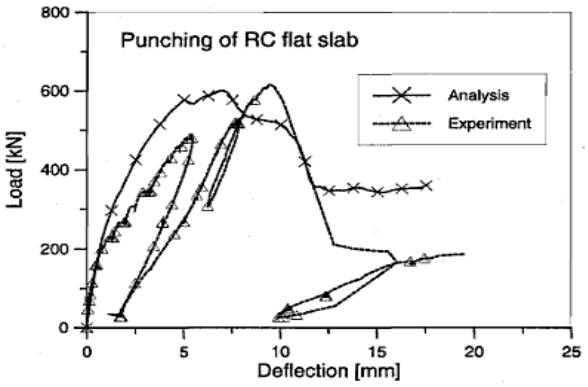

Figure 2.16: Numerical versus experimental load-deflection curves (Ožbolt *et al*., 2000).

Beutel, Schmidt & Landaure (2000)

Beutel *et al*., (2000) carried out numerical simulation of slab-column connections with shear reinforcement in order to define the optimum distance of the first row of shear reinforcement from the column face. The authors used two sets of experimental results from Beutel *et al*., (2000), one with a shear reinforcement ratio $\rho = 0.8\%$ (Slab P2-II) in which the failure occurs within the shear reinforcement, and one with a shear reinforcement ratio, $\rho = 1.75\%$ (Slab P6-I) where the failure took place at the column face.

The load-deflection curves from FE and experiments for both slabs are shown in Figure 2.18. In Figure 2.17 (a), the FE curve identifies with the test curve up to the service load and then it becomes stiffer reaching a peak load equal to 90% of the experimental failure load. The difference in peak loads in this slab was attributed to not including the dowel action in the FE simulation. The load-deflection curves for the slab with the greater ρ are shown in Figure 2.17 (b). The greater difference in peak load is similarly attributed to neglecting dowel action.

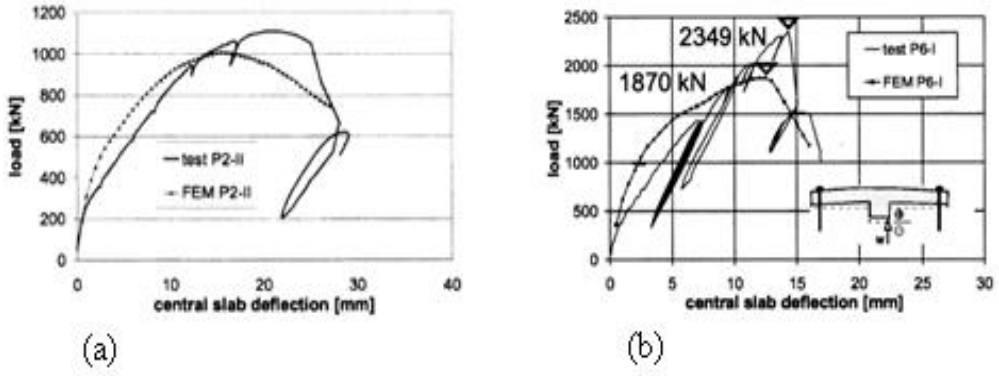

Figure 2.17: Simulation of a punching failure (a) Slab P2-II (b) Slab P6-I (Beutel *et al*., 2000).

2.3.3.4 Discussion of finite element analysis

Of the studies presented on the numerical modelling of slabs by different researchers, there has not been any model that performs completely satisfactorily. Since the punching shear mechanism of RC flat slabs is still not theoretically well understood, it is not suprising that there has been little success in numerically modelling of RC slabs. Furthermore, it is usually difficult to determine the values of material parameters used

in FE analyses prior to undertaking the finite element analysis. Therefore, FE analysis is capable of depicting the behaviour observed in any given experiment but is less successful in predicting the results of an experiment. On the other hand, FE analysis of RC slabs can help the understanding of the mechanism of punching shear failure as well as effects of different parameters such as concrete strength, reinforcement ratio, slab depth, and shear reinforcement on enhancing the shear strength.

Chapter 3

PUNCHING SHEAR DATABASE AND EVALUATION OF PUNCHING SHEAR DESIGN CODE PROVISIONS

3.1 Introduction

In this chapter, the author has constructed the biggest database using 549 punching shear experiments from literature. A detailed description of the database of punching shear tests without shear reinforcement is given. The distribution of data in the punching shear test database is briefly explained. The database is used to evaluate the predictions of existing shear design provisions. This is achieved by comparing the punching shear test results in the database with the failure punching shear strength predicted by the ACI 318-08, British standard (BS 8110: 1997), the CEB-FIP Model Code (MC 1991) and the Eurocode (EC 2-2004). The database is then used to assess the effect of parameters, such as top and bottom reinforcement ratios, column dimension, slab depth, concrete compressive strength and span to depth ratio, on the prediction of punching shear strength of slab-column connections.

3.2 Database on punching tests

The first report associated with punching shear strength was published by Talbot (1913) at the University of Illinois. Since then, a large number of experimental investigations in the field of the punching shear problem with different aims have been published all over the world. Gardner (1996) established a data bank of 142 tests published on punching shear of slabs. Later in 2001, the *fib* Bulletin 12 (2001) published 250 tests collected on slabs without shear reinforcement. The latest data bank was published by Hamada *et al*., (2008). The data bank comprised of 300 tests on slabs without shear reinforcement including the data from *fib* Bulletin 12, (2001) and more than 130 experiments which were carried out by Japanese researchers published in the Japanese language. However, Hamada *et al*., (2008) did not provide the full details in

his database. The author constructed a database that comprised of 549 experiments on slab-column connections.

To study experimentally, the load deformation behaviour of complete flat slab systems requires considerable expenditure. Therefore, most of experimental investigations reduce the complete slab system to an approximate system. The entire test specimens in the database are based on tests carried out on isolated slab-column connections.

3.2.1 Explanation to the database on slabs without shear reinforcement

The geometric properties of the RC slabs in the experimental database are shown in Figure 3.1. The material properties obtained for the slabs include concrete compressive strength ($f_c^{'}$) and yield strength of the flexural reinforcement (f_y).

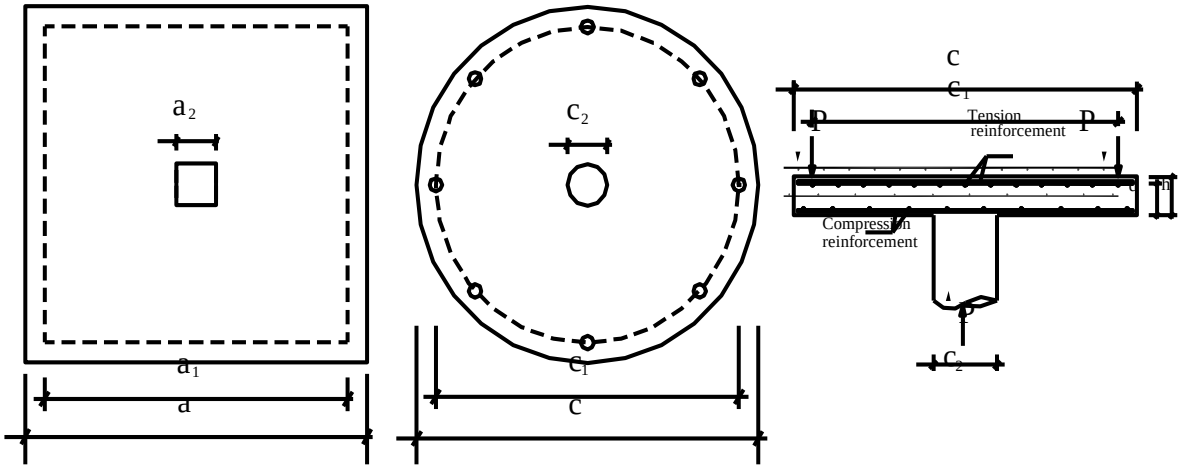

Figure 3.1: Geometric properties of slabs in experimental database.

To determine the concrete compressive strength, different control specimens are used in experiments from different parts of the world. To make comparison between different experiments and code equations, it is important to normalize strength values. Conversion factors used in this database are taken from *fib* Bulletin 12 (2001) and are summarised in Table 3.1.

Table 3.1: Conversion factors of concrete compressive strength of different control specimens

Specimen type and size, mm	Relation	Specimen type and size, mm
Cylinder $\Phi 150 \times H300$	$f'_{c,cyl,150,300} = 1.05 f'_{c,cyl,100,300}$	Cylinder $\Phi 100 \times H300$
Cube 150×150	$f'_{c,cube,150} = 0.90 f'_{c,cyl,100}$	Cube 100×100
Cylinder $\Phi 150 \times H300$	$f'_{c,cyl,150,300} = 0.8 f'_{c,cube,150}$	Cube 150×150

The distribution of the properties of slabs without shear reinforcement is shown in Figure 3.2. Details including geometry, material strength, boundary conditions and failure loads of all slab specimens in the database are given in Appendix A.

It can be observed from Figure 3.2 that the distribution of slab depth is poor since there are few tests for thicker slabs. Only less than 4% of the experiments belong to slab depths more than 250 mm. The same applies to concrete strength. Only 17% of the experiments belong to higher concrete strengths ($f'_c > 51$ MPa). 24% of the experiments belong to the slabs with flexural reinforcement higher that 1.5% ratio. The bias of shear parameters suggests the need for further experimental investigations especially for thicker slabs ($h > 250$ mm), higher concrete strength ($f'_c > 51$ MPa) and slabs with higher flexural reinforcement ratios. Poor distribution of shear parameters of the experimental database can make the predictions obtained from empirical equations poor, especially if certain categories of slab specimens are either deficient or unavailable, for developing the empirical equation.

Experimental tests of RC slabs are becoming more challenging with the increase in costs and laboratory constraints of such RC slabs. On the other hand, in order to further understand the behaviour of such members, until more test data are available, sophisticated statistical approaches (e.g. ANN) along with analytical approaches such as Finite Element Analysis can serve as useful tool.

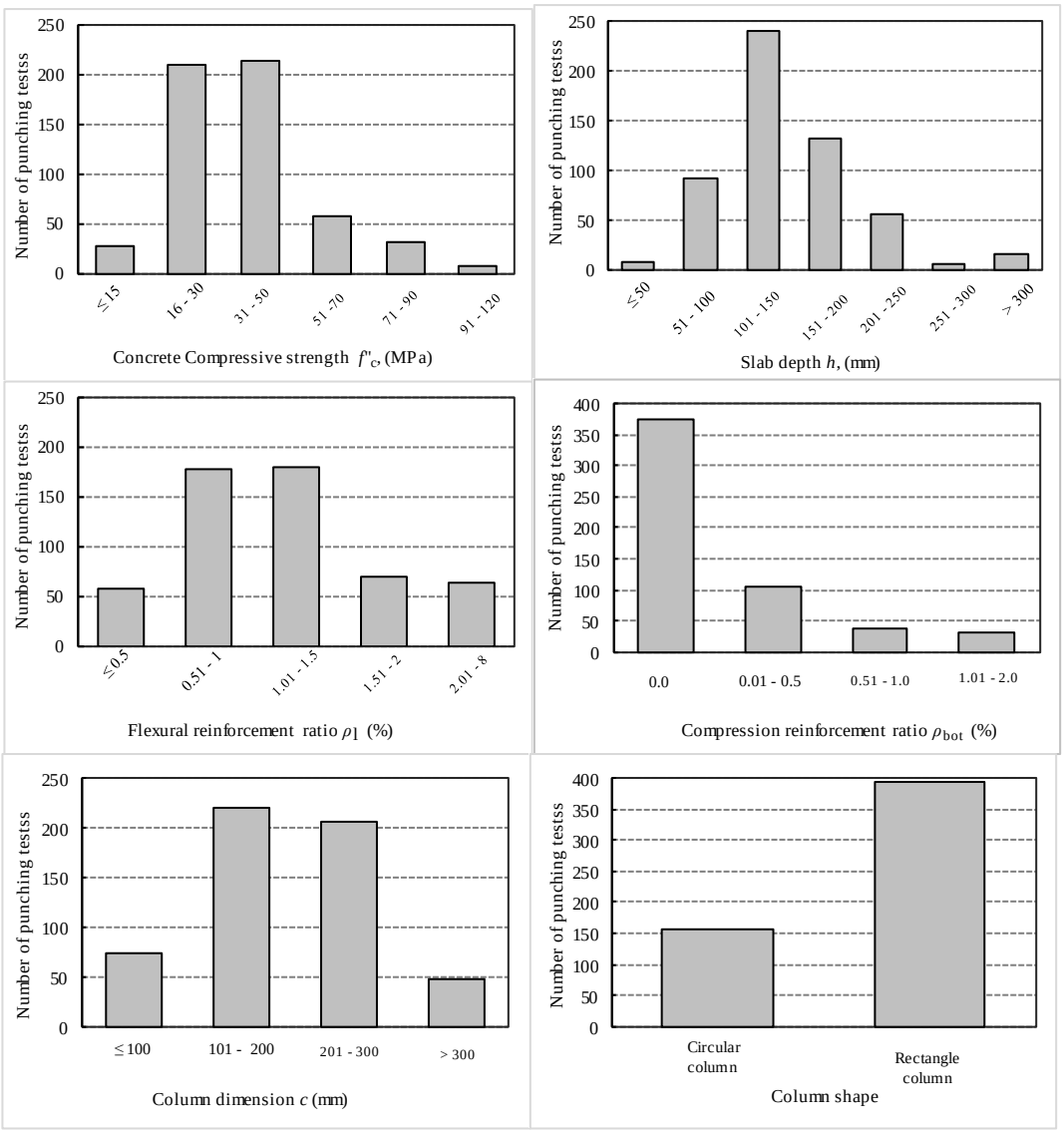

Figure 3.2: Distribution of the data of punching tests without shear reinforcement in database.

A total of 680 slab-column connections without shear reinforcement were collected initially by the author however, another 131 experiments which do not fulfil the following three criteria were disregarded for further evaluation.

- Membrane action: A lot of tests have demonstrated that the membrane action influences the punching shear capacity and ductility of slabs. Therefore experiments on these types of slabs are excluded. It has to be noted that the membrane action is not considered in this thesis.

- Bond failure: Tests that failed due to bond are excluded from database. Due to insufficient data provided on the detailing of flexural reinforcement, provisions of strain gauges and boundary condition of tests specimens, bond failures at end supports could only be established by reading the reports. For example, bond failure of 12 experiments of Gardner (1990) are reported.

- Influence of the shear slenderness: Tests with slenderness less than 2.5 are excluded from the database. The database contains tests with shear slenderness (a/d) between 1.40 and 24. The shear slenderness is the ratio of a/d where a is the radial distance from the column face to the bearing points and d is the effective depth. It is known that the shear resisting capacity is influenced by the shear slenderness and the codes of practice account for slenderness in beams. Tests carried out on slabs with different slenderness ratios by Lovorovich and McLean (1990) are shown in Figure 3.3. It can be seen that there is a sharp increase in strength of the connection when the slab to depth ratio decreases below 2.5.

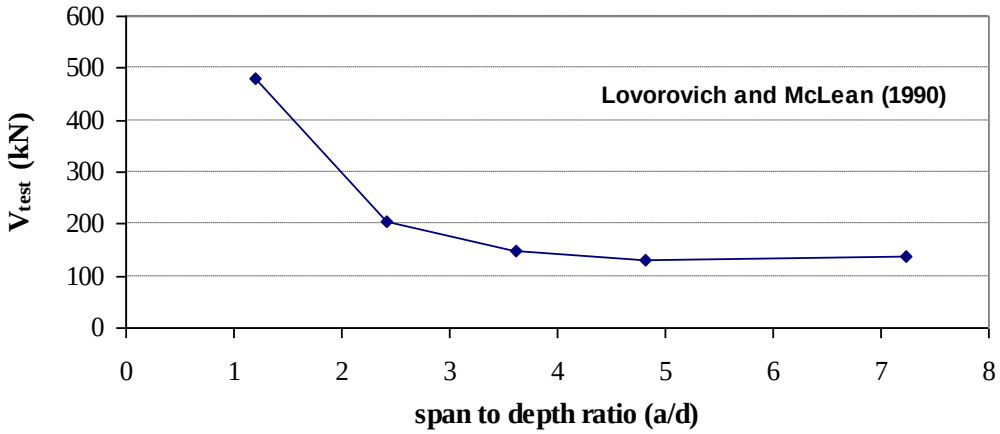

Figure 3.3: Punching shear strength versus span to depth ratios.

3.3 Procedure for evaluating code equations

The strength reduction factors and material strength factors are set to be equal to 1 when the code equations were used to predict the failure load in experiments in the database. The mean, Standard Deviation (SD) and Coefficient of Variation (COV) of the ratio V_{test}/V_{calc} is used to examine the accuracy of the code provisions. Besides, the proposed classification system by Collins (2001) is used to examine the distribution of V_{test}/V_{calc}

(see Table 3.2). Classification system for distribution of V_{test}/V_{calc} (adopted from Collins, 2001) are summarised in Table 3.2.

Table 3.2: Classification system for distribution of V_{test}/V_{calc} (adopted from Collins, 2001)

V_{test}/V_{calc}	Classification
< 0.5	Extremely dangerous
0.5 – 0.65	Dangerous
0.65-0.85	Low safety
0.85-1.30	Approximately safe
1.30-2.00	Conservative
>2.00	Extremely Conservative

The performance (i.e. V_{test}/V_{calc}) of the code provisions are assessed in two stages. First, the comparison is carried out for all the slabs in the database which consists of 549 slabs without shear reinforcement. Second, the comparison was carried out on different subsets created from the database. This was necessary to reduce the influence of the bias of shear parameters observed in the database. It also allowed the deficiencies of each code equation to be characterised. In addition, the distribution of the performance of each code provision is also examined.

3.4 Evaluation of the performance of code provisions

Table 3.3 summarises the experimental punching load and the calculated punching load (V_{test}/V_{calc}) in terms of mean value, standard deviation (SD) and the coefficient of variation (COV) for comparison using Code equations of ACI 318-08, EC 2-2004, CEB-FIP 90 and BS 8110.

Table 3.3: Summary of the experimental punching load and the calculated punching load (V_{test}/V_{calc})

Code	ACI 318-08	EC 2-2004	CEB- FIP 1990	BS 8110, 1997
RC slabs without shear reinforcement				
Mean	1.35	1.34	1.33	1.18
SD	0.49	0.43	0.44	0.34
COV	0.36	0.32	0.33	0.28

The following observations can be made from and examination of the data in Table 3.3.

- The ACI 318-08 shear design provision gave the poorest prediction for members without shear reinforcement with a mean and COV of 1.35 and 0.36 respectively. This is due to the fact that ACI 318-08 is dependent only on concrete strength and ignores the influence of other shear parameters such as reinforcement ratio and effective depth. Better predictions obtained from BS 8110- 1997, EC 2-2004 and CEB FIP MC (1991) take the influence of flexural reinforcement ratio and the effective depth into account along with the concrete strength.
- It was observed that the BS 8110 has the lowest mean for the ratio of V_{test}/V_{calc}. A detail investigation on the distribution of V_{test}/V_{calc} reveals that most of the RC slabs had V_{test}/V_{calc} bigger than 1.00 (see Figure 3.7). This is due to the fact that BS 8110 limits the concrete compressive strength to 40 MPa.

3.4.1 ACI 318-08

The predictions obtained from ACI 318-08 are shown in Figure 3.4 and 3.5. As it is discussed earlier in the chapter, members without shear reinforcement exhibit large scatters and this is also shown in Figure 3.4.

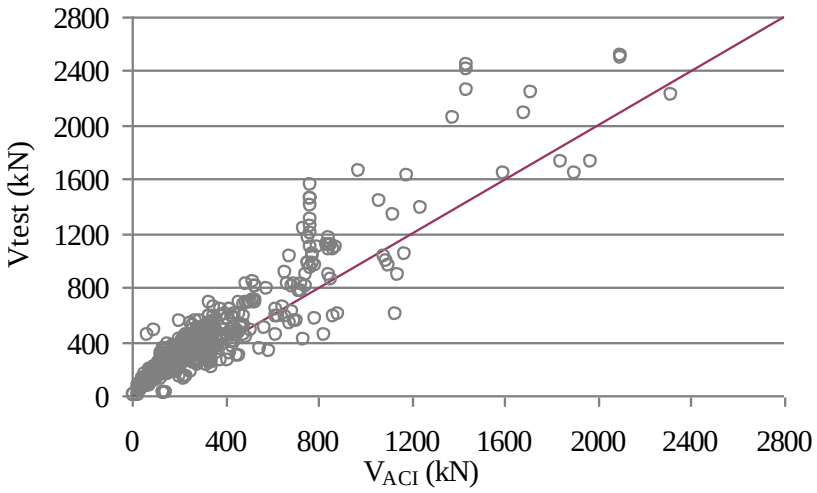

Figure 3.4: Comparison of ACI 318-08 procedures with empirical tests for slabs without shear reinforcement.

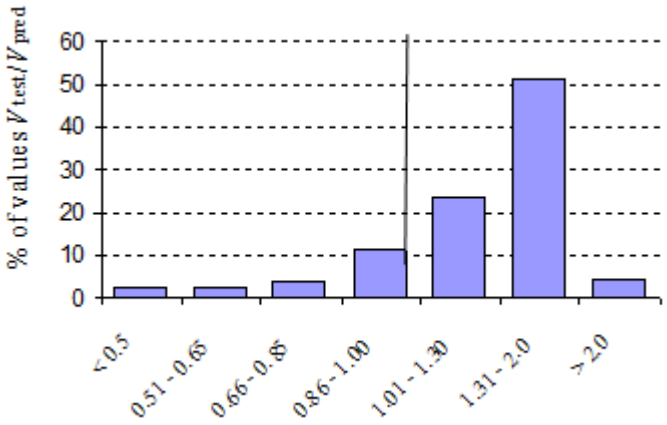

Figure 3.5: Distribution of strength ratio for ACI 318-08 for slabs without shear reinforcement.

Studies on the distribution of strength ratios V_{test}/V_{pred} show that large scatter is also evident for members without shear reinforcement. Over 50% of the predictions obtained from the ACI 318-08 design procedure had strength ratios V_{test}/V_{pred} between 1.31 to 2.00 for members without shear reinforcement. These are considered to be conservative according to Collins classification criteria (see Table 3.2). However, ACI 318-08 can make extremely dangerous predictions for members without shear reinforcement (*i.e.* $V_{test}/V_{pred} < 0.5$ - see Figure 3.5). Nearly 20% of the predictions of ACI 318-08 procedure had strength ratio V_{test}/V_{pred} less than one for members without shear reinforcement.

3.4.2 BS8110-1997

The predictions obtained from the BS 8110 and the empirical test results are shown in Figure 3.6 for comparison. The distribution of the strength ratios is shown in Figure 3.7.

Over 55 % of the predictions obtained from BS8110 design procedure for slabs without shear reinforcement are categorized in approximately safety according to Collins classification criteria. Less than 35 % of the predictions had strength ratios V_{test}/V_{pred} in the range of 1.31 to 2.00 which are categorized as conservative according to Collins classification criteria.

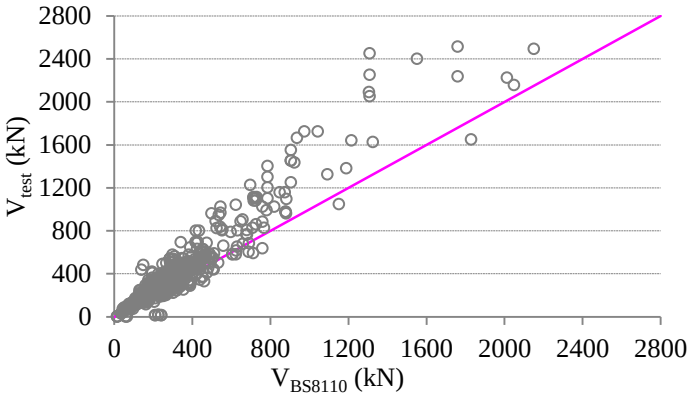

Figure 3.6: Comparison of BS 8110 procedures with empirical tests for slabs without shear reinforcement.

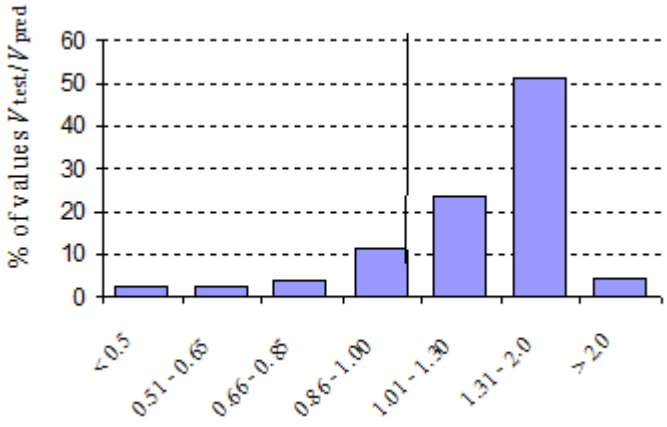

Figure 3.7: Distribution of strength ratio for BS 8110 for slabs without shear reinforcement.

3.4.3 EC 2-2004

Figure 3.8 and 3.9 show the predictions obtained from EC2-2004. It has been pointed out earlier in this chapter that there is a very large scatter for members without shear reinforcement as shown in Figure 3.8. Above 45% of the predictions from EC 2 provide strength ratios V_{test}/V_{pred} in the range of 1.30 to 2.0 which is categorized as conservative according to Collins criteria. 40% of the predictions from EC 2 provide strength ratios V_{test}/V_{pred} in the range of 0.85 to 1.30 which is categorized as appropriate safety according to Collins criteria. EC 2-2004 can produce extremely conservative predictions since V_{test}/V_{pred} >2.0.

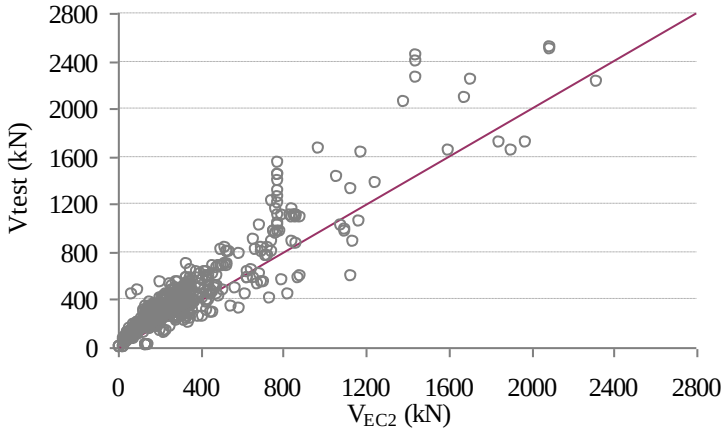

Figure 3.8: Comparison of EC2-2004 procedures with empirical tests for slabs without shear reinforcement.

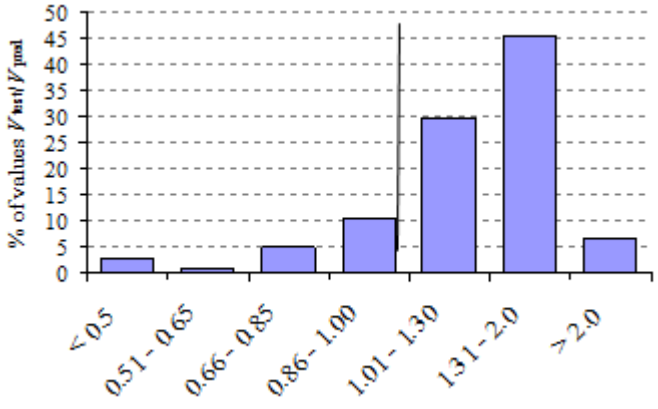

Figure 3.9: Distribution of strength ratio for EC2-2004 for slabs without shear reinforcement.

3.4.4 FIP CEB Model Code

The comparison of CEB FIP model code procedures with empirical tests and the distribution of strength ratio for CEB FIP model code for slabs without shear reinforcement are shown in Figure 3.10 and Figure 3.11 respectively.

The difference in the predictions obtained using CEB FIP model code and EC 2-2004 is overall not very significant. ACI 318-08, however, produces less conservative predictions and reduced scatter for members without shear reinforcement (see Figures 3.4 and 3.5). The predictions by CEB FIP model code and EC 2-2004 can be extremely dangerous as well as exceptionally conservative.

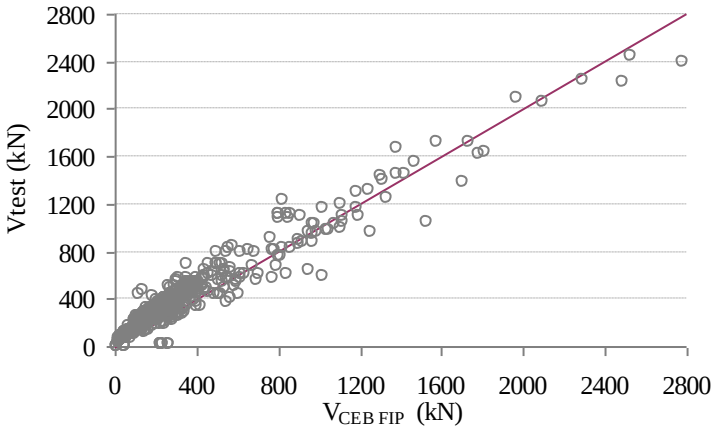

Figure 3.10: Comparison of CEB FIP model code procedures with empirical tests for slabs without shear reinforcement.

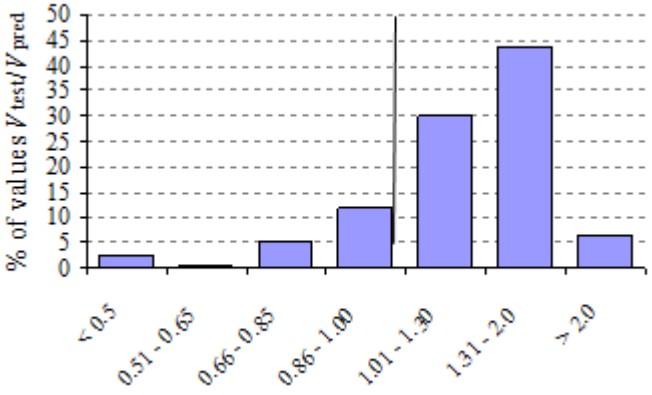

Figure 3.11: Distribution of strength ratio for CEB FIP model code for slabs without shear reinforcement.

3.4.5 Concluding remarks

A database constructed using published punching shear test results was used in the assessment of the code provisions for the predictions of the punching shear capacity. The majority of previous research has focused on testing slabs that are less than 200 mm deep, members that have rectangular column-sections, members that are simply supported, and members that are moderately reinforced in flexure. However, in practice, slabs designed to the codes are usually large, non-rectangular, continuous and lightly reinforced.

A comparison of the predictions from the code provisions does not sufficiently correlate with the experimental test results for the majority of the members, which are not well represented in the experimental database. This is to be expected as these code provisions rely on empirical expressions that were calibrated on test data that did not contain a significant number of slabs with low flexural reinforcement ratios. Using the variations in the means and the values of the COVs, the punching shear design provisions of BS 8110-1997 provide the most accurate and consistent predictions of capacity. A significant drawback however of the BS 8110 approach is that the equation limits the use of concrete compressive strength up to 40 MPa.

3.5 Parameters affecting the punching shear strength of connection

It has to be emphasised that the large number of interrelated variables present in the reported experiments makes the isolation of individual parameters very challenging. It is particularly very difficult to eliminate the effect of other parameters when the influence of one specific variable is of concern. In fact, the influence of major variables such as column dimension, concrete strength, slabs thickness and flexural reinforcement ratio are still not accurately understood.

For instance, when the reinforcement ratio is kept constant whilst the slab thickness is increased, flexural capacity is decreased considerably. Factors such as test set-up, quality control and test equipment influence the test results and are very difficult to account for. Test set-up can result in rotational and lateral restraints of varying degrees at their supports. It is crucial to focus on particular test results that have the same experimental configuration and the same test equipment to avoid uncontrollable variables.

3.5.1 Effect of bottom reinforcement on the punching shear strength

Existing mechanical models and design standards generally ignore the shear force carried by bottom reinforcement in compression. Based on experimental tests conducted by Elstner and Hognestad (1956), it was concluded that "the ultimate shearing capacity is not dependent upon the compressive reinforcement". This conclusion was derived based on the experimental tests with tensile reinforcement ratios larger than 2% that failed in shear. However this statement cannot be applied to lightly reinforced slabs. Experimental results of eight specimens reported in Manterola (1966) (cited by CEB FIP Bulletin No. 12), Binici and Bayrak (2003), Yamada *et al*., (1992) and Tomaszevicz (1993) (cited by CEB FIP Bulletin No. 12) are summarised in Table 3.4 together with the geometrical and material properties for evaluation.

Table 3.4: Contribution of compression flexural reinforcement on punching shear strength

	Slab thickness (mm)	d (mm)	c (mm)	f_c' (MPa)	ρ_{Top} (%)	ρf_y (MPa)	ρ_{Bot} (%)	Dim. of slab (mm)	V_u (kN)	$\frac{V_u}{\sqrt{\rho f_y f_c'}}$
P2-S1	125	107	250	33.8	1.04	3.16	0	3250	257	24.87
P2-S2	125	107	250	33.1	1.04	3.37	0.52	3250	283	26.80
Control 1	152	114	304	28.3	1.76	7.89	0	2133	404	27.04
Control 2	152	114	304	28.3	1.76	7.89	0.12	2133	510	34.13
T1	200	160	300	21.58	1.23	9.97	0.62	2000	441	30.07
K1	200	156	300	26	1.53	8.7	1.53	2000	658	43.75
ND95-2-1	240	200	150	88	1.7	8.5	0	2600	1100	40.21
ND95-2-1D	240	200	150	86.5	1.7	8.5	0.9	2600	1300	47.94

The specimens P2-S1 and P2-S2, by Manterola (1966) show that the strength of the connection is increased up to 11% when the compressive mat of slab reinforcement is provided. However, the bottom reinforcement provided in Slab Control 2 in Binici *et al*., (2003) is placed only within the column width and showed 26% increase in punching strength of the connection when compared to Slab Control 1 where bottom compression reinforcement is not used at all. The percentage of flexural reinforcement and concrete compressive strength was slightly different in Slab T1 when compared to Slab K1 (Yamada *et al*., 1992). To eliminate the effect of material strength on specimen capacity, the test results were evaluated using the ratio of V_u to $\sqrt{\rho f_y f_c'}$. From the normalised strength of the connection shown in the last column of Table 3.4, it is concluded that the increase in the compressive reinforcement resulted in an increase in the strength of the connection by 44%. The normalised strength for specimens, ND95-2-1 and ND95-2-1D from Tomaszevicz, also resulted in an increase in the strength of the connection by 20%.

3.5.2 Effects of Span to depth ratio on the punching shear strength

Lovorovich and McLean (1990) investigated the punching shear strength of reinforced slab-column connections with varying span to depth ratios. They conducted five experiments on slab-column connections where flexural reinforcement, concrete compressive strength and column dimension were kept the same but spans width varied each time. The experimental results showed a dramatic increase in strength of the connection when the span to depth ratio decrease below 4.

It can also be concluded from the Figure 3.12 that the punching shear strength was significantly increased as the span to depth ratio decreased below 4. Figure 3.12 also indicates that the code equations (ACI 318-05, Eurocode 2 (2004) and BS 8110 (1997)) underestimate the strength of the connections as the span to depth ratio decrease below 4. Lovorovich and McLean (1990) concluded that the strength increase could be due to the development of arch mechanism in slabs and in-plane compressive forces resulting from friction at the support.

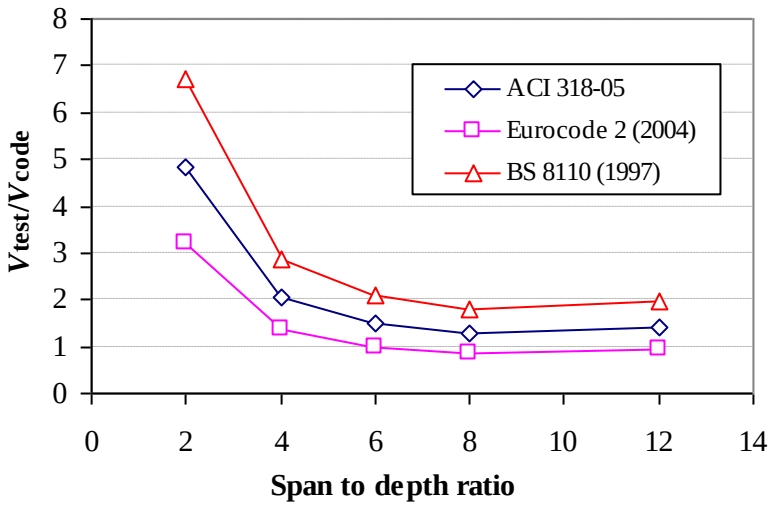

Figure 3.12: Normalised punching shear strength versus span to depth ratio.

3.5.3 Size effect on the punching shear strength

Although the effect of the slab thickness on the punching shear resistance had been recognised as early as 1938 by Graf (cited by Birkle and Dilger, 2008), it is difficult to carry out experiments only on the size effect. Most experimental studies in the literature, not only varied in slab thickness but also in concrete compressive strength, flexural reinforcement and column size. Keeping the reinforcement ratio constant while increasing the slab thickness, leads to a decrease in the reinforcement ratio. Thus using low reinforcement ratio leads to a lower flexural capacity in the connection. Slabs with lower flexural capacity have more flexural cracks which lead in reducing the punching shear capacity. Experiments with small slab size also affect the punching shear capacity by means of yielding the flexural reinforcement or bond failure in flexural reinforcement (Mitchell *et al*., 2005).

Richart (1948) carried out experiments on punching behaviour of column footings and concluded that shear stress at failure is decreased as the effective depth is increased in the testing foots. Guandalini *et al*., (2009) conducted experiments of low reinforcement ratio slabs with different thicknesses of specimens. The overall slab thicknesses, *h*, used in the experiments were 125 mm, 250 mm and 500 mm. To eliminate the effect of low span to depth ratio (discussed in 3.5.2) longer spans were used with higher thicknesses of the slabs. Li (2000) reported 6 experiments on slab-column connections with different slab thicknesses. The overall thickness, *h*, of the slabs varied from 135 mm to

550 mm. Since the spans length of the slabs were kept constant in Li's experiments (lower span to depth ratio for thick slabs), only limited conclusions can be made for size effect. Figure 3.13 shows the variation of normalised shear stress versus slab effective depth for experiments conducted by Li (2000), Birkle and Dilger, (2008) and Guandalini *et al.* (2009). The results re-plotted in Figure 3.13 indicate that increase in the slab thickness has resulted in a decrease in shear stress of the connection.

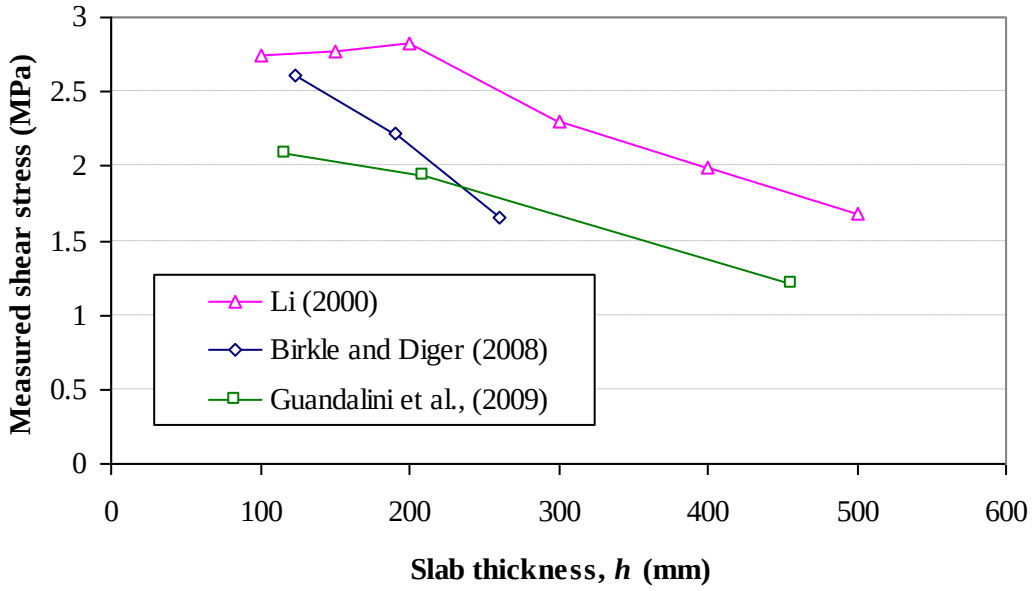

Figure 3.13: Normalised punching shear stress ($V_u / b_o d$) versus slab thickness by Li (2000), Birkle and Dilger, (2008) and Guandalini *et al*., (2009).

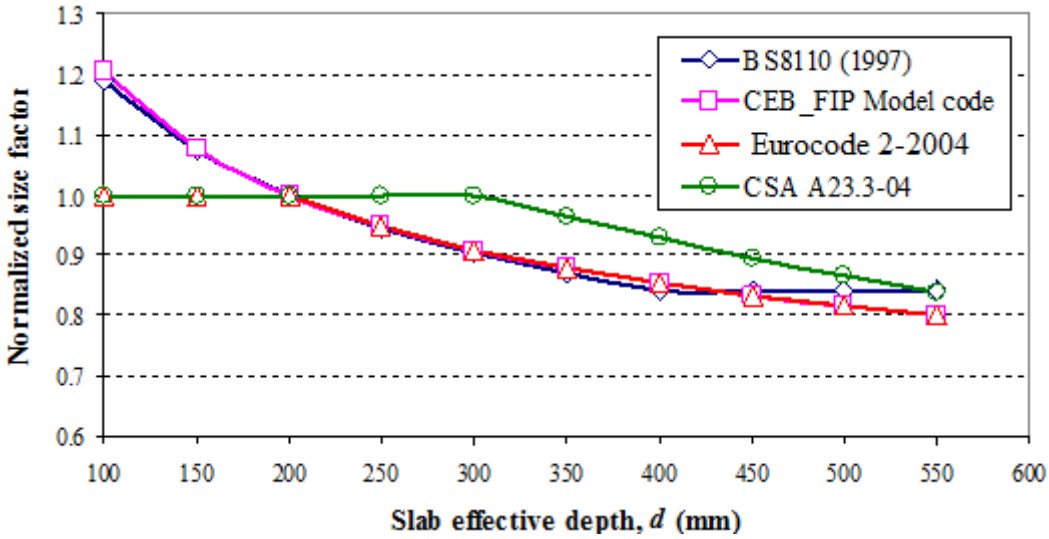

Figure 3.14: Size effect factors normalised to an average effective depth of 200 mm.

Apart from ACI 318-08, all other codes such as Eurocode 2 (2004), BS 8110 (1997), CSA A23.3-04 and CEB FIP model code (1990) take the size effect into account when calculating the punching shear capacity of the connections (as discussed in Chapter 2). Figure 3.14 compares the different size effect expressions using the Code Equations in Eurocode 2 (2004), BS 8110 (1997), CSA A23.3-04 and CEB FIP model code (1990). The size effect factors were normalized to an average effective depth of 200 mm to give a value of 1 when the effective depth is 200 mm. BS 8110 (1997) has a size effect factor that does not decrease beyond an average effective depth of 400 mm. The CSA A23.3-04 gives an expression for slabs with effective depth factor greater than 300 mm. Eurocode 2 (2004) has a size effect factor that does not decrease beyond an effective slab depth of 200 mm; however, only CEB-FIP Model code 1990 expression for size effect factor increases when the effective depth is less than 200 mm.

3.5.4 Effect of column size and shape on the punching shear strength

There are two different sets of experiments on the effects of column dimension on strength of connections: Slabs with square columns (aspect ratio, β=1) and slabs with rectangular columns ($\beta \neq 1$). Aspect ratio, β, is the ratio of the larger to the smaller column dimension. Marzouk and Hussein (1991): specimens HS14 and HS 15l; Corley and Hawkins (1968) cited by CEB FIP Bulletin No.12: specimens AN1 and AN2, Manterola (1966) cited by CEB FIP Bulletin No.12: specimens P1-S4, P2-S4 and P3-S4 and Lander *et al*., (1977) cited by CEB FIP Bulletin No.12: specimens DA6, DA&, DA10 and DA11 are reviewed here to examine the effect of square columns dimension on the punching capacity of the connection while all other parameters were kept constant. Figure 3.15 shows the variation of measured punching capacity versus square column dimensions. The results presented in Figure 3.15 demonstrate that the punching shear resistance of slabs are influenced by the size of the supports.

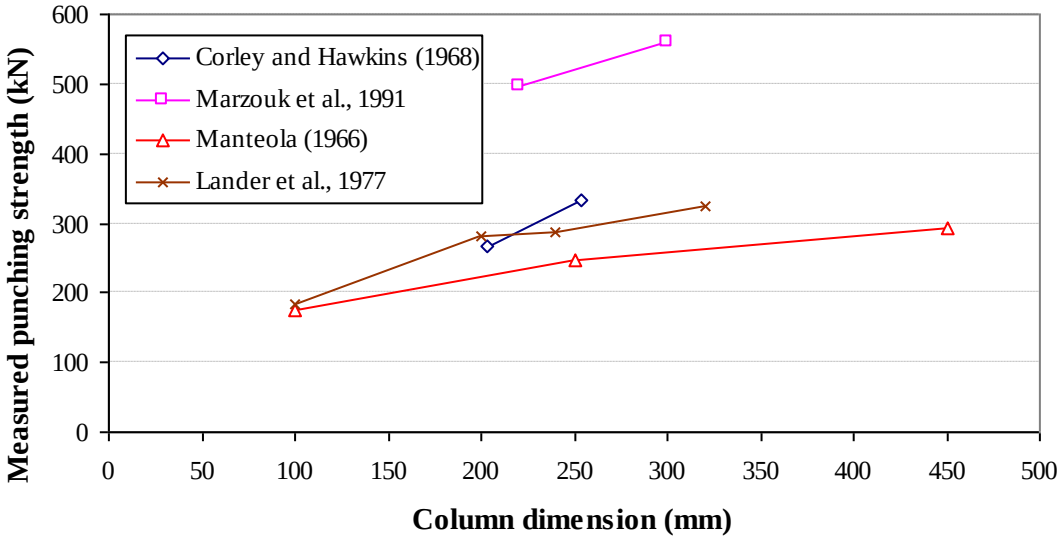

Figure 3.15: Punching shear strength versus square column dimension.

The first series of experiments on slab-column connections with rectangular columns was reported by Corley and Hawkins in 1968 (cited by CEB FIP Bulletin No. 12). These experiments were the base to introduce the aspect ratio to the ACI punching shear equation (Eq. 2.15). However ACI 318-08 indicates that when the aspect ratio is over 2, shear stress predictions by ACI is unconservative. "The actual shear stress on the critical section at punching shear failure varies from a maximum of about $0.33\sqrt{f_c'}$ around the corners of the column or loaded area, down to $0.166\sqrt{f_c'}$ or less along the long sides between the two end sections" (ACI 318-08).

Experimental data in Hawkins *et al*., (1971), Mahmood (1978) and Oliviera *et al*., (2004) are re-plotted in Figure 3.16 in order to examine the effects of column aspect ratio on the shear stress (v_u) of the connections. Three specimens from Hawkins *et al*., (1971): Slabs 7, 8 and 9; eight specimens from Mahmood (1978): Slabs L42 and L41 with thickness of 130 mm and Slabs L42a, L45, L46, L41a, L43 and L44 with thickness of 164 mm and three specimens from Oliviera *et al*., (2004): Slabs L3c, L4c and L5c (all cited in Oliviera *et al*., 2004) were used in Figure 3.16. Hawkins suggested an aspect ratio in the range of 2 to 4.5, while this was varied from 1.67 to 4 in the experiments reported in Mahmood (1978). Oliviera *et al*., (2004) used columns 120 mm wide and 120, 240, 360, 480 and 600 mm long. It can generally be concluded that the

increase in the aspect ratio of columns resulted in a decrease in the shear stress of the connection and this is also shown in Figure 3.16.

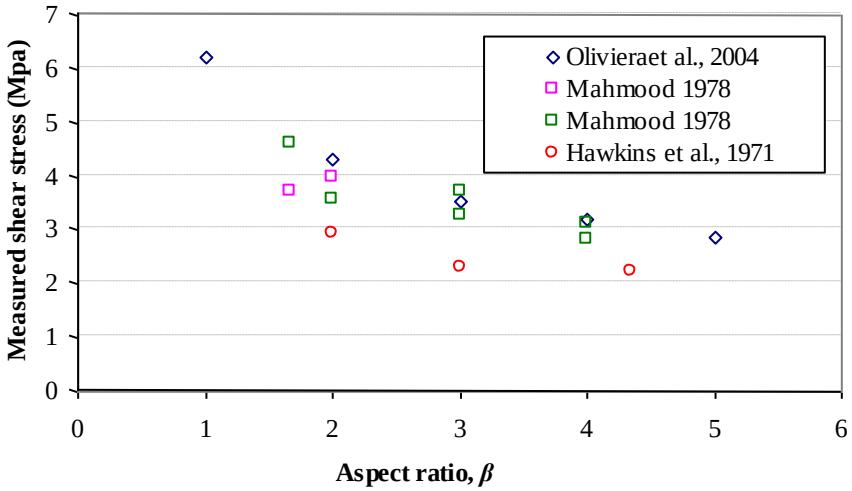

Figure 3.16: Punching shear strength versus aspect ratio.

Although the effect of column size and shape were ignored in most of the code equations (BS 8110, 1997; Eurocode 2, 2004; CEB FIP Model code 1990, 1991) the influence of column size is somehow accounted by comparing the shear stress along the critical sections. For instance, the critical section is located at a distance of $0.5d_{avg}$, $1.5d_{avg}$ and $2.0d_{avg}$ from the column face for ACI 318-08, BS 8110 (1997) and Eurocode 2 (2004) respectively.

3.5.5 Effect of flexural reinforcement on punching shear strength

The effect of flexural reinforcement ratio on the assessment of the punching shear resistance of slab-column connections was recognised since 1950. However, based on the available experimental data in the literature, it is difficult to assess the influence of flexural reinforcement only while the influence of other parameters had to be ignored.

On the other hand, experiments from Marzouk and Hussein (1991), Alexander and Simmonds (1992), Elstner and Hognestad (1956) and Guandalini *et al.*, (2009) studied the effects of flexural reinforcement ratio on the shear capacity more precisely and are chosen to be re-viewed in this section. In these experiments, apart from the slab flexural reinforcement ratio, all other parameters were kept the same. These results are summarised in Figure 3.17.

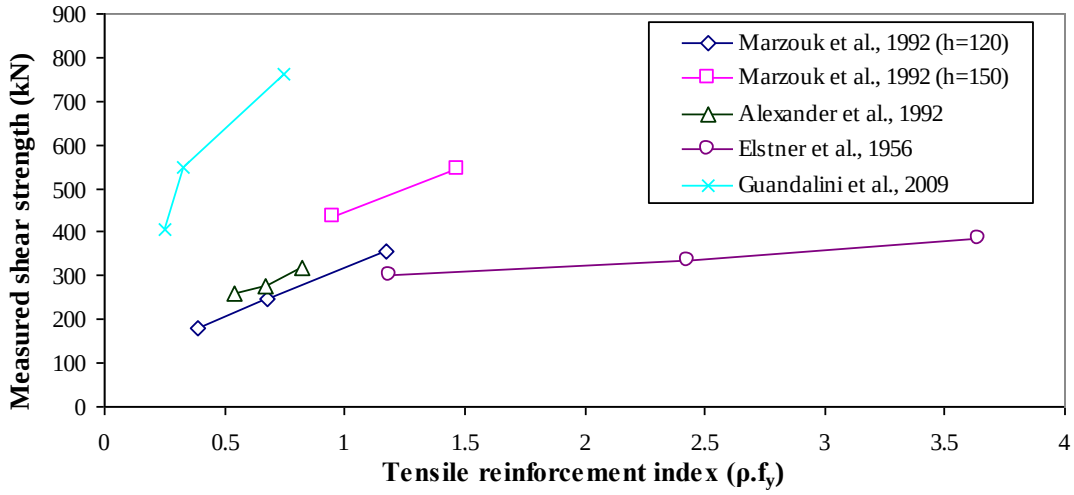

Figure 3.17: Measured shear strength versus $\rho.f_y$.

Figure 3.17 consists of experiments on slabs with two different depths (h = 120 mm and h = 150 mm) of Marzouk and Hussein (1991), three experiments out of six from Alexander and Simmonds (1992) with the slab thickness of 155 mm and the concrete compressive strength was 26 MPa, three experiments from Elstner and Hognestad (1956) with specimen's slab thicknesses of 152 mm and a very low concrete compressive strength and three specimens with slab thicknesses of 250 mm by Guandalini *et al*., (2009).

The measured shear strength versus tensile reinforcement index ($\rho.f_y$) shown in Figure 3.17 indicates that the tensile reinforce index increases with an increase in the shear strength of the connection.

There are two methods of spacing the flexural reinforcement on slabs in construction: Uniform spacing in the slab width and concentration of flexural reinforcement in the column region. Both spacings are allowed in codes. Moe (1961) conducted series of experiments while the flexural reinforcement was concentrated in column regions and the percentage of reinforcement was kept constant. Moe concluded that the concentration of flexural reinforcement in a narrow width in the column region does not increase the shear strength of the connection. However, the flexural rigidity of slab was increased. The same conclusion was achieved by Regan (1986) where experiments were conducted on slabs with concentrated reinforcement in the column region. Dilger *et al*., (2005) stated that Hawkins *et al*., (1974) reported the same conclusion that the

concentration of flexural reinforcement increases the load to yield the flexural reinforcement and consequently results in maximum crack width to decrease for the given load.

ACI 318-08 requires that a band width of $c+3h$ (a slab width extending a distance of 1.5 times the slab thickness on either side of column) could be designed to resist the negative moment. However Regan (1986) suggested extending the effective width 3 times the slab thickness from the face of the column. FEMA 356 also suggested that the effective width should be considered as 5 times the slab thickness from the column face.

3.5.6 Effect of concrete strength on punching shear strength

The shear stresses reported in the experiments on punching shear strengths in the literature and the ACI code for different concrete compressive strengths are compared in Figure 3.18. The results shown in Figure 3.18 are slightly spread out. This is mainly because of the other parameters that affect the shear capacity. Slabs that failed in flexure also contributed in the scatter.

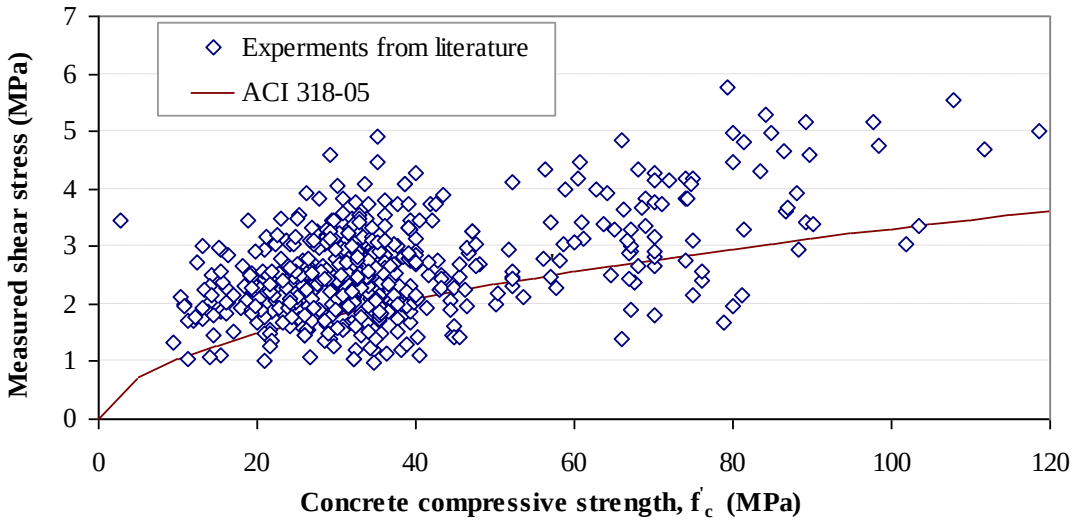

Figure 3.18: Influence of concrete strength on shear strength.

Ramadan in 1996 (cited by Theodorakopolus and Swamy 2003) conducted experiments on the slab-column connections to assess the effect of compressive concrete strength on the capacity of the connection. Although the reinforcement ratio and concrete strength varied in these experiments, the specimen thickness was constant to 125 mm. Out of 9

specimens re-examined here, 5 of the specimens had 0.58% flexural reinforcement while other four specimens had 1.28%. Experiments from Regan (1986) were also chosen to investigate the concrete strength on shear capacity. Three specimens with a thickness of 80 mm and a flexural reinforcement of 0.98% are reviewed. Six other slabs with a thickness of 120 mm were chosen where they split into 2 groups (Group 1 with a flexural reinforcement of 0.83% and Group 2 with a flexural reinforcement of 1.52%). These experiments are used to calculate the shear stress at failure, based on the ACI 318-08 critical shear periphery and re-plotted in Figure 3.19. Figure 3.19 re-plots the values of shear stresses versus the concrete stresses values of the experiments and compares this with ACI 318-08. The results illustrate the calculated shear stress values of experiments together with the shear stress values obtained from the ACI 318-08 based on the concrete strength for four different power of $\left(f_c^{'}\right)^n$, when n=1/4, n=1/3, n=1/2 and n=2/3. It is clear from Figure 3.19 that the overall trend is reasonably represented by n=1/4.

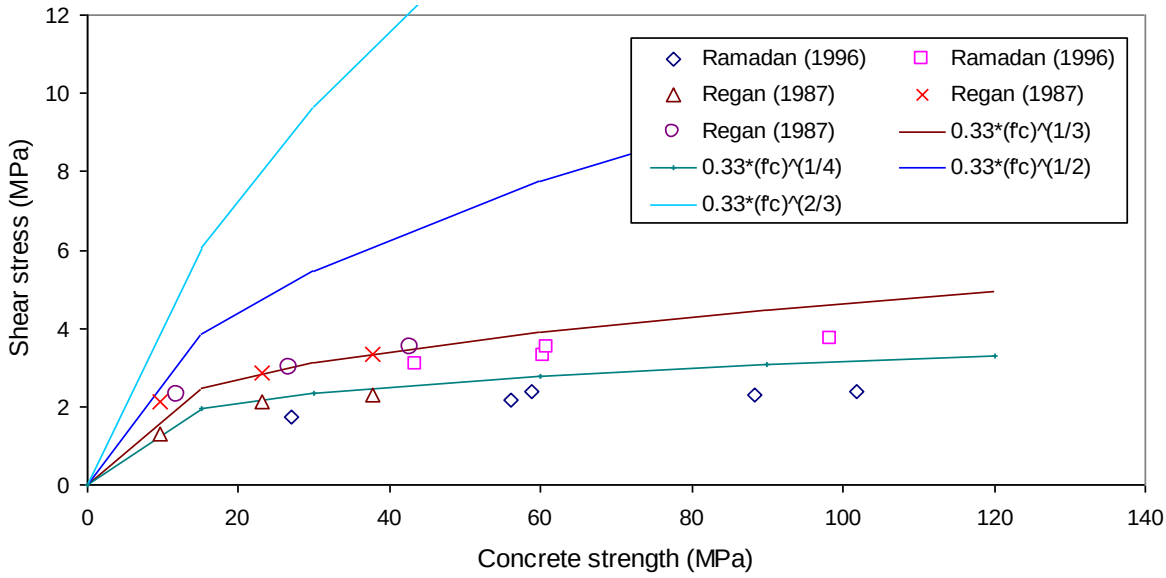

Figure 3.19: Influence of the concrete strength on shear stress

However, Marzouk and Hussein (1991) and Gardner (1996) propose using a punching shear equation that is proportional to $\sqrt[3]{f_c^{'}}$ rather than $\sqrt{f_c^{'}}$.

3.5.7 Concluding remarks

Parameters that affect the punching shear strength of the connection are reviewed here. These parameters included bottom reinforcement, span to depth ratio, slab thickness, column size and shape, flexural reinforcement and concrete compressive strength. The main conclusions are summarised here.

- Although the code equations (ACI 318-08, Eurocode 2 (2004) and BS 8110 (1997)) underestimate the punching shear strength of the connections, the experimental results showed a dramatic increase in the strength of the connection when the slab to depth ratio decreases below 4.
- The shear stress at punching failure decreases with increasing effective depth and with increasing rectangularity of the column. (The size effect and the geometric feature, also expressed as the aspect ratio, are significant aspects in punching shear resistance and should be included in code design expressions).
- The shear stress at punching failure is increased with an increasing compressive strength of concrete. The author suggests that in order to develop a new design expression for punching shear experimental research should also be conducted on high-strength concretes.
- The punching shear resistance showed a significant decrease with decreasing reinforcement ratio. It was concluded that the punching load is not influenced by the yield strength if punching failure occurred prior to reaching yield. Small increase of punching shear strength can be observed with a concentration of flexural reinforcement in the vicinity of the column.
- The influence of the reinforcement ratio on the punching shear capacity of flat slabs is not considered in ACI 318-08 while EC2 (2004), BS 8110 (1997) and CEB FIP model code (1990) takes the influence of the flexural reinforcement ratio into account.

Chapter 4

PUNCHING SHEAR STRENGTHENING OF CONCENTRICALLY LOADED RC FLAT SLABS

4.1 Introduction

Experiments on slabs with Lenton steel fortress (LSF) shear reinforcement are limited to the tests carried out by Li (1997). An increase in punching shear capacity could normally be achieved by the use of shear reinforcement. However, experiments carried out by Li (1997) were designed with low flexural reinforcement ratios and therefore the additional shear reinforcement used in those experiments was only sufficient to increase the flexural capacity (Stein *et al*., 2007). Li (1997) also used both a higher strength of steel strip (f_y=1100 N/mm^2) and bent strips in some of his experiments to increase the vertical stiffness of the LSF shear reinforcement however, the requirement for bending made the production of such strips more expensive.

Two series of experiments are described in this chapter: Pullout tests and Punching shear tests. In the first series, pullout tests were carried out on unbent strips in order to investigate the maximum strength that could be developed in the LSF strip and its anchorage behaviour. In the second series, three real scale punching shear test were conducted on slabs. Slab 1 is left without shear reinforcement as a control specimen, while Slabs 2 and 3 were strengthened with LSF type of shear reinforcement.

In the following sections, the general experimental considerations for both pullout tests and RC flat slabs are given first. The configuration of the specimens and the loading procedures are also provided and the test results are reported and discussed in detail.

4.2 First series: Pullout tests

A series of 42 pullout tests were carried out on a range of unbent LSF strip anchorages embedded in concrete. Tests were conducted to examine the anchorage characteristics

of the unbent LSF strips with and without holes. Both L shape and U shape LSF strips with and without holes were tested and these are shown in Figure 4.1. Different hook lengths (50, 100, and 380 mm), "flat" lengths (50, 76 mm) and bending radiuses (4.8 and 8.0 mm) were examined. 1.6 mm thick strips were supplied by Erico Inc. Pullout tests were carried out in the Heavy Structures Laboratory of the Department of Civil and Structural Engineering in the University of Sheffield by the author.

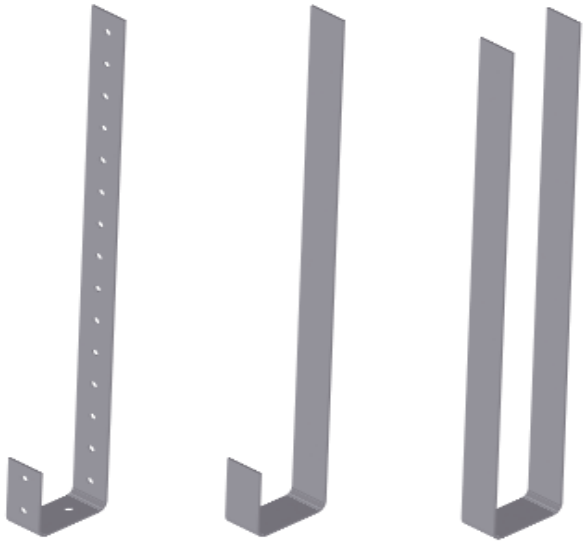

Figure 4.1: Lenton Steel Fortress (LSF) strips for pullout tests.

4.2.1 Material Characteristics

4.2.1.1 Concrete

The concrete used for the pullout specimens was prepared in the structural and material laboratory. Due to limited capacity of the laboratory mixers, two batches of concrete were prepared. Ordinary Portland cement was used and the maximum aggregate size was 10 mm. The compressive strength of the concrete was examined by testing four cubes for each batch (100x100 mm) according to BS 1881-116 (1983a). The mean compressive strength values obtained were 56.0 and 54.0 MPa for Batch 1 and 2, respectively.

4.2.1.2 Lenton Steel Fortress (LSF) strips

The Lenton Steel Fortress (LSF) is a form of shear reinforcement intended to increase the punching resistance of reinforced concrete flat slabs. They were manufactured from

a 25 mm wide flat steel strip. ERICO Inc. provided the strips and the mill certificate is given in Appendix B. The yield strength and the tensile strength of the strip are 538 MPa and 580 MPa respectively while the elongation is 18% (Manufacturer's data).

Two different strips were used in the pullout tests; strips with holes and strips without holes. The strips with holes are perforated with 5 mm circular holes at 25 mm spacing along the centre line. A perforation process was carried out during manufacturing.

4.2.2 Specimen classification and instrumentation

The main variables examined were hook length, h_2, 'flat' length, w, and bending radius, R, are summarised in Table 4.1. Three types of pullout specimens (Type P1, P2 and P3) were prepared to examine the possibility of pullout and these are shown in Figure 4.2.

Table 4.1: Summary of the Specimens

Specimen Type	Length (Unit: mm)			Bending radius, R	No. of strip specimens	Remarks
	h_1	w	h_2			
P1	380	50	50	3t	3	With holes
P1	380	50	50	3t	3	Without holes
P1	380	50	50	5t	3	With holes
P1	380	50	50	5t	3	Without holes
P1	380	50	100	3t	3	Without holes
P1	380	50	100	5t	3	Without holes
P2	380	76	50	5t	3	Without holes
P2	380	76	100	5t	3	Without holes
P3	380	50	380	3t	9	Without holes
P3	380	50	380	5t	9	Without holes

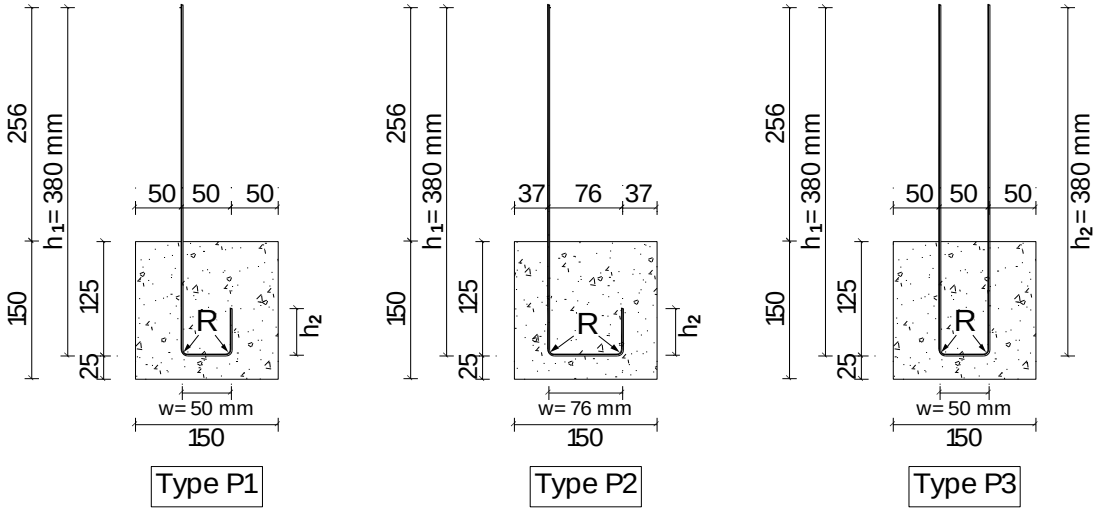

Figure 4.2: Pullout specimens

(Variables: R=internal bending radius, h_2=hooks length in vertical direction).

4.2.2.1 Mould manufacturing

Polystyrene 150 mm cubes were used in the laboratory to cast the concrete. The mould was made of 25 mm thick Polystyrene. The inside of the mould was coated with a thin layer of mould-releasing agent to make de-moulding of the concrete blocks easier. The strips were held rigidly on the bottom surface of the cubes by spacers and plastic ties and were positioned vertically in the moulds.

4.2.2.2 Casting and curing

The concrete was cast vertically in three successive layers of approximately equal thickness. Each layer was vibrated using a poker vibrator to minimise voids and achieve a more uniform and homogenous distribution of concrete. Extra care was taken during casting and vibrating so as not to disturb the verticality of the strips. Adequate compaction and levelling were applied on the top surface to eliminate voids and minimise geometric irregularities. Control specimens were cast using the same batch of concrete for subsequent evaluation of concrete strength. After casting, all specimens were covered with wet hessian and polythene sheets, cured for one week and subsequently stored under standard laboratory conditions. Figure 4.3 shows the pullout specimens after casting.

Figure 4.3: Pullout specimens after casting.

4.2.2.3 Test set-up

The pullout test was performed in a universal testing machine and is shown in Figure 4.4.

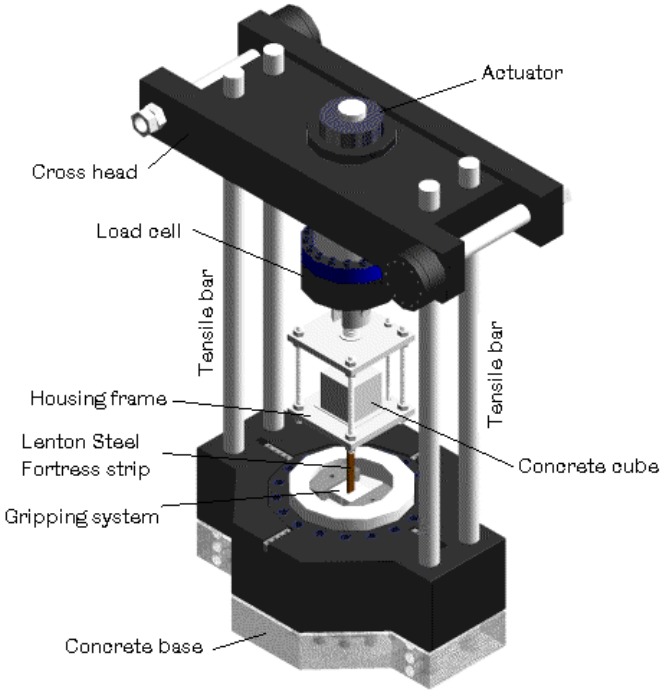

Figure 4.4: The loading frame and test set-up for the pullout test.

This servo-controlled machine is capable of delivering 1 MN force, in tension or compression. The machine rig consists of a heavy static base with a moveable cross-

head supported on four steel posts of 100 mm diameter. The height of the cross head can be adjusted by using secondary hydraulic rams, allowing the cross head to slide up or down the supporting posts. The main 150 mm-diameter hydraulic actuator is mounted in the centre of the cross-head and connected to the top plate of the steel housing frame which provides the reaction to the pullout load imposed to the specimen.

The housing frame comprises of two steel plates that are 38 mm thick. These plates are connected via 24 mm diameter bolts at each corner and this is shown in Figure 4.5. In order to strengthen the connections of the top and bottom plates 20 mm diameter two other bolts were used. The housing frame was designed to rotate independently, allowing the portion of the strip projecting from the concrete cube to be inserted in the jaw in a vertical position. A 2 mm thick rubber plate was used to secure contact between the bottom face of the concrete cube and the steel bearing-plate. This was essential to reduce stress concentrations due to small irregularities on the surface of the concrete cube and minimise possible bending effects on the bar during testing.

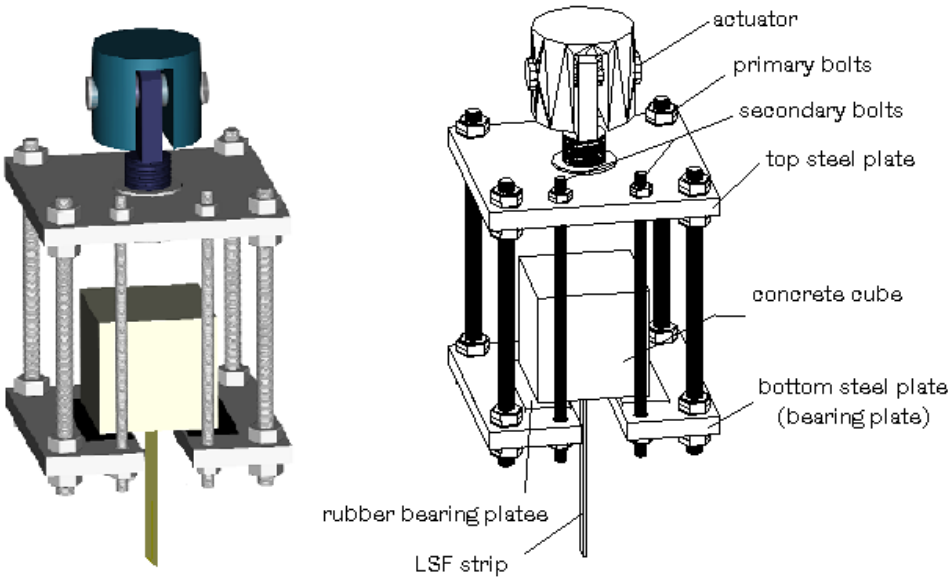

Figure 4.5: Testing arrangement for pullout test.

For L shaped strips, in the middle of the bottom bearing plate, a main 50 mm-circular hole allowed the strip to run through a slot which connects the central hole to the plate boundary as shown in Figure 4.6. For U shaped strips a 70 mm hole allowed the strips to run through a slot, as shown in Figure 4.7.

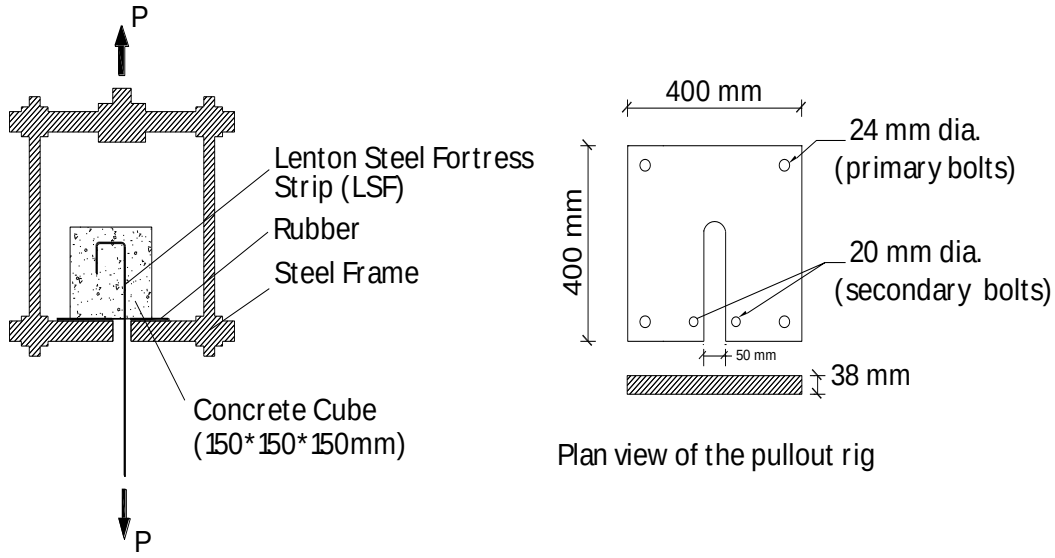

Figure 4.6: Details of pullout housing frame for specimens type P1, and P2

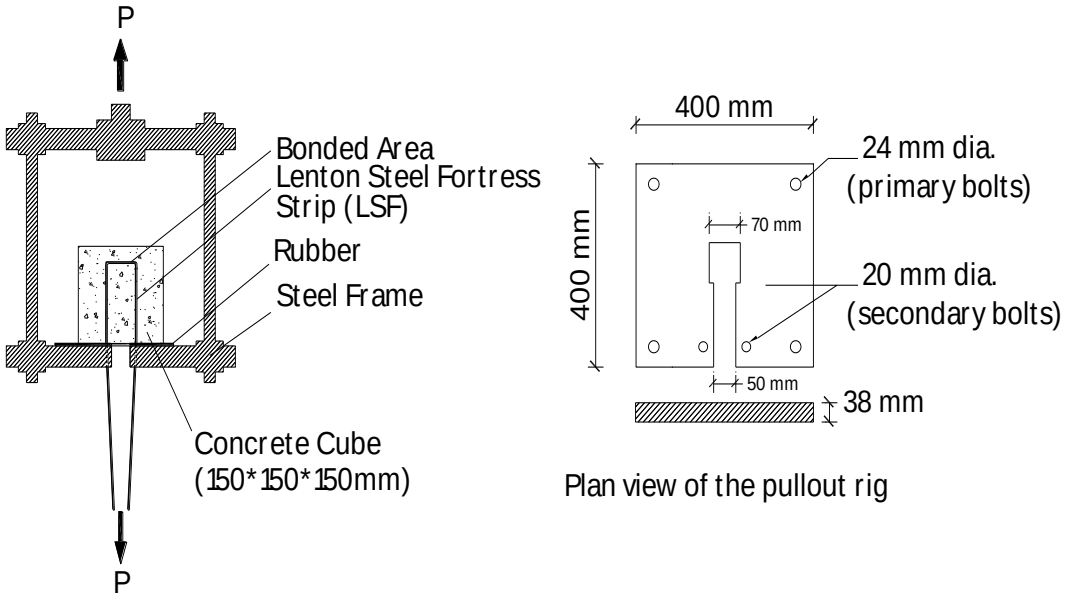

Figure 4.7: Details of pullout housing frame for specimens type P3.

4.2.3 Test results and discussion

The stress versus displacement results are shown in Table 4.2 and the full details are provided in Appendix B.

Table 4.2: Summary of test results

Specimen I.D.	t	t'	h_1	W	h_2	R	f'_c	f'_{c1}	F_{max}	f_{max}	f_{ave}	σ_1	σ_2	μ	Failure Mode
P1-h-50-3t#1	1.6	1.57	381	50	50	4.8	56	46	18.6	574	574	0	4.1	1.9	BC
P1-h-50-3t#2	1.6	1.58	381	50	50	4.8	56	41	18.6	574		0	4.0	1.9	BC
P1-h-50-3t#3	1.6	1.6	381	50	50	4.8	56	46	18.6	574		0	4.3	1.7	BC
P1-w-50-3t#1	1.6	1.57	381	50	50	4.8	56	47	23.6	581	577	NA	37	9.1	BC
P1-w-50-3t#2	1.6	1.58	381	50	50	4.8	56	39	23.3	575		NA	29	8	BC
P1-w-50-3t#3	1.6	1.57	381	50	50	4.8	56	46	23.4	576		NA	17	3.5	BC
P1-h-50-5t#1	1.6	1.6	381	50	50	8.0	56	45	18.7	575	575	0	4.8	2.2	BC
P1-h-50-5t#2	1.6	1.58	381	50	50	8.0	56	42	18.7	576		0	4.8	1.8	BC
P1-h-50-5t#3	1.6	1.54	381	50	50	8.0	56	38	18.6	574		0	5.2	1.6	BC
P1-w-50-5t#1	1.6	1.6	381	50	50	8.0	56	39	23.2	571	571	4.5	23	9	BC
P1-w-50-5t#2	1.6	1.6	381	50	50	8.0	56	48	23.2	570		4	29	7.7	BC
P1-w-50-5t#3	1.6	1.58	381	50	50	8.0	56	35	23.2	571		NA	29	7	BC
P1-w-100-3t#1	1.6	1.6	381	50	100	4.8	56	39	23.0	565	565	7	29	8	BC
P1-w-100-3t#2	1.6	1.6	381	50	100	4.8	56	45	23.2	572		6	22	6	BC
P1-w-100-3t#3	1.6	1.59	381	50	100	4.8	56	40	22.7	559		5	31	6.7	BC
P1-w-100-5t#1	1.6	1.58	381	50	100	8.0	56	38	22.9	564	566	9	31	8	BC
P1-w-100-5t#2	1.6	1.6	381	50	100	8.0	56	37	23.1	568		6	25	6.4	BC
P1-w-100-5t#3	1.6	1.56	381	50	100	8.0	56	37	23.0	567		6	28	8	BC
P2-w-50-5t#1	1.6	1.54	381	76	50	8.0	56	39	23.2	572	556	4.5	24	7	BC
P2-w-50-5t#2	1.6	1.56	381	76	50	8.0	56	46	21.5	529		5.5	--	-	BR→PO
P2-w-50-5t#3	1.6	1.53	381	76	50	8.0	56	48	23.1	568		5.0	26	7	BC
P2-w-100-5t#1	1.6	1.54	381	76	100	8.0	54	46	22.5	554	564	7.0	26	6	BC
P2-w-100-5t#2	1.6	1.6	381	76	100	8.0	54	43	23.0	567		5.0	22	5	BC
P2-w-100-5t#3	1.6	1.56	381	76	100	8.0	54	47	23.2	571		7.0	29	9	BC
P3-w-380-3t#1	1.6	1.53	381	50	381	4.8	54	36	23.0	565	575	5.0	22	5	BR→BR
P3-w-380-3t#2	1.6	1.57	381	50	381	4.8	54	48	23.1	568		NA	25	5.6	BR→PO
P3-w-380-3t#3	1.6	1.57	381	50	381	4.8	54	46	23.0	566		4.0	18	4	BR→BR
P3-w-380-3t#4	1.6	1.58	381	50	381	4.8	54	39	23.1	570		NA	27	5	BR→PO
P3-w-380-3t#5	1.6	1.57	381	50	381	4.8	54	47	23.1	568		6.0	19	4.3	BR→BR
P3-w-380-3t#6	1.6	1.6	381	50	381	4.8	54	40	23.1	568		5.0	21	3.6	BR→BR
P3-w-380-3t#7	1.6	1.6	381	50	381	4.8	54	46	23.0	570		7.0	26	6	BR→BR
P3-w-380-3t#8	1.6	1.58	381	50	381	4.8	54	40	23.2	567		NA	19	3	BR→PO
P3-w-380-3t#9	1.6	1.57	381	50	381	4.8	54	39	22.7	571		NA	19	4	BR→PO
P3-w-380-5t#1	1.6	1.57	381	50	381	8.0	54	45	23.1	568	570	NA	23	5.7	BR→PO
P3-w-380-5t#2	1.6	1.58	381	50	381	8.0	54	48	23.1	568		NA	17	3	BR→PO
P3-w-380-5t#3	1.6	1.58	381	50	381	8.0	54	45	23.4	576		NA	24	5.5	BR→PO
P3-w-380-5t#4	1.6	1.57	381	50	381	8.0	54	46	23.2	572		NA	24	6.3	BR→PO
P3-w-380-5t#5	1.6	1.56	381	50	381	8.0	54	44	23.2	571		NA	25	6.5	BR→PO
P3-w-380-5t#6	1.6	1.56	381	50	381	8.0	54	46	23.2	571		NA	25	6	BR→PO
P3-w-380-5t#7	1.6	1.57	381	50	381	8.0	54	40	23.1	568		NA	20	5.4	BR→PO
P3-w-380-5t#8	1.6	1.57	381	50	381	8.0	54	42	23.0	566		NA	26	6.9	BR→PO
P3-w-380-5t#9	1.6	1.56	381	50	381	8.0	54	45	23.1	570		NA	20	4.8	BR→PO

Notation: Specimen P3-w-380-5t#3 stands for [test type (Fig. B.1) strip type (with or without holes)]-[hook length (h_2)]-[bent radius]-[# sample no.]

h_1= Length of the strip
w= Tail length
h_2= Hook length
R= Internal bending radius (mm)
t= Nominal thickness (mm)
t'= Actual thickness (mm)
f'_c = concrete compressive strength (MPa)
f'_{c1}=Concrete compressive strength of cubes after pull out tests (MPa)
F_{max}= Maximum pullout load (kN)
f_{max}= Maximum pullout stress (MPa)
f_{ave}= Average pullout stress (MPa)
σ_1= Slip inside the concrete cube (mm)
σ_2= Overall slip along the bar (mm)
PO= Pullout failure
BC= Bar break at outside the concrete
BR= Bar rupture at the bend zone
BR→PO =First, failure occurs as rapture on the weaker leg of the strip then pullout.
Ductility =$\mu=D_u/D_y$
D_u= Displacement at ultimate load
D_y= Displacement at yielding

For L shaped strips, bar rupture occurred outside the concrete in all cases except for specimen P2-w-50-5t#2, for which rupture occurred on the bent zone and then the strip pulled out from the concrete cube.

The ductility of the strips was determined using the ratio of ultimate to yield displacement. The strips with holes showed a limited ductility (1.6 – 2.2) while the strips without holes showed much higher ductility (3 – 9).

By considering the elongation of the strips, it is clear that the strips with holes anchored the strip better and that little plastic elongation took place inside the concrete, whilst the strips without holes elongated considerably within the concrete but appeared to be perfectly anchored at the first bent.

The U shaped strips were tested to examine the possibility of concrete pullout in between two strips in tension. This did not happen and failure occurred by the strip fracture.

Finally, it can be concluded that the strips with holes show limited ductility though they anchor well in the concrete limiting slip displacements. The strips without holes anchor well at the first bent and fail after considerable ductility. The down side is that they show higher slip displacements than the strips with holes.

4.3 Second series: Slab-column connection tests

In the beginning of this section it is essential to provide a brief description of the experiments carried out by Li (1997) as these experiments are used for comparison purposes. Experiments by Li (1997) are also used in the numerical modelling and are reported in Chapters 5 and 6 in this thesis. Li (1997) referred experimental test series as PSS in his thesis and the same reference is used in this thesis for simplicity.

Li (1997) carried out seven tests on slab-column connections. The control specimen was left without shear reinforcement and referred in this thesis as PSSA. The effectiveness of the different arrangements of the Shearband in slab-column connections was assessed by Li (1997). The shear reinforcement in PSSB, PSSC and PSSE are along the main axes while shear reinforcement in PSSD distributed around the column. In PSSF and PSSG the shear reinforcement is distributed uniformly over the slab. In these experiments the placement angles (vertical or inclined) and the anchorage properties of

the LSF type of shear reinforcement (punched with holes or solid) were investigated. Schematic drawings of slabs (PSSA, PSSB, PSSC, PSSD, PSSE, PSSF and PSSG) are shown in Figure 4.8 and their details are provided in Table 4.3.

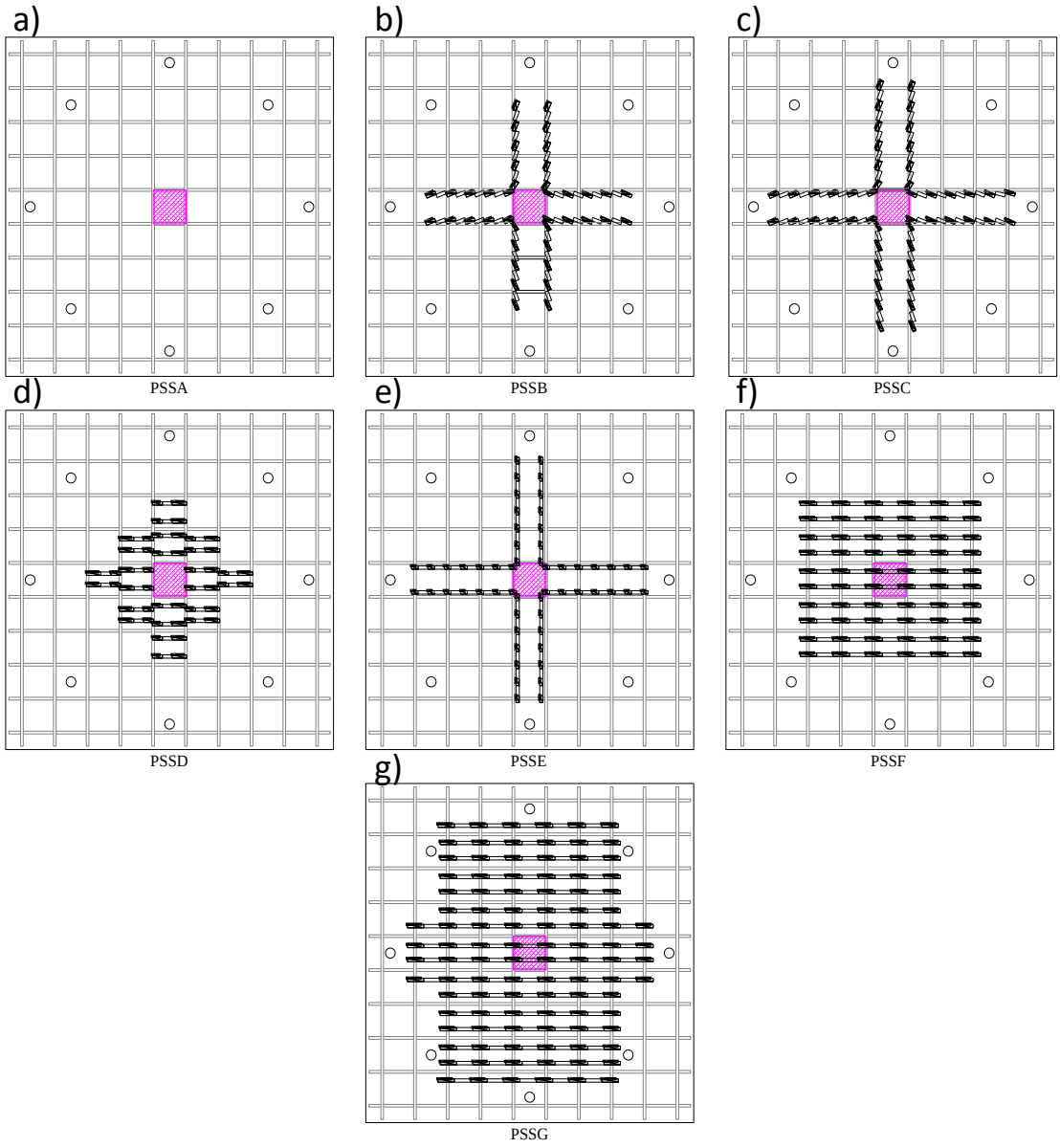

Figure 4.8: Test series PSS (Li, 1997). a; PSSA, b; PSSB, c; PSSC, d; PSSD, e; PSSE, f; PSSF, g; PSSG.

Table 4.3: Details of series PSS (Li, 1997)

		PSSA	PSSB	PSSC	PSSD	PSSE	PSSF	PSSG
	f'_c (cube) (MPa)	32.3	39	41.2	42.2	43.4	43.4	38
	***h* (mm)**	175	175	175	175	175	175	175
	***d* (mm)**	139	139	139	139	139	139	139
	ρ (%)	0.7	0.7	0.7	0.7	0.7	0.7	0.7
Top Reinforcement	**Bar diameter (mm)**	16	16	16	16	16	16	16
	f_y (MPa)	500	500	500	500	500	500	500
	Spacing of the bars (mm)	200	200	200	200	200	200	200
Bottom Reinforcement	**Bar diameter (mm)**	12	12	12	12	12	12	12
	f_y (MPa)	480	480	480	480	480	480	480
	Spacing of the bars (mm)	200	200	200	200	200	200	200
Shear Reinforcement	**f_y (MPa)**	-	1100	1100	1100	1100	1100	1100
	Cross Section (mm^2)	-	20.32	20.32	20.32	20.32	20.32	20.32
	No of legs	-	80	88	94	80	100	184
	Failure Load (kN)	454	560	560	560	573	598	590

The experiments in this section were commissioned by Erico Inc. for accreditation purposes. These tests were carried out by Taylor Woodrow Technology in their centre at Leighton Buzzard. Three tests on interior slab-column connections were conducted: one specimen without shear reinforcement and two specimens strengthened with LSF shear reinforcement.

4.3.1 Test configuration

A total of three full scale interior slab-column connections were tested. Design of the experiments was aided by studies conducted on prototype specimens designed to satisfy typical requirements for construction of slabs in low-rise buildings used in UK. These specimens can be regarded as part of a prototype structure of which the flat concrete

slab spans 6-6.5 m between columns. The slab thickness was 200 mm. A depth of 200 mm for current slab was chosen since it is the minimum required depth for the use of shear reinforcement to increase the punching shear capacity in BS 8110 (1997). The tested slabs represent interior slab-column connections with plan dimensions of 2750×2750 mm and loads were applied at lines of 1220 mm from the column centre corresponding to the lines of contraflexure.

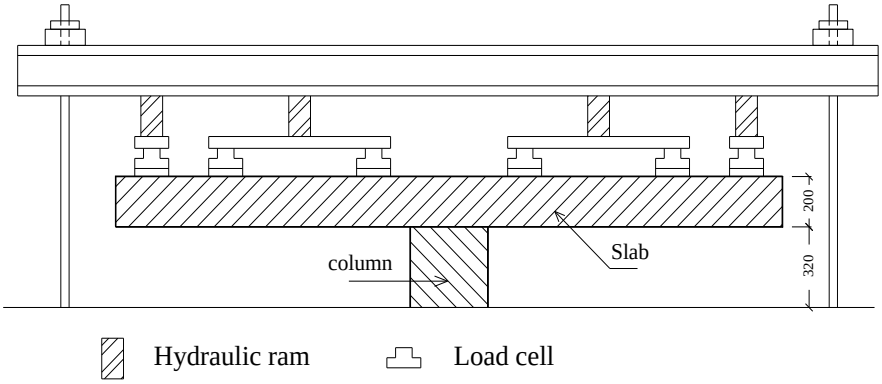

Figure 4.9: Test rig general arrangement.

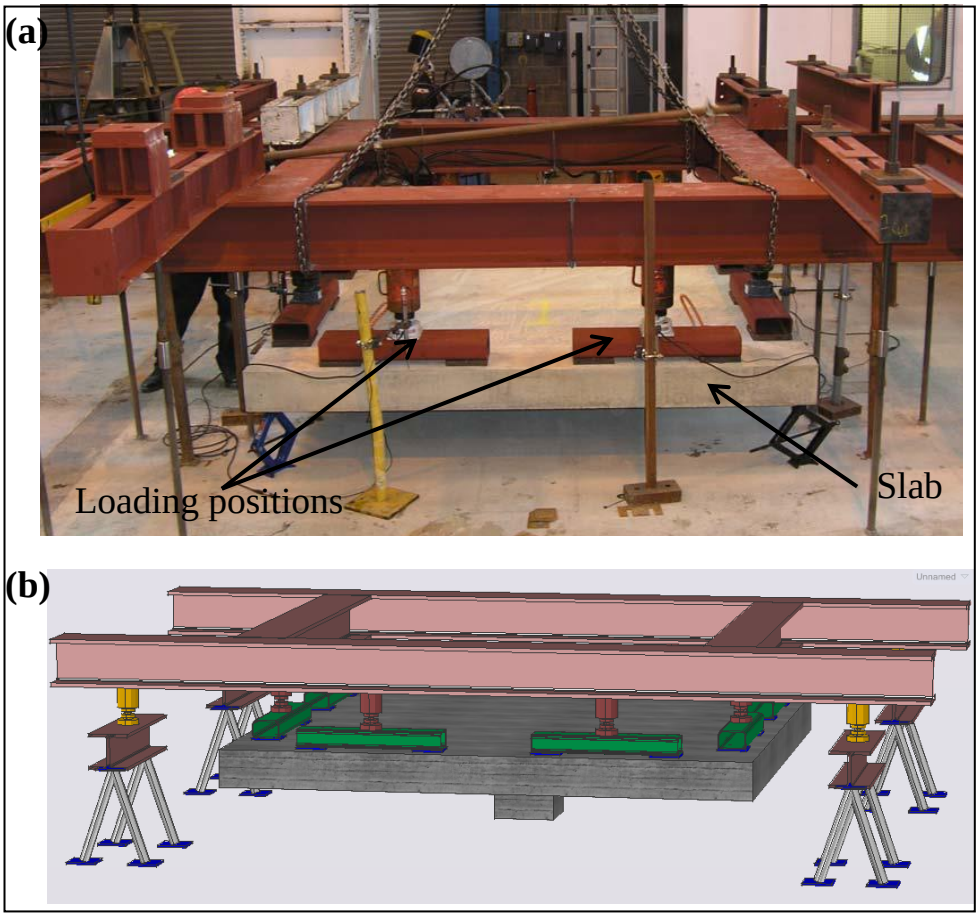

Figure 4.10: (a) A picture of test rig; (b) the schematic plot of the test configuration.

The test rig arrangements are shown in Figures 4.9. A photograph that was taken prior to the experiment of the rig and the schematic plot of the test configuration are shown in Figures 4.10 (a) and (b) respectively. A 320 mm square column section was used in the experiments which is appropriate for slabs with 6-6.5 m spans in low rise buildings.

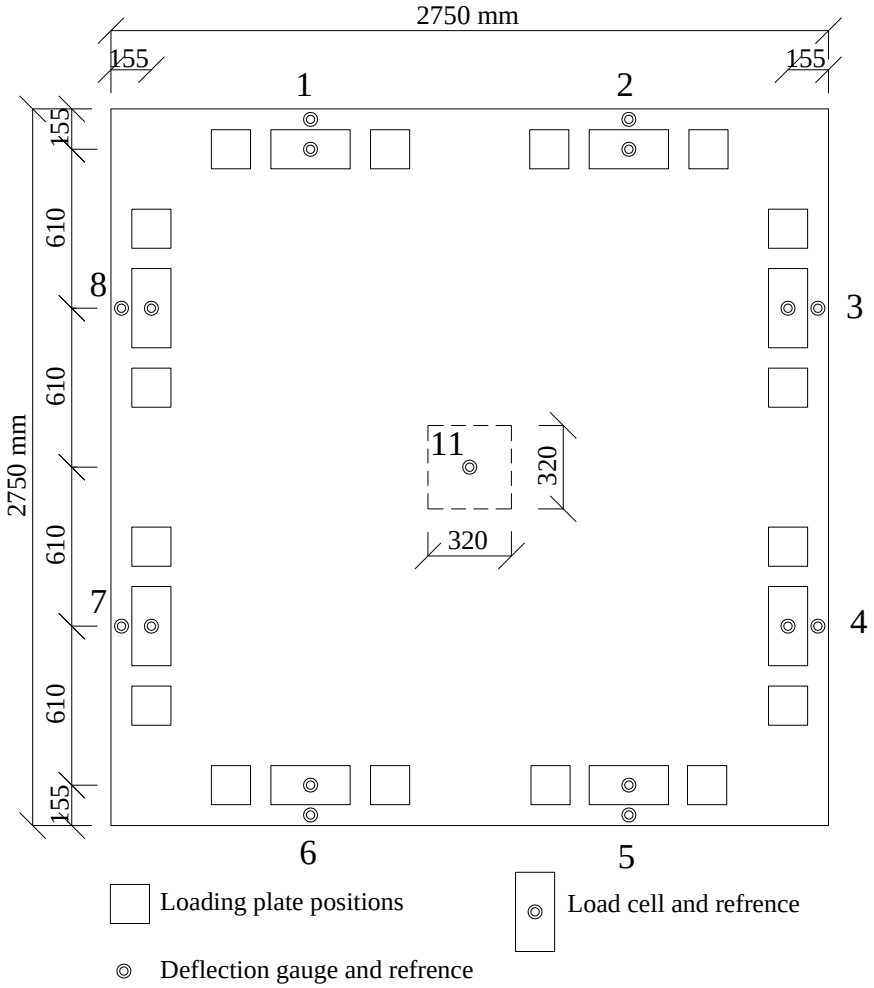

Figure 4.11: Plan view of test specimens.

The slab was supported through a column stub on the floor. Equal point loads were applied downwards symmetrically at eight points on a circle of diameter 2750 mm which were distributed to the 16 load points shown in Figure 4.11 by spreader beams. Eight hydraulic jacks were connected to a single pump and the force from each jack was centred by a spherical bearing and monitored continuously by a load cell placed between the bearing and the spreader. The jacks were mounted on a steel framework tied to the laboratory floor by high tensile bars. Restrained forces produced by the

lateral movement between the jack and the slab are negligible considering the height of the jacks and the horizontal flexibility of the steel frame and its supports.

On interior slab-column connections of flat slabs, three types of boundary conditions were considered for the experimental study regarding the support and loading positions. The first boundary condition assumed that the slab was supported along its edges and was loaded through a column or a plate at the centre (Elstner and Hognestad, 1956). The second boundary condition was arranged according to Kinnunen and Nylander (1960), where the slab was supported through a column or plate at the centre and loaded at the perimeter. Kuang and Morley (1992), also suggested that the slab can be supported along its edges with some or full lateral restraint and loaded through a column or plate in the centre which is intended to model the membrane action in RC flat slabs and therefore were not addressed in this thesis.

According to Kinnunen and Nylander (1960), the load is applied to the column through a single hydraulic jack. The column load is then transferred to a strong floor by means of a number of tie rods which are fitted along the circumference of the test slab. Tie rods act as a rocker support and are normally provided with a spherical ball bearing at each end. In Elstner and Hognestad (1956), the test specimens are simply supported along their edges and the column load is applied downwards, also by a single hydraulic jack through a reaction frame. This may allow redistribution of moment after yielding of flexural reinforcement due to the uniform deflections being imposed at the boundary. This is the major disadvantage of this arrangement. The deflections at each loading point are expected to be different since the reinforced concrete slabs are not isotropic and the stiffness of the actual structure varies in different directions with the same column load. The same problem is valid for test specimens supported along the four edges.

Normally full redistribution of moment occurs for interior columns in buildings, however, Clyde and Carmichael (1974) stated that the conventional punching shear tests do not allow full redistribution of moment. This results in the flexural collapse load from the test to be less than that of the prototype.

The test configuration adopted in this thesis consists of a slab which is supported through a column stub on a beam reacting against two reaction ring frames. Figure 4.11 shows the positioning of the equal point loads that are applied downwards at eight

locations on a circle of diameter 2750 mm symmetrically. Eight hydraulic jacks of 100 kN capacity are used in this configuration. Each jack had a spherical ball bearing. This allowed jacks to be connected to the same pump in order to receive the same pressure and apply the same load to the specimen. Bending effects as a result of the lateral expansion of the slab or the inclination of the slab during testing are minimised by tying the jacks just above the load point. A Teflon sheet between the loading plate and each spherical ball bearing of the jacks is used. Therefore no horizontal confinement to the specimen is provided at the loading points since the spherical ball bearing could move freely in the horizontal direction.

The deformation on the specimens both in the horizontal and vertical directions are not imposed in the test-rig used. Although the load at each loading point is kept the same, each loading point could have different deflection. Compared to the all other deformation control arrangements carried out by previous researchers, the author strongly recommends that the applied loading in practice is more precisely simulated with this type of loading.

4.3.2 Materials

4.3.2.1 Concrete

The concrete used was a normal weight concrete with a target cube strength of 35 N/mm^2. This value is close to the maximum compressive strength which BS 8110 allows to be taken into account in calculation of shear resistance. The concrete was obtained from a local ready-mix supplier and was made with limestone aggregate with a 20 mm maximum size and water cement ratio of 0.54. All the slabs were cast together. Poker-vibrators were used to compact the concrete. The development of concrete strength was monitored by tests of 100 mm cubes. After casting, the slabs were cured with plenty of water and covered with polythene sheeting for one week. The cubes were cured under water and were tested in accordance with BS 12390 Part 3: 2002 on the same day as the slabs. Slab 1 was tested on day 26 while Slab 2 and 3 were tested 28 and 32 days from the casting date respectively. The test results for these 100 mm cubes are summarised in Table 4.4.

The equivalent 150 mm cube strengths have been obtained as (fib Bulletin 12, 2001) $f_{cu,150}=0.9f_{cu,100}$. Yield strength of 550 MPa for flexural reinforcement was used in these experiments.

Table 4.4: Concrete strength of slabs

Slab	Slab 1	Slab 2	Slab 3
Cube strength (N/mm^2)	38.5	38.6	38.6

4.3.2.2 Mechanical properties of unbent LSF shear reinforcement

The characteristics of the unbent LSF strips are given in Table 4.5.

Table 4.5: Mechanical properties of LSF reinforcement strip

Nominal section (mm×mm)	Imperforated				Perforated				$\frac{f_y^2}{f_y^1}$	$\frac{f_u^2}{f_u^1}$
	Actual section (mm×mm)	f_y^1 (N/mm^2)	f_u^1 (N/mm^2)	Elongation (%)	Actual section (mm×mm)	f_y^2 (N/mm^2)	f_u^2 (N/mm^2)	Elongation (%)		
25×2.0	25.09×2.01	589	648	11.0	25.06×2.01	476	511	4.0	0.81	0.79
25×1.6	25.06×1.62	548	606	12.5	25.0×1.62	442	470	5.5	0.81	0.78
25×1.2	25.04×1.21	574	620	18.0	25.0×1.21	492	512	11.0	0.89	0.89

Note: Stresses f_y and f_u for perforated strip are calculated for the gross (imperforated) sections.

The application of 0.8 times the gross area and the yield stress in structural calculations is supported by the experiments summarised in Table 4.5 where the ratio of the perforated to imperforated strengths of the stirps at yield and ultimate load is approximately 0.8.

The criteria for properties of reinforcement from EC 2-2004, Annex C (2004) was used to evaluate the LSF reinforcement (Table 4.6). The imperforated strip material categorised as type C reinforcement in terms of elongation. The type of the reinforcement for perforated strips varied considerably with the strip thickness. For instance, the strip with a thickness of 1.2 mm categorised to type C, while the strips with thicknesses of 1.6 mm and 2.0 mm were classified to type B and A respectively. In

terms of the ratio f_u / f_y, of the imperforated strip, all three thicknesses corresponded to class B while for perforated strips with the same thicknesses are categorised to class A.

Table 4.6: Classification of perforated LSF strips according to EC 2-2004, Annex C

Nominal section (mm×mm)	25×2.0	25×1.6	25×1.2
Classification by f_u / f_y	A	A	A
Classification by ε_u (%)	A	B	C

4.3.3 Flexural design of slab tests

Yield line analysis was used to compute the approximate flexural capacity. For determining the flexural capacity, assumptions regarding the possible yield line failures need to be made. Failure is likely to occur by four diagonal yield lines or by a simple yield line at the face of the slab. For the four diagonal yield line mechanism, by using virtual work (Stein *et al*., 2007), the force that produces flexural failure is

$$V_f = \frac{8ml_s}{l_1 - c} \quad [\text{kN}] \ . \tag{4.1}$$

For the simple yield line at the face of column, the force that produces flexural failure is

$$V_f = \frac{8ml_s}{(l_1 - c) + (\frac{l_1}{2} - c)} \quad [\text{kN}] \tag{4.2}$$

where m is the bending moment per unit slab width at yielding of the top flexural reinforcement, l_s is dimension of the slab specimen (2750 mm), l_1 is the span between the supports (loading points, 2440 mm) and c is the column dimension (320 mm). Since the simple yield line gives less capacity, it is conservative to accept the yield moment for the first test series.

The layout and the reinforcement details (bottom flexural reinforcement, top flexural reinforcement and section) for Slab 1, 2 and 3 are shown in Figures 4.12, 4.13 and 4.14 respectively.

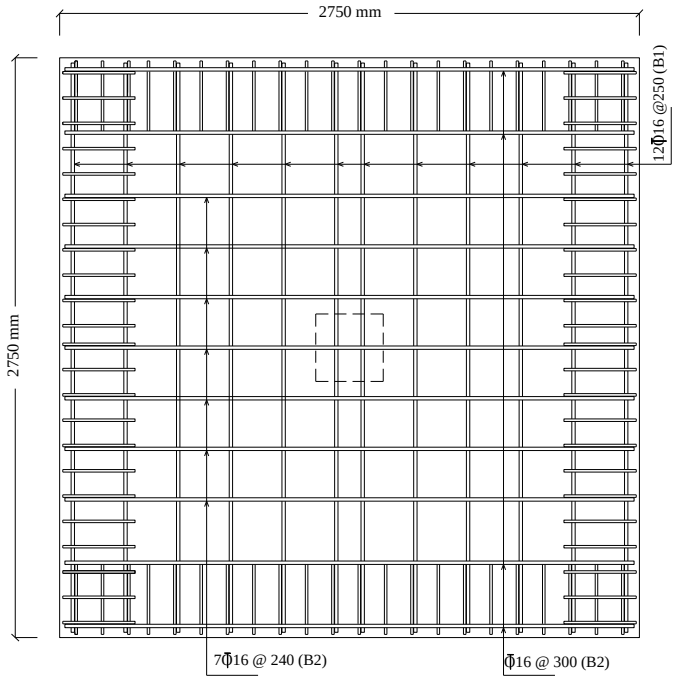

(a) Bottom flexural reinforcement

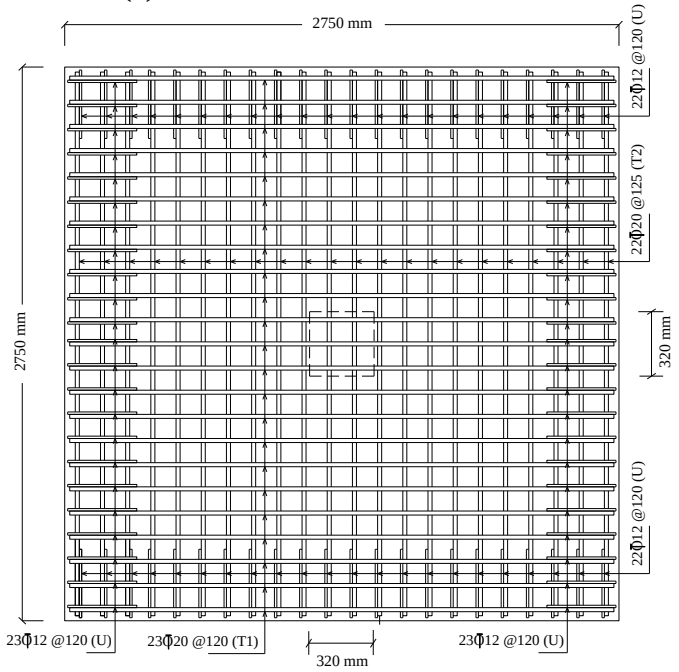

(b) Top flexural reinforcement

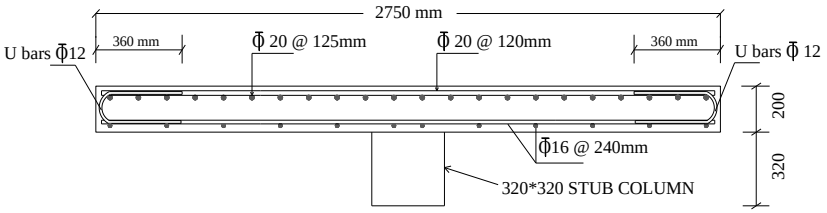

(c) Section

Figure 4.12: Layout and reinforcement details for Slab 1.

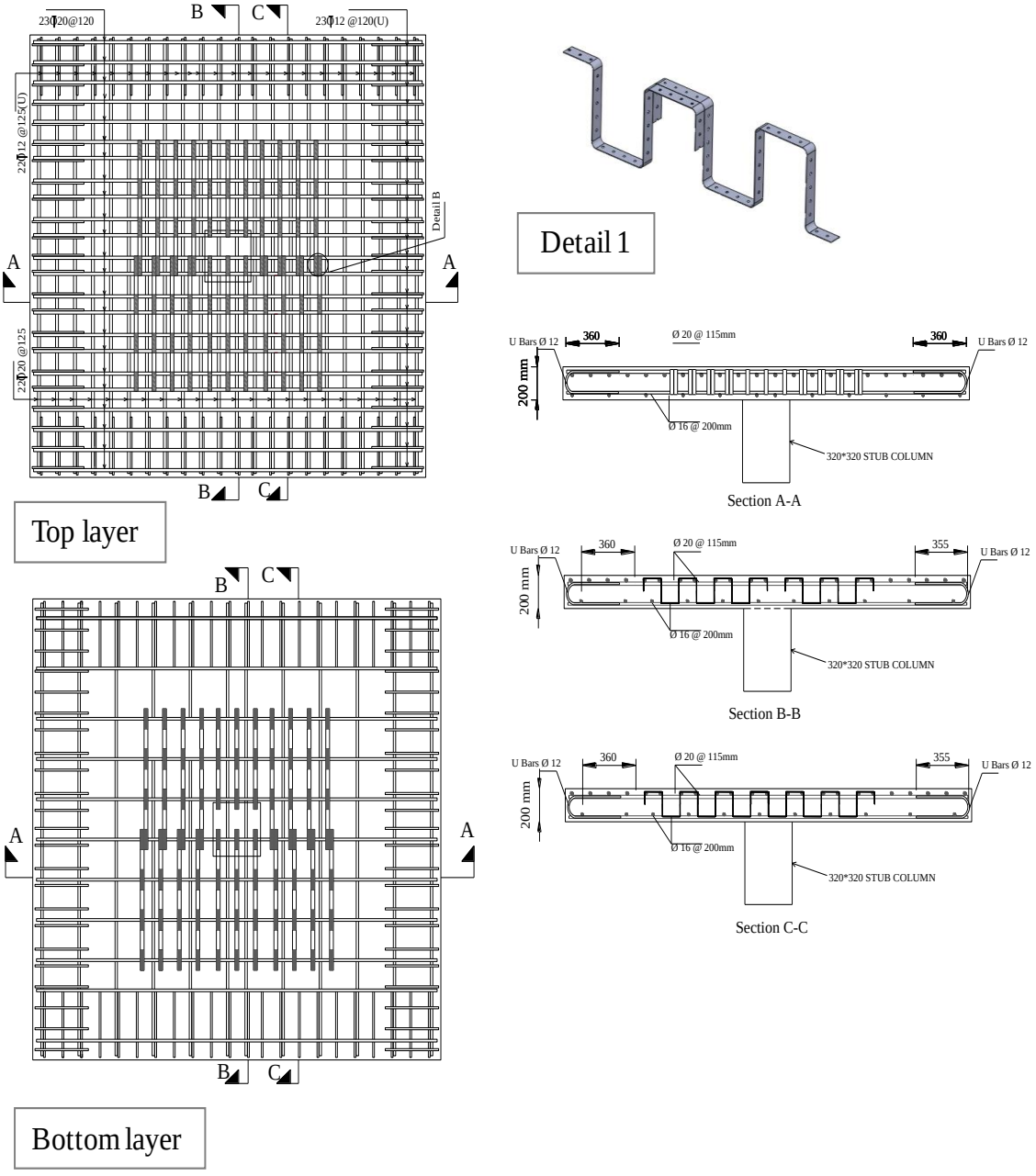

Figure 4.13: Layout and reinforcement details for Slab 2.

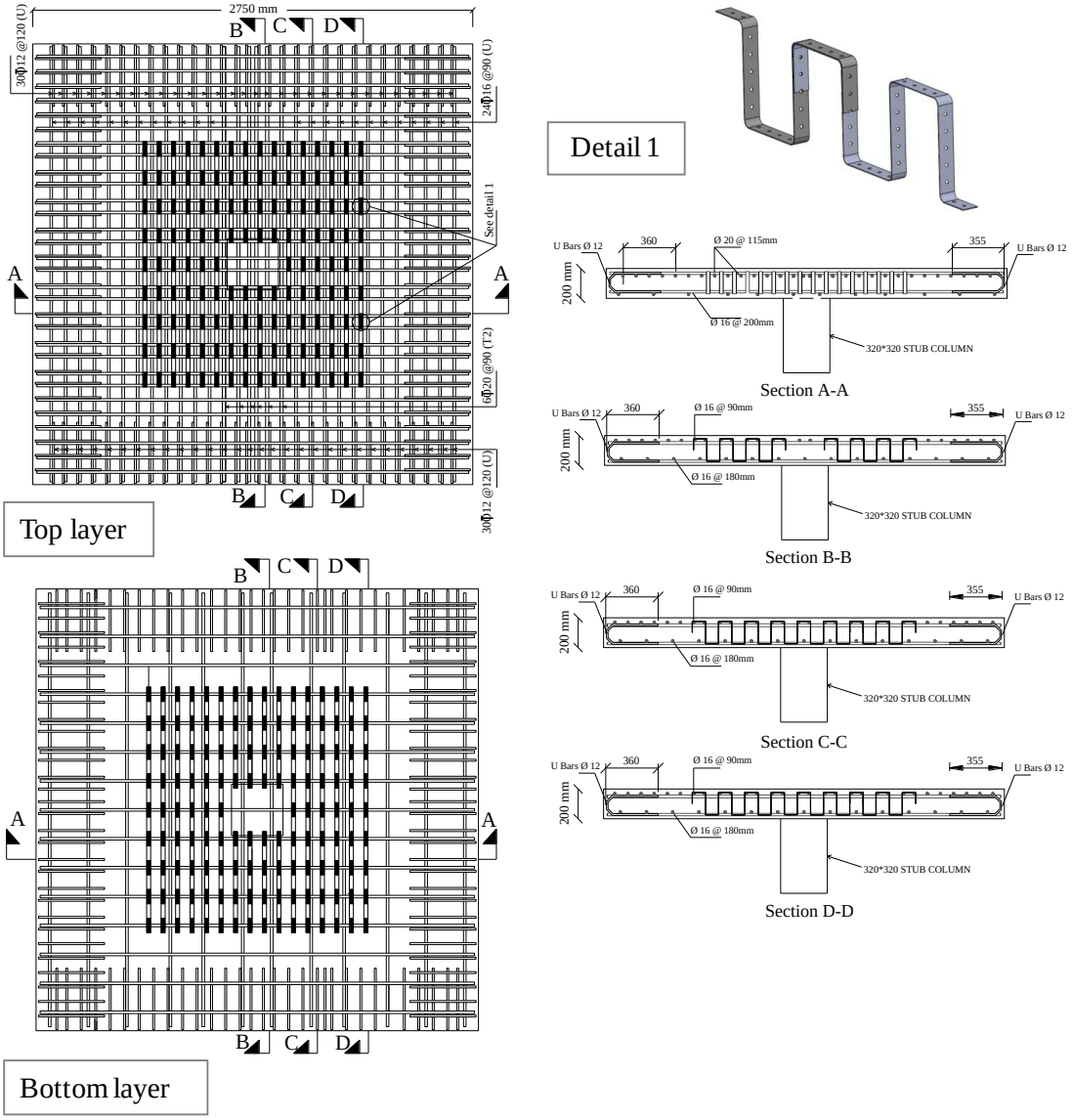

Figure 4.14: Layout and reinforcement details for Slab 3.

4.3.4 Strains in Shear Reinforcement

Electrical resistance strain gauges were used to measure the strain in the shear reinforcement in the vertical legs. Pairs of strain gauges were positioned in the mid height on opposite faces of a number of legs at sections away from perforations. To avoid difficulties during placing the gauges in perforated sections and effects of variations of strain across the width near perforations, the gauges were positioned away from the perforations. Figure 4.15 shows the position of strain gauges in the shear reinforcement for Slabs 2 and 3 respectively. In each pair, gauges were on opposite faces of the leg, so the average of two measurements should give the mean axial strain

which is free from any effects of bending. The measured strain, $1.25E_s\varepsilon$, is used in the estimation of the mean stress at perforated sections where E_s is the elastic modulus of the steel, and is assumed to be 200 kN/mm^2 and ε is the average measured strain.

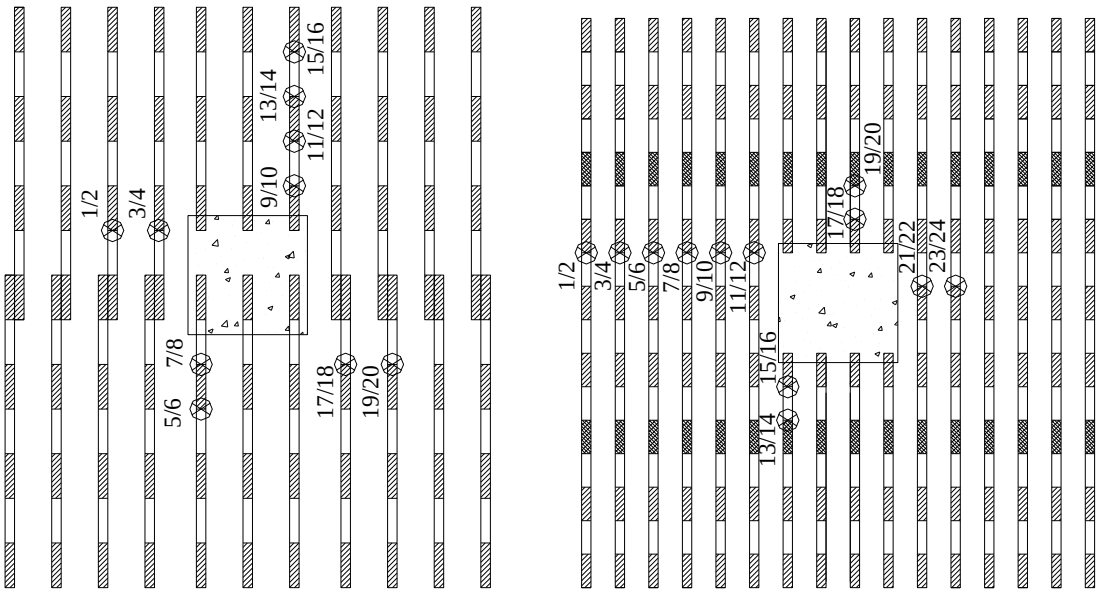

Slab 2 Slab 3

Figure 4.15: Position of strain gauges in the shear reinforcement layers for Slab 2 and Slab 3.

4.3.5 Testing

Load was applied gradually and continuously however, Slab 1 was unloaded and reloaded at a load of 500 kN and Slabs 2 and 3 were unloaded and reloaded at 600 kN. The total durations of the experiments were about 45 minutes for Slab 1 and 65 and 95 minutes for Slabs 2 and 3 respectively.

4.3.6 Test results

Test results of slabs loaded concentrically are summarised in this section. Load deformation characteristics, strain gauge measurements on shear reinforcement, and crack patterns are discussed here.

4.3.6.1 Load deformation

The average displacement was calculated by subtracting the average displacements of linear potentiometers 1, 2, 3, 4, 5, 6, 7, and 8 from displacement linear potentiometer 11 (as previously shown in Figure 4.11). Applied load versus average deflection plots for the test specimens are given in Figure 4.16 to Figure 4.18. The solid blue lines, shown in Figures 4.16, 4.17 and 4.18 are the results of linear elastic analysis using gross section properties and measured material properties of the tested slabs which could also be classified as initial tangents. Linear elastic analysis was performed using ABAQUS (2008).

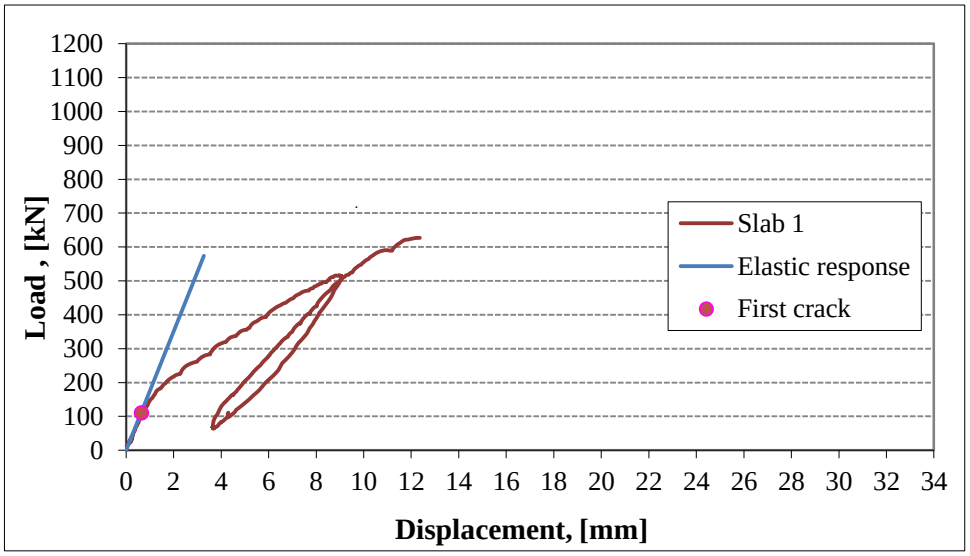

Figure 4.16: Load deformation behaviour of control specimen, Slab 1.

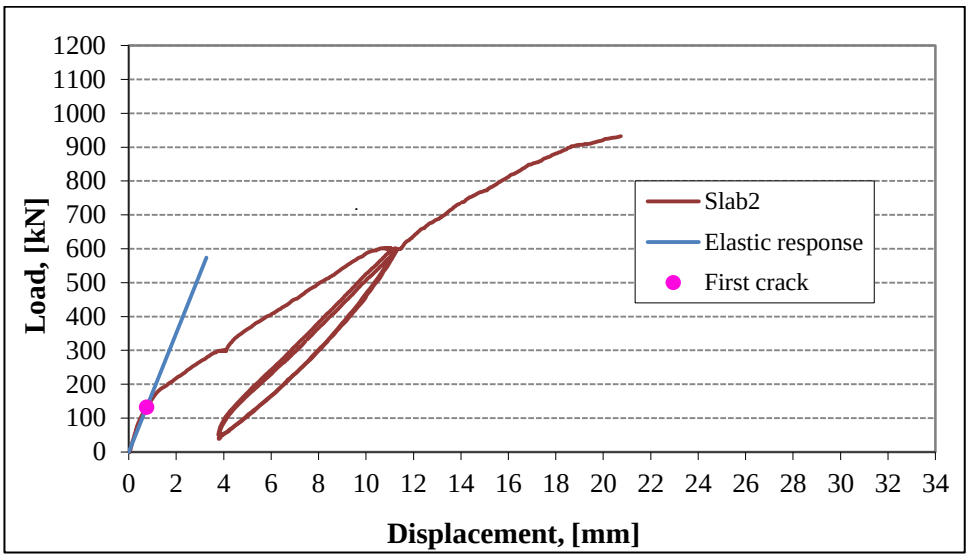

Figure 4.17: Load deformation behaviour of Slab 2.

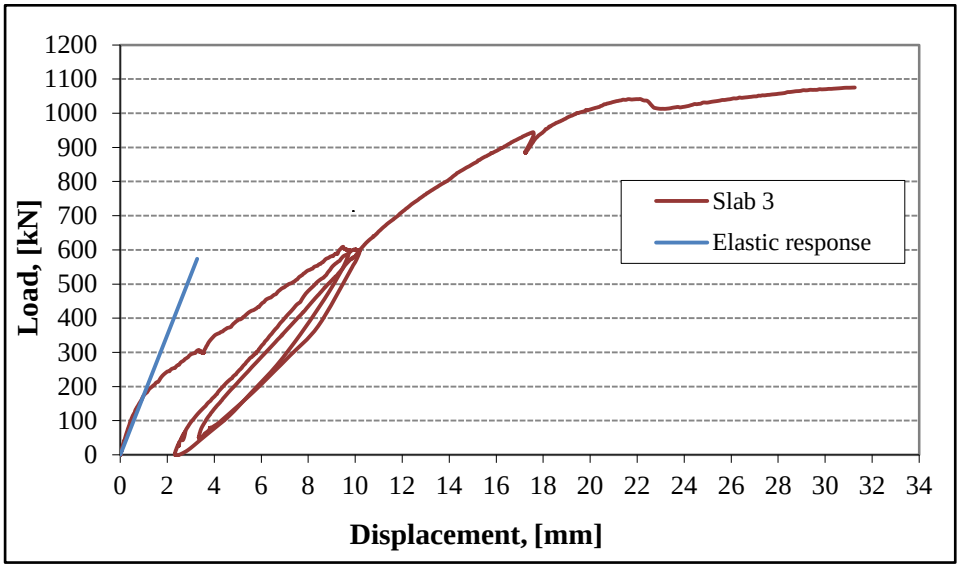

Figure 4.18: Load deformation behaviour of Slab 3.

As shown in Figures 4.16, 4.17 and 4.18 until first cracking, the slopes of the measured responses were in a good agreement with the elastic response. Due to difficulties in visually determining first cracking in the tested specimens, the point where the load-deflection response deviated from the initial elastic response gives an indication of the point of first cracking.

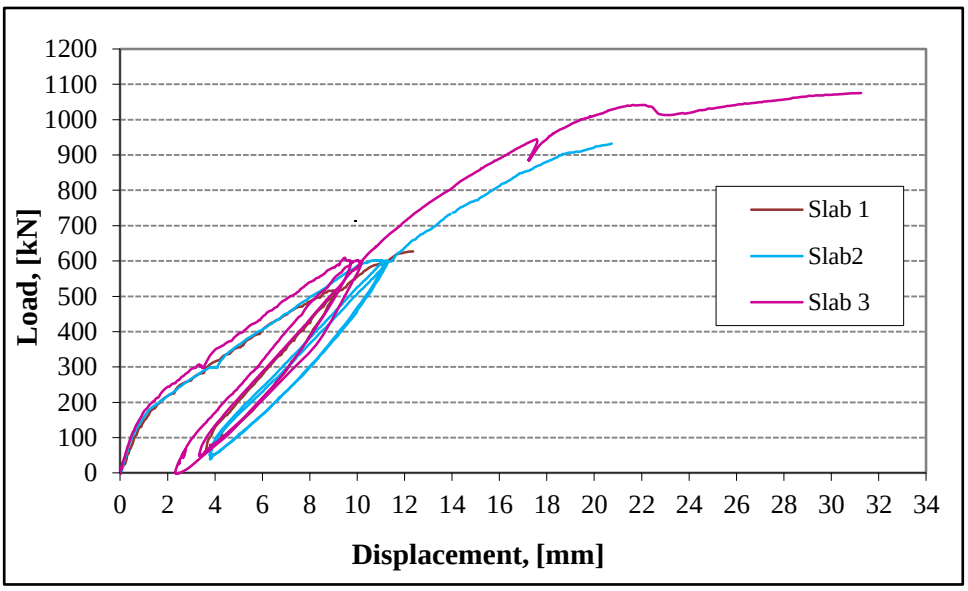

Figure 4.19: Comparison of load displacement behaviour of all tested slabs.

Load displacement behaviour of tested specimens shown in Figure 4.19 demonstrates that the use of shear reinforcement has negligible effect on initial stiffness and cracked stiffness. Slab 3 showed slightly higher crack stiffness compared to Slabs 1 and 2. This agrees with research results reported by Polak (1998b). They showed that for a given reinforcing ratio, the diameter of the reinforcing bars as well as spacing significantly affects the stiffness of the reinforced concrete member. Slabs with lower diameter of bars showed higher crack stiffness in their experiments. Table 4.7 summarizes the results of load-displacement measurements for all specimens.

Table 4.7: Properties of the tested slabs

Slab no.	f_{cu} (MPa)	ρ (%)	LSF shear reinforcement		Self weight (kN)	P_u (kN)	V_{test} * (kN)	Ultimate deflection (mm)
			First layer	Second layer				
Slab 1	34.7	1.61	No shear reinforcement		37	627	664	12.36
Slab 2	34.7	1.61	16	24	37	932	969	21.6
Slab 3	34.7	1.57	20	28	37	1075	1112	31.3

* V_{test}=Ultimate applied load to slab (P_u) + self-weight of the slab

4.3.6.2 Energy absorption capacity

The energy absorption capacity, *U*, of slab column connection referred to the area under the load-deflection curve of the slab (Figures 4.20 to 4.22) can be calculated by:

$$U = \int_0^{\Delta u} P d\Delta \qquad (4.3)$$

where *P* is the load applied and Δ is the displacement of the slab under loading. Table 4.8 shows the calculated values for energy absorption capacity parameters for the tested slab herein. The energy absorption capacities of Slab 2 and Slab 3 were 245 and 495 percents higher than the energy absorption capacity of control specimen (Slab 1). This was expected since Slab 2 and Slab 3 demonstrated more ductile behaviour compared to

control slab. Slab 3 had 202% higher energy absorptions compared to Slab 2 due to the higher amount of shear reinforcement.

Table 4.8: Calculated values for energy absorption capacity parameters for all slabs tested.

Test	Energy absorption capacity (kN.mm)
Slab 1	4853.3
Slab 2	11833
Slab 3	23902

4.3.6.3 Test Observations

Radial cracks formed in the middle of the slabs were observed to extend gradually toward the edges of slab. This was followed by the developments of circumferential cracks prior to punching shear failure. Typical development of cracking on the top face of the slab is shown in Figure 4.20.

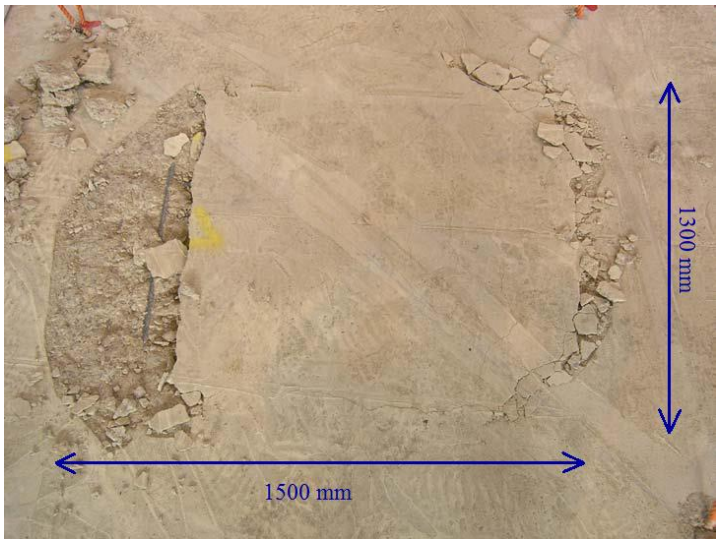

Figure 4.20: Typical development of cracking on the top face of the slab.

4.3.6.4 Strain Measurements in Shear Reinforcement

The details of measured load/strain relationships of testes slabs are given in Appendix C. Figures 4.21, 4.22 and 4.23 show the load/average strain relationship for typical legs of the shear reinforcement.

The gauges were deliberately positioned away from perforations as it was difficult to place them at perforated sections. By positioning the gauges away from the perforations, the effects of variations of strain across the width near perforations became negligible. The mean stresses at perforated sections can be estimated from the measured strains as $1.25E_s\varepsilon$ where E_s is the elastic modulus of the steel, assumed as 200 kN/mm^2, and ε is the average measured strain.

The applied load versus strain measurements with the their positions in the Slab 3 are shown in Figure 4.23 while for Slab 2, only the measured load-average strain are given on specific incremental load. In some cases both gauges in a pair failed to function due to damage during casting. The lines are drawn from readings at chosen load stages in 200 kN increments for Slabs 2 and 3. Prior to the onset of failure, they are continued up to the last stages at which stable readings were obtained. In Appendix C, the complete load/strain relationships for all gauges of each experiment are given.

The inner two layers of shear reinforcement developed strains distinctly higher than those in the outer layers in both the slabs examined here. Table 4.9 summarises the results for the inner layers at the last load increment for which strains are plotted.

Table 4.9: Strains of inner layers of shear reinforcement

Slab no.	Load (kN)	V/V_u	Microstrain		Stress (MPa)	
			Layer 1	Layer 2	Layer 1	Layer 2
Slab 2	900	0.97	1462	991	366	248
			(3589)	1217	-	304
				1303		326
				1495		375
Slab3	1000	0.93	805	730	201	183
			1322	1040	330	260
			1553	1122	388	280

Note 1) Strains given in parenthesis are values from single gauges and not means from pairs of measurements. Due to the unknown influence of bending in these cases, no stress values are given.
2) Stresses are values calculated as $1.25E_s\varepsilon$ (see text), i.e. for the net widths of the perforated sections.

From the five other cases listed above, the mean stress at 93% to 97% of ultimate load was 297 N/mm^2, with the means in the separate cases varying from 241 to 313 N/mm^2. The actual stresses at the most stressed levels of the legs would have been somewhat higher, due to bond between the locations of the gauges and those of maximum stresses. The bond was probably not very high as the strips are of smooth steel, thus the stresses above are probably consistent with EC2's unfactored limit stress of 334 N/mm^2 for slabs of the depth in question.

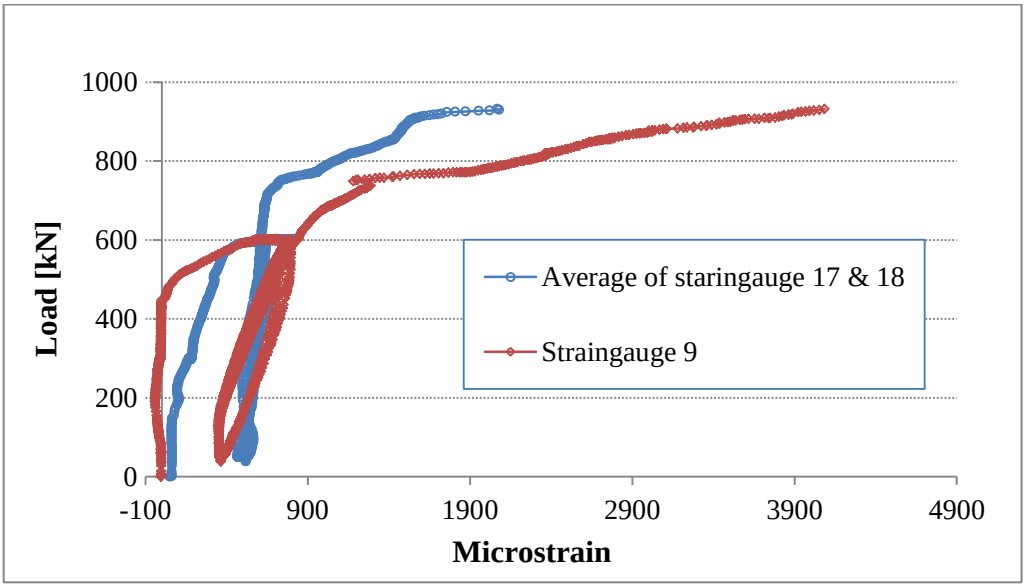

Figure 4.21: Load – average strain behaviour of shear reinforcement of Slab 3.

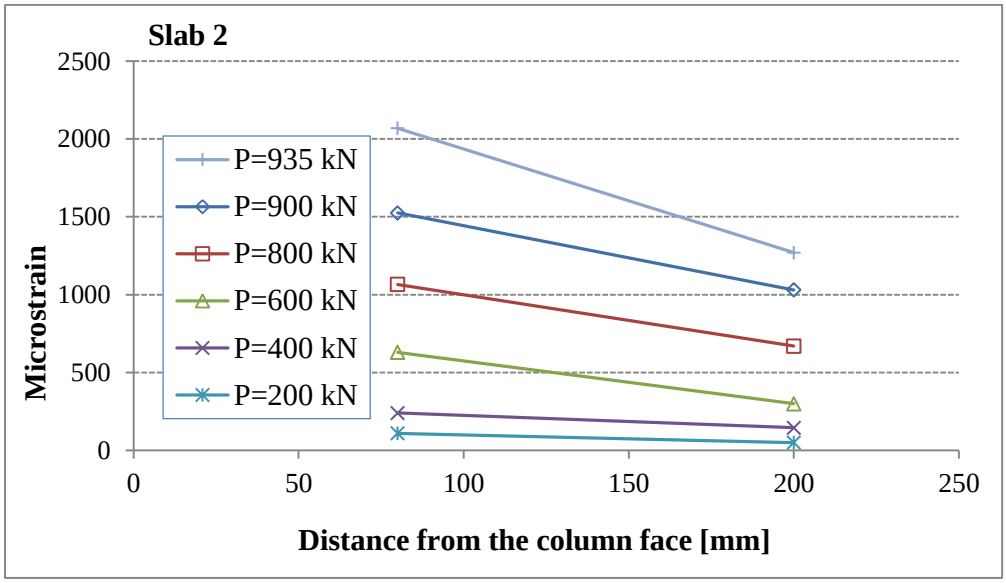

Figure 4.22: Strain gauge measurements of Slab 2.

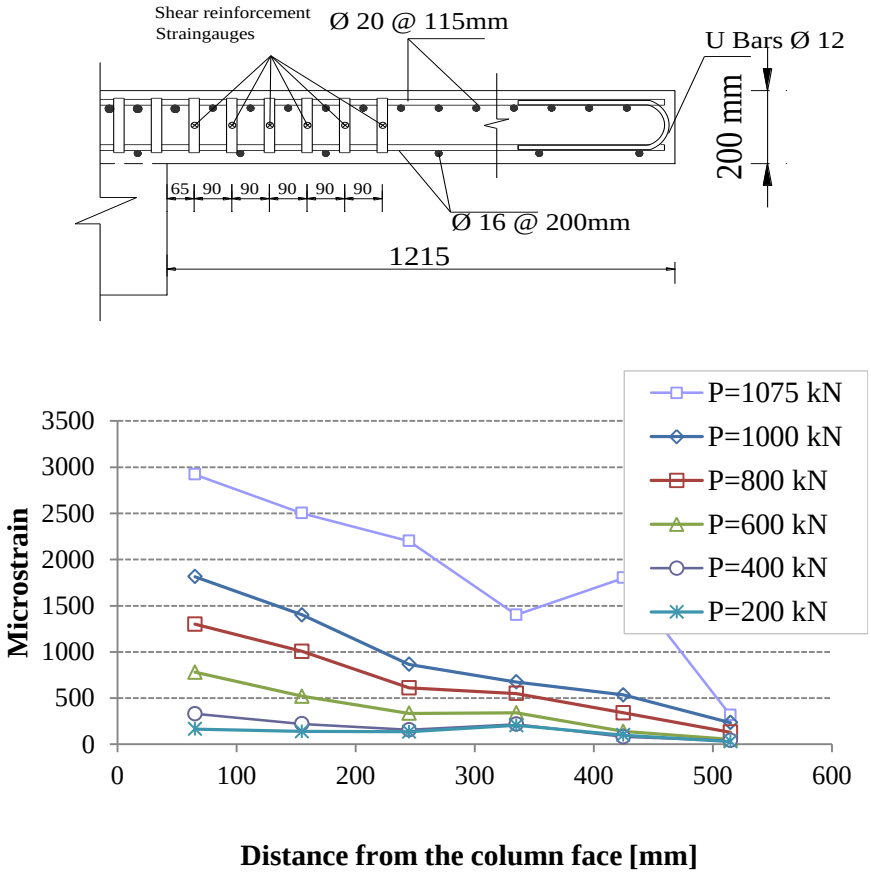

Figure 4.23: Strain gauge measurements of Slab 3.

Figures 4.22 and 4.23 show the applied load versus strain measurements of the LSF shear reinforcement from column face. In all two slabs the inner two layers of shear reinforcement developed strains distinctly higher than those in the outer layers and the Table 4.9 summarises the results for the inner layers at the last loads for which strains are plotted.

4.4 Comparisons with Code Predictions

In flat slab-column connections, the prediction of ultimate capacity is defined as the minimum of the flexural and the punching shear capacity of the slab. The flexural strength of the slab was determined using BS8110 based on the yield line method. Predictions of the code of standards and experimental results are compared and are

reported here. The calculated unfactored flexural capacity of Slabs 1 and 2 are 1350 kN while for Slab 3 is 1200 kN.

The partial safety factors or strength reduction factors are set equal to 1.0 for calculation of the shear capacity of the slabs according to BS8110, ACI 318-08 and EC2. The actual concrete compressive strength was taken from the control specimens and was used in the calculation of the punching shear capacity in the code equation. The prediction of the codes are summarised in Tables 4.10, 4.12 and 4.13. The yield strength of the steel strip was taken as 500 N/mm^2 as reported by the manufacturer.

4.4.1 ACI Prediction

It is worth mentioning that the shear reinforcement distribution did not meet the ACI code requirement totally, as for Slab 2 and 3, the shear reinforcement was spaced more than 0.5*d* and the first layer of the shear reinforcement was more than 0.5*d* away from column face for Slab 2. For Slab 3 the distance between the column face and the first line of LSF shear reinforcement was 60 mm which is in accordance with the ACI 318-08 design method. Considering the small thickness of LSF shear reinforcement, the contribution of LSF to the punching shear capacity was limited only for the first perimeter according to ACI 318-08 design method.

Failure loads and failure modes of experimental results using Code equations in ACI 318-08 are summarized in Table 4.10 for comparison. ACI 318-08 underestimates the punching shear capacity of slabs with shear reinforcement as it is clearly summarized in Table 4.10. The reason for this underestimation is the concrete contribution which was taken as 50% in the calculation of punching shear capacity where as full contribution of shear reinforcement legs within the perimeter was taken into consideration.

In the slabs tested with LSF shear reinforcement, the shear reinforcement contribution is less than half the concrete contribution. Hence, the total shear capacity of Slab 2, with the presence of LSF reinforcement, is calculated to be less than of shear capacity of a similar slab without LSF type of shear reinforcement, as shown in columns 2 and 4 of Table 4.10. The outcome of this approach obviously leads to very conservative results.

Table 4.10: Comparison of actual and predicted strength and modes of failures of tested slabs using ACI 318-08

Slab	Shear reinf. region within			Outside	V_{calc} (5)	V_{test}	$\frac{V_{test}}{V_{calc}}$	Mode of failure	
	V_n (1) (kN)	V_{max} (2) (kN)	V_n (3) (kN)	V_c (4) (kN)	(kN)	(kN)	(kN)	predicted	actual
Slab 1	-	-	534.5	-	534.5	664	1.24	punching	punching
Slab 2	459	810.0	534.5	1058	459	969	2.11	within	flexural + punching.
Slab 3	674	830.0	548.0	1235	674	1112	1.65	within	flexural + punching.

(1) $V_n = V_c + V_s$, $V_c = 0.167\sqrt{f_c}b_o d$, $b_o = 4(c+d)$

(2) $V_{max} = 0.5\sqrt{f_c}b_o d$

(3) $V_n = V_c$, $V_c = 0.33\sqrt{f_c}b_o d$, $b_o = 4(c+d)$ (considering similar slab without shear reinforcement)

(4) $V_c = 0.33\sqrt{f_c}b_o d$, (considering perimeter chamfered $d/2$ from the outermost shear reinforcement)

(5) $V_{calc} \leq \begin{bmatrix} V_n^{(1)} \\ V_{max}^{(2)} \\ V_c^{(4)} \end{bmatrix}$, while $\geq V_n^{(3)}$

4.4.2 BS 8110 and EC 2 Predictions

BS 8110 (1997) and EC2 (2004) require the provision of at least two layers of shear reinforcement within the control perimeter from the loaded area. The BS and EC design methods limit the spacing of the shear reinforcement not to exceed 0.75*d*. Slabs 2 and 3 were detailed in accordance with the BS 8110 (1997) design method. Tables 4.11 and 4.12 compare the predictions by BS 8110 and EC2 with the experimental results respectively.

Although the punching shear strength of the slab without shear reinforcement (Slab 1) is equal to the resistance predicted by BS, the ultimate resistance of the slabs with LSF shear reinforcements (Slab 2 and Slab 3) are lower than the predictions by BS. Due to the limited experiments on slabs with LSF shear reinforcement, it can be concluded that the BS 8110 method for slabs with stirrups cannot be applied directly to the slabs with LSF unless necessary modifications are made.

As shown in Table 4.12, the predictions by the EC 2 design method are not exactly the same as the experiments. This variation can be due to the detailing of the experiments in accordance with BS design method. Also, it should be noticed that EC 2 does not consider the grid type arrangement of shear reinforcement in the code and therefore more tests on grid type arrangement will be useful in order to adopt this arrangement in the code.

Table 4.11: Comparison of actual and predicted strength and modes of failures of tested slabs using BS8110 (1997)

SLAB	Within shear reinf. region		Without or outside shear reinf. region	$V_{max}^{(4)}$	$V_{test}^{(5)}$	$V_{calc}^{(6)}$	$\frac{V_{test}}{V_{calc}}$	Mode of failure	
	$V_k^{(1)}$ (kN)	$V_{max}^{(2)}$ (kN)	$V_{ck}^{(3)}$ (kN)	(kN)	(kN)	(kN)		pred.	actual
Slab 1	-	-	665	1205	664	665	1.00	Punching	
Slab 2	1087	1330	1263	1205	969	1087	0.89	within	Flexural + Punching
Slab 3	1240	1352	1361	1229	1112	1240	0.90	within	Flexural + Punching.

(1) $V_k = A_{sv} f_{yv} + v_{ck} Ud$, $v_{ck} = 0.79 (100A_s/bdf_{cu})^{1/3} (400/d_{eff})^{1/4}$, $U=4c + 12d$ considering that shear reinforcement within first perimeter 1.5d from column face.

(2) $V_{max} = 2V_c$ considering a similar slab without shear reinforcement at critical section 1.5d from column face.

(3) $V_{ck} = v_{ck}Ud$, using square perimeter 1.5d from the last layer or using $U=4c+12d$ for Slab 1

"Contd"

(4) Maximum shear capacity at column face, shear stress less than $0.8\sqrt{f_{cu}} = 4.71$ N/mm^2 or 5 N/mm^2

(5) V_{test} = ultimate load applied to slab + self weight of slab

(6) V_{calc} is the lesser of $V_k^{(1)}$, $V_{max}^{(2)}$, $V_{ck}^{(3)}$, $V_{ck}^{(4)}$, V_{flex}, V_{flex} is the flexural capacity based on yield line method by using BS8110

Table 4.12: Comparison of actual and predicted strength and modes of failures of tested slabs using EC2 (2004)

Slab	Within shear rein. region		Without shear rein.	$V_{calc}^{(4)}$	$V_{test}^{(5)}$	$\frac{V_{test}}{V_{calc}}$	Mode of failure	
	$V_{Rd,cs}^{(1)}$ (kN)	$V_{max}^{(2)}$ (kN)	$V_{Rd,c}^{(3)}$ (kN)	(kN)	(kN)		pred.	Actual
Slab 1	-	-	713	713	664	0.93	punching	
Slab 2	824	1546	1366	824	969	1.18	within	flexural + punching
Slab3	1185	1546	1780	1185	1112	0.94	within	flexural + punching

(1) $V_k = A_{sv} f_{yv} + v_{Rd,c} Ud$, $v_{Rd,c}$, where $v_{Rd,c} = 0.18 \times \xi \times (100 \times \rho \times f_{ck})^{1/3}$, $U=4(c + \pi d)$, considering that shear reinforcement within first perimeter 2.0d from column face

(2) Maximum shear stress at the column face $v_{max} = 0.5v.f_{cd}$, where $v=0.6[1-f_{ck}/250]$

(3) $V_{ck} = v_{Rd1}Ud$, using square perimeter 1.5d from the last layer or using $U= 4(c+\pi d)$ for Slab 1

(4) V_{calc} is the lesser of $V_{Rd,cs}^{(1)}$, $V_{max}^{(2)}$, $V_{Rd,c}^{(3)}$

(5) V_{test} = ultimate load applied to slab + self weight of slab

4.5 Discussions and Conclusions

The samples of LSF shear reinforcement tested under unbent conditions demonstrated that the imperforated strip were equivalent to Class C reinforcement; however, the effects of perforation were to reduce the thicker sizes to a thickness of 1.6 mm for Class B and 2.0 mm for Class A. For the strip with 1.2 mm thickness, the LSF was categorized to type C. It is worth noting that above statement is based on very limited tests.

Observations from the test slabs demonstrated that the rupture of the LSF leg occurred at perforated section closed to bend therefore, perforations at the bend region of LSF strips during manufacturing process is not recommended.

Out of all the slabs tested, the LSF type of shear reinforcement was found to be very effective against punching shear. Increases of strength at internal columns reached about 46% and 67% for slabs 2 and 3 respectively as compared with slab 1 which was left with no shear reinforcement (control specimen). Also increases of 74 % and 152 % in ultimate displacements were achieved for Slab 2 and Slab 3 compared to the control slab (Slab 1) respectively. Slabs with LSF shear reinforcement showed higher energy absorption capacities compared to the control specimen. The effective depth and ratio of flexural reinforcement between these slabs were very small and were negligible.

It is observed that the ultimate strength of the internal slab without shear reinforcement (Slab 1) is equal to the resistance predicted by BS8110's expression for characteristic punching strength. However, the experimental strengths of the two slabs with LSF shear reinforcement are below the calculated values. Therefore, the BS8110 design method for slabs with stirrups as shear reinforcement needs necessary modifications in order to be directly applicable to the slabs with LSF reinforcement. Since the test slabs were detailed in accordance with BS8110, the analysis might therefore not be in a good agreement with EC2 and ACI 318-08. It was also shown that the predictions of punching shear capacity of Slabs 2 and 3 by ACI were very conservative since detailing of the LSF shear reinforcement was not in accordance to the ACI design method.

EC 2-2004 suggests the usage of lower stresses for shear reinforcement in thin slabs which is in good agreement with the measurement of strains of LSF strips in the tested slabs. Although the predictions of punching shear capacities obtained by EC2 were

satisfactory, EC2 does not consider the grid-type arrangement for shear reinforcement and therefore further experiments is essential to adopt this arrangement in the code.

Both types of laps for the LSF shear reinforcement used in the tests appeared to behave satisfactorily.

Chapter 5
NUMERICAL MODELING

5.1 Introduction

This chapter is a study on the numerical modelling on punching shear behaviour of slab column connections. The finite element analysis was carried out using ABAQUS, a general purpose FE package. This chapter provides further insights into the experimental results in Chapter 4 to evaluate the capability of the corresponding theoretical predictions and to support the parametric studies in Chapter 6. The material properties and nonlinear solutions were implemented in the FE model and are therefore discussed here in detail for completeness and are not the major focus of the thesis. A sensitivity study based on an FE model of Slab 1 (Chapter 4) is reported, which examines the model's dependence on the variation of user defined parameters. Following a detailed understanding of the advantages and the limitations of the package, experiments in Chapter 3 and experiments carried out by Li (1997) were re-analyzed. Finally, conclusions were drawn regarding the applicability and limitations of the current model in the analysis of perforated LSF strips.

5.2 Material properties

5.2.1 "Concrete smeared cracking" vs. "Concrete damage plasticity"

In this section different constitutive material models for concrete are discussed. ABAQUS offers three material models for modelling the nonlinear behaviour of concrete. These are namely: *concrete smeared cracking*, *brittle cracking* and *concrete damage plasticity*. Brittle cracking can only be used in dynamic analysis in ABAQUS/Explicit therefore is not addressed in this thesis. *Concrete smeared cracking* and *concrete damage plasticity*, were evaluated to verify their capabilities in modelling the slabs tested herein. For this purpose, Slab 1 was used to perform the evaluation. The disadvantages of smeared cracking model are also briefly explained. The concrete damage plasticity model is described in detail in Appendix D which was implemented in the finite element program used in this thesis. Further details on constitutive material

models for concrete can be found in Karihaloo (2003), Chen (1982), Kupfer *et al*., (1969), Malm (2006) and Malm (2009).

As briefly discussed in Appendix D, Concrete smeared cracking uses the associated flow rule which overestimates the volumetric plastic strain due to simplification of the compressive behaviour. The model uses a fixed angle crack model to detect the cracks results in shear stress locking problem. This can lead to convergence problems and causes the analysis to stop in early loading due to numerical instability.

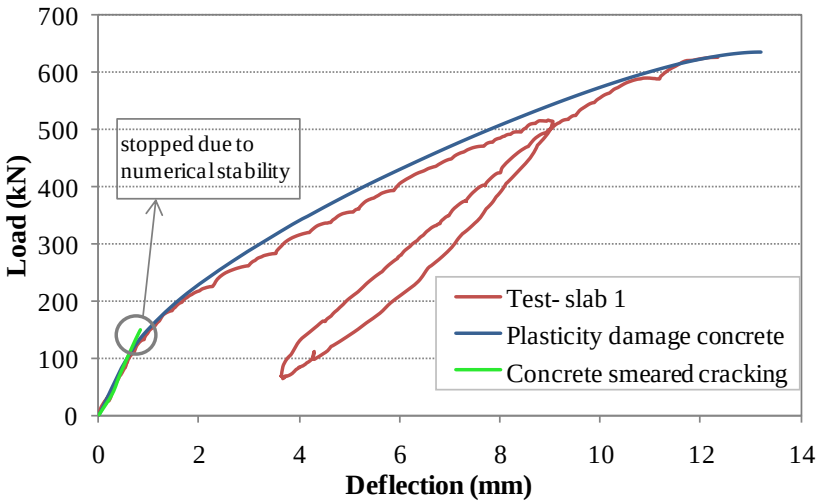

Figure 5.1: Comparison of load-deflection behaviour of Slab 1 based on smeared cracking and damage plasticity models.

Figure 5.1 shows that the concrete damage plasticity model is able to predict the behaviour of Slab 1 up to failure while smeared cracking model stops in early stage of loading due to numerical stability problems.

5.2.2 Concrete Damage Plasticity

Plasticity theory is a mathematical representation of the mechanical behaviour of solids. It can be used for translation of physical reality for ductile materials such as metals or a model that approximates the behaviour under certain circumstances for brittle materials such as concrete. In problems where the tension, with the crack development, plays a significant role, such as shear failure in reinforced concrete structures, the usual procedure is to apply plasticity theory in the compression zone and treat the zones in

which at least one principal stress is tensile by one of several versions of fracture mechanics (Lubliner *et al*., 1989).

Kupfer *et al*., (1969) carried out tests on biaxial loading of concrete specimens (200×200×50 mm). They found that the various critical surfaces in stress space are usually similar. Concrete can show a significant volume change when subjected to severe inelastic loading. Figure 5.2 (a) shows that the increase in volume can be more than twice as large for the hydrostatic compressive stress state σ_1/σ_2= -1/-1. The points marked in stress-volumetric strain diagram (Figure 5.2 (a)) represent the limit of elasticity, the point of inflection in the volumetric strain, the 'bendover' point corresponding to the onset of instability or localisation of deformation and the ultimate load. The critical stress surfaces related to these material states are shown in Figure 5.2 (b) (Kupfer *et al*., 1969). The same results were not found for concrete under triaxial compression tests specially for the case of hydrostatic pressure; under these condition it was found that the hardening goes on indefinitely (Lubliner *et al*., 1989). This means that while the yield surface is closed, the failure surface is open in the direction of hydrostatic pressure.

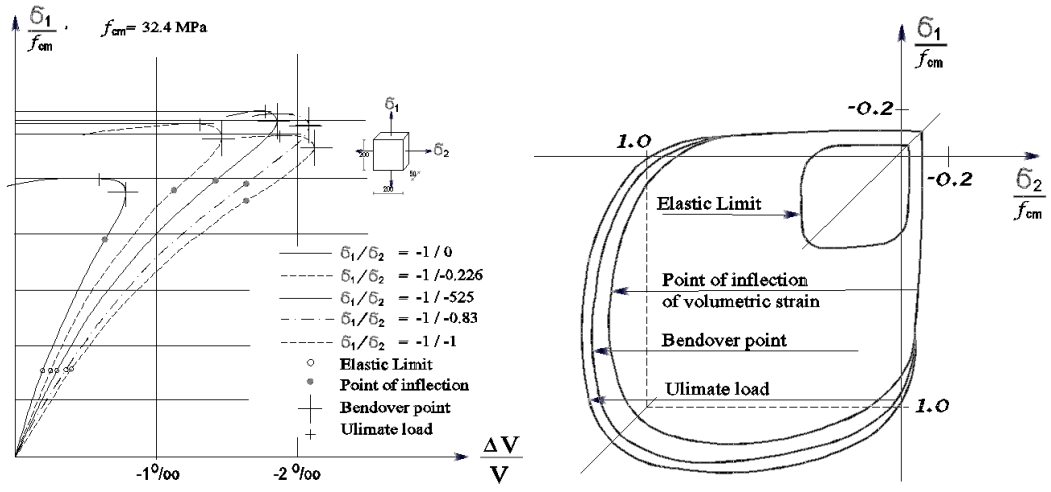

(a) (b)

Figure 5.2: (a) Volumetric strain of concrete under biaxial compression, (b) typical loading curves of concrete subjected to biaxial stresses. (Adopted from Kupfer *et al*., 1969).

Since the critical surfaces are similar in the biaxial behaviour of concrete, a yield function is used in plasticity based models. The size of yield function is based on the

material properties defined for the uniaxial behaviour of concrete. The yield surface is defined as the material no longer acts elastic and the failure surface is based on the ultimate strengths. This means that in the biaxial tensile meridian of the yield surface is equal to the failure surface. In compression, the material is usually assumed to be initially elastic up to 30-60 % of the compressive strength (Chen, 1982). There are several failure (or yield) criteria developed for concrete materials (reported by Lubliner *et al*., 1989) such as Drucker-Prager and Mohr-Coulomb criteria. For steel usually the Von Mises failure criteria is used (further details can be obtained in ABAQUS user's manual, 2008). According to Lubliner *et al*., (1989), these criteria do not represent experimental results for concrete precisely unless they are suitably modified. For instance, one modification is to use a combination of the Mohr-Coulomb and Drucker-Prager yield functions, where the Drucker-Prager is used for biaxial compression and the Mohr-Coulomb is used otherwise. In Figure 5.3, the Drucker-Prager and concrete failure surfaces in three dimension are shown schematically.

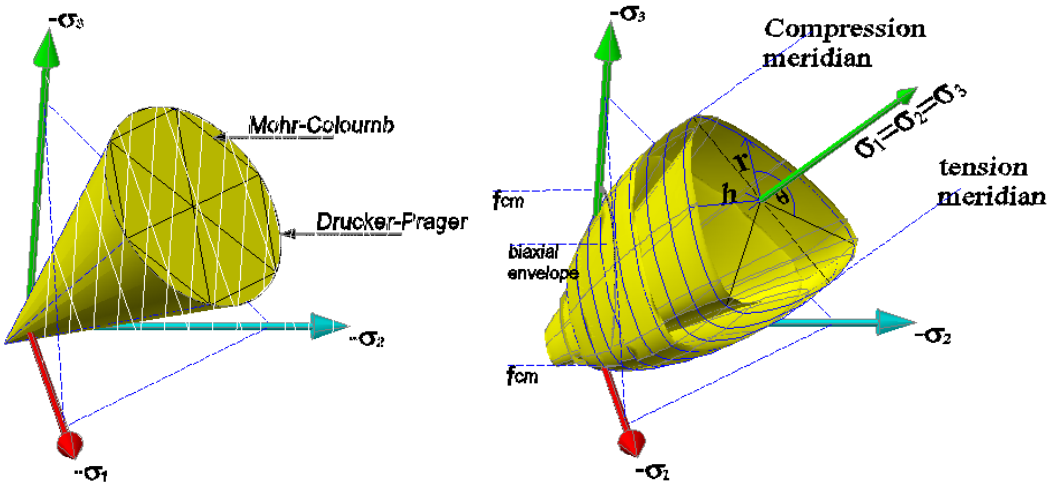

Figure 5.3: Drucker-prager failure surface and concrete triaxial failure space.

The biaxial yield function used in concrete damage plasticity was developed by Lubliner *et al*., (1989) which also includes the modifications that was proposed by Lee and Fenves (1998) (cited in ABAQUS Manual). It is vital to understand the constitutive parameters which describe the material properties in finite element modelling to obtain

authentic results. Therefore, brief descriptions of "failure criteria of concrete", "flow rule" and "dilatancy in the concrete damages plasticity model" are given in Appendix D.

A parametric study for dilation angle is carried out in order to determine the optimised value to be implemented in the numerical analysis. Dilation angle measures the inclination of the plastic potential which reaches for high confining pressure. Low values of the dilation angle produce brittle behaviour while higher values produce more ductile behaviour. A parametric study on dilation angle for Slab 1 is presented in Figure 5.4. Figure 5.4 shows that the difference in the behaviour of the slab is fairly small when the dilation angle is between 20º to 40º. It is noticed that the difference is insignificant when the dilation angle is between 30º to 40º. In this thesis a dilation angle of 31º was used. Malm (2009) also made the same conclusion on dilation angle for the analysis of a reinforced concrete beam subjected to four-point bending test. He used a dilation angle of 35º and 38º in his analysis. Jankowiak and Lodygowski (2005) presented a work on identification of dilation angle for the use in ABAQUS. They determined a dilation angle of 38º based on minimisation of the error of the biaxial failure envelope of Kupfer et *al*., (1969) and the yield surface in ABAQUS.

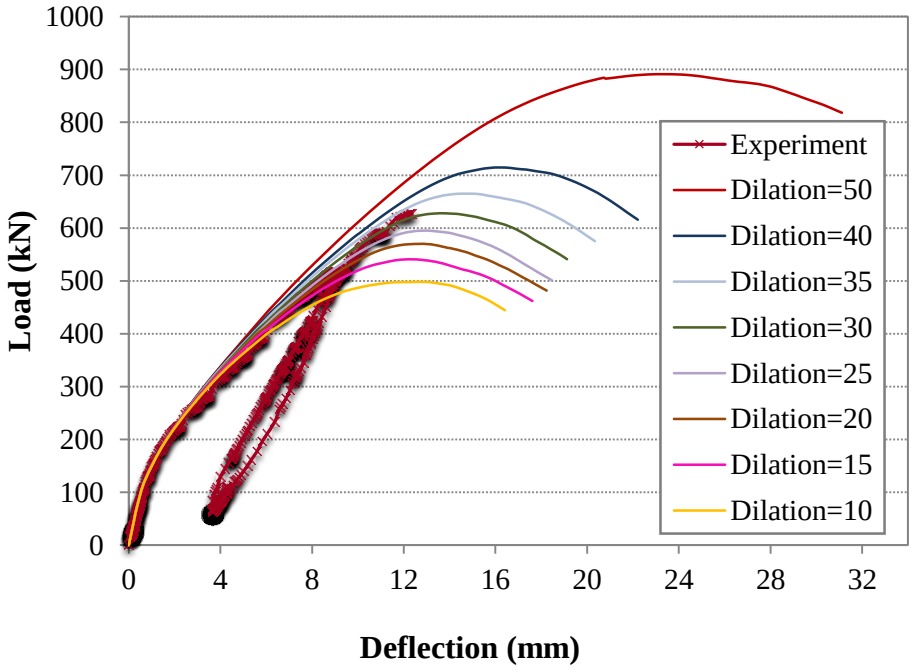

Figure 5.4: Parametric study on the effect of dilation angle on the response for Slab 1.

5.2.3 Compressive Behaviour

In this study the uniaxial tensile and compressive responses of the concrete are used along with the concept of a damage plasticity model. The uniaxial compressive concrete model from Eurocode 2 (EC-2, 2004) was adopted in this thesis (Figure 5.5). The stress-strain relationship is expressed as follows

$$\sigma_c = f_{cm}\frac{K\eta - \eta^2}{1+(K-2)\eta} \tag{5.1}$$

where $\eta=\varepsilon_c/\varepsilon_{c1}$, $\varepsilon_c=0.0007f_{cm}^{0.31}<0.0028$, $K=22[f_{cm}/10]^{0.3}$ and $\varepsilon_{cu1}=0.0035$ for $f_{cm}<58$MPa.

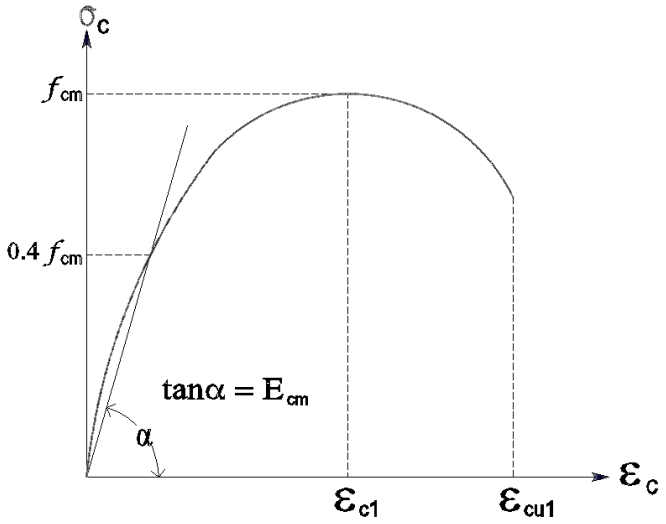

Figure 5.5: Stress-strain compression curve for concrete

In this thesis, the concrete stress strain curve was adjusted to continue beyond the crushing point to avoid stopping the analysis.

5.2.4 Tensile Behaviour

Under uniaxial tension the stress strain response follows a linear elastic relationship until the value of the failure stress, f_t, is reached and this is shown in Figure 5.6. The failure stress corresponds to the start of micro-cracking in the concrete material. A softening stress-strain response is used beyond the failure stress to represent the formation of macro cracks, which induces strain localization in the concrete structure. ABAQUS provides two approaches to describe the softening behaviour of cracked

concrete. The first method is based on strength criteria whereas the other approach adopts fracture energy cracking criteria. The approach based on the stress-strain relationship will introduce mesh sensitivity into the results if significant regions of the model do not contain reinforcement, (ABAQUS user's manual, 2008). It means that the analysis will not converge to a unique solution.

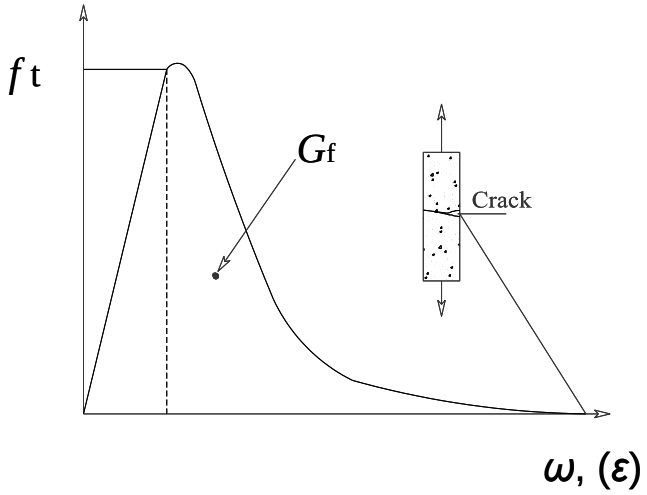

Figure 5.6: Crack opening with fracture energy (adopted from Malm 2006).

The fracture energy criterion which was developed by Hillerborg *et al*., (1976) overcomes the mesh sensitivity issues for the former approach. The crack behaviour of concrete was described based on the fracture energy. The fracture energy, G_f, is a material parameter that describes the amount of energy required to open a unit area of a crack. The area under stress-displacement curve (Figure 5.6) corresponds to the fracture energy.

Three different stress-displacement curves can be used to model tension softening. They are linear, bilinear and exponential which are based on analytical expressions derived from curve-fitting of experimental test data. The simplest way to introduce crack is to use linear approximation. The crack opening corresponding to a stress free crack with linear tension stiffening can be calculated as shown in the Equation 5.2.

$$\omega_c = \frac{2G_f}{f_t}. \tag{5.2}$$

Linear and bilinear tension softening models are used extensively in modelling plain concrete however, Malm (2006) reported that according to Karihaloo (2003) the exponential tension softening model is by far the best and most accurate model. Figure 5.7 illustrates the bilinear and exponential tension softening models.

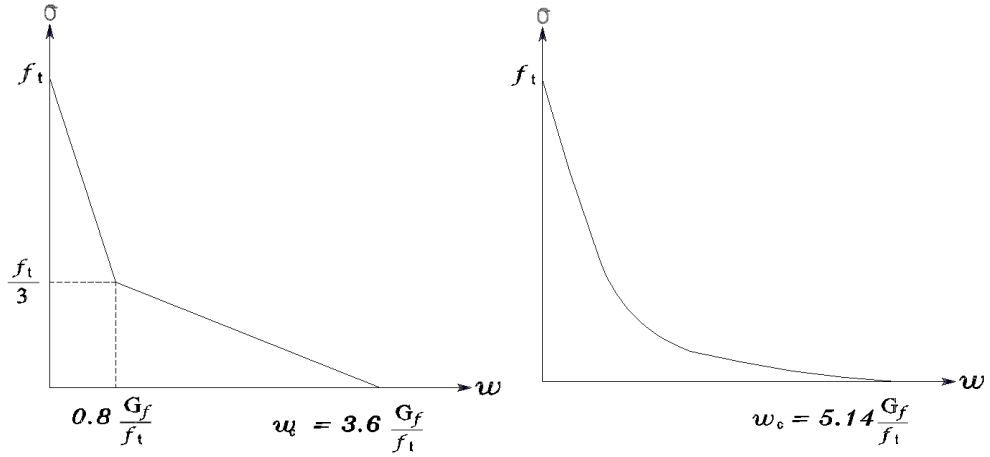

(a) (b)

Figure 5.7: (a) Bilinear and (b) exponential tension softening model.

The following equations were used to developed exponential tension softening model:

$$\frac{\sigma}{f_t} = f(\omega) - \frac{\omega}{\omega_c} f(\omega_c) \tag{5.3}$$

where $f(\omega)$ is a displacement function given by

$$f(\omega) = \left[1 + \left(\frac{c_1\omega}{\omega_c}\right)^3\right] \exp\left(-\frac{c_2\omega}{\omega_c}\right) \tag{5.4}$$

where, ω is the crack opening displacement and ω_c is the crack opening displacement at which stress can no longer be transferred (ω_c=5.14 G_f /f_t for normal weight concrete). c_1 is a material constant and is 3.0 for normal weight concrete. c_2 is a material constant and is 6.93 for normal weight concrete.

The fracture energy of concrete, G_f, is calculated from Equation 5.5 suggested by MC90 (1991) is used to estimate G_f in this chapter.

$$G_f = G_{f0}\left(\frac{f_{cm}}{f_{cm0}}\right)^{0.7} \tag{5.5}$$

where $G_{f0} = 0.0024 + \frac{0.0053 d_{max}^{0.95}}{8}$, d_{max} is the maximum aggregate size, f_{cm} is the mean concrete compressive strength, and f_{cm0}=10MPa.

5.3 Nonlinear solution

In this section, the solutions for numerical instability are discussed. The Newton-Raphson technique, given in Appendix E, is implemented for the FE analysis in ABAQUS.

5.3.1 Numerical Instability

Concrete material models which develop strain softening and stiffness degradation, often experience severe convergence problems. To avoid some of these convergence difficulties, viscoplastic regularisation of the constitutive equation could be used. Another way of reducing convergence difficulties is the use of artificial damping in combination with concrete damaged plasticity model. This may introduce large artificial damping forces on elements undergoing severe damage since ABAQUS calculates the damping stress based on the undamaged elastic stiffness (ABAQUS, User's Manual 2008). Another technique is to change the convergence criteria and allow a larger number of iterations before convergence is checked. The other option also suggested by Malm and Holmgren, (2008) is the possibility of converting a static problem to a quasi-static problem to use an explicit solution. Malm (2006) also suggested reducing the tolerances to 10% of default value and increasing the number of iterations between to two and four times of default value, before the rate of convergence is checked.

Analysis presented in this thesis, are performed with an implicit solution scheme. Also the simulations performed in ABAQUS had a trend to interrupt due to convergence difficulties. The most effective method to continue beyond this in the analysis suggested by the author was to increase the number of iterations. This will lead in small time increments when reaching a point with convergence difficulties and thereby increasing the time. This would be done by addition of Volume-proportional damping to the model to stabilize the unstable static problem in ABAQUS/Standard (ABAQUS user's manual, 2008). To obtain an optimum value for the damping factor requires performing post-

analysis comparison of the energy dissipated by viscous damping (ALLSD) to the total strain energy (ALLIE) (ABAQUS user's manual, 2008).

5.4 Slab modelling techniques

Reinforced concrete slabs can be modelled by layered or discrete modelling techniques. In a layered approach the concrete section is divided into a set of layers by employing layered shell elements, whereas the reinforcement is smeared into a layer between concrete layers. However, shell elements in ABAQUS cannot model a punching shear failure since this type of elements treat the shear based on computing the elastic shear and superimposing them onto the flexural deformations (ABAQUS Theory manual). The total transverse deformation is essentially flexural deformation which incorporates the transverse shear deformation. This leads to the total deformations reasonably approaching the actual deformation, indicating predictions of the load displacement curves of the experiments. Although shell elements are able to predict the structural responses reasonably well, it is not possible to model the shear cracking. Therefore, a do you mean plate as in a particular FE element or do you mean plate as in slab? plate discretised with shell element cannot fail in shear. This allowed the total deformations to approach the actual deformation accurately, representing the predictions of the load displacement curves of the experiments.

In the discrete approach which was adopted in this thesis, concrete is modelled by three dimensional solid elements while the reinforcement is modelled by beam, truss or shell elements (beam elements are used to model the flexural reinforcement and shell elements are used to model the LSF reinforcement strips). The concrete and reinforcement can be connected by two mehods. In the first method, a bond element is inserted at the interface to connect the corresponding degrees of freedom for both concrete and reinforcement nodes, while the interaction response can be modelled. In the second method a perfect bond is assumed between concrete and reinforcement by embedding the reinforcement to the concrete. The later method was adopted in this study since it is computationally more efficient when used with a damaged plasticity model.

5.5 Solid element

Wide ranges of three-dimensional (3D) continuum elements are offered by ABAQUS. For instance, the ABAQUS/Standard solid element library includes first-order (linear) interpolation elements and second-order (quadratic) interpolation elements in one, two, or three dimensions. They can be used in almost any linear/nonlinear stress-displacement analysis and to model nearly any shape. They are more accurate, provided they are not distorted, particularly for hexahedral elements.

5.6 Investigation of model parameters

After identifying the material models and analysis techniques as well as choosing an appropriate meshing element, the various modelling parameters were investigated next. For this purpose, a sensitivity study which investigates the effect of user-defined parameters values on the FE structural response was performed. Mesh sensitivity was carried out to define the appropriate mesh size. Then, the effect of tension stiffening was investigated in order to accurately predict the behaviour of test slabs.

5.6.1 Description of the model

Depending on the geometry of the slabs, symmetric in one axis or symmetric in two axes (bisymmetric or mono-symmetric), either one-quarter or one-half of the slabs was modelled. The loads were applied through the periphery of the slabs.

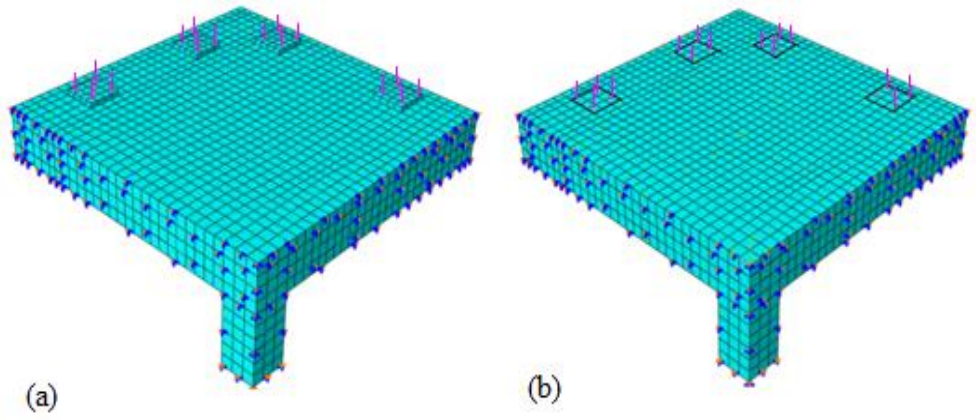

Figure 5.8: (a) Load applied through the steel loading plates to the slab, and (b) Load applied as pressure to the surface of the slab.

As shown in Figure 5.8, the load can be applied by two methods in the FE analysis: (a) the load can be applied on steel plates which are tied to the slab top surface, and (b) the load can be applied directly on the surface of the slab as a pressure force on the surface. It was found that the behaviour of slab is nearly the same for both methods however introducing the plates can cause significant numerical convergence problems in some slabs. Therefore method (b) in which the load is applied directly to the surface of the slab was adopted in this study.

5.6.2 Mesh Sensitivity

Since punching shear failure is characterized by crack localisation in certain areas, the mesh density is a key factor. Therefore, a mesh sensitivity analysis was carried out in this study. Also the sensitivity to the mesh size is linked to the tension stiffening option. Hence, the sensitivity of the FE model to mesh size should be seen in view of the tension stiffening values used. As discussed in section 5.2.4, tension stiffening in ABAQUS can be introduced by the strain approach and the displacement approach (fracture energy approach). In strain approach, for the same tension stiffening, the response for the denser mesh becomes softer.

For this purpose, Slab 1 with different mesh sizes was considered here. The nominal mesh sizes were 160 mm, 100 mm, 70 mm, 50 mm and 25 mm. For every case, the aspect ratio was kept to one as far as possible. As shown in Figure 5.9, the mesh is assumed to be converged when an increase in mesh density had negligible effect on the results obtained. For mesh sensitivity, a linear displacement-type, tension stiffening curve based on fracture energy which defines the ultimate displacement value u_0 at the crack when the tensile strength drops to zero. A typical displacement value of u_0=0.15 mm yielded different responses for the meshes examined here.

Based on the results shown in Figure 5.9, the convergence study implies that the 50 mm mesh size converges to both 25 mm and 75 mm mesh sizes. A mesh size of 160 mm appears to have unstable behaviour after first cracking. Therefore, a mesh size of 50 mm was adopted for the rest of the analysis.

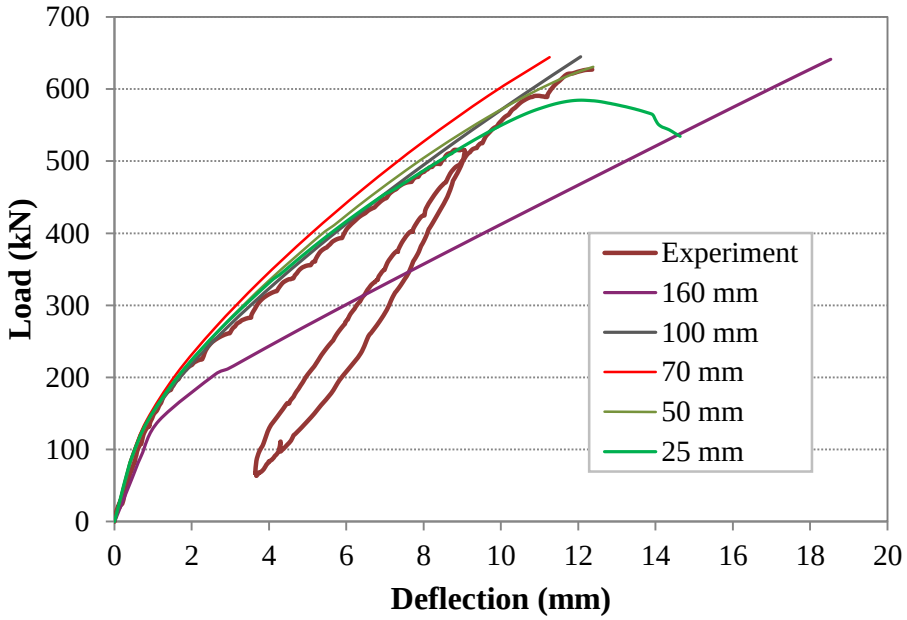

Figure 5.9: Mesh sensitivity for Slab 1.

5.6.3 Tensile Strain Sensitivity

Tension stiffening can be used to describe the stiffness reduction behaviour of concrete after cracking. It accounts for the contribution of concrete in handling the tensile stress in the post-cracking stage. For reinforced concrete members, the bond interaction contributes to the stiffening in the post-cracking behaviour. It is well established that the tension stiffening effect of reinforced concrete is dependent on the percentage of steel, diameter of steel reinforcement, distribution of reinforcement and bond stresses. For over-reinforced structural elements, the ultimate load capacity prediction is not affected by the tension stiffening since the ultimate capacity could be reached prior to yielding of the reinforcement.

The same value of the strain-type tension stiffening is expected to yield softer responses for denser meshes and stiffer responses for coarser meshes. This could be roughly explained by the definition of the cracking strain as $\varepsilon = u_0 / L$. If ε is the tensile strain at which concrete loses its tensile strength and u_o is the opening of crack at which the concrete tensile strength becomes zero, then ε equals u_o/L, where L is the characteristic element size. Since the crack opening u_o is independent of the element size, it is seen that for an increase in the element's characteristic length L, the strain-type tension stiffening value ε is decreased.

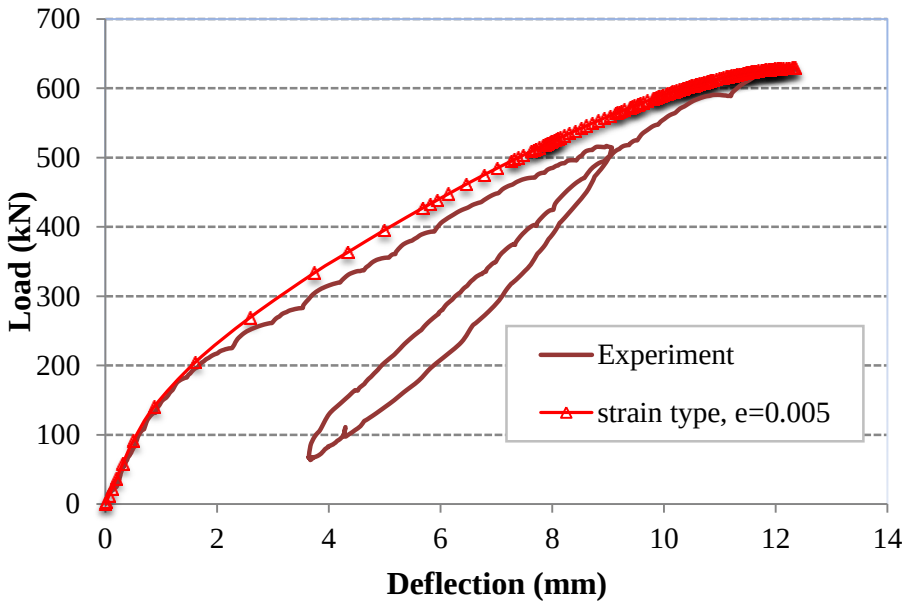

Figure 5.10: Load-deflection curve based on two tension stiffening approaches (strain type and displacement type).

The selection of appropriate values for the tension stiffening parameter depends on the modelling experience of the user. For example, for a linear descending stress strain CEB-FIP (cited in Barzegar and Schnobrich, 1990) suggested the use of 20 to 80 times of the cracking strain, where the higher values corresponds to high reinforcement ratios. However, in this study the value of tensile strain when the tensile stress vanishes was calibrated. The calibration was based on the agreement of the FE results and the available experimental results.

5.6.4 Effect of concrete tensile strength

For the tests carried out in this thesis, the tensile strength was not measured experimentally however, the empirical equation for the calculation of tensile strength of concrete beams and slabs suggested by EC2 (2004) was adopted. As shown in Figure 5.11, the tensile strength of the slab has a significant effect on the first crack load. It is observed that the use of lower tensile strength leads to underestimation of the applied load at a given displacement in the model. This is true because the lower tensile strength, results in earlier microcracking which leads to lower stiffness behaviour of the slab up to failure.

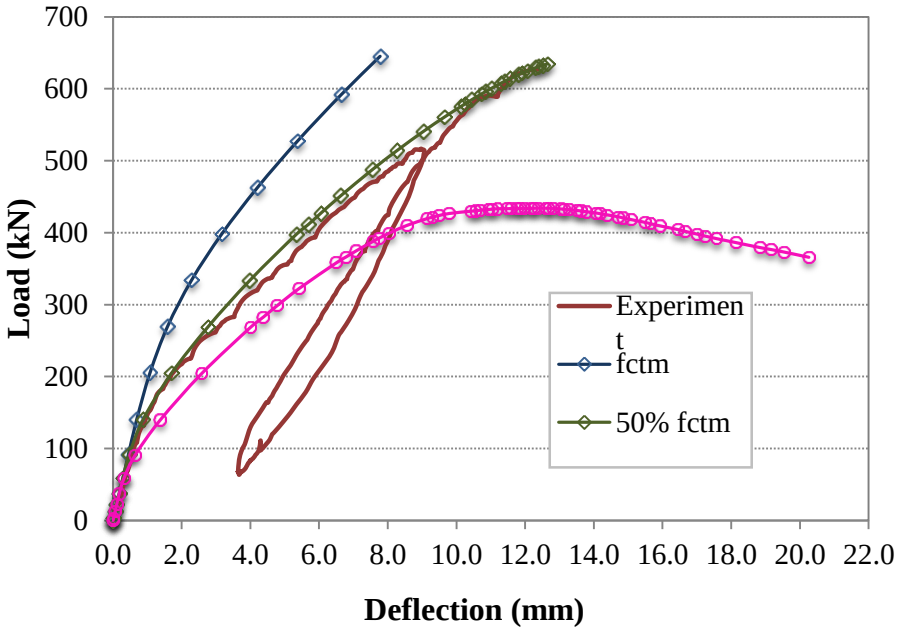

Figure 5.11: Load-deflection curve of Slab 1 for different values of concrete tensile strength.

In this study, a reduced concrete tensile strength ($f_{ct} = 0.5 f_{ctm}$) was adopted for the analysis of slabs. This can be accepted based on the fact that the rupture modulus of slabs mostly depends on the reinforcement ratio since it affects the drying shrinkages of the surrounding concrete. Therefore, low reinforced slabs could easily allow development of shrinkage cracks between the reinforcing bars. Subsequently, such slabs may experience lower cracking loads compared to beam members. The Canadian standard (CSA, A 23.3-04) also suggests using 50% of the mean tensile splitting strength to account for the shrinkage effects in the slabs.

5.6.5 Element Type

Solid brick elements were used to model the slabs. ABAQUS /Standard library includes first-order (linear) interpolation elements and second-order (quadratic) elements. Figure 5.12 compares the predictions from FE analysis using first-order (e.g. C3D8, C3D8R) and second-order (e.g. C3D20R) elements while typical values were used for other parameters. The element adopted for the analysis was element C3D8, as other element types had convergence problems and were stopped in early loading stage.

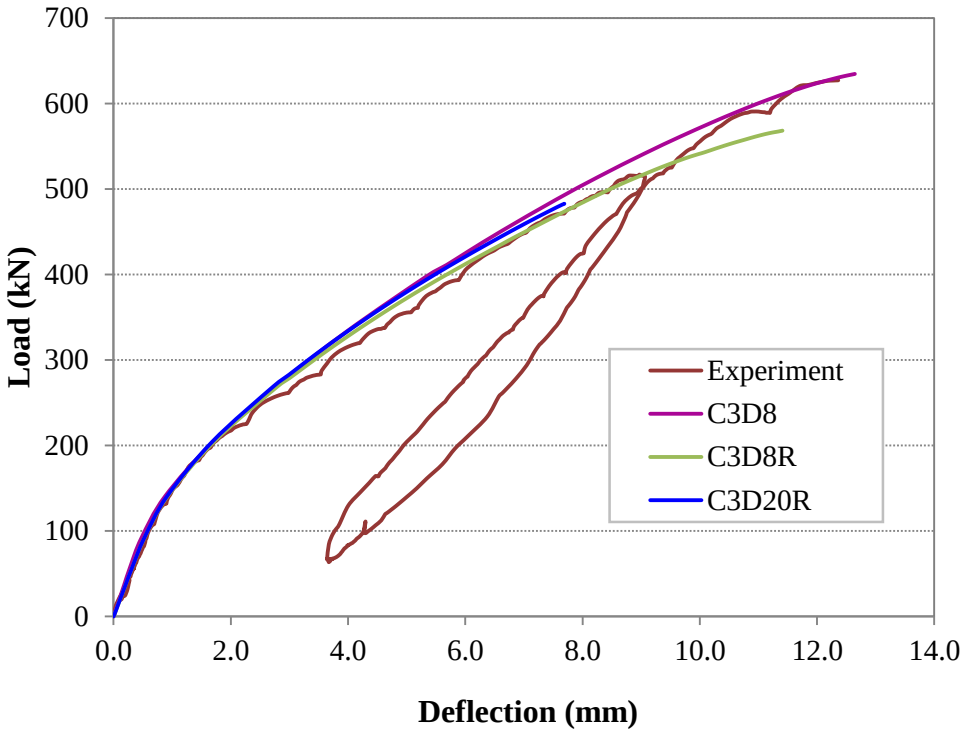

Figure 5.12: Load deformation behaviour of Slab 1 with different element types.

5.7 Failure Type

Three main types of failure are:

- Steel yielding spreads over a wide area of the slab (flexural failure)
- Steel yielding followed by concrete crushing (flexural punching failure);
- Concrete compressive crushing (pure punching shear failure)

If flexural reinforcement yields well before failure and yielding spreads over a wide area of the slab at failure, the slab fails in a pure flexural mode. In this scenario the yield line pattern is fully developed.

The next failure mode is somewhere between the pure flexural failure and pure punching failure. The flexural strength may be reached with yielding of the tensile steel reinforcement locally around the column followed by crushing of the concrete in the compression zone. In this case the yield line pattern is not fully developed.

Higher flexural reinforcement ratios provide higher flexural capacities in slabs. Therefore, the typical failure mode is the crushing of the concrete rather than yielding in flexural reinforcement. This type of failure is obviously brittle.

5.8 Discussion on Numerical Results

The punching behaviour of the test slabs reported in Chapter 4 and experiments carried out by Li (1997) are discussed in this section. The behaviour depicted by FE analysis was investigated and compared to the experimental results. The comparison between the experiments and predicted values was based on the following aspects of structural behaviour:

- The load deflection behaviour;
- Strains in LSF shear reinforcement and internal steel reinforcement;
- Distribution of concrete strains;
- Crack pattern;
- The mode of failure.

The discussion on punching shear behaviour of slab-column connections concludes with a summary of factors that affect behaviour such connections. Also the adequacy of numerical analysis technique used here is discussed.

5.8.1 Slabs without shear reinforcement

In this section Slab 1 reported in Chapter 4 and Slab PSSA from Li (1997) were investigated using numerical simulations. Slab 1 was designed to have a high flexural capacity while Slab PSSA was designed for a low reinforcement ratio. Due to double symmetry both in geometry and loading of Slab 1 and Slab PSSA, only a quarter of the tested slabs were modelled. Based on the mesh sensitivity analysis carried out in the previous section, a mesh size of 40 mm was used for modelling Slab 1 while a mesh size of 25 mm was used for Slab PSSA. In order to get the best fit of results with experminet with experiments, the level of tension stiffening was calibrated.

5.8.1.1 Load deformation behaviour

Figure 5.13 (a, b) shows the comparison of load deformation of Slab 1 and Slab PSSA with the ABAQUS models.

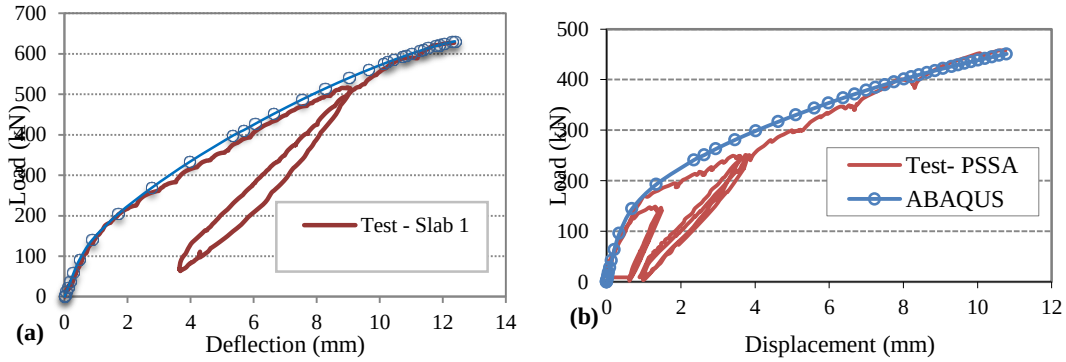

Figure 5.13: Comparison between experimental and model predictions of slabs without shear reinforcement: (a) Slab 1, (b) Slab PSSA.

It can be seen from the Figure 5.13 that both models are in good agreement with the experiments. ABAQUS models for both the slabs showed stiffer behaviour when the slabs start to have flexural cracks compared to the test results. Flexural cracks start to happen at loads over 200 kN. This is expected since in the FE model, a full bond between the flexural reinforcement and concrete was assumed by embedding the flexural reinforcement to the concrete.

5.8.1.2 Internal steel reinforcement

No strain gauges in the flexural reinforcements of Slab 1 were used in the experiments however strain gauges on the flexural reinforcement were installed for Slab PSSA as reported by Li (1997).

Slab1

Based on the yield-line analysis carried out in Chapter 4, it was shown that flexural reinforcement in Slab 1 yields when the load approaches 1100 kN. Figure 5.14 shows the load-stress relationship for the flexural reinforcement in Slab 1 which is in good agreement with yield line analysis as well. Figure 5.14 shows that the maximum stress

in the flexural reinforcement which is 320 MPa. As shown in Figure 5.15 only very limited areas of the top reinforcement which are close to the column faces have stresses higher than 200 MPa while for compression reinforcement only one reinforcement bar inside the column reaches 200 MPa as shown in Figure 5.15.

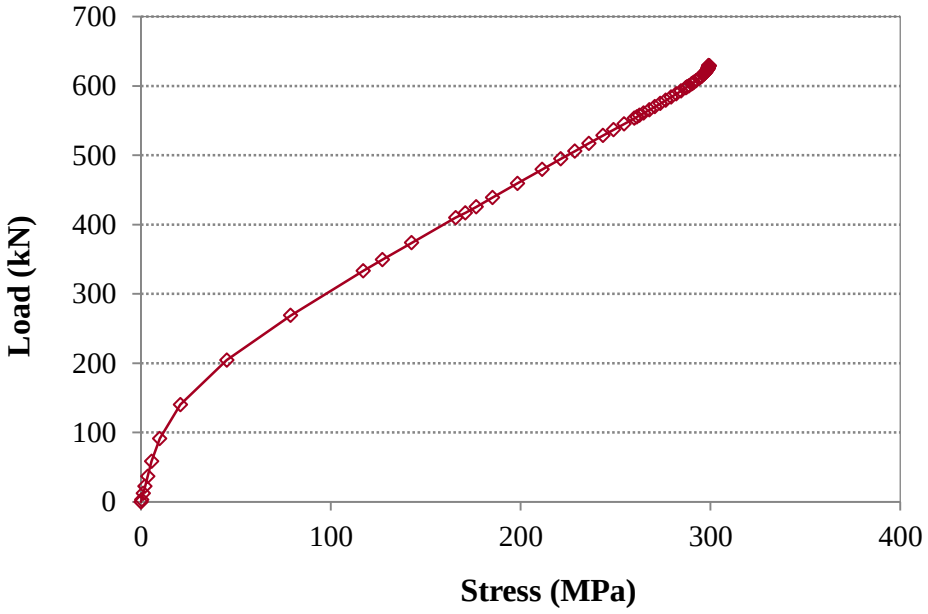

Figure 5.14: Load-Stress behaviour of flexural reinforcement at the column face of the Slab 1.

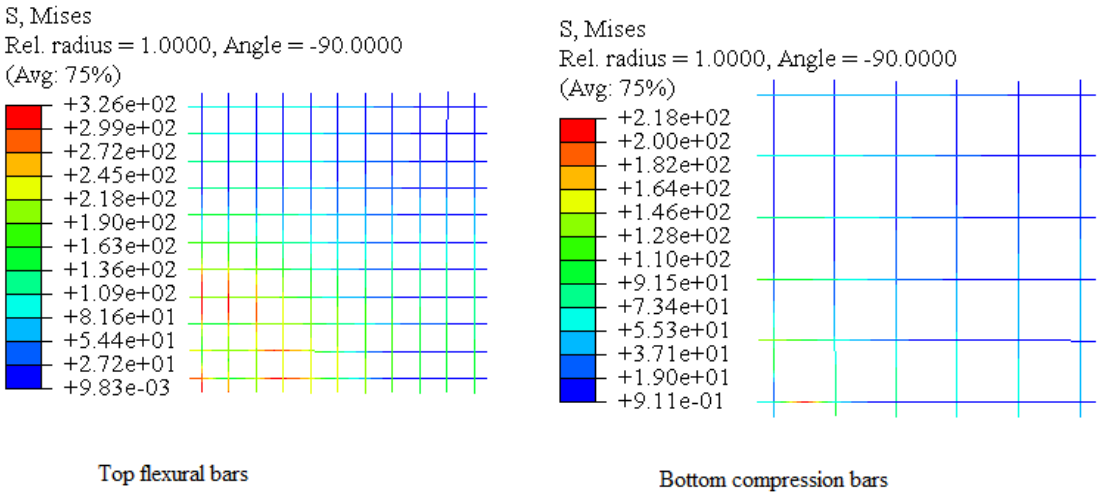

Figure 5.15: Stresses on the tensile and compression reinforcement of Slab 1 under loading.

Slab PSSA

It has been highlighted earlier in this chapter that FE analysis smears the effect of cracks and, in itself, does not differentiate between cracked and uncracked sections. The possible prediction of the experimental deflection is obtained by the level of tension stiffening in FE analysis. Therefore, prediction of the average rebar strain between cracks is likely to be obtained by FE analysis. This strain is usually less than that of an individual rebar and this is shown in Figure 5.16.

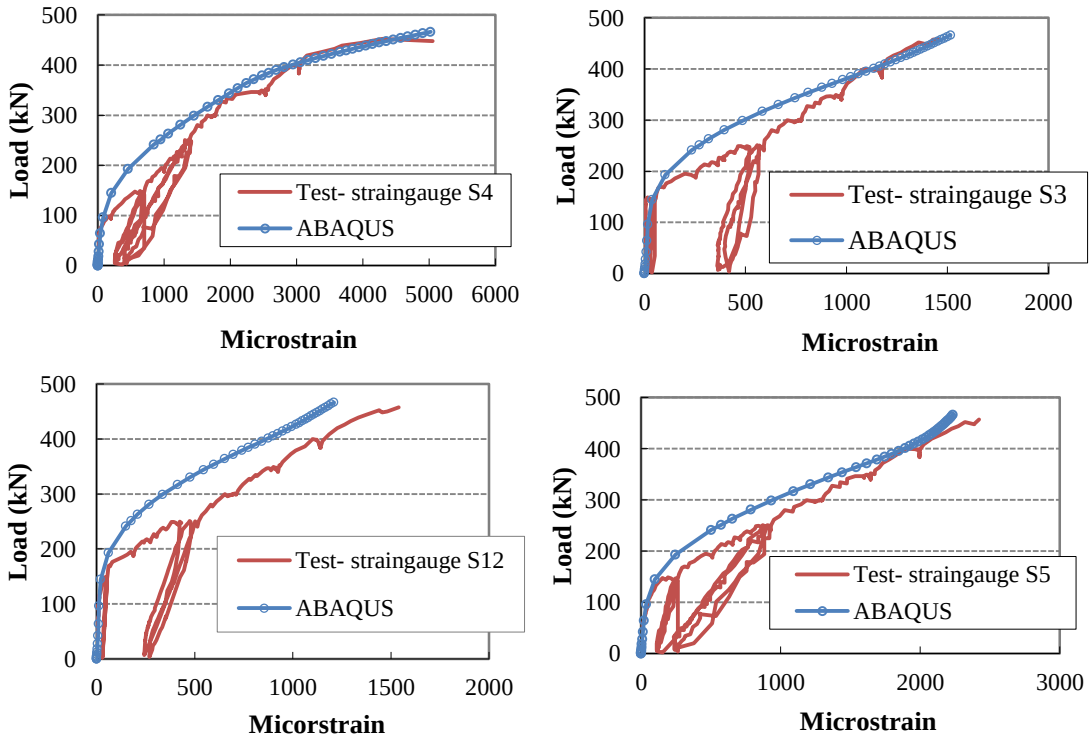

Figure 5.16: Comparison between strain gauge measurements of flexural reinforcement in Slab PSSA with ABAQUS predictions.

It is clear from Figure 5.16 that the predictions of reinforcement strains using FE model reasonably well. However, the rebar strain predicted by the model is less than the actual reinforcement strain in Gauges S3 and S4. On the other hand, up to a load of about 400 kN, the strain predicted by the model compares very well with the measured strain in strain gauge S3 and S4. It has to be noted that predicted strain is underestimated in the model beyond this load. The amount of tension stiffening added to the concrete model

could be the possible explanation for such discrepancies. As it is well recognised, the punching behaviour is characterised by localization of strains near to the loading area, contrary to the flexural behaviour in which cracking is nearly distributed all over the member. Hence, the model may overestimate the strains in some regions while underestimating them in other regions. It is shown here that Slab 1 failed in pure punching failure mode while Slab PSSA failed by flexural and punching shear mode.

5.8.1.3 Strain in Concrete

Unlike the smeared crack concrete model, the concrete damaged plasticity model does not have the notion of crack developing at the material integration point. However, it is possible to introduce the concept of an effective crack direction with the purpose of obtaining a graphical visualization of the crack pattern in the concrete structure. Different criteria can be adopted within the framework of scalar-damage plasticity for the definition of the direction of cracking. Following the model presented in Lubliner *et al*., 1989, it is assumed that the crack initiates at points where the tensile equivalent plastic strain (ABAQUS parameter PEEQT) is greater than zero and the maximum principal plastic strain is positive. The direction of the vector normal to the crack plane is assumed to be parallel to the direction of the maximum principal plastic tensile strain. Using this approach, the coloured area shown in Figure 5.17 indicates places where the concrete tensile equivalent plastic strain value was greater than zero. Figure 5.17 shows the direction of cracks parallel to the maximum principal plastic compressive strain (red arrows).

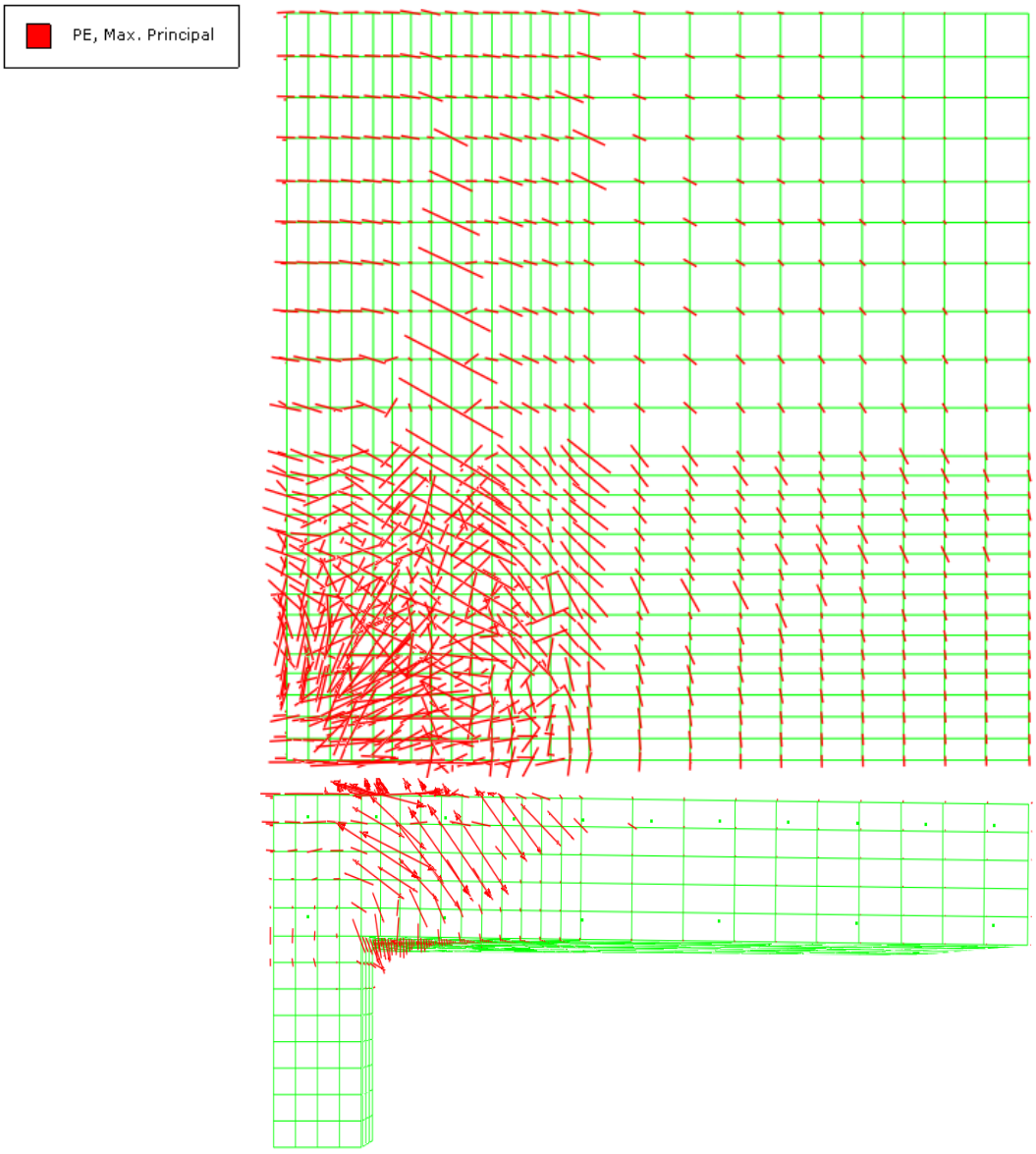

Figure 5.17: Crack pattern of Slab 1 at failure load.

Figure 5.18 shows the failure cone which was developed at failure load from FE analysis for Slab 1 and Slab PSSA.

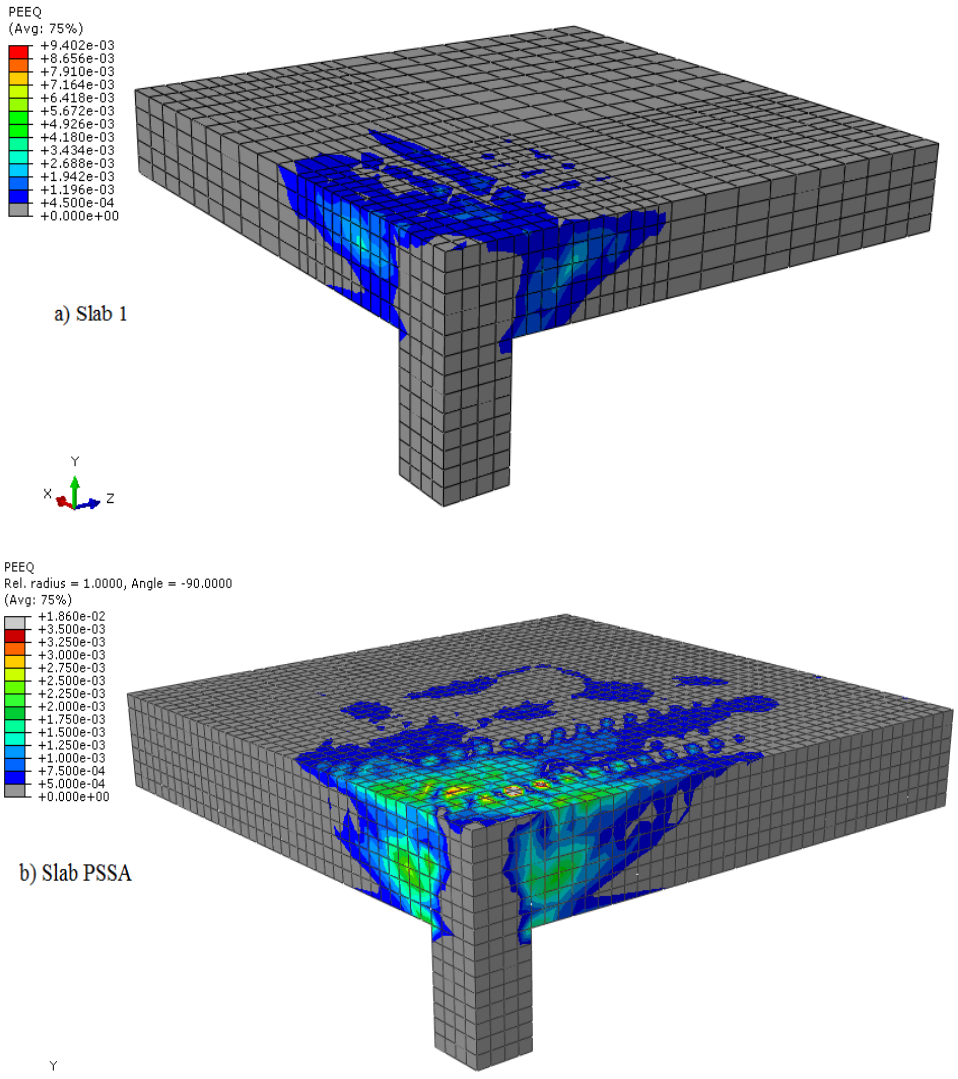

Figure 5.18: Crack pattern in the post-peak regime- simulation in terms of maximum principle strains.

5.8.2 Slabs with Shear reinforcement

Due to symmetry both in geometry and loading of Slab 2, only half of the slabs tested were modelled while a quarter of Slab 3 was modelled due to double symmetry of the Slab 3 in geometry and loading. Mesh sizes of 35 mm and 45 mm were used for Slab 2 and Slab 3 respectively. Flexural reinforcement was modelled using 2D beam elements while LSF shear reinforcement was modelled using shell element as shown in Figure 5.19.

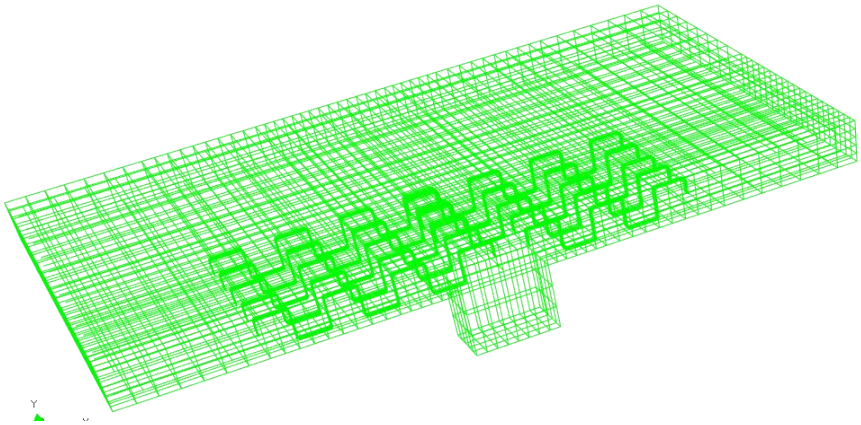

Figure 5.19: Typical view of Slab 3 modelled in ABAQUS.

Figure 5.20 (a, b) show the comparison of load deformation of Slab 2 and Slab 3 with the ABAQUS model. It can be seen from the Figure 5.20 that the load deflection predictions of both models are in a very good agreement with the experiments.

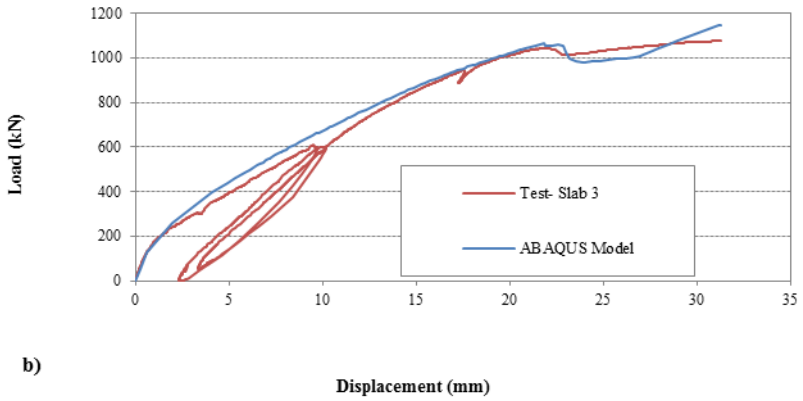

Figure 5.20: Comparison between experimental and model prediction of slabs with shear reinforcement: (a) Slab 2, (b) Slab 3.

Unless low tension stiffening is used in the FE model, which is adopting a smeared cracking approach with full bond assumption, the additional deflection due to the slip between concrete and steel reinforcement cannot be predicted. However, the ultimate load and corresponding deflection are underestimated by such low tension stiffening.

Figure 5.20 (b) shows that the model slightly underestimates the load capacity of connection when the deflection of slab is between 23 to 27 mm.

Internal steel reinforcement

No strain gauges were installed in flexural reinforcement of Slabs 2 and 3. Therefore, the stress-strain behaviour of the steel bars is investigated only numerically here. Both Slabs 2 and 3 showed yielding of the steel reinforcement in a very small area of the bars close to the column. Comparison of the stress-strain behaviour of steel bars of Slab 1 with Slab 2 and 3 confirms the failure type of the Slab 2 and 3 to be flexural and punching.

LSF reinforcements

As discussed in Chapter 4, strain gauges for LSF shear reinforcement were installed for both Slabs 2 and 3. In this section, the predicted stress-strains from the numerical models are compared with the experimental results. The details of the position of the strain gauges for Slab 2 and 3 are given in Figure 4.15 in Chapter 4.

5.8.2.1 Slab 2 and Slab 3

Slab 2

Figures 5.21, 5.22 and 5.23 show the FE predictions of the stress-strain curves of LSF shear reinforcement in perimeter 1, 2 and 4 respectively compared to measured stress-strain curves. These figures show a good agreement with experiments up to the failure load.

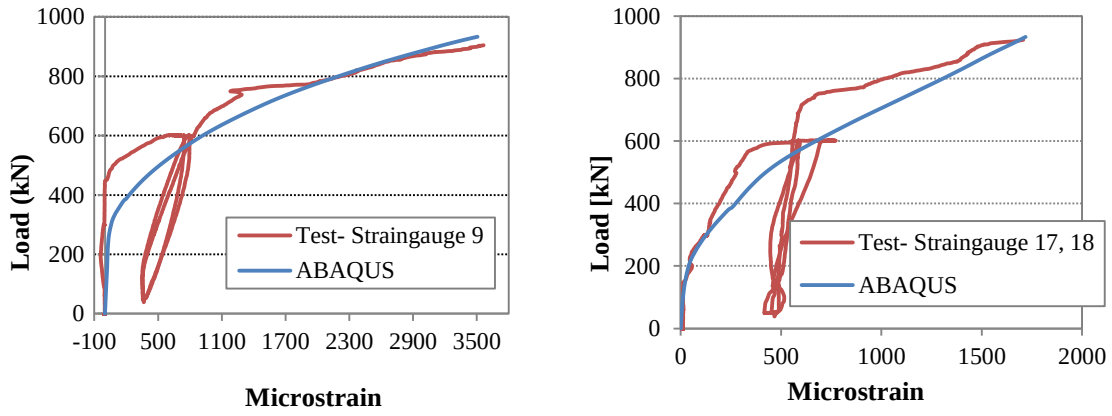

Figure 5.21: Comparison between strain gauge measurements of Slab 2 with ABAQUS model for shear reinforcement in first perimeter.

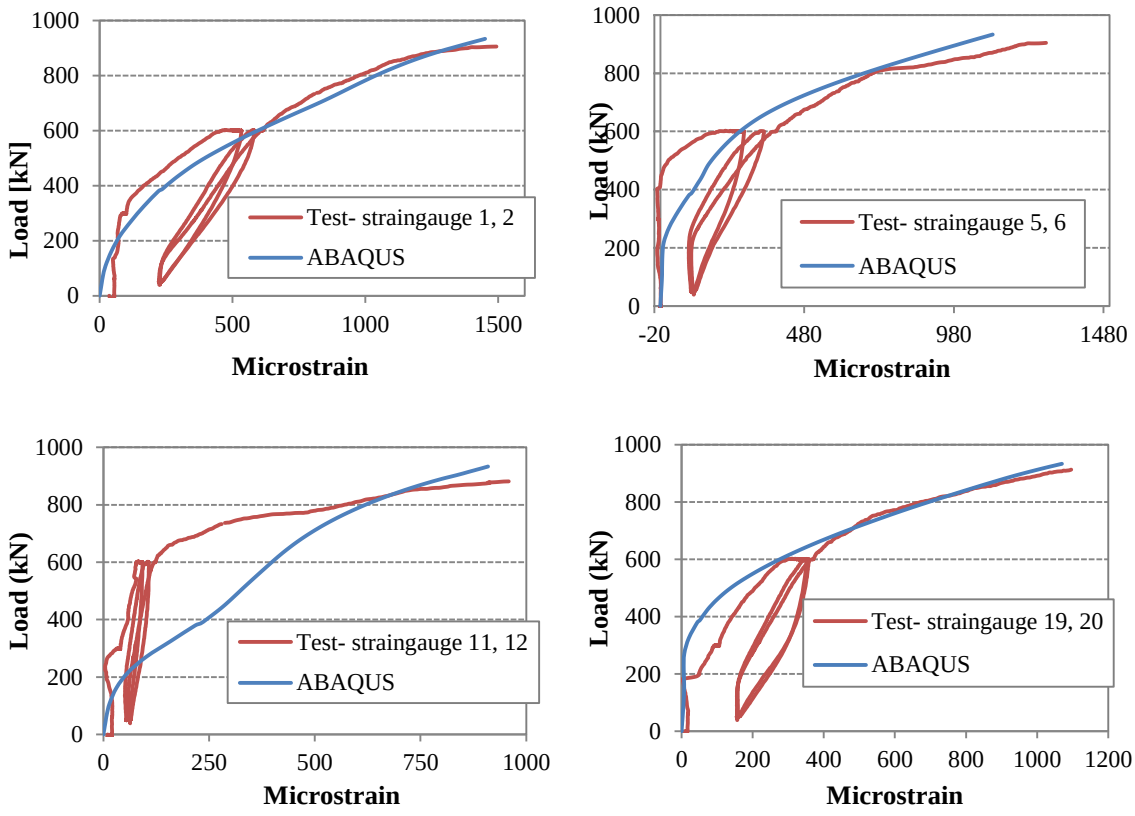

Figure 5.22: Comparison between strain gauge measurements of Slab 2 with ABAQUS model for shear reinforcement in the second perimeter.

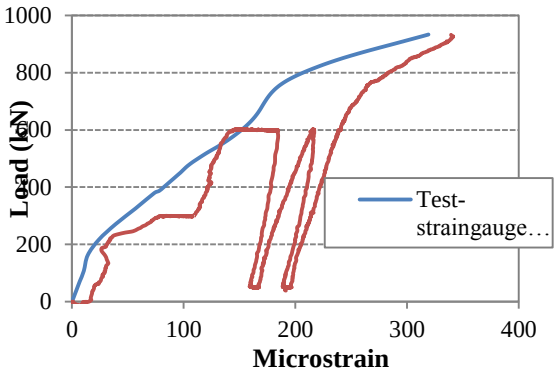

Figure 5.23: Comparison between strain gauge measurements of Slab 2 with ABAQUS model for shear reinforcement in the fourth perimeter.

Readings from strain gauges of 5-6 and 19-20 showed a stiffer behaviour in the elastic region at the beginning. The stress-strain curves (such as 11- 12, 7 and 17-18) predicted by FE model showed lower stiffness compared to the experiments. A probable explanation for this behaviour is that the strain gauges were installed in the middle of the vertical direction of the LSF reinforcement between two holes. Therefore, the exact place of strain gauges could be somewhere very close to the middle of the LSF strips.

Slab 3

Figures 5.24 to 5.29 present the comparisons of the stress-strain curves predicted by FE models with the experiment results. As shown in these figures, the FE model shows a perfect agreement with the experimental results. Predictions from strain gauges 15-16 are slightly different, this could be due to the fact the LSF strip become stressed while casting the concrete to the slab mould.

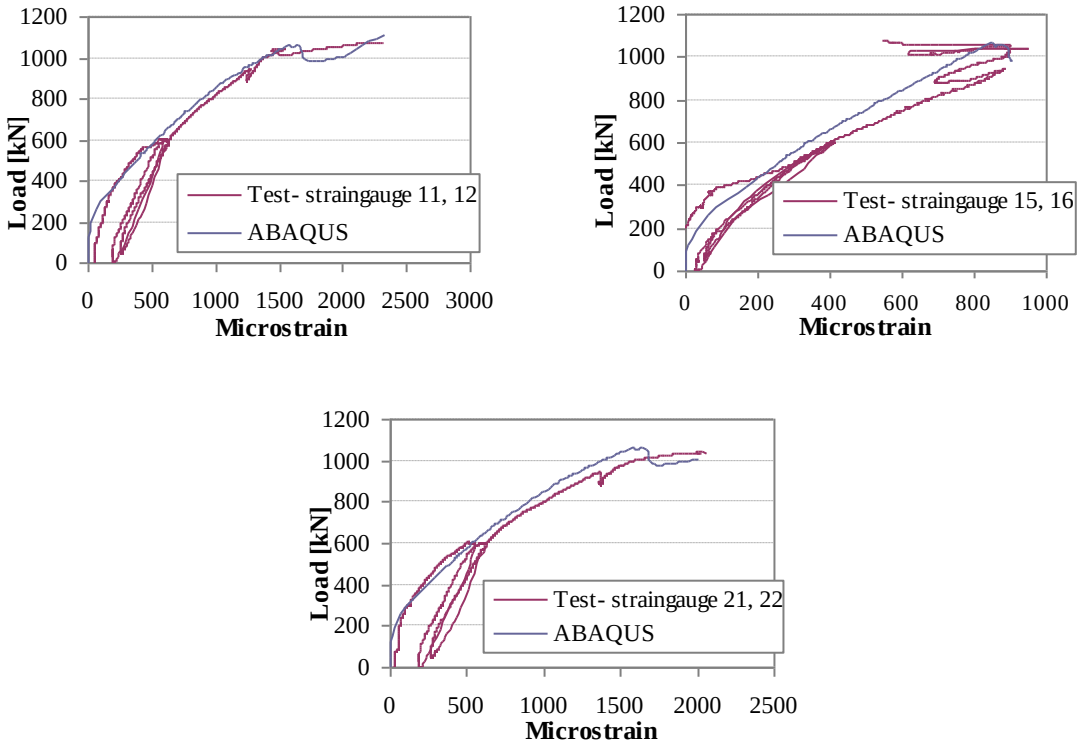

Figure 5.24: Comparison between strain gauge measurements of Slab 3 with ABAQUS model for shear reinforcement in first layer.

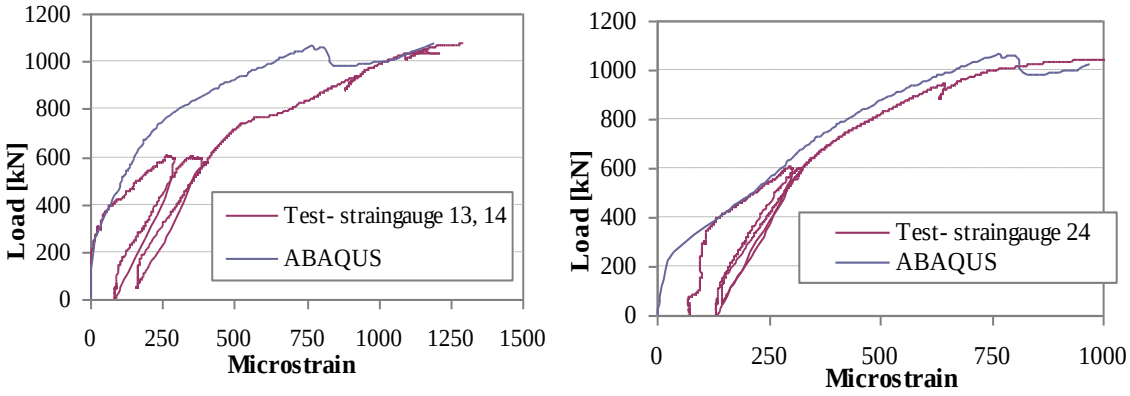

Figure 5.25: Comparison between strain gauge measurements of Slab 3 with ABAQUS model for shear reinforcement in second layer.

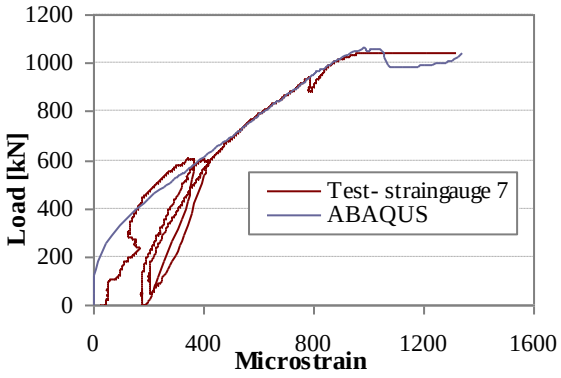

Figure 5.26: Comparison between strain gauge measurements of Slab 3 with ABAQUS model for shear reinforcement in third layer.

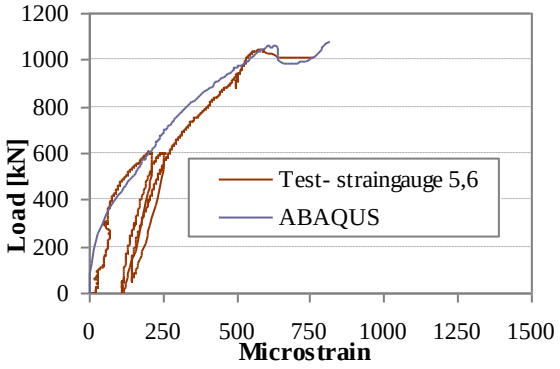

Figure 5.27: Comparison between strain gauge measurements of Slab 3 with ABAQUS model for shear reinforcement in fourth layer.

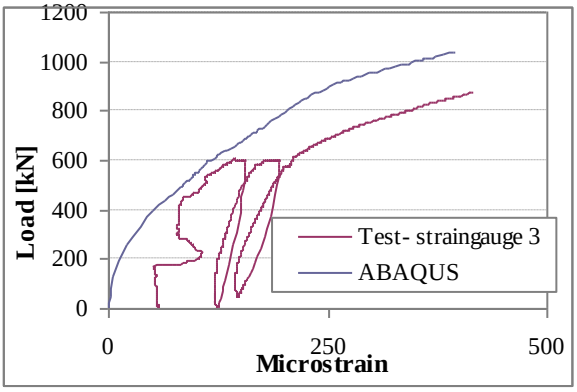

Figure 5.28: Comparison between strain gauge measurements of Slab 3 with ABAQUS model for shear reinforcement in fifth layer.

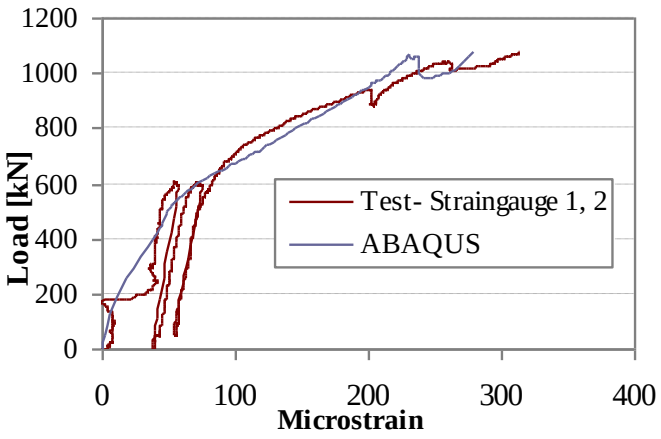

Figure 5.29: Comparison between strain gauge measurements of Slab 3 with ABAQUS model for shear reinforcement in sixth layer.

Crack opening displacement

The serviceability of structural members is significantly influenced by large deflections and excessive cracking. It is recognized that the crack width of the concrete is controlled by the usage of shear reinforcement. However experimental work reported in Chapter 4 did not include the measurements for concrete cracks. The effectiveness of the shear reinforcement was confirmed by the load versus crack mouth opening displacement (CMOD) obtained at the strain localization area within a distance of 1.5*d* from the column face which was recorded from the FE models. In this particular case, the CMOD can be assumed equal to the tensile equivalent plastic strain, $\varepsilon^{pl}_{t,}$ at the tension face of the slab multiplied by the characteristic length of the FE mesh.

The use of LSF shear reinforcement resulted in a significant decrease of crack opening displacement and this is clearly demonstrated in Figure 5.30. For instance, for Slab 3, at a load level of 500 kN, the percentage reduction in the CMOD is about 15% of the reference Slab (Slab1), the percentage reduction in the CMOD is about 45% of the reference slab (Slab 1) for Slab 3. Therefore, it is clear that Slabs 2 and 3 which are strengthened by LSF shear reinforcement demonstrated enhanced serviceability behaviour.

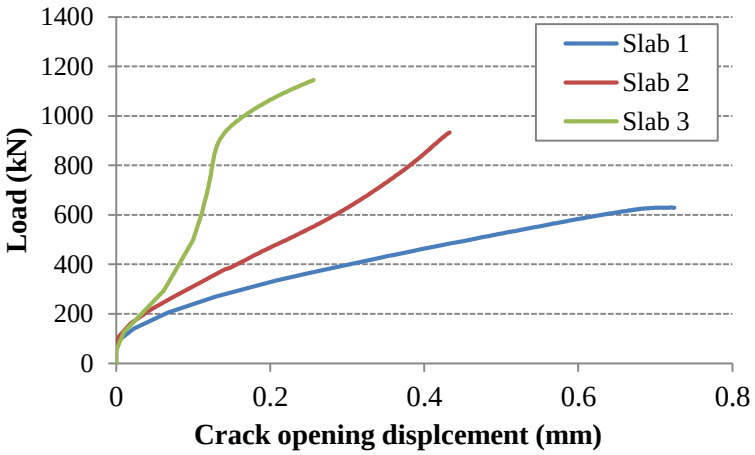

Figure 5.30: Load-CMOD obtained at distance 1.5*d* from the column face along the centreline of the slab.

5.8.2.2 Experiments from Li (1997)

Slabs PSSB, PSSE and Slab PSSF

The shear reinforcement in Slabs PSSB and PSSE were arranged according to ACI shear arrangements while for the Slab PSSF it was made according to BS 8110-1997 arrangement. Figure 5.31 compares the load deflection behaviour of slabs predicted by FE model with the experiments.

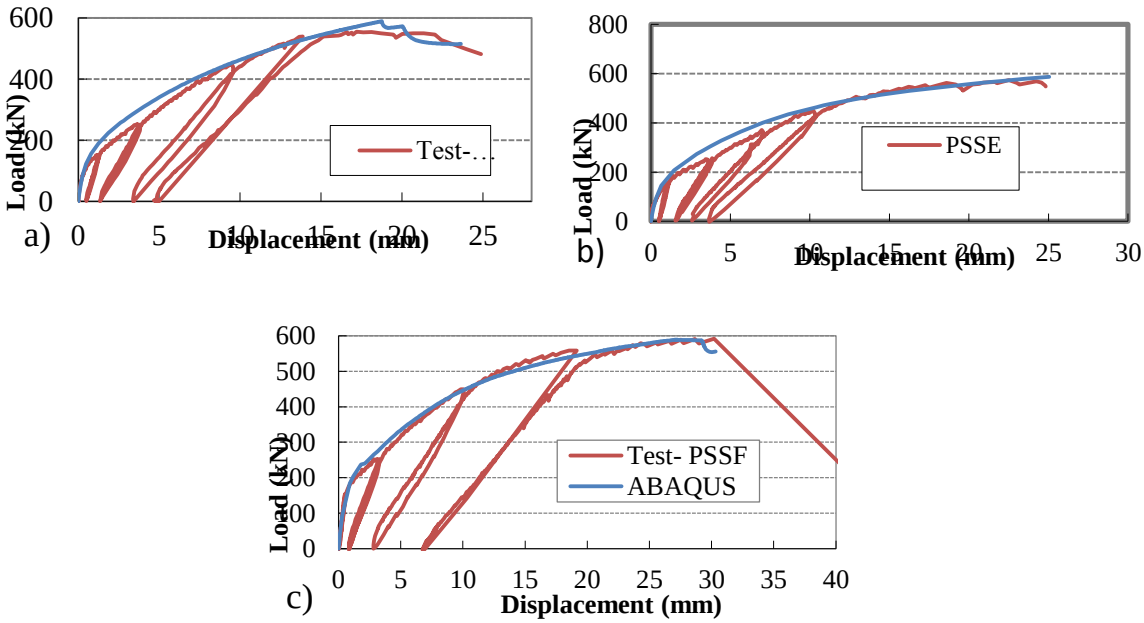

Figure 5.31: Comparison between experimental and model prediction, (a) Slab PSSB, (b) Slab PSSE (c) Slab PSSF.

The stress-strain behaviour of the flexural and shear reinforcement of the modelled slabs showed very good agreement with the experimental results.

5.9 Conclusions

In this chapter, nonlinear finite element analyses were carried out to simulate the deflection behaviour of slab column connection. Experiments from Chapter 3 as well as experiments by Li (1997) consisting of slabs without and with LSF shear reinforcement were used in the simulations. The simulations also showed good agreement with the yield line analysis for both the series of the experiments.

The nonlinear finite element analysis with ABAQUS can simulate slab-column connections behaviour in terms of load-deflection behaviour and stiffness in both the pre- and the post-cracking stages. However, for such analysis, a proper evaluation of tension stiffening is vital. For slabs with low reinforcement ratio such as reported in Li (1997), the ultimate load is attained while the flexural reinforcements are yielding therefore, an accurate estimation of the tension stiffening is essential. For this type of structure, an underestimation of tension stiffness leads to underestimating the post cracking stiffness. For lightly reinforced slabs (such as slabs reported in Li, 1997), the shape of tension stiffening curve is also important. For lightly reinforced slabs, it is noteworthy that a lower energy will be required to open a crack of unit width in the early stage of loading, while more energy might be required later to increase the crack area due to bond between concrete and reinforcement. It was found that the tensile strength has a significant effect on the first crack load.

Chapter 6

PARAMETRIC STUDY: EFFECT OF DIFFERENT DESIGN PARAMETERS

6.1 Introduction

Codes or standards (e.g. ACI 318-08) often use semi-empirical methods to calculate punching shear capacity of flat slabs, as was discussed in Chapter 3. A series of parametric studies were conducted using the validated numerical models presented in Chapter 5 of this thesis to investigate the sensitivity of certain parameters and to gain a better understanding of how flat slabs behave in punching. The major aim of the parametric study was to investigate the influence of key parameters such as thickness of slab, tensile reinforcemnent, compression reinforcement, concrete compressive strength, shear reinforcement on the performance of slab-column connections under gravity loads.

6.2 Effect of column size on punching shear capacity

Four numerical models of slab-column connections are analysed in this section: - Slab 1, adopted from Chapter 5 which has a column size of 320 mm, along with 3 other models, choosen with column sizes of 200, 260 and 380 mm. In all cases the other parameters such as slab depth, concrete compressive strength, tensile and compression reinforcement ratios were deliberately selected to be identical to Slab 1.

Figure 6.1 compares the load deformation behaviour of slabs with different column sizes. Figure 6.1 shows that the variation in column dimension size has no significant influence on the elastic behaviour of such connections. Following the occurrence of first crack, it is clearly shown that the increase in the column dimension has resulted in an increase in stiffness of the connection. For instance increasing the column dimension from 260 mm to 320 mm has results in a nearly 8% increase of punching shear capacity.

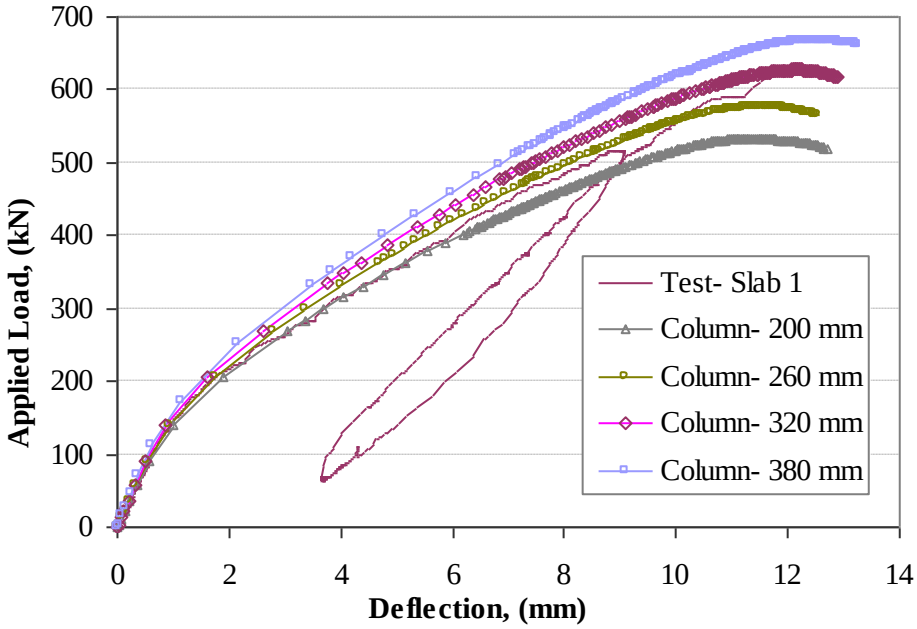

Figure 6.1: Effect of column dimension on the load-deflection behaviour of slabs failed in punching shear.

It is also observed from the analyses that the increase in column dimension has resulted in a decrease in maximum strain in the tension part of the concrete. For instance, the maximum tensile strain at the tensile surface of the slab is 0.0093 and 0.0087 for slabs with column dimensions 320 mm and 380 mm respectively. Table 6.1 summarises the prediction of the FE model on maximum plastic principle strains at the tensile surface of the slabs.

Table 6.1 Maximum plastic strain at tensile surface of concrete

Specimen	Maximum Plastic strain
Slab with column size of 200 mm	0.0104
Slab with column size of 260 mm	0.00977
Slab with column size of 320 mm	0.00928
Slab with column size of 380 mm	0.00878

Observations from the FE analyses also revealed typical truncated conical failure surfaces which tended to be a steeper for slabs with smaller column dimensions.

6.3 Effect of compressive reinforcement on punching shear capacity

As discussed earlier in Chapter 3, mechanical models and codes or standards do not consider the contribution of compression reinforcement in transferring shear loads on slabs. For this reason, two series of parametric studies were performed for slabs with low and high flexural capacities. The previously validated models in Chapter 5 were used to perform the parametric study in this section. Slab 1 was selected to be a representative typical example of high flexural capacity slab and Slab PSSA was then selected to be a typical representative of low flexural capacity slab. From each representative specimen, two other models were developed with all other parameters identical to their validated control experimental results so that compression reinforcement ratio was the only variable.

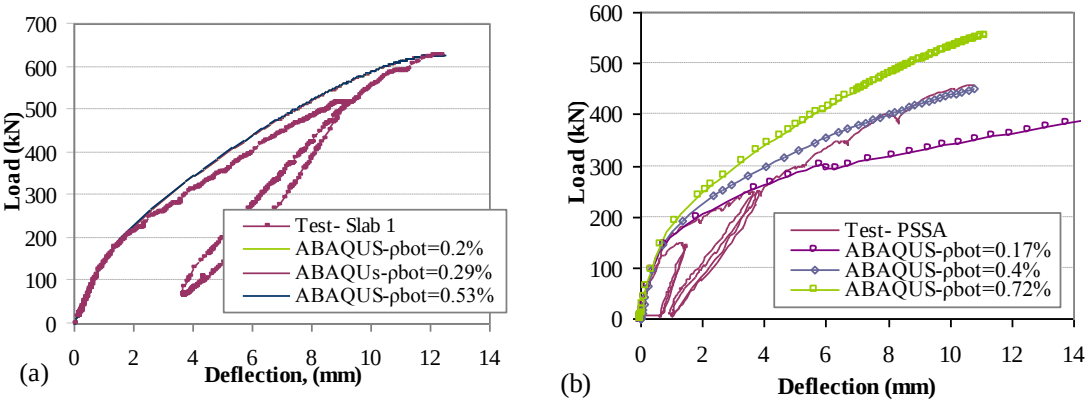

Figure 6.2: Effect of bottom reinforcement on load deflection behaviour of slabs: (a) slabs with higher flexural reinforcement ratio, (b) slabs with lower flexural reinforcement ratio.

Figure 6.2 shows the load deflection behaviour of FE models of slab-column connections with varying compression reinforcement ratios. Figure 6.2 (a) and (b) show different bottom reinforcement for Slab 1 and PSSA respectively. It is clearly demonstrated in Figure 6.2 (a) that the effect of compression reinforcement on load deflection behaviour is insignificant while there is a considerable increase in punching shear capacity with an increase in compression reinforcement in Figure 6.2 (b). These results mean that the punching shear capacity of a slab is influenced by the compression reinforcement for slabs only with low flexural capacity. In addition, slabs with low

flexural capacity demonstrated similar load deformation behaviour until the concrete is cracked. However, slabs with low reinforcement ratio, although they behave in a similar manner until the first crack has formed, the increase in compression reinforcement ratio results in a stiffer behaviour of these connections.

As the results clearly demonstrated, the effect of compression reinforcement ratio plays a significant role on the load deflection behaviour of low flexural capacity slabs. It is also known that in practice, such connections are generally designed to have low flexural capacity in order to have a more ductile behaviour in seismic scenarios. Therefore, the significance of the effect of compression reinforcement in design of such connections has to be emphasised.

6.4 Effect of tension reinforcement ratio on punching shear capacity

The validated numerical model of Slab 1 presented in Chapter 5, was used to assess the effect of flexural reinforcement ratio on punching shear behaviour of slabs. In addition to Slab 1, three other slabs, particularly developed for these analyses, with different percentages of reinforcement ratios of 1.61, 1.0, 1.97 and 2.6% respectively were analyzed. The variation in tensile reinforcement ratio was achieved by keeping the spacing the same as in Slab 1, and varying the bar diameter.

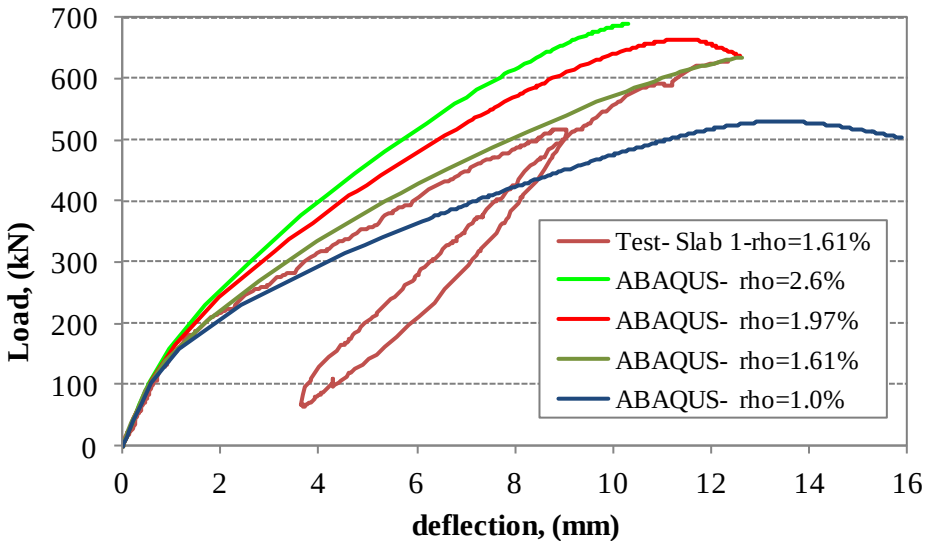

Figure 6.3: Effect of flexural reinforcement.

Figure 6.3 shows the load deflection predictions of the FE analyses for different reinforcement ratios of the slabs. All the slabs have demonstrated similar elastic behaviour until the occurrence of the cracks in the concrete, and beyond this point, the increased in percentage of reinforcement ratio has resulted in an increase in both the punching load and stiffness of the connection. Figure 6.3 also demonstrates that decreasing the flexural reinforcement caused an increase in ductility of the connection.

The observations from FE analysis shows that for slabs with low flexural reinforcement ratio, the tensile cracks spread into a very large area; whereas, with high flexural reinforcement ratios, the tensile cracks were grouped into a smaller area within the slab immediately around the column periphery. It was also observed that the increase in the reinforcement ratio resulted in a decrease in the maximum stress within the tensile reinforcement.

6.5 Size effect

The size effect was also studied with the FE model of Slab 1. It has to be emphasised that the size effect (slab depth) cannot be considered as an independent variable as the change in slab depth would significantly alter other parameters of the slabs. For instance, when the flexural reinforcement ratio is kept constant, the increase in the slab depth would result in a decrease in flexural capacity of the connection and this can further cause excessive cracks in the tension part and change the failure mode from punching to flexure. In order to asses the size effect on punching shear capacity of slab-column connections in a more realistic manner, it is necessary to keep the span to depth ratio, column dimension to depth ratio and reinforcement ratio constant and identical to Slab 1 for comparison purpose. Table 6.2 summarises the geometry of the models developed such as slab's depth, effective depth, column size, reinforcement ratio and span of the slabs as well as predicted values of shear stresses of the slabs modelled. The shear stress was calculated at a distance of $d/2$ from the column face.

Table 6.2: Poperties of developed models of slab-column connection

Specimen name	Slab depth, h (mm)	Effective depth, d (mm)	Column size, c (mm)	Reinforcement ratio, ρ (%)	Span (mm)	v_u (MPa)
1	160	120	250	1.54	2140	2.02
2 (Slab 1)	200	160	320	1.54	2750	2.04
3	240	200	360	1.54	3360	1.88
4	280	240	420	1.54	3970	1.79

It was observed from the FE analyses that all the slabs demonstrated typical truncated conical failure surfaces. Increase in the depth of the slab has resulted in an increase in angle of the truncated conical failure surface.

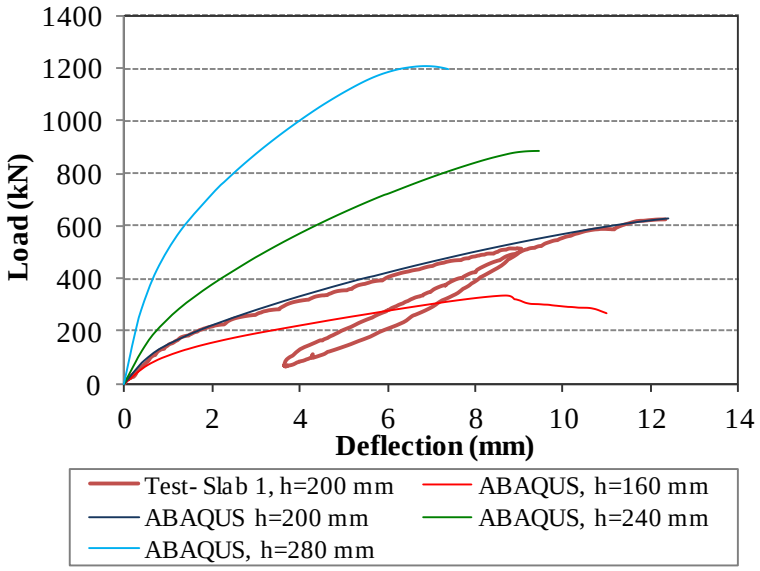

Figure 6.4: Load deflection behaviour of Slab1 with different depths.

Figure 6.4 presents the predicted load deflection behaviour of slabs with varying slab depth. Increase in the slab depth caused a significant increase in both elastic and plastic stiffness of the connection.

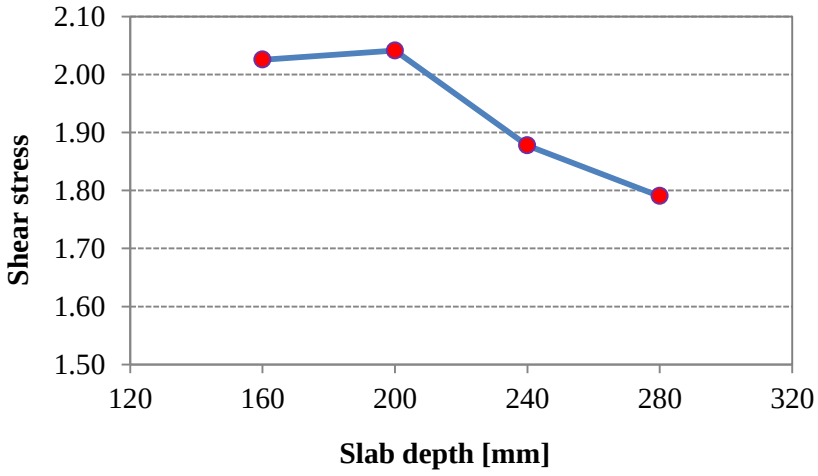

Figure 6.5: Punching shear stress vs. slab depth based from numerical modelling.

The increase in the slab depth resulted in a rapid decrease in the shear stress resistance, v_u, at the critical section $d/2$ from the column as shown in Figure 6.5. Experiments carried out by Birckle and Dilger (2008) and Guandalini *et al*., (2009) also showed similar trends. The influence of maximum aggregate size on the punching shear capacity is outside the scope of this thesis, however, it must be noted that the aggregate size is expected to have a limited effect on punching shear capacity (Birckle and Dilger, 2008).

6.6 Effect of shear reinforcement on punching shear capacity

Assessment of the effectiveness of shear reinforcement in punching shear experiment can be extremely tricky. This is mainly because of the difficulty in positioning the strain gauges at locations either very close or at the intersection of cracks however, obtaining measurements at these critical points is essential for the assessment of the effectiveness of the shear reinforcement. In addition to this, it is also very expensive to perform an experiment for each particular parameter to be investigated to assess the effectiveness of shear reinforcement. Therefore, two series of parametric studies were performed to assess the possible influences of the cross sectional area and the length of LSF shear reinforcement on punching shear capacity. The validated FE model of Slab 3was used to perform the parametric study in this section.

6.6.1 Effect of the cross sectional area of the LSF shear reinforcement on punching shear capacity

The influence of the cross sectional area of the LSF shear reinforcement on punching shear behaviour was investigated using the parameters of Slab 3 and two other cases with different shear reinforcement thickness. In those two cases, slab depth, column size, reinforcement ratio, span length and concrete compressive strength were kept constant and identical to Slab 3, while the thickness of the LSF strip was the varying parameter. Thicknesses of 1.2, 1.6 and 2 mm were used.

Figure 6.6 compares the predicted load deformation behaviour of slabs with varying thicknesses of LSF shear reinforcement. As it is demonstrated in Figure 6.6, the elastic behaviour of the slab-column connection is not influenced by the change in cross sectional area of LSF shear reinforcement. Furthermore, after the cracking of concrete,

the decrease in the cross sectional area of the LSF shear reinforcement causes, although negligible, a decrease in the stiffness of the connection.

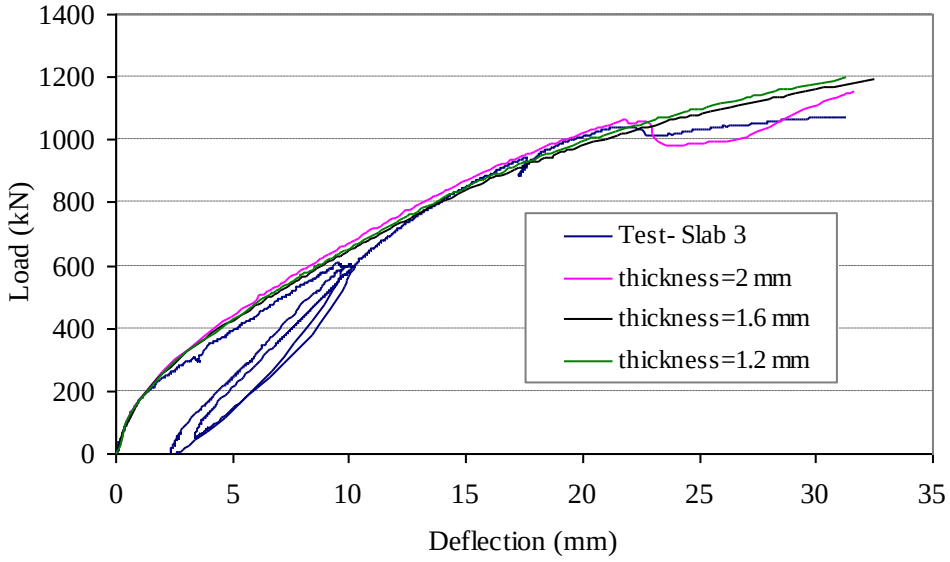

Figure 6.6: Load deflection behaviour of test specimens with varying cross sectional area of LSF shear reinforcement.

After carrying out a detailed analysis of the equivalent plastic strain at the tensile surface of the concrete, it was observed that the decrease in the cross sectional area of the LSF shear reinforcement resulted in a decrease in maximum equivalent plastic strain. As yielding in flexural reinforcement of Slab 3 was evident in Chapter 5, the FE results showed that even though the cross sectional area of the LSF shear reinforcement has decreased, the mode of failure was still observed to be a combination of flexure and punching.

Figure 6.7 shows the distribution of Von Misses stresses of LSF shear reinforcement under loading. It is clearly demonstrated in Figure 6.7 that for the slab with 2 mm thick LSF reinforcement, the yielding took place at the first perimeter from column face, while for the slab with 1.6 mm thick LSF reinforcement, the yielding occurred both within the first and second perimeters; and for the slab with 1.2 mm thick LSF reinforcement, yielding occurred at the first, second and third perimeters.

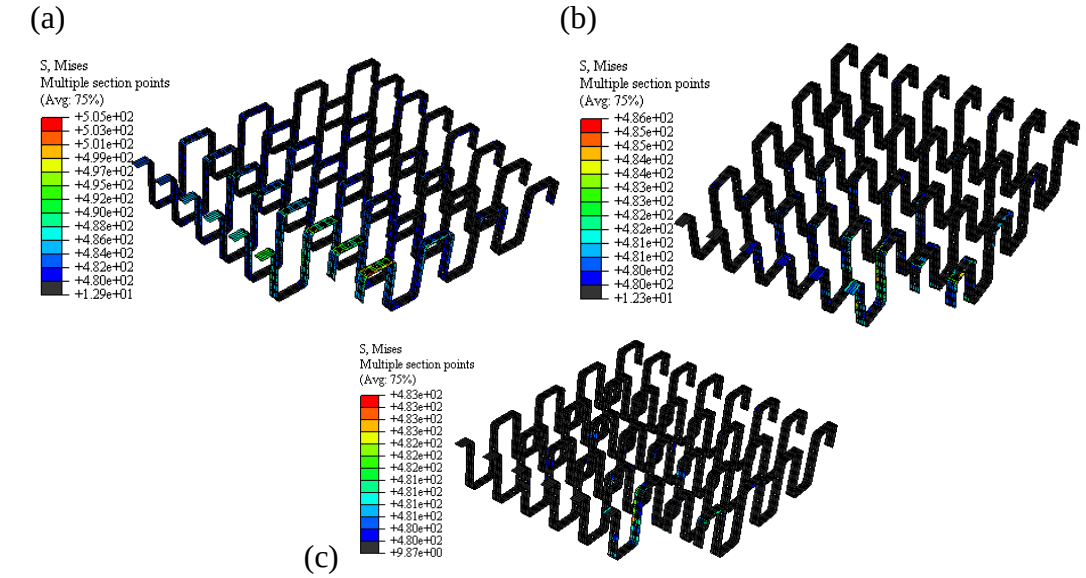

Figure 6.7: Stress distribution following yield stress at 480 MPa for slabs, (a); LSF thickness of 1.2 mm, (b); LSF thickness of 1.6 mm, (c); LSF thickness of 2 mm.

6.6.2 Effect of the number of layers of the LSF shear reinforcement on punching shear capacity

It is significant to study the effect of varying the number of layers of the LSF reinforcement on punching shear behaviour. Hence, three experiments with varying numbers of layers were analysed.

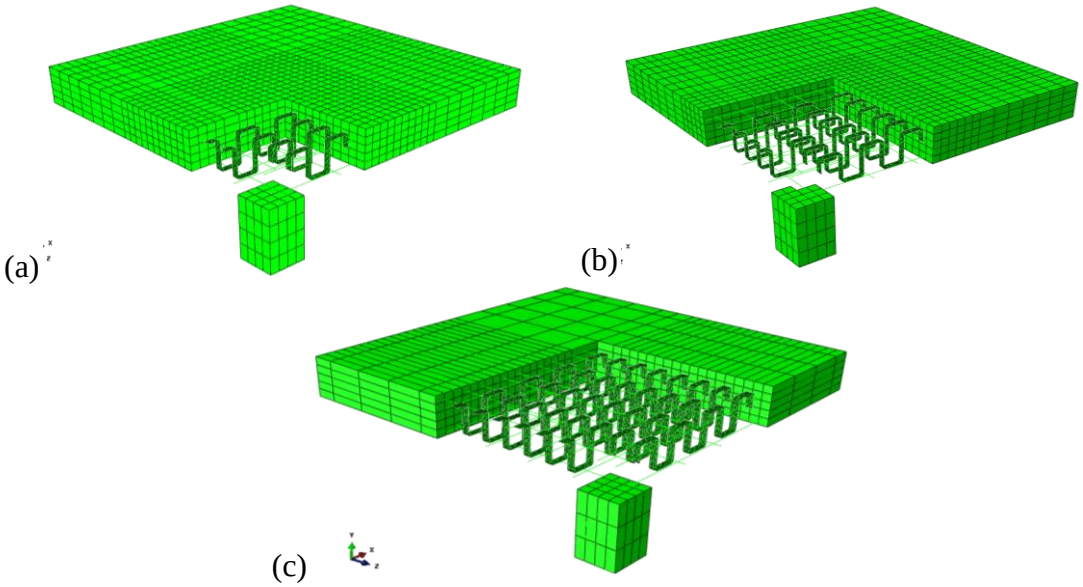

Figure 6.8: Schematic drawing of the shear reinforcement for analysed slabs; (a) slab with 2 layers of LSF, (b) slabs with 4 layers of LSF, (c) slab with 6 layers of LSF.

Slab 3 and two other cases with LSF layer numbers of 6, 4 and 2 were investigated in this section and the results are shown in Figure 6.8. The two virtual cases had all the parameters identical to Slab 3 except the number of layers of LSF.

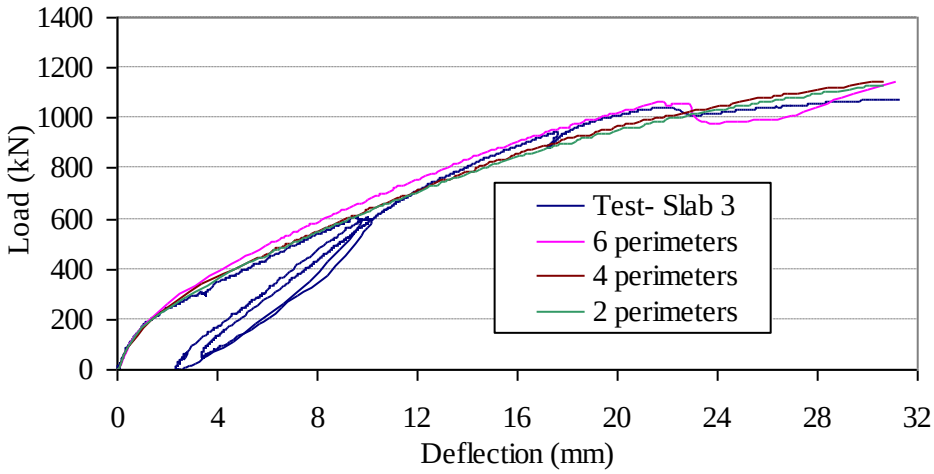

Figure 6.9: Load deflection behaviour of test specimens with different number of layers of LSF shear reinforcement.

Figure 6.9 shows the load deflection behaviour of the test specimens with different number of layers of LSF shear reinforcement. It is clearly seen from the Figure 6.9 that the decrease in the number of layers of LSF shear reinforcement has no significant effect on the load deflection behaviour of the connection. However, the use of two layers of LSF shear reinforcement caused the slab to fail outside the shear reinforcement area. It is also observed that the increase in the number of perimeters restricted the equivalent plastic strain at concrete tensile surface.

6.7 Conclusion

A series of parametric studies was carried out using the experiments reported in Chapter 5 as controls of the numerical models. These showed that the amount of compression reinforcement can play a significant role in changing the punching shear capacity. The influence of compression reinforcement ratio should be taken into account and necessary modifications should be performed to increase the accuracy of the Code Provisions.

A parametric study to investigate the varying column sizes was performed. The results showed that increase in the column size resulted in an increase in the punching shear capacity of the connection.

It can also be concluded that an increase of slab depth may result in a decrease in stress, and an increase in flexural reinforcement ratio increases the stiffness of the slab in both elastic and plastic regions of load-deflection behaviour.

One of the most important parameters that significantly affects the punching shear capacity was shear reinforcement. It can be concluded that the use of shear reinforcement can significantly enhance the capacity and ductility of such connections. Therefore, it is suggested that the future versions of the design codes should make appropriate recommendations on this aspect.

Chapter 7

DEVELOPMENT OF BAYESIAN NEURAL NETWORK

7.1 Introduction

Prediction of the punching shear capacity of slab-column connections was carried out by developing a Bayesian Neural Network (NN) model described in this chapter. First of all, a brief description of Artificial Neural Networks is given and back propagation Neural Networks are then discussed. Previous work on back propagation Neural Networks is then summarised. The experimental database reported in Chapter 3 was used to develop a Bayesian Neural Network model to predict the punching shear capacity of slab-column connections.

7.2 Artificial Neural Networks

Artificial Neural Networks (ANN) allows the structural and/or functional aspects of biological neural networks to be simulated. They are composed of neurons that have large number of simple processing units, known as nodes or units. These neurons are connected to each other to form a network (Anderson, 1995; Gesoglu *et al*., 2010; Iruansi *et al*., 2011). A simplified model of an artificial neuron is shown in Figure 7.1. It is shown that the input signals have synaptic weights w associated with them which are multiplied with the signals travelling along each connection.

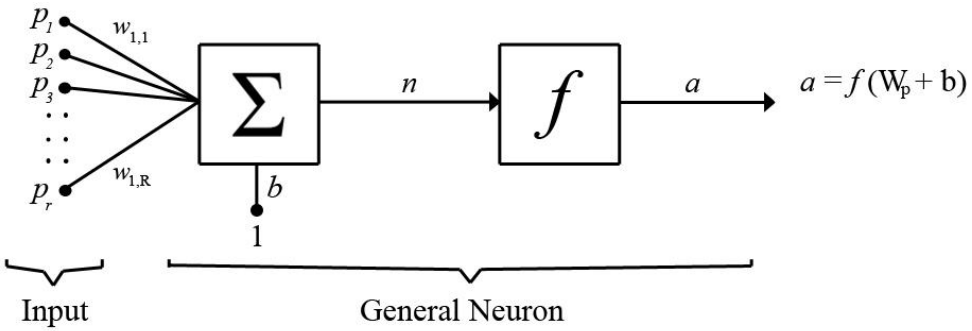

Figure 7.1: Simplified model of artificial neuron (Kose, 2007).

It is reported in literature that complex functions such as function approximation, regression analysis, pattern recognition, vision and speech identification can be dealt with the Artificial Neural Network. The back propagation Neural Network, often used for regression analysis, is briefly discussed in the next section.

7.3 Back Propagation Neural Networks

The back-propagation Neural Network (NN) is a class of Neural Network that is often used for practical applications (Bishop, 1995; Iruansi *et al*., 2011). The back propagation is a combination of a number of series of layers. The first and last layers are the input and output layers respectively. Hidden layers are located between the input and output layers. As shown in Figure 7.1, each layer is made up of neurons and they are also known as processing units. These layers are responsible for receiving inputs and processing inputs in order to provide a corresponding output. The significant variables which affect the network outputs are represented by the input layers. The output layer also contains neurons representing the network outputs. Thus, the punching shear parameters can be represented by the neurons in the input layer and punching shear strength can be represented by the neurons in the output layer and this is shown in Figure 7.2.

A complexity of a given model determines the number and size of the hidden layers and is usually unknown (Kingston *et al*., 2005). Normally, the network is constructed with the smallest number of hidden neurons to imitate the optimal complexity (Bishop, 1995; Kingston *et al*., 2005; Iruansi *et al*., 2011).

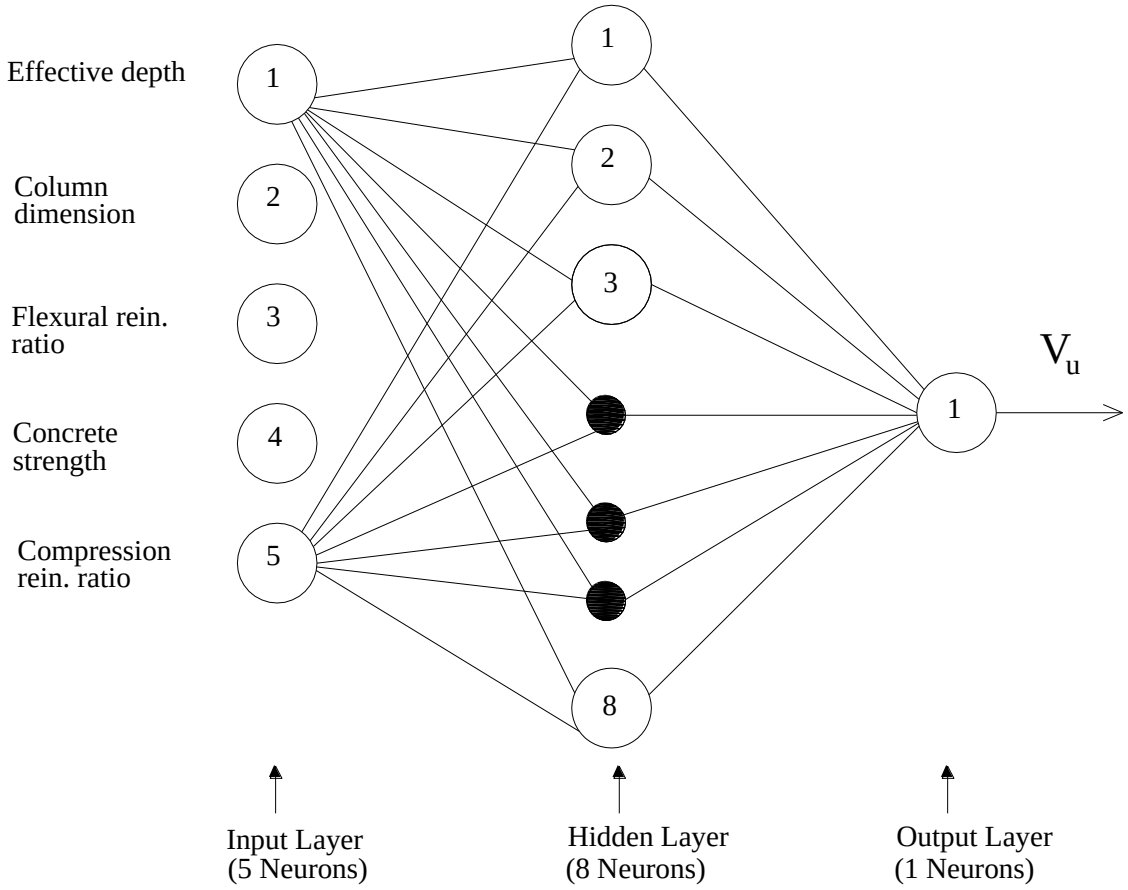

Figure 7.2: Architecture of a typical NN model for predicting the punching shear strength of slabs.

Optimal complexity of a network is very difficult to determine as there are no systematic methods yet reported on determining the optimal network architecture (Iruansi *et al*., 2011; Kingston *et al*., 2005; Mansour *et al*., 2004). Therefore, according to Bishop, (1995), Mansour *et al*., 2004, and Iruansi *et al*., 2011, a trial and error approach should be implemented to select the number of hidden layer neurons. To find the best performance of the network, the number of hidden nodes is systematically increased and decreased with the coefficient of determination (r^2) and the root mean squared error (RMSE) being used to assess this best performance.

To find an appropriate relationship between the set of input variables (x) and the system response (y), Equation 7.1 which characterises the relationship between the input parameters can be given as

$$y = R(x;w) \tag{7.1}$$

where $R()$ is the function described by the ANN and w is a vector of connection and bias weights (Kingston *et al*., 2005). The relationship between input x, and output y, for a two-layer network can be described as

$$h_j = f^1\left(\sum w_{jk}^{(1)} x_k + b_j^{(1)}\right); \quad y_i = f^2\left(\sum w_{ij}^{(2)} h_j + b_i^{(2)}\right) \tag{7.2}$$

where f is a linear or nonlinear activation function allocated to each neuron in the network. In Equation 7.2 the layer of the neurons is represented by the superscripts. In fact, activation functions at the hidden nodes and output node are represented by f^1 and f^2 respectively.

The activation function for the output neurons is linear and each of the hidden neurons is assumed to have a nonlinear activation function. The computational flexibility of Neural Networks can be achieved by a nonlinear activation function at the hidden neurons (Mansour *et al*., 2004). The log-sigmoid and tan-sigmoid type of nonlinear activation functions are often used in engineering applications. The log-sigmoid and tan-sigmoid provide ranges of output between 0 and 1 and between −1 and 1 respectively. The tan-sigmoid activation function was adopted in this study.

The training process is carried out following the determination of the architecture of the network. Training of the neural network is an iterative adjustment of the network parameters such as biases and connection weights. This iteration is carried out until the difference between the expected output and the network output is minimised and this is schematically shown in Figure 7.3 (Goh *et al*., 2005; Iruansi *et al*., 2011). It is crucial to minimise the error function, $E_D(w)$ by using the back-propagation algorithm, which is usually the sum of squares error between the experimental and the network output $y(x_i, w)$, and is expressed as:

$$E_D(\omega) = \frac{1}{2}\sum_{i=1}^{N}\{y(x_i,\omega) - t_i\}^2 = \frac{1}{2}\sum e_i^2 \tag{7.3}$$

Weight adjustment during the training process is performed using an optimisation algorithm such as the popular gradient-descent method. (see Bishop, 1995).

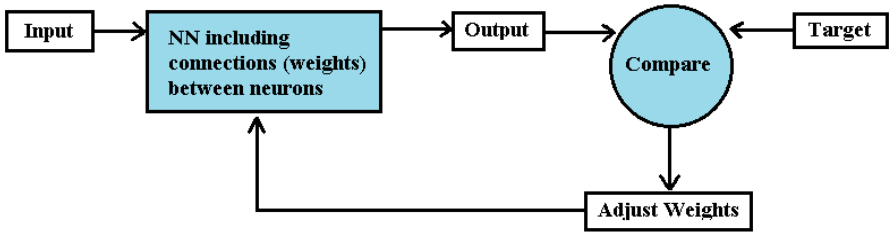

Figure 7.3: Basic methodology used in Neural Network training.

The efficiency of the trained Neural Network model is assessed on a set of data (testing data) that the network has not seen during training (Kingston *et al*., 2005).

It has been emphasised earlier on in this chapter that the determination of the optimal network architecture is a very difficult task when developing a neural network model using conventional back propagation (Iruansi *et al*., 2011; Chang and Yang, 2006).

It is computationally time-consuming when an excessive number of hidden layer neurons are used in a model. This can also result in a "memorised dataset", which is not able to capture the general trend in the dataset. This is shown in Figure 7.4, and is known as over-fitting. This problem can cause the generalisation ability of the network to be significantly damaged. On the other hand, the same problem can arise from an overly simple network, where the model cannot capture the trend in the dataset and also yields poor results.

As previously noted, a trial and error approach is used in determining the optimal numbers of hidden neurons as there is no existing approach to estimate the optimal number of hidden neurons. In order to reduce the tendency of over-fitting, early stopping and regularisation techniques are implemented in the Neural Network model (Iruansi *et al*., 2011).

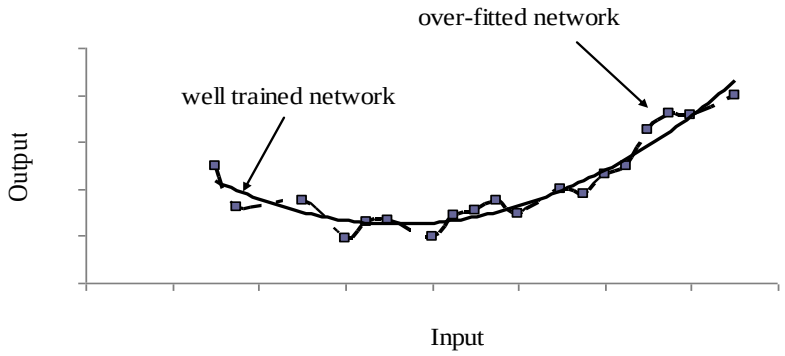

Figure 7.4: Example of an over-fitted network versus well-trained network.

The dataset is divided into two independent sets such as training and testing datasets. Increase in the error in the testing data results in a distraction of the network. This is not only tedious but also computationally expensive. For the case of a limited database, dividing the dataset in two independent sets with similar data trends can become impractical which is the case of the available experimental data on slab-column connections.

By means of adding a weight decay term, E_W, (regulariser) the objective function can be modified. This is also known as regularisation technique. The resulting new objective function becomes:

$$S(\omega) = E_D(\omega) + \mu E_W(\omega) \tag{7.4}$$

where the parameter μ is a regularization coefficient that controls the degree of regularisation and the regulariser, E_W is the sum squares of network weights and is given as:

$$E_w(\omega) = (1/2)\sum_{i=2}^{m} \omega_i^2 \tag{7.5}$$

where m is the total number of parameters in the network. The regulariser aims to penalize the more complex weight functions in favour of simpler functions (Bishop, 1995).

Optimum value of the regularisation coefficient is very difficult to determine and the over fitting may result if a very large coefficient is assigned. On the other hand, the network may not fit the training data sufficiently if a very small coefficient is assigned. This coefficient is also selected using a trial and error approach.

It can be concluded that, the selection of the optimum number of hidden neuron and learning parameters (i.e. regulariser) can be crucial to the performance of an ANN.

Integration of the Bayesian framework into the back-propagation algorithm was proposed by MacKay (1992) in order to enhance the generalization capabilities of the conventional back propagation neural network. The method is based on the Bayesian statistical approach. It is worth mentioning that to select the optimum network architecture and learning parameters, Bayesian framework provides a systematic approach. The parameter uncertainty is taken into account in the Bayesian framework and therefore the over-fitting is resolved (Bishop, 1995) and as a result the network generalisation capabilities are enhanced. The confidence level can be determined by an

error bar following the prediction generated by the network. The relative importance of different input variables can be determined by the use of Automatic Relevance Determination (ARD).

Conventional back propagation with early stopping technique had commonly been used to predict the punching shear strength of slab-column connections (Shah and Ribakov, 2011, Elshafey *et al*., 2011). It is unfortunate that the Bayesian approach has not been exploited to date to predict punching shear capacity. A full description of the Bayesian Neural Network can be found in Bishop (1995); MacKay (1992). The technical development of the Bayesian Neural Network is not the topic under discussion in this thesis and is not covered in detail. Instead this thesis focuses on the applicability of such networks in predicting the punching shear capacity of the slab-column connections.

7.4 Experimental Database

The experimental database reported in Chapter 3 was adopted here to develop a Bayesian Neural network. The distributions of the test specimen parameters are shown in Figure 7.5. It can be observed that the database is not uniformly distributed across the range of shear parameters as discussed in Chapter 3. Owing to the distribution of the available data, a Bayesian regularised NN was proposed instead of adopting the early stopping technique. Bayesian learning technique allows the use of the whole dataset to be trained in the network and therefore this technique not only eliminates the need for a testing dataset, but also guarantees optimal generalisation quality (MacKay, 1992).

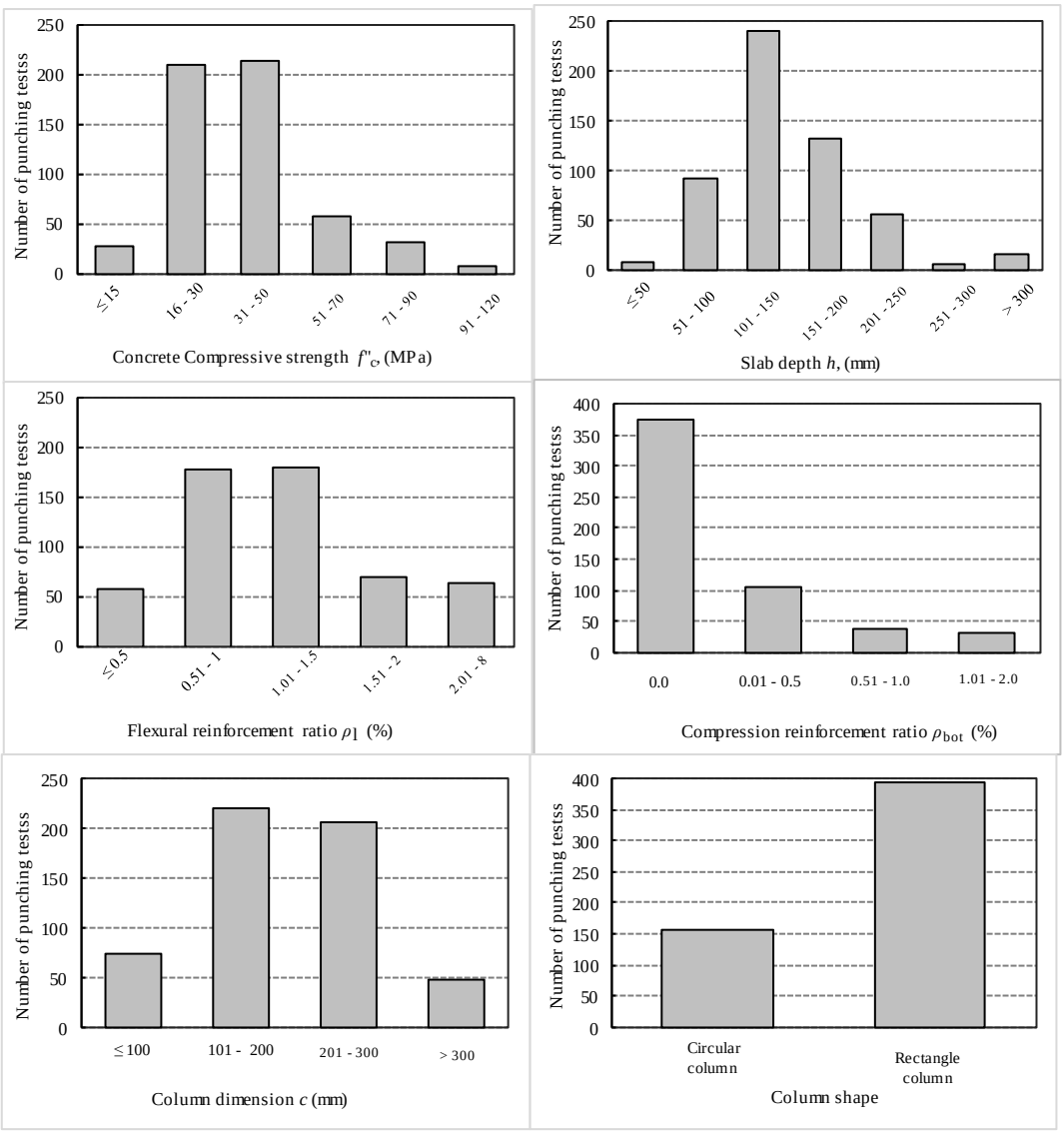

Figure 7.5: Distribution of the data of punching tests without shear reinforcement in the database.

7.5 Neural Network Architecture

The neural network architecture proposed in this study comprises of an input layer, one hidden layer and an output layer. The number of neurons in the input layer was determined from the parameters that affect the punching shear capacity of reinforced concrete slabs which was six (6) for slab-column connections without shear reinforcement. The number of neurons in the output layer was one (1) which represents the punching shear strength of the slab-column connections with parameters in the input layer neurons. The optimal number of neurons in the hidden layer was obtained by comparing the log of the evidence of a range of NN models.

In the proposed neural networks, tan-sigmoid and linear transform functions were employed in the hidden and output layers, respectively as shown in Figure 7.6.

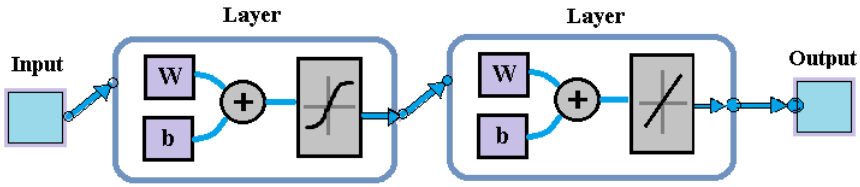

Figure 7.6: Flowchart for training Bayesian neural network.

7.5.1 Normalisation

It is essential to normalise the input variables in order to allow the network weights to have similar values in case of input variables being equally important when developing a Neural Network. Iruansi *et al*., 2011 reported normalised input and output variables to improve the performance of Neural Networks. Normalisation is vital to prevent network training from distractions in a local optimum, and without normalisation prediction of the best values is impossible. The comparison of the relative importance of the input to the Automatic Relevance Determination (ARD) process can be achieved by the normalisation of the input variables within the Bayesian framework. For this reason, Equation 7.6 was used to normalise the input data in order to have a zero mean and a unit variance. Equation 7.6 is

$$(x_i)_n = \frac{x_i - x_{min}}{\sigma_i} \tag{7.6}$$

where $(x_i)_n$ and x_i are the normalized and original values of data set, and x_{min} and σ_i are the mean and standard deviation of the parameter under normalization, respectively. Using the following equation, the output variables were normalised.

$$(y_i)_n = \frac{2(y_i - (y)_{min})}{(y)_{max} - (y)_{min}} - 1 \tag{7.7}$$

where $(y_i)_n$ and y_i are the normalized and original values of data set, while $(y)_{min}$ is the minimum values of parameters and $(y)_{max}$ is the maximum values of the parameter under normalization. Equation 7.8 was used to re-scale the values of the output to their original magnitudes. Equation 7.8 is

$$y_i = \frac{[(y_i)_n + 1][(y)_{max} - (y)_{min}]}{2} + (y)_{min}. \quad (7.8)$$

7.6 Implementation of Bayesian

A learning algorithm, to capture appropriately the weight of the structure, is used in the training of the Neural Network (Iruansi *et al*., 2011).

MATLAB toolbox called NETLAB was used in the training phase of the neural network (Nabney, 2002). The Bayesian framework into the back-propagation algorithm was implemented using an iterative procedure. Optimal values of α and β, and the optimum weight parameter ω_{MP} was found by the following iterative procedure in a neural network model:

1. α and β, the initial values for the hyperparameters, were set to 0.01 and 50, respectively.

2- The weights in the network were randomly initialised and were drawn from the prior distribution defined by α.

3. Then the network was trained. In order to minimise the regularised error function $S(\omega)$, weight optimisation was performed using the scale conjugate gradient algorithm shown in Equation 7.9. The total number of training cycles was set to 5000. The tolerance of the weight was set to 10^{-7}.

$$S(w) = \alpha E_D + \beta E_w \quad (7.9)$$

where E_D is given in Equation 7.3 and E_W is given in Equation 7.5 while β and α are termed hyper-parameters (regularisation parameter).

4. The hyper-parameters β and α were captured using gaussian approximation given in Equation 7.10 and 7.11 respectively after every 500 training cycles.

$$\alpha_{MP} = \frac{\gamma}{2E_W^{MP}} \quad (7.10)$$

$$\beta_{MP} = \frac{N - \gamma}{2E_D^{MP}} \quad (7.11)$$

with $E_W^{MP} = E_W(\omega_{MP})$; $E_D^{MP} = E_D(\omega_{MP})$; the quantity $\gamma = m - 2\alpha_{MP} tr(H^{MP})^{-1}$ is the number of well determined parameters and m is the total number of parameters in the

network. The hessian matrix was also computed during this procedure using Equation 7.12 as given below:

$$H = \nabla^2 S(\omega) = \beta \nabla^2 E_D + \alpha \nabla^2 E_W \quad (7.12)$$

5- Until the hyper-parameters and weights had converged, steps 2, 3 and 4 were repeated.

The number of hidden neurons is varied between 1 to 30, the above mentioned steps from 1 to 5 are repeated. The evidence of each network was computed using Equation 7.12 to select the optimum network. By different random initial conditions, each network was trained 20 times separately. This was necessary to ensure that the optimal network parameters were obtained for different network architecture.

7.7 Results and Discussions

7.7.1 Optimal network model

A plot of log evidence and R-Squared versus different hidden layer neurons for slab-column connections without shear reinforcement is shown in Figure 7.7. The optimal structure, shown in Figure 7.7, consisted of a number of hidden layer neurons, corresponding to a neural network that has eight hidden neurons (i.e. maximum of the log evidence) for slabs without shear reinforcement. Therefore, the optimum network architecture was constructed by five input neurons, eight hidden neurons and one output neuron (5: 8: 1).

Figure 7.7 clearly demonstrates that an increased number of hidden layer neurons results in an increase in R-Squared which is opposite to the log of evidence. The increase in R-Squared is expected as the increase in the network complexity would result in an increase in its ability to map to nonlinear functions. The R-Squared values obtained for the optimal network with eight hidden neurons is 0.9906 where for the network with 30 hidden neurons is 0.99748. Therefore, it is obvious that there is no significant difference between R-Squared obtained for the optimal network and the network with a very high number of neurons.

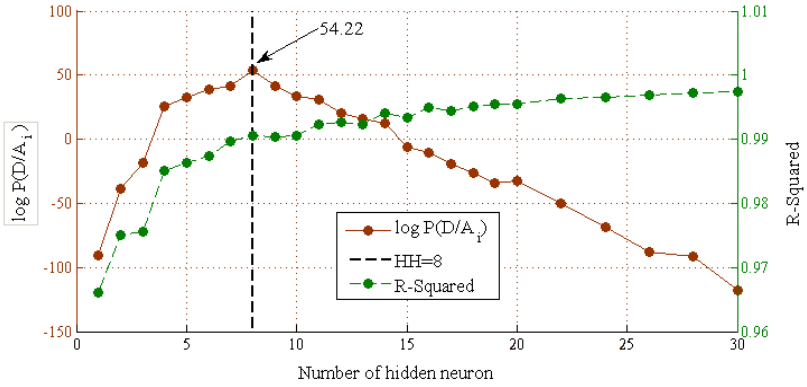

Figure 7.7: Plot of Log evidence and R-Squared vs. number of hidden layer neurons.

To check the convergence of the NN model, fifty iterations have been performed for the selected NN architecture (5:8:1) for the slabs without shear reinforcement. It is worth noting that 500 training cycles correspond to one single iteration. It was observed that 25 iterations were sufficient for the convergence to be achieved.

7.7.2 Connection weight and biases

For slabs without shear reinforcement, the selected NN architecture (5:8:1) has five input neurons (slab effective depth (*d*), column dimension (*c*), flexural reinforcement ratio (ρ_{Top}), concrete compressive strength ($f_c^{'}$) and compression reinforcement ratio (ρ_{Bot})); eight hidden layer neurons; and one output neuron representing the ultimate punching shear strength (V_{test}). Table 7.1 and 7.2 summarise the matrices of connection weights and biases for the developed NN model respectively.

Table 7.1: Connection weights for 5:8:1 ANN model

Slabs without shear reinforcement						
	$w_{jk}^{(1)}$					$w_{ij}^{(2)}$
Hidden neuron j=1	Input 1 d k=1	Input 2 c k=2	Input 3 ρ_{Top} k=3	Input 1 $f_c^{'}$ k=4	Input 1 ρ_{Bot} k=5	Output layer i=1
1	0.723	-0.820	0.2503	0.296	-0.571	-1.038
2	-0.077	-1.052	0.494	0.636	-0.287	-1.987
3	-0.175	0.428	0.0007	-0.365	0.763	0.667
4	0.217	0.2438	0.126	0.518	-0.134	1.4718
5	0.269	0.8707	-0.454	-0.459	0.134	-2.136
6	0.703	0.2821	0.0496	-0.784	-0.035	-0.978
7	0.818	0.2276	0.392	-0.237	1.177	-0.3420
8	-1.978	-0.224	-1.363	0.302	0.718	0.287

Table 7.2: Connection biases for 5:8:1 ANN model

Slabs without shear reinforcement		
	$b_j^{(1)}$	$b_i^{(2)}$
Hidden neuron j=1	Hidden layer j	Output layer i=1
1	2.843	0.168
2	1.816	-
3	0.406	-
4	1.443	-
5	-1.752	-
6	1.826	-
7	-0.868	-
8	-1.262	-

In order to determine the explicit formulation which relates the input variables *x* and the output variable *y*, the connection weights and biases are used as shown in the following equations:

$$a_j = \sum\left(w_{jk}^{(1)} x_k + b_j^{(1)}\right) \text{ and } y_j = \tanh(a_j) \tag{7.13}$$

$$y_i = \sum\left(w_{ij}^{(2)} y_j + b_i^{(2)}\right) \tag{7.14}$$

where the input variables are normalized using Equation 7.6 and then used in Equation 7.13.

7.7.3 Relative Relevance of Input variables

The relevance of the input variables can be determined by the implementation of the Automatic Relevance Determination (ARD) within the Bayesian inference learning. Figure 7.8 shows the inverse of the values of the hyper-parameters (*i.e.* relevance) of each input variable used in the developed neural network. For slabs without shear reinforcement, it was observed that slab depth (*d*), concrete compressive strength ($f_c^{'}$) and slab flexural reinforcement ratio (ρ) are the variables that influence the output most significantly. This is comparable with the results of various experimental and theoretical studies (e.g. Guandalini *et al*., 2009, Bazanat and Cao, 1987).

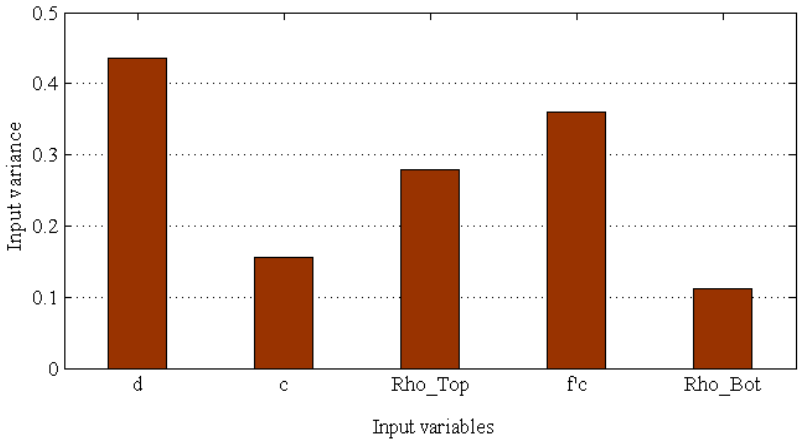

Figure 7.8: Relevance of input variables to punching shear strength.

7.7.4 Validation of ANN

Comparison of the experimental test data, V_{test}, and the predictions by the selected NN model is shown in Figure 7.9. As it is clearly seen in Figure 7.9, there is a very good agreement between the experimental test data and the predictions by the selected NN. For instance, the sum squared error (SSE) and R-Squared of the network's prediction are 315.5 and 0.9933, respectively and the mean and COV of the strength ratios are 1:0038 and 0:15, respectively. It should be emphasized that the selected NN model predicts the punching shear strength of slab-column connections very well and shows only very little scatter.

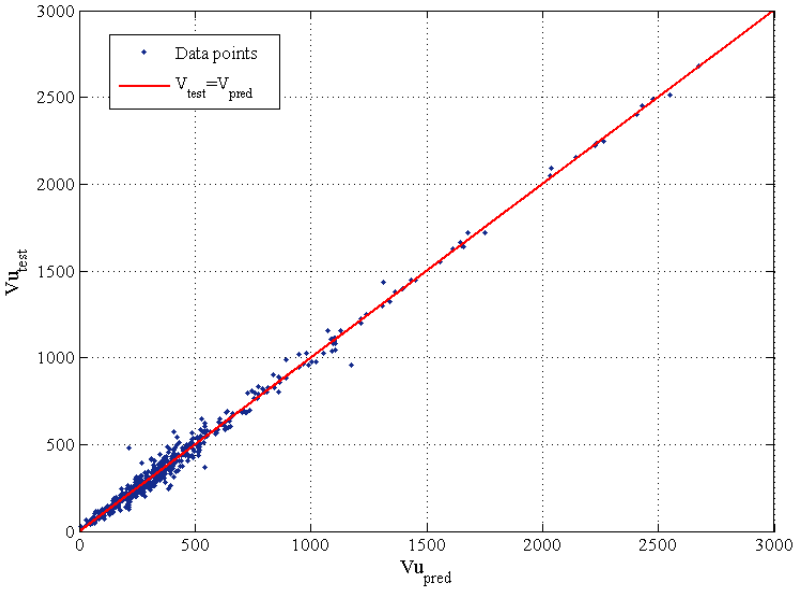

Figure 7.9: A plot of shear strength vs. ANN predictions.

The strength ratios V_{test}/V_{pred} for the 5:8:1 neural network were compared with EC-2 (2004) and ACI 318-08 in Figures 7.10 and 7-11 respectively. Parameters used in comparison were the effective depth, concrete strength, longitudinal tensile reinforcement ratio and compression reinforcement ratio. As it is clearly shown in Figures 7.10 and 7-11, ANN predictions (left columns) demonstrated much less scatter in each parameter examined compared to EC 2-2004 and ACI 318-08 (right columns).

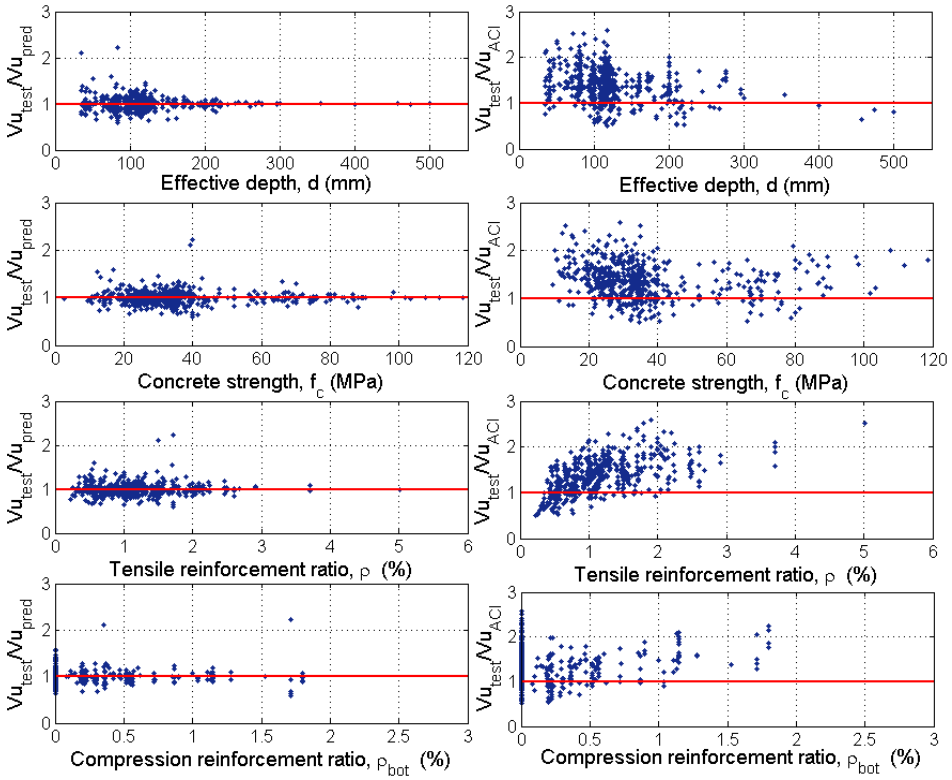

Figure 7.10: Strength ratios, Vtest/Vpred and Vtest/V_{ACI} vs. shear parameters for slabs without shear reinforcement.

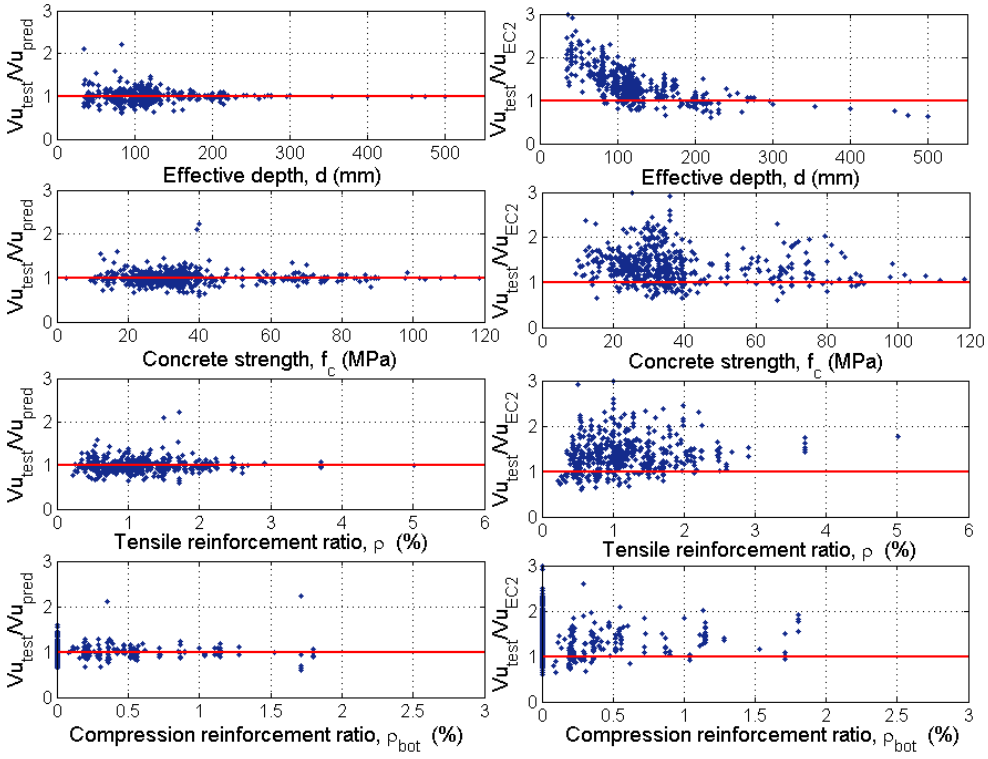

Figure 7.11: Strength ratios, Vtest/Vpred and Vtest/V_{EC} vs. shear parameters for slabs without shear reinforcement.

7.7.5 Simulation of Shear Strength of Slabs without Shear reinforcement

An independent dataset of slabs that is not included in the training was used to assess the ability of ANN to simulate the punching shear strength of slabs. Experiments carried out by Ghannoum (1998), Schaefers (1978) (cited in FIB bulletin 12) and Guandalini *et al*., (2009), which were not included in the initial training set, were used in the newly developed NN model to simulate the punching shear strength of the slabs.

Experiments by Schaefers (1978) (cited in FIB bulletin 12) was designed to investigate the influence of the slab depth on ultimate strength of slabs. Column dimensions and concrete strength were kept constant in the experiment and were 210 mm and 31 MPa respectively. Tensile reinforcement of the two slabs used in the tests was 0.8% and 0.6%. The NN predictions for these two slabs are shown in Figure 7.12 and are compared with predictions by ACI 318-08 and EC 2-2004. Although the ACI predictions were found to be conservative, it was concluded that ANN predictions were able to capture the experimental results better.

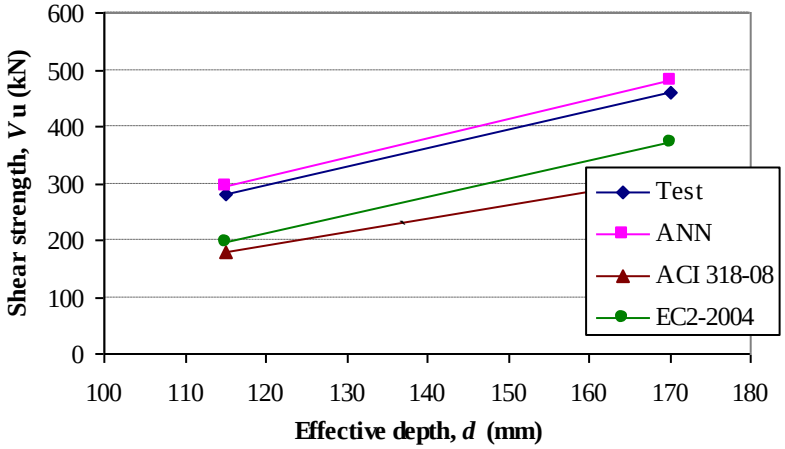

Figure 7.12: NN prediction for slabs tested by Schaefers, 1978 (cited in FIB bulletin 12).

Ghannoum's (1998) experiments were designed to investigate the influence of concrete strength on the ultimate strength of slabs. Tensile and compression reinforcement ratio, slab depth, and column dimensions were kept constant for all the slabs and were 1.11%, 0.36%, 110 mm, 225 mm respectively. Figure 7.13 shows the ANN predictions as well as the prediction by ACI 318-08 and EC 2-2004. It is clear that the ANN predicts the

punching shear capacity of the slabs more accurately compared to ACI and EC recommendations. Predictions by EC are found to be more conservative for these test series.

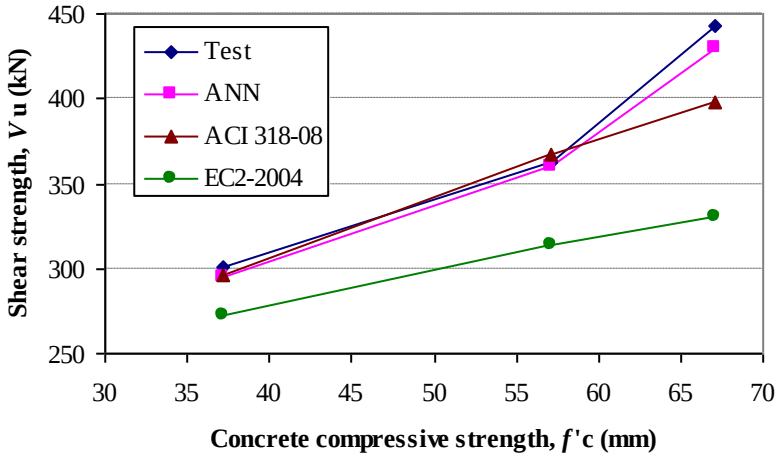

Figure 7.13: NN prediction for slabs tested by Ghannoum (1998).

Guandalini *et al*., (2009) developed experiments to assess the effects of flexural reinforcement on the ultimate strength of slabs. Four experiments from those were used in the simulation of the developed ANN model. The flexural reinforcement varied between 0.25% and 1.50%. Slab depth, column dimensions and compression reinforcement ratio were kept constant and were 250 mm, 260 mm, 0.2% respectively. Figure 7.14 shows the predictions by the ANN model, ACI 318-08, and EC 2-2004. As it is expected, the predictions by the ANN model captured the experimental data more adequately once again. ACI 318-08 predictions were unconservative for low reinforced slabs and conservative for slabs with high amount of reinforcement ratio.

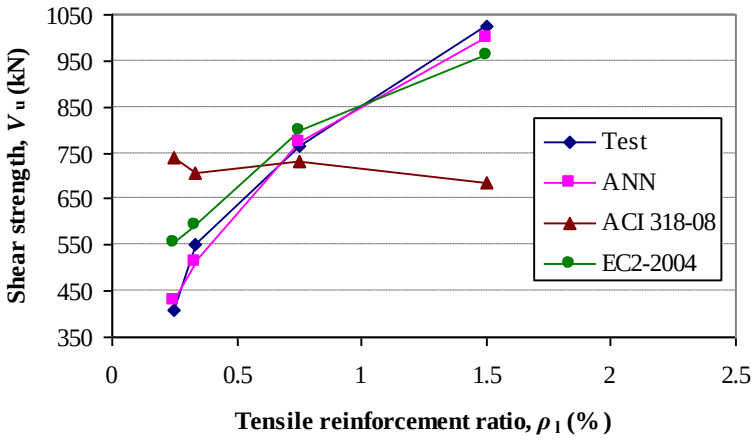

Figure 7.14: NN prediction for slabs tested by Guandalini *et al*., (2009).

7.8 Validation of Code Provisions and Numerical Models:

In order to investigate the performance of the design methods, numerical methods and Artificial Neural Network model, the influence of tensile reinforcement and compression reinforcement ratios, depth of the slab and amount of shear reinforcement on punching shear capacity were analyzed. The used formulations of the code provisions have been presented in Chapter 2. Also the results of the numerical analysis from Chapters 4, 5, 6, and 7 are used in this section. Non-dimensional punching shear strength ($V_u/(f_c^{'} b_o d)$) was used in all the comparisons, where V_u is the ultimate punching shear strength, $f_c^{'}$ is the compressive strength of concrete, b_o is the critical surface at half the effective depth (d) away from the perimeter of the loaded area.

7.8.1 Slab Thickness

Figure 7.15 compares the predictions of code equations with respect to the effective depth of the slabs for the experiments from Li (2000), and Muttoni et *al.*, 2009. The variation of the effective depth for Li's experiments was between 100 mm and 500 mm, whereas this variation for Muttoni's experiments was between 100 mm and 450 mm. The reinforcement ratios for Li experiment varied between 0.75% and 1.00% whereas for Muttoni's experiment the variation was between 0.25% and 0.35%. The ANN predictions for Li and Muttoni's experiments are not used here since these dataset were used in the training of the ANN model.

ACI does not account for the influence of the effective depth on the normalized punching strength. Therefore, the calculation leads to a horizontal line for slabs without shear reinforcement as shown in Figure 7.15. Strength is generally well predicted for EC2-2004 and BS 8110-1997 while the slab effective depth is limited to 400 mm. It was shown in Chapter 3 that there are limited experiments in literature on slabs with higher depth and this bias affected the code equations which were developed empirically. BS 8110 formulation includes a size effect term while the punching shear strength is calculated. The size effect term cannot be taken less than one which means that the shear resistance can be reduced for slabs with effective depth up to 400mm and for effective depth higher than 400 mm the shear stress will remain constant.

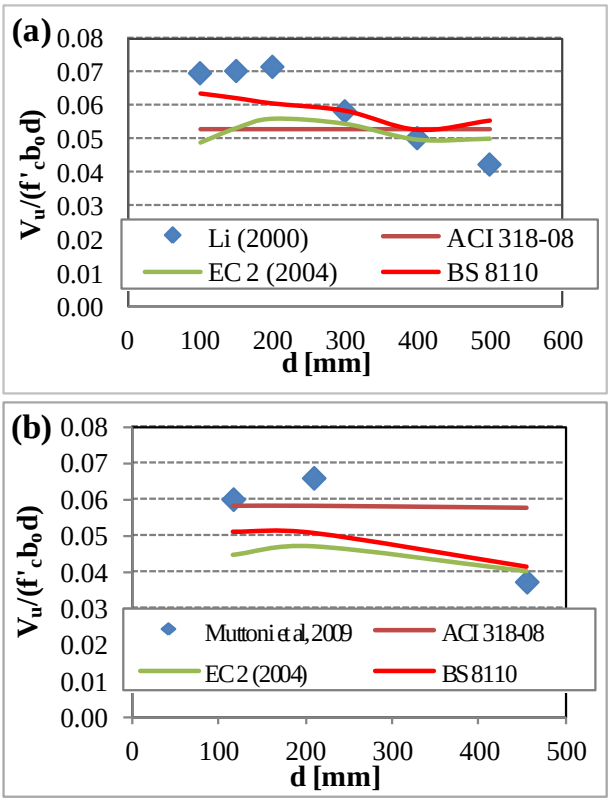

Figure 7.15: Comparison of non-dimensional shear strength versus effective depth: a) experiments by Li (2000), (b) Experiments by Muttoni et *al.*, 2009,

Slab 1 from chapter 4 which was validated numerically in Chapter 5 and three new numerical cases developed in Chapter 6 were used here to assess the size effect on the normalized punching shear. Parameters such as reinforcement ratio, span to depth ratio (c/d), column size to depth ratio (c/d), and concrete compressive strength were identical for all the experiments and only slab depth varied between 160 mm and 280 mm for these experiments. The normalized predicted punching strength from the numerical analysis and their normalized predictions using the code equations as a function of the effective depth is shown on Figure 7.16. ACI does not account for the effect of the effective depth and a horizontal line for slabs is shown in Figure 7.16. EC 2 on the other hand accounts for the size effect in the punching shear strength formulation. The size effect term in EC-2 is limited to 2 and it means that the shear strength of the slab can be reduced if the slab effective depth is greater than 200 mm. EC 2 slightly overestimated the shear strength of the slabs. BS 8110 overestimated the strength for slab with effective depth of 125 mm while for other slabs BS 8110 showed good agreement with numerical results.

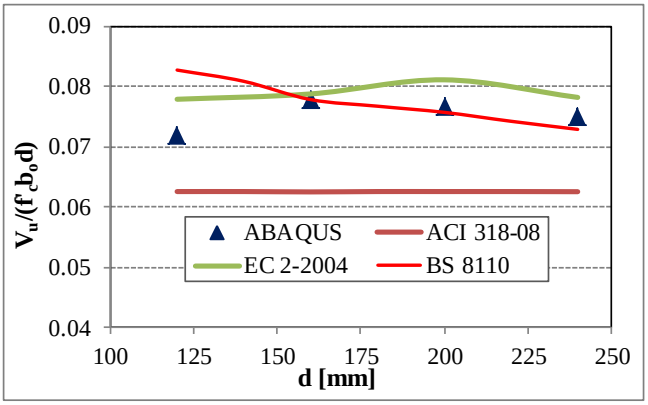

Figure 7.16: Comparison of non-dimensional shear strength versus effective depth.

Figure 7.17 shows the normalized predicted punching strength of the experiments from Schaefers (1978) as well as the predicted values from ANN and their normalized predictions using the code equations as a function of the effective depth. Schaefers's experiments were not used in the training process of ANN and these experiments were used for validation of the ANN shear model. The prediction of the punching shear strength from ANN model is very close to the experiments, therefore the normalized punching strength from ANN is in excellent agreement with the experimental values. All the code equations provided conservative predictions for those experiments.

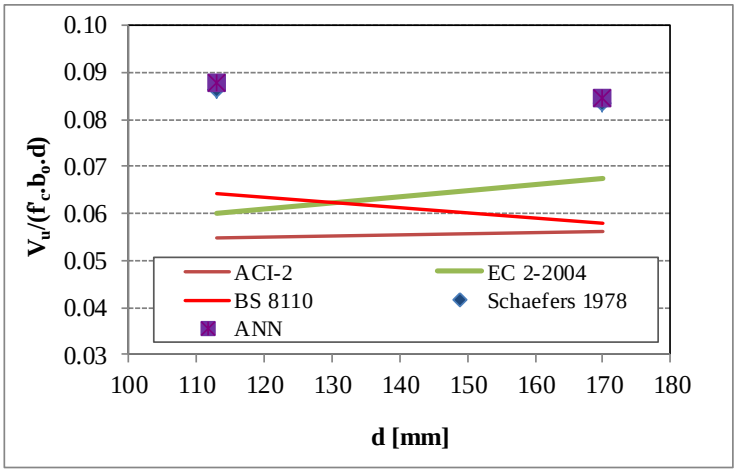

Figure 7.17: Comparison of non-dimensional shear strength (experiments by Schaefers (1978)) versus effective depth.

7.8.2 Reinforcement Ratio

Figure 7.18 compares experiments from Marzouk et *al.*, 2000, Alexander and Simmonds (1992), Guandalini et *al.*, 2009, and Elstner and Hogneted (1956) and the

code predictions with respect to their tensile reinforcement ratio. The variation of the tensile reinforcement ratio for Elstner and Hogneted experiments varied between 1.20% and 3.65% while for the other experiments the variation was between 0.5% and 1.25%. Other parameters such as slab effective depth, span to depth ratio (*c/d*), column size to effective depth ratio (*c/d*), and concrete compressive strength were identical for all the experiments and only concrete compressive strength slightly differed in Marzouk et *al.*, 2000 and Guandalini et *al.*, 2009. ACI does not account for the influence of the tensile reinforcement ratio on the normalized punching strength. Therefore, the calculation leads to a horizontal line for the slabs without shear reinforcement as shown in Figure 7.18. Strength is generally well predicted for EC2-2004 and BS 8110-1997 when the tensile reinforcement ratios are less than 2.00%. EC 2 and BS formulations account for the effect of reinforcement ratio while the strength of slabs are calculated. BS do not recommend increase of shear strength of slabs beyond 3.0% of reinforcement ratio while the similar limit for EC2 is 2.0%.. It can be seen from Figure 7.18 (d), that the code equations provide an uneconomical design when high tensile reinforcement ratios are used in the slabs.

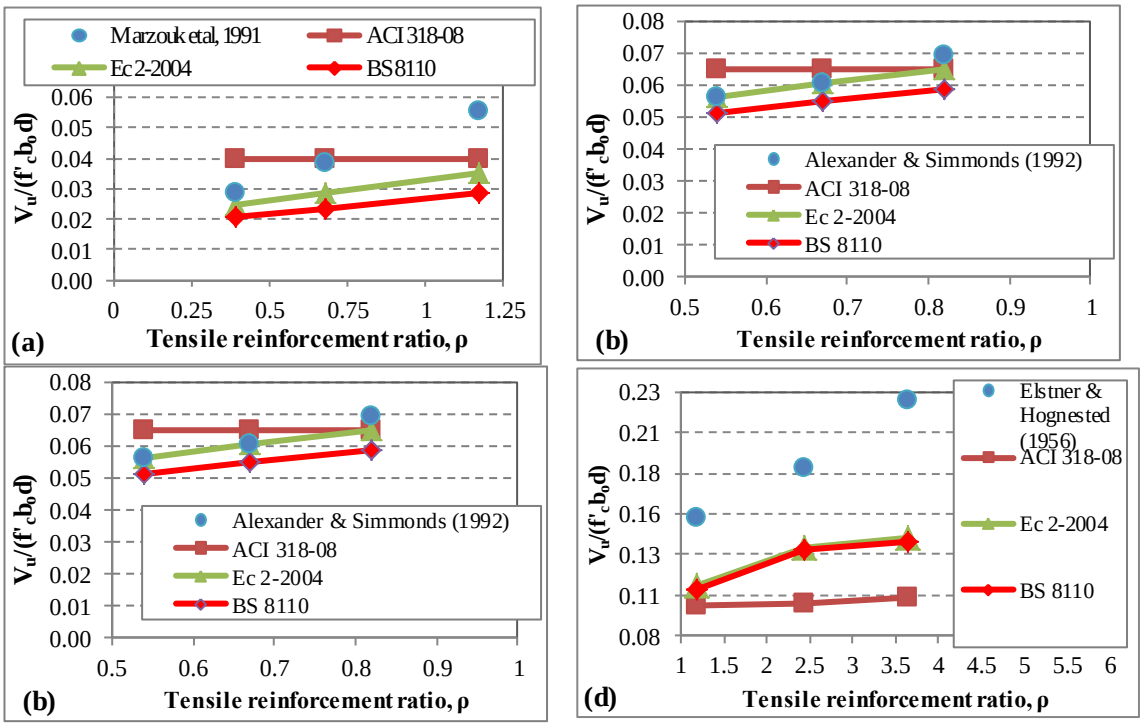

Figure 7.18: Comparison of non-dimensional shear strength versus tensile reinforcement ratio: a) experiments by Marzouk et *al.*, 1991. (b) Experiments by Alexander and Simmonds (1992), (c) Experiments by Guandalini et *al.*, 2008, and (d) experiments by Elstner and Hognested (1956).

Slab 1 from chapter 4 which was validated numerically in Chapter 5 and three new numerical cases developed in Chapter 6 were used to assess the effect of reinforcement ratio on the normalized punching shear strength. Parameters such as slab effective depth, span to depth ratio (*c/d*), column size to depth ratio (*c/d*), and concrete compressive strength were identical for all the experiments and only reinforcement ratio varied between 1.00% and 2.60% for these experiments. The normalized predicted punching strength from the numerical analysis in Chapter 6 and their normalized predictions using the code equations as a function of the effective depth are shown in Figure 7.19. ACI does not account for the effect of the tensile reinforcement ratio and a horizontal line for slabs are shown in Figure 7.19. BS 8110 and EC 2-2004 provide good approximations of these cases.

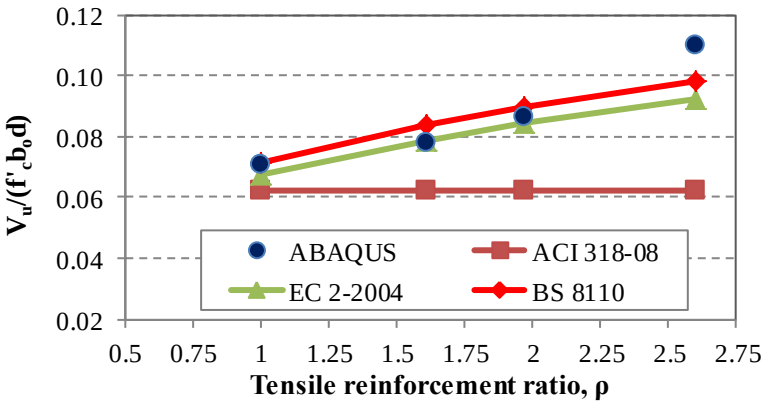

Figure 7.19: Comparison of non-dimensional shear strength (from the numerical results in chapter 6) versus effective depth.

Figure 7.20 shows the normalized predicted punching strength of the experiments from Guandalini et *al.*, 2009 as well as the predicted values from ANN model and their normalized predictions using the code equations as a function of the tensile reinforcement ratio. Experiments by Guandalini et *al.*, 2009 were used to validate the ANN shear model in this Chapter. The prediction of the punching shear strength from ANN model is very close to the experiments, therefore the normalized punching strength from ANN is in a very good agreement when compared with the experiments. All the code equations provided conservative predictions for Muttoni's experiments. ACI predictions provided a horizontal line and overestimated the shear strength of the slabs with low flexural capacity. This is due to the fact that ACI empirical formula was developed based on the experiments which all failed in shear.

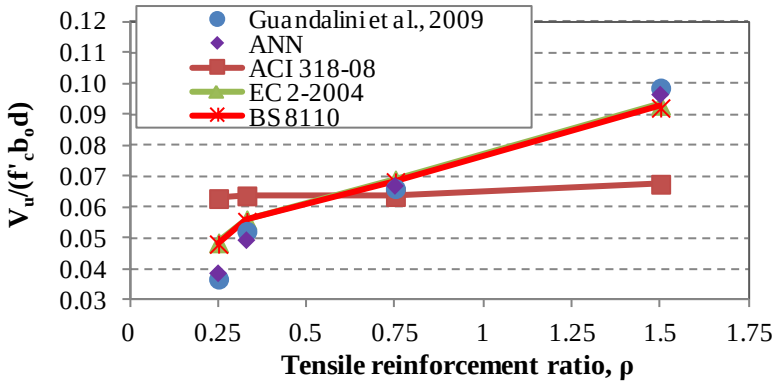

Figure 7.20: Comparison of non-dimensional shear strength (experiments by Guandalini et *al.*, 2009) versus effective depth.

7.8.3 Compression Reinforcement Ratio:

Figure 7.21 shows the normalized predicted punching strength as a function of the compression reinforcement ratio. It was shown in Chapter 6 that the punching strength of the slabs are influenced by the compression reinforcement for slabs with low flexural capacity. Therefore, experiments from Manterola (1996) as low flexural capacity and experiments from Birinici and Bayrak (2003) as approximately high flexural capacity slabs were chosen here for comparison. It was shown in Chapter 3 that none of the code equations account for the effect of the compression reinforcement and therefore a horizontal line for slabs are shown in Figure 7.21. ACI 318-08 slightly overestimates the punching strength of experiments with low flexural capacity while the BS 8110 and EC 2 provides safe predictions of the punching strength for low and moderate tensile reinforced slabs.

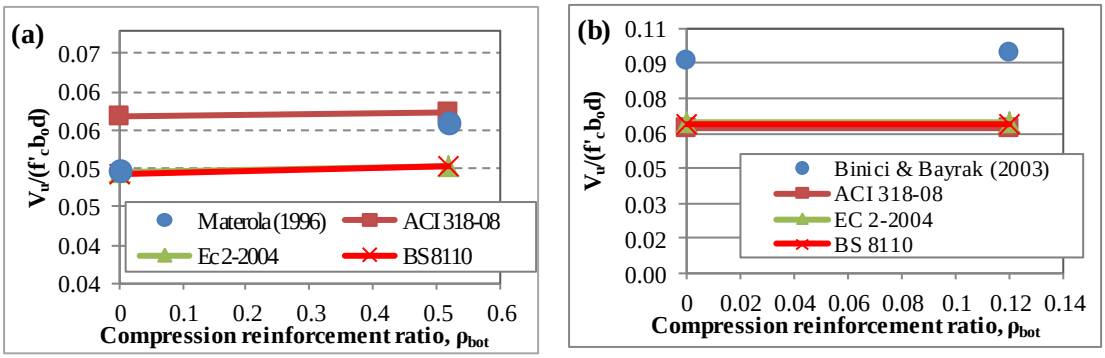

Figure 7.21: Comparison of non-dimensional shear strength versus compression reinforcement ratio: (a) experiments by Manterola (1996). (b) Experiments by Birinici and Bayrak (2003).

The numerically validated model, slab PSSA (Li (1997)), and two numerical cases developed in Chapter 6 with different slab compression reinforcement were used here to assess the effect of compression reinforcement here. Figure 7.22 shows the normalized predicted punching strength from the numerical analysis in Chapter 6 and their normalized predictions using the code equations as a function of the compressive reinforcement ratio. It can be seen that none of the codes adequately consider the effect of the compression reinforcement on the punching shear strength.

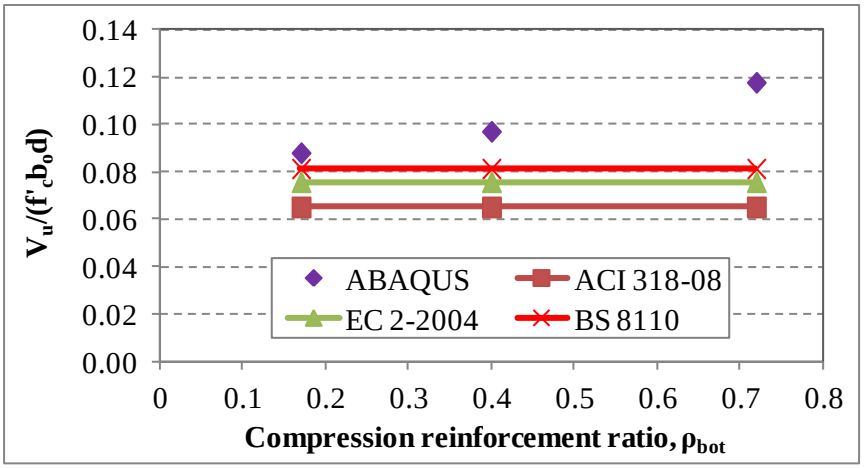

Figure 7.22: Comparison of non-dimensional shear strength (from the numerical model developed in chapter 6) versus compression reinforcement ratio

7.8.4 Shear Reinforcement Ratio

Figure 7.23 shows the normalized punching strength of Slab 2 and Slab 3, conducted by the author in Chapter 4, as a function of the shear reinforcement ratio. Both of the experiments failed within the shear-reinforced area. It was shown in Chapter 4 that all the code equations predicted failure within the shear-reinforced zones. ACI considers only 50% of concrete contribution for the punching shear capacity of the slabs. Therefore, ACI underestimated the punching strength capacity of the slabs as clearly shown in Figure 7.23. Slab 2 and Slab 3 were detailed according to BS 8110 requirements. Also the BS method was developed for slabs with stirrup shear reinforcement. BS 8110 provided a safe prediction of the shear strength of the slabs. Considering the fact that EC 2 does not consider the grid type arrangement of the shear

reinforcement in the code and the shear reinforcements were not detailed according to EC 2, it can be seen that the EC 2 slightly overestimated the shear strength for Slab 3.

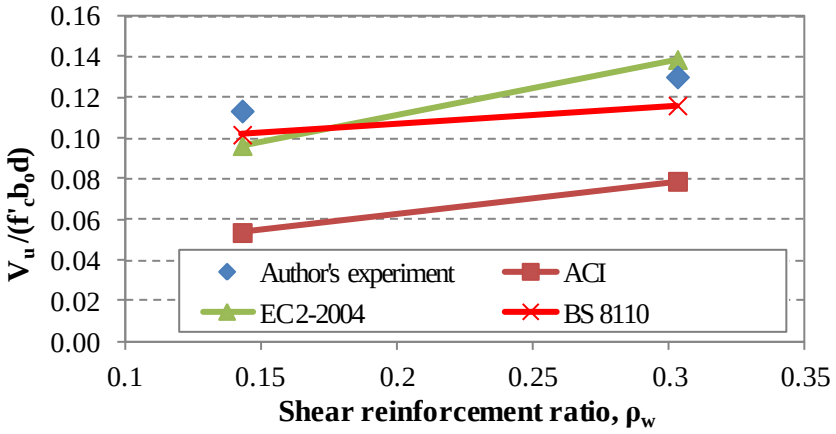

Figure 7.23: Comparison of non-dimensional shear strength (experiments by the author) versus effective depth.

7.9 Conclusion

In order to predict the punching shear strength of slab-column connections without shear reinforcement, a Bayesian Neural Network with five input neurons, eight hidden neurons and one output neuron was developed for the first time. The use of conventional back propagation neural network was abandoned in this study as the distribution of available test data was not sufficiently good to deal with the model complexity and therefore, a Bayesian approach was implemented preventing the overall dataset being separated into the training and test set, with the whole dataset being used in the training.

Analytical results demonstrated clearly that there is a very good agreement between the punching shear strength obtained from the experiments and the corresponding values predicted by the ANN model. Comparison of the V_{test}/V_{pred} for neural network and EC 2-2004 and ACI 318-08 showed that the ANN model was able to predict the punching shear strength with higher accuracy and much less scatter.

Chapter 8

CONCLUSIONS

8.1 Conclusions

8.1.1 Review of the punching shear failure

A comprehensive literature review was carried out to gain an insight into the underlying mechanisms and the fundamental causes of punching shear failure in flat slab column connections. Shear reinforcement types including stirrups and bent-up bars, shear studs and thin plate stirrups were reviewed along with the Lenton Steel Fortress (LSF) type of shear reinforcement, which due to its enhanced anchorage behaviour was adopted to be used in the experimental work and the numerical analysis of this thesis.

Available mechanical models on slab-column connections have been reviewed in detail and it was concluded that they are too complex to be used by engineers without simplification that could quite possibly compromise their overall accuracy as a result. Punching shear provisions in codes such as ACI 318-08 (2008), Eurocode 2-2004, CEB-FIP model code 1990 and BS 8118-1997 have been reviewed and the conclusion was that ACI 318-08 (2008) only considers the contribution of concrete for punching shear while BS 8118-1997, Eurocode 2-2004 and CEB-FIP model code 1990 also consider size effect and reinforcement based on empirically developed equations. Numerical models of punching behaviour of slab-column connections were reviewed. Different element types and material models were briefly discussed. It is concluded that the numerical models are able to predict the load deformation behaviour of slab-column connections and therefore it was adopted in this thesis to gain a further insight into the punching shear experiments.

8.1.2 Evaluation of punching shear design Code provisions

Previously the assessments of the Code equations were restricted with experiments reported by researchers. In order to examine the accuracy of the Code equations, the

author has constructed the biggest database on punching shear tests to evaluate the predictions of the Code Provisions such as ACI 318-08 (2008), Eurocode 2-2004, CEB-FIP model code 1990 and BS 8118-1997. It is shown that majority of the punching shear experiments were limited to slab depth less than 200 mm, members that have rectangular column-sections, members that are simply supported, and members that are moderately reinforced in flexure. It was also concluded that the punching shear design provisions of BS 8110-1997 provides the most accurate and consistent predictions of capacity using the variations in the Means and the values of the Coefficients of Variations (COVs).

8.1.3Pullout and Punching shear experiments

8.1.3.1 Pullout experiments

Previously, Lenton Steel Fortress (LSF) shear reinforcement was tensioned at middle sections of the strip to have a higher resistance. However, this process made the production of the this type of LSF reinforcement expensive and therefore, the author eliminated the use of such bent strip and developed a series of pullout experiments in order to assess the effectiveness of un-bent strips of LSF type of shear reinforcement.

It was concluded that the LSF strip both with and without holes showed very good anchorage behaviour. Another significant conclusion was that, the strips without holes demonstrated high ductile behaviour compared to the strips with holes. The strips with holes demonstrated a better anchorage behaviour and little plastic deformation inside the concrete compared to the strips without holes. Therefore, the modified LSF type of shear reinforcement was implemented to be used in punching shear experiment.

8.1.3.2 Punching shear experiments

Three real scale slab-column connections with and without LSF type of shear reinforcement were designed and tested to gain an in-depth understanding of the punching shear behaviour of such connections. Slab 1 was left with no shear reinforcement as control specimen and Slabs 2 and 3 were reinforced with LSF shear reinforcement. Experiments showed that Slab 1 failed in brittle punching shear while the mode of failure changed in Slab 2 and 3 where they failed in combination of flexure

and punching. The use of LSF shear reinforcement enhanced the punching shear capacity by 46% and 67% in Slab 2 and 3 respectively compared to the control specimen. The use of LSF shear reinforcement resulted in 75% and 153% increase of the ultimate displacement at failure compared to the control specimen.

8.1.4 Numerical modelling

Due to the limitations of the experimental configurations, it is vital to perform a numerical study to have a better insight into the behaviour of flat slab-column connections. For this purpose, the author adopted the ABAQUS FE package in this thesis. Available material models in ABAQUS were assessed and a plasticity concrete damage model was adopted and used in the numerical modelling. A sensitivity study was carried out both on mesh size and user defined parameters of concrete in order to define the appropriate model that predicts the punching shear behaviour. Punching shear experiments reported in Chapter 4 and four punching shear experiments carried out by Li (1997); PSSA, PSSB, PSSE and PSSF were modelled using ABAQUS. It can be concluded that there is a good agreement between the predictions of the FE analysis and experiments in terms of load deformation, stress-strain behaviour of flexural and shear reinforcements. Crack mouth opening displacement (CMOD) values showed an enhanced punching shear behaviour of slabs with LSF shear reinforcement as this was limiting the crack width significantly.

8.1.5 Parametric study

Using the validated models reported in Chapter 4, a parametric study was carried out on parameters that affect the punching shear behaviour of slab column connections. The effects of most important parameters such as compression reinforcement, column dimensions, slab to depth ratio and reinforcement ratio, on the capacity of punching shear capacity were studied. It is concluded that compression reinforcement has no significant effect on the punching shear capacity of slabs with high flexural reinforcement whereas slabs with low flexural reinforcement showed that the increase in compression reinforcement resulted in an enhanced behaviour of such connections. Increase in the column dimension also resulted in an increase in punching shear capacity. In order to assess the size effect precisely, all parameters such as span to depth

ratio, reinforcement ratio, column to depth ratio were kept constant; slab depth was left to be the only variable. For this reason, 4 series of experiments on slab-column connections with depth of 160, 200, 260 and 320 mm were modelled and analysed. Increase in the depth of the slabs resulted in a decrease in the nominal strength of the slab. It was also concluded that an increase in the flexural reinforcement ratio results in an enhanced load deflection behaviour in both elastic and plastic regions. The use of shear reinforcement on slab-column connections significantly increases the punching shear capacity. However, the influence of shear reinforcement on such connections has not received much attention in the Codes.

8.1.6 Bayesian Neural Network

The Bayesian Neural Network, a very recent approach to deal with complex models, was adopted here to predict the punching shear capacity of slab-column connections. The accuracy in prediction of punching shear capacity was significantly increased by implementing the Bayesian Neural Network.

8.2 Suggested future work

- In this thesis, real scale slab-column connections with and without LSF type of shear reinforcement were designed and tested to investigate the punching shear behaviour of such connections. However, it is essential to perform experiments on slab-column connections under intially gravity and then seismic loading in order to gain a deep understanding of punching shear behaviour in seismic scenarios.
- It is also suggested that further real scale experiments on slab-column connections need to be carried out using unbent LSF shear reinforcement without holes. Pullout and punching shear experiments need to be carried out to assess the performance of such shear reinforcement on punching shear capacity.
- The database for punching shear experiments that has been developed in this thesis needs to be updated with any future experiments on the topic. This will make it possible to formulate more precise and simplified models of punching shear capacity.

REFERENCES

ABAQUS User's Manual, Vol.: Materials, 2008, Version 6.8.

ABAQUS Theory Manual, User Manual and Example Manual, Version 6.8, Providence, RI. 2009.

ACI 318-08. Building Code Requirements for Structural Concrete. Farmington Hills, Mich.: American Concrete Institute, 2008.

Abdullah, A.M., 2010, "Analysis of Repaired/Strengthened R.C. Structures Using Composite Materials: Punching Shear" PhD Thesis, Faculty of Engineering and Physical Sciences, The University of Manchester.

Agbossou, A., michel, L., Lagache, M., Hamelin, P., 2008, "Strengthening slabs using externally-bonded strip composites: Analysis of concrete covers on the strengthening" Composites Part B: Engineering, Vo. 39, No.7–8, pp. 1125–1135.

Alam, A.K.M.J., Amanat, K.M., and Seraj, S.M., 2009 "An experimental study on punching shear behaviour of concrete slabs." Advances in Structural Engineering, Vol. 12, No. 2, pp. 257-265.

Alander, C. 2000. "Punching Prevention in Flat RC Slabs." International Workshop on Punching Shear Capacity of RC Slabs, Proceedings, Royal Institute of Technology, Stockholm, pp. 145-154.

Alexander, S. D. B. and Simmonds, S. H. 1992. Punching shear tests of concrete slab–column joints containing fibre reinforcement. ACI Structural Journal. Vol. 89, No. 4, pp. 425–432.

Anderson, J.A., 1995, "An introduction to neural networks." A bradford book, MIT press, Cambridge, MA.

Barzegar, F., Schnobrich, W.C., 1990, "Post-cracking analysis of reinforced concrete panels including tension stiffening" Canadian Journal of Civil Engineering, Vol. 17, No. 3, pp. 311-320.

Bazant, Z. P., and Cao, Z. 1987. "Size Effect in Punching Shear Failure of Slabs." ACI Structural Journal, Vol. 84, No. 1, pp. 44-53.

Beutel, R., Hegger, J., 2002, "The effect of anchorage on the effectiveness of the shear reinforcement in the punching zone" Cement and Concrete Composites, Vol. 24, No. 6, pp. 539–549.

Beutel, R., Schmidt, M., and Landauer, A. 2000. "3D numerical punching analysis of shear reinforced flat slabs - variation of quantity and arrangement of stirrups." Proceedings of the International Workshop on Punching Shear Capacity of RC Slabs, Stockholm, Kungl Tekniska Hogskolan - Royal Technical University, pp. 181-189.

Bhatt, P., and Lim, B.T. 2000. Punching shear failure of flat slabs: a comparison between nonlinear finite element analysis predictions and experiments. Proceedings of the International Workshop on Punching Shear Capacity of RC Slabs, Stockholm, Kungl Tekniska Hogskolan - Royal Technical University, pp. 47-55.

Binici, B., and Bayrak, O., 2003. Punching shear strengthening of reinforced concrete flat plates using carbon fiber reinforced polymers. Journal of Structural Engineering, ASCE, Vol. 129, pp. 1173-1182.

Birkle, G., Dilger, W.H., 2008. Influence of Slab Thickness on Punching Shear Strength. ACI Structural Journal, Vol. 105, No. 2, Title no. 105-S19, pp. 180-188.

Bishop, C.M., 1995, Neural network for pattern recognition." Oxford University Press, Oxford.

Broms, C.E., 1990, "Punching of flat plates - A question of concrete properties in biaxial compression and size effect." ACI Structural Journal, Vol. 87, no. 3, pp. 292–304.

Broms C. E. 2000. Elimination of Flat Plate Punching Failure Mode, ACI Structural Journal, Vol. 97, No. 1, pp. 94-101.

BS 8110, 1997, British Standards Institution. Structural Use of Concrete, Part 1 – Code of Practice for Design and Construction. London: British Standards Institution.

BS 1881-116: 1983, Testing concrete - Part 116: Method for determination of compressive strength of concrete cubes. British Standards Institution.

BS EN 12390-3:2002, British Standards Institution. Testing hardened concrete - Part 3: Compressive strength of test specimens. British Standards Institution.

CEB FIP Bulletin 12, 2001, "Punching of structural concrete slabs" FIB

CEB-FIP Model Code 1990: Design Code, Comitee Euro-International De Beton, Bulletin D'Information No. 203–305, Lausanne, Switzerland.

Cervera, M., Hinton, E., and Hassan, O., 1987, "Nonlinear analysis of reinforced concrete plate and shell structures using 20-noded isoperimetric brick elements." Computer and Structures, Vol.25, No. 6, pp. 845-869.

Cervenkaa, J., Vassilis, K., Papanikolaoub, V.K., 2008, "Three dimensional combined fracture-plastic material model for concrete." International Journal of Plasticity, Vol. 24, No. 12, pp. 2192-2220.

Chana, P.S., and Desai, S. B. 1992. "Design of shear reinforcement against punching" The Structural Engineer Vol. 70, No. 9, pp. 159–164.

Chen, W.F., 1982, "Plasticity in reinforced concrete", McGraw-Hill Book Company Inc., New York.

Cheng, M.Y., and Parra-Montesinos, G., 2010, "Evaluation of Steel Fiber Reinforcement for Punching Shear Resistance in Slab-Column Connections. Part I: Monotonically Increased Loading", ACI Structural Journal, Vol. 107, No. 1, pp. 101-109.

Clyde D. H. and Carmichael D., 1974 "Lower bound flexural fields and slab shear", Publication SP- 42 Vol. 2, ACI, pp 769 - 784.

Chang, C.H., and Yang, C.C., 2006, "Artificial neural networks in prediction of concrete strength reduction due to high temperature." ACI Materials Journal, Vol. 103, No. 1, pp. 68–69.

Chen, C.C., Li, C.Y., 2000. "An experimental study on the punching shear behaviour of RC slabs strengthened by GFRP" Proceedings, Royal Institute of Technology, Stockholm, pp. 415-422.

Cho, Y.S., Noh, S.Y., Kim, H.W., 2010. Punching shear reinforcing using studs with steel plates in reinforced concrete flat plates. Magazine of Concrete Research, Volume 61, Issue 9, pp. 721 –729 , ISSN: 0024-9831, E-ISSN: 1751-763X.

Collins, M.P., 2000, "Evaluation of Shear Design Procedures for Concrete Structures – A report prepared for the CSA Technical Committee on Reinforced Concrete Design".

Corley, W. G., and Hawkins, N. M., 1968, “Shearhead Reinforcement for Slabs,” ACI JOURNAL, Proceedings Vol. 65, No. 10, pp. 811-824.

CSA standard A 23.3-04: Design of concrete structures. 3rd ed. 2006, Ottawa: Cement Association of Canada.Reinforcement Ratios. ACI Structural Journal, V. 106, No. 1, January-February 2009.

Dilger, W., Birkle, G., Mitchell. D., 2005,”Effect of flexural reinforcement on punching shear resistance” SP-232, American Concrete Institute Special Publication, pp. 57-74.

Ebead, U.A., Marzouk, H., 2005, “Tension-stiffening model for FRP-strengthening RC concrete two-way slabs” Materials and Structures, 38, March 2005, pp. 193-200.

Elshafey, A. A. Rizk, E. Marzouk, H. Haddara, M. R. 2011. Prediction of punching shear strength of two-way slabs. Engineering Structures, Vol. 33, No. 5, pp. 1742-1753.

Elstner, RC, Hognestad, E., 1956, “Shearing strength of reinforced concrete slabs.” Structural Journal of ACI. Vol. 53, No. 7, pp.59–29.

EN 1992-1-1: 2004, Eurocode 2: Design of Cncrete Structures, Part 1-1: General rules and rules for buildings, December 2004.

Esfahani, M. R. Kianoush, M. R. 2009. Punching Shear Strength of Interior Slab-Column Connections Strengthened with Carbon Fiber Reinforced Polymer Sheets. Engineering Structures, Vol.7, Pages 1535-1542.

Erdogan, H., Ozcebe, G., and Binici, B., 2007, “A new CFRP strengthening technique to enhance punching shear strength of RC slab-column connections.” Asia-Pacific on FRP in Structures (APFIS 2007).

Faria, D. M. V. Lúcio, V. J. G. Ramos, A. P. 2011. Strengthening of flat slabs with post-tensioning using anchorages by bonding. Engineering Structures, Vol. 33, No. 6, pp. 2025-2043.

Galvez, J.C., Cervenka, J. C., Cendon, D.A., Saouma, V., 2002, “A discrete crack approach to normal/shear cracking of concrete” Cement and Concrete Research, Vol. 32, pp. 1567–1585.

Gardner, N. J. 1990. Relationship of Punching shear capacity of reinforced concrete slabs with concrete strength. ACI Structural Journal, Vol. 87, No. 1, pp. 66-71.

Gardner, N.J., 1996, "Punching shear provisions for reinforced and pressurised concrete flat slabs." Canadian journal of civil engineering, Vol. 23, No. 2, pp. 502-510.

Gardner N.J., Huh J., Chung L., 2002, "Lessons from Sampoong Department Store Collapse." Cement and Concrete Composites, 24(2), 523-529.

Gardner, N.J. and Shao, X.Y., 1995, "Punching Shear of Continuous Flat Reinforced Concrete Slabs," ACI Structural Journal, Vol. 93, No. 2, March-April 1996, pp.218-228.

Gesoglu, M., Guneyisi, E., Ozturan, T., and Ozbay, E. (2010). "Modeling the mechanical properties of rubberized concretes by neural network and genetic programming." Materials and Structures, Vol. 43, No. 10, pp. 31–45.

Ghannoum, C.M., 1998. Effect of High–Strength Concrete on the Performance of Slab-Column Specimens. MSc thesis, Dep. of Civil Engineering and Applied Mechanics, McGill University, Montreal, Canada.

Goh, A.T.C., Kulhawy, F.H., and Chua, C.G., 2005, "Bayesian neural network analysis of undrained side resistance of drilled shafts." Journal of Geotechnical and Geo-Environmental Engineering, vol. 131, no. 1, pp. 84–93.

Gomes, R.B., and Regan, P.E., 1999. "Punching Resistance of RC Flat Slabs with Shear Reinforcement." ASCE, Journal of Structural Engineering, Vol. 125, No. 6, pp. 684-692.

Gonzalez-Vidosa, F., Kotsovos, M. D. & Pavlovic, M. N., 1987, "Symmetrical punching of reinforced concrete slabs: an analytical ivestigation based on nonlinear finite element modelling." ACI Structural Journal, May-June, pp. 241-50.

Gonzalez-Vidosa, F., Kotsovos, M. D., & Pavlovic, M. N., 1991, "Three-dimensional finite-element model for structural concrete. Part 2: generality study." Proc. Inst. Civil Engineers, Vol. 91, No. 2, pp. 545-60.

Grassl, P., Jirasek, M., 2006, "Damage-plastic model for concrete failure." International Journal of Solids and Structures" Vol. 43, pp. 7166-7196 (doi:10.1016/j.ijsolstr.2006.06.032).

Muttoni A., Burdet, O., Guandalini, S., 2009, "Punching tests of slabs with low reinforcement ratios" ACI Structural Journal, Vol. 106, No1, USA, pp. 87-95.

Guidotti R., Fernández Ruiz M., Muttoni A., 2011, " Behaviour and design of slab-column joints" fib Symposium Prague 2011, Prague, Czech Republic, pp. 399-402.

Hamada, S., Yang, Q., Mao, M., 2008, "Evaluation of punching shear strength of reinforced concrete slabs based on database." Journal of Advanced Concrete Technology, Vol. 6, No. 1, pp. 205-214.

Hawkins, N. M., 1974, "Shear strength of slabs with shear reinforcement", ACI SP-42 Shear in Reinforced Concrete, 785–816.

Hawkins, N.W., Criswell, U.M.E., & Roll, F., 1974, "Shear strength of slabs without shear reinforcement." Shear in Reinforced Concrete (SP-42). American Concrete Institute, Detroit, MI, USA, pp. 677-720.

Hawkins, N.M., Fallsen, G.B., and Hinojosa, R.C., 1971, "Influence of Column Rectangularity on the Behaviour of Flat Plate Structures", SP-30, American Concrete Institute, Farmington Hills, Mich., pp.127-146.

Harajli, M.H. and Soudki, K.A., 2003. Shear Strengthening of Interior Slab-Column Connections using CFRP Sheets. ASCE Journal of Composites in Construction, Vol. 7, No. 2, pp. 145-153.

Harajli, M.H. and Soudki, K.A., Kudsi, T., 2006, "Strengthening of Interior Slab–Column Connections Using a Combination of FRP Sheets and Steel Bolts"Journal of Composite for Construction, Vol.10, No.5, pp. 399-409.

Hillerborg, A., Modeer, M., Petersson, P.E., 1976, "Analysis of crack formation and crack growth in concrete by means of fracture mechanics and finite elements" Vol. 6, No. 6, pp. 773-782.

Hughes, B.P., Xiao, Y., 1995, "Flat slabs with fibre or link reinforcement at slab-column connections." Proceedings of the Institution of Civil Engineers and Buildings, Vol. 110, No. 3, pp. 308-321.

Ioannou, C., 2001. "Behaviour of flat slabs with openings". PhD Thesis, Dep. Of Civil and Structural Engineering, The University of Sheffield, UK.

Iruansi, O., Guadagini, M., Pilakoutas, K., Neocleous, K., 2011, Predicting the shear strength of RC beams without stirrups using bayesian neural network." International Journal of Reliability and Safety, Vol. 5 , No. 1, pp. 82-109.

Israel, R. 1959. Experimental Investigation of Flat Floor Syystems. ACI Journal Proceedings, Vol 56, No. 8, pp. 153-166.

Jankowiak, T., Lodygowski, T., 2005, Identification of parameters of concrete damage plasticity constitutive model" Foundation of Civil and Environmental Engineering, No 6, ISSN 1642-9303, pp. 53-69.

Kang, T. H.-K., and Wallace, J. W., 2005. "Dynamic responses of flat plate systems with shear reinforcement", ACI Structural Journal, Vol. 102, No. 5, pp. 763-773.

Karihaloo, B., 2003, "Failure of concrete" Comprehensive Structural Integrity, Vol. 2, No. 10, pp. 475-546.

Kamaraldinm K., 1990, "Punching shear and moment transfer in reinforced concrete flat slabs" PhD Thesis, The Polytechnic of Central London, UK.

Kim, Y. J. Longworth, J. M. Wight. R. G. Green, M. F. 2009. Punching Shear of Two-way Slabs Retrofitted with Prestressed or Non-prestressed CFRP Sheets. Journal of Reinforced Plastics and Composites, Vol. 00, No. 00/2009, DOI: 10.1177/0731684409103143.

Kingston, G.B., Maier, H.R., and Lambert, M.F., 2005. "A bayesian approach to artificial neural network model selection." pp. 1853-1859.

Kinnuen, S., and Nylander, H., 1960, "Punching of Concrete Slab Without Shear Reinforcement". Transaction of the Royal Institute of Technology. Stockholm, Sweden.

Kose, M.M., 2007, "Prediction of transfer length of prestressing strands using neural networks" ACI Structural Journal, 104(2):162–169.

Krüger, G. Burdet, O. Favre, R. 2000. "Punching strength of RC flat slabs with moment transfer" International Workshop on Punching Shear Capacity of RC Slabs – Proceedings, Royal Institute of Technology, Stockholm, pp. 333-341.

Kuang, J. S., & Morley, C.T., 1992, "Punching shear behavior of restrained reinforced concrete slabs." ACI Structural Journal, Vol. 89, No. 1, pp. 13–19.

Kunz, J. Fernández R. M. Muttoni, A. 2008. "Enhanced safety with post-installed punching shear reinforcement." FIB Symposium, Amsterdam, Netherlands, ISBN 978-0-415-47535-8.

Kupfer, H., Hilsdorf, H. K., Rusch, H., 1969, "Behaviour of concrete under biaxial stresses." ACI Structural Journal, Vol. 65, No. 8, pp. 656-666.

Lee, J., and Fenves, G.L., 1998 "A plastic-damage concrete model for earthquake analysis of dams" Earthquake Engineering & Structural Dynamics, Vol. 27, No. 9, pp. 937–956.

Li, K.K.L., 2000. Influence of Size on Punching Shear Strength of Concrete Slabs. MSc thesis, Dep. of Civil Engineering and Applied Mechanics. McGill University, Montreal, Canada.

Lips, S. And Muttoni, A. 2010. Experimental investigation of reinforced concrete slabs with punchig shear reinforcement. Proceeding of the 8th fib-PhD Symposium, Copenhagen, Denmark, pp. 105-110.

Li, X. 1997. Punching Shear Behaviour of Slab-Column Connections. PhD Thesis, Dep. Of Civil and Structural Engineering, The University of Sheffield, UK.

Lovorovich, J.S., and McLean, D.I., 1990 "Punching Shear Behaviour of Slabs With Varying Span-Depth Ratios" ACI Structural Journal, vol. 87, No. 5, pp. 507-512.

Lubliner, J.J., Oliver, S.O., Oñate, E., 1989, "A plastic-damage model for concrete." International Journal of Solids and Structures, Vol. 25, No. 3, pp. 229-326.

MacKay, D.J.C. 1992, "A practical bayesian framework for back-propagation networks." Neural Computation, vol. 4, No. 3, pp. 448–72.

Malm, R., 2006, "Shear cracks in concrete structures subjected to in-plane stresses"

Lic. Thesis, Royal Institute of Technology (KTH), Stockholm.

Malm, R., 2009, "Predicting shear type crack initiation and growth in concrete with non-linear finite element method." TRITA-BKN. Bulletin 97, Royal Institute of Technology (KTH), Stockholm.

Malm, R., and Holgren, J., 2008"Cracking in deep beams owing to shear loading. Part 2: Non-linear analysis."Magazine of Concrete Research, Vol. 60, No. 5, pp. 381-388.

Mansour, M.Y., Dicleli, M., Lee, J.Y., and Zhang, J., 2004, "Predicting the shear strength of reinforced concrete beams using artificial neural networks." Engineering Structures, Vol. 26, No. 6, pp. 781- 799.

Marzouk, H., and Chen, Z., 1993. Finite element analysis of high strength concrete slabs. Structural Journal of ACI, Vol. 90, pp. 505-513.

Marzouk, H., Emam, M., and Hilal, M.S., 1996, "Effect of high-strength concrete columns on the behaviour of slab-column connections" ACI Structural Journal, Proceedings, Vol. 93, No. 5.

Marzouk, H., Emam, M., and Hilal, M.S., 1998, "Effect of high-strength concrete slabs on the behaviour of slab-column connections" ACI Structural Journal, Proceedings, Vol. 95, No. 3.

Marzouk, H., Hussein, A., 1991. Experimental Investigation on the Behaviour of High-Strength Concrete Slabs. ACI Structural Journal, Proceedings, Vol. 88, No. 6, pp. 701-713.

Marzouk, H., Jiang, D. 1996. Finite Element Evaluation of Shear Enhancement of High-Strength Concrete Plates. ACI Structural Journal, Vol. 93, No. 5, pp. 667-673.

Marzouk, H., and Jiang, D., 1997, "Experimental Investigation on Shear Enhancement Types for High-Strength Concrete Plates" ACI Structural Journal, Vol. 94, No. 1.

Matthys, S. Taerwe, L. 2000. Verification of the punching resistance of concrete slabs reinforced with FRP grids. International Workshop on Punching Shear Capacity of RC Slabs – Proceedings, Royal Institute of Technology, Stockholm, pp. 475-484.

McHarg P. J. Cook W. D. Mitchell D. and Young-Soo Y. 2000. Benefits of concentrated slab reinforcement and steel fibers on performance of slab–column connections. ACI Structural Journal. Vol. 97, No.2, pp. 225–234.

Megally, S., 1998, "Punching shear resistance of slabs in gravity and earthquake forces" PhD Thesis, Dep. of Civil Engineering, The University of Calgary, Calgary, Alberta.

Megally, S., and Ghali, A., 1994, "Design Considerations for Slab-Column Connections in Seismic Zones," ACI Structural Journal, V. 91, No. 3, May-June, pp. 303-314.

Megally, S. and Ghali, A., 2000, "Seismic Behaviour of Edge Column-Slab Connections with Stud Shear Reinforcement.", ACI Structural Journal, Vol. 97, No. 1, Jan.-Feb., pp. 53-60.

Menetrey, Ph., 1994,"Numerical analysis of punching failure in reinforced concrete structures." 179 pp., Thesis No. 1279, Dep. De Genie Civil, EPFL Lausanne.

Menetrey, P., 1996. “Analytical Computation of the Punching Strength of Reinforced Concrete.” Structural Journal of ACI, Vol. 93, No. 5, pp.503-501.

Menetrey, P., 2002, “Synthesis of punching failure in reinforced concrete” Cement and Concrete Composites, Vol. 24, No. 6, pp. 497-507.

Michell, D., Cook, W.D., Dilger, W., 2005, “Effects of Size, Geometry and Material Properties on Punching Shear Resistance” SP-232, American Concrete Institute Special Publication, pp. 39-59.

Mitchell, D., DeVall, R. H., Saatcioglu, M., Simpson, R., Tinawi, R., and Tremblay, R., 1995. “Damage to Concrete Structures due to the 1994 Northridge Earthquake.” Canadian Journal of Civil Engineering, Vol.22, No.4, pp-361-377.

Michel, L. Ferrier, E. Bigaud, D. Agbossou, A. 2007. Criteria for punching failure mode in RC slabs reinforced by externally bonded CFRP. Composite Structures 81 (2007) 438–449.

Moe, J., 1961. “Shearing Strength of Reinforced Concrete Slabs and Footings under Concentrated Loads.” Development Department Bulletin D 47, PCA Research and Development Laboratories, Illinois, 130 pp.

Mokhtar, A. Ghali, A. and Dilger, W., 1985. Stud Shear Reinforcement for Flat Concrete Plates. ACI JOURNAL, Proceedings Vol. 82, No. 5, pp. 676-683.

Mowrer, R. D. and Vanderbilt, M. D. 1967. Shear Strength of lightweight aggregate reinforced concrete flat plates. Journal of ACI, Vol. 64, No. 11, pp. 722-727.

Nguyen-Minh, L., Rovanak, M., Tran-Quoc, T., Nguyenkim, K., 2011, “Punching Shear Resistance of Steel Fiber Reinforced Concrete Flat Slabs” Procedia Engineering, Vol. 14, 2011, pp. 1830–1837.

Oliveira, D.R., Melo, G.S., and Regan, P. E., 2000, “Punching Strengths of Flat Plates with Vertical or Inclined Stirrups”, ACI Structural Journal, Vol. 97, pp. 485-491.

Oliveira, D.R.C., Regan, P. And Melo, G.S.S., 2004. Punching Resistance of RC Slabs with Rectangular Column. Magazine of Concrete Research, Vol.56, No. 3, London, pp. 123-138.

Osman, M. Marzouk, H. and Helmy, S., 2000. Behavior of High-StrengthLightweight Concrete Slabs under Punching Loads. ACI Structural Journal,Vol. 97, No. 3, pp. 492-498.

Ospina, C.E. Alexander, S.D. B., and Roger Cheng, J.J. 2003. Punching of two-way concrete slabs with fiber-reinforced polymer reinforcing bars or grids. ACI structural Journal, Vol. 100, No. 5, pp. 589-598.

Ozawa, M. Uchida, Y. Koyanagi, W. 2000. Study on the process on punching shear failure of RC slabs. International Workshop on Punching Shear Capacity of RC Slabs – Proceedings, Royal Institute of Technology, Stockholm, pp. 145-154.

Ožbolt, J., Vocke, H. and Eligehausen, R. 2000. "Three-dimensional numerical analysis of punching failure." Proceedings of the International Workshop on Punching Shear Capacity of RC Slabs, Stockholm, Kungl Tekniska Hogskolan - Royal Technical University, pp. 65-74.

Ozden, S. Ersoy, U. Ozturan, T. 2006. Punching shear tests of normal- and high-strength concrete flat plates. Canadian Journal of Civil Engineering, Vol. 33, No. 11, pp. 1389-1400 doi: 10.1139/l06-089.

Papanikolaou, K. V. Tegos, I. A. and Kappos, A. J. 2005. Punching Shear Testing of Reinforced Concrete Slabs, and Design Implications. Magazine of Concrete Research, Vol. 57, No. 3, pp. 167–177.

Pisanty, A. 2005. Eurocodes and North American Codes Predictions of Punching Shear Capacity in View of Experimental Evidence. Special Publication SP-232, pp. 257-276.

Polak, M., 1998b, "Modelling punching shear of reinforce concrete slabs using layered finite elements." ACI Structural Journal, Vol. 95, No. 1, pp. 71-80.

Polak, M., 1998b, "Shear analysis of reinforced concrete shells using degenerate elements" Computers & Structures, Vol. 68, No. 1–3, pp. 17–29.

Polak, M. A.; El-Salakawy, E., and Hammill, N. L., 2005 "Shear Reinforcement for Concrete Flat Slabs.", Punching Shear in Reinforced Concrete Slabs, SP-232, American Concrete Institute Special Publication, pp. 75-95.

Ramos, A.P., Lucio, V.J.G., Regan, P.E., 2011, "Punching of flat-slabs with in-plane forces" Engineering Structures, Vol. 33, No. 3, pp. 894-902.

Rankin, G.I.B. and Long, A.E., 1987 "Predicting the punching strength of conventional slab-column specimens", Proceedings of the Institution of Civil Engineers, Part I, Vol 82, April, pp 327-346.

Rankin, G.I.B. and Long, A.E., 1987 "'Predicting the enhanced punching strength of interior slab-column connections", Proceedings of the Institution of Civil Engineers, Part I, Vol 82, December, pp 1165-1186.

Regan, P.E., 1981 "Behaviour of Reinforced Concrete Flat Slabs," CIRIA Report No.89, Construction Industry Research and Information Association, London, United, Kingdom.

Regan, P.E., 2000. "Shear reinforcement of flat slabs". International Workshop on Punching Shear Capacity of RC Slabs – Proceedings, Royal Institute of Technology, Stockholm, pp. 99-108.

Regan, P.E., 2004, "Punching of slabs under highly concentrated loads" Proceedings of the Institution of Civil Engineers, Structures and Buildings 157, Issue SB2, pp. 165-171.

Regan, P. E. and Samadian, F.2001. Shear Reinforcement against punching in reinforced concrete flat slabs, The Structural Engineer, pp. 24-31, London, England.

Robertson, I., Kawai, T., Lee, J., and Enomoto, B., 2002, "Cyclic Testing of Slab-Column Connections with Shear Reinforcement," ACI Structural Journal, Vol. 99, No. 5, Sept.-Oct., pp. 605-613.

Regan, P. E. 1986. Symmetric punching of reinforced concrete slabs. Magazine of Concrete Research, Volume 38, Issue 136, pp. 115 –128 , ISSN: 0024-9831, E-ISSN: 1751-763X.

Richart, F.E., 1948, "Reinforced Concrete Wall and Column Footings, Part 1," Journal of the American Concrete Institute, V. 45, No. 2, 1948, pp. 97-127.

Rizk, E. And Marzouk, H. 2011. Experimental validation of minimum flexural reinforcement for thick high-strength concrete plates. ACI Structural Journal, Vol. 108, No. 3. pp. 332-340.

Rizk, E., Marzouk, H., Hussein, A., 2011. Punching Shear of Thick Plates with and without Shear Reinforcement" ACI Structural Journal, Vol. 108, No. 5. pp. 581-591.

Ruiz, Muttoni, 2010,3rd Fib Congress, Performance and design of punching shear reinforcement systems.

Sakinis, D. Vainiunas, P. 2009. Influence of longitudinal reinforcement on the punching shear resistance of reinforced concrete slabs /Isilginio armavimo poveikis gelzbetonines

plokstes praspaudziamajai laikomajai galiai. Engineering Structures and Technologies, Vol. 1, No. 2, pp. 73–79.

Scordelis, A. C., et al. (1958). Shearing strength of prestressed lift slabs. Journal of American Concrete Institute, Vol. 55, No. 32, pp. 485–506.

Shah,A.A., Ribakov, Y., 2011, "Estimation of Rc slab-column joints effective strength using neural networks" Latin American Journal of Solids and Structures, Vol 8, No 4.

Shehata, I.A.E.M., 1990, "Rational Method For Designing R.C. Slabs To Resist Punching", Journal of the American Society of Civil Engineeris, Structure Division, ASCE, vol. 116, No. 7, pp. 2055 – 2060.

Shehata, I.A. E. M., 1990 "Simplified model for the estimating the punching resistance of reinforced concrete slabs" Materials and Structures, Vol. 23, No. 137, pp. 364-370.

Shehata, I.A. E. M., and Regan, P.E., 1989, "Punching in RC slabs" ASCE Journal of Structural Engineering, Vol. 115, No. 7, pp. 1726-1740.

Sissakis, K. and Sheikh, S. A. 2007. Strengthening Concrete Slabs for Punching Shear with Carbon Fiber-Reinforced Polymer Laminates. ACI Structural Journal, Vol. 104, No. 1, pp. 49-59.

Sistonen, E., Huovinen, S., 2011, "Results of the new reinforcing technology Project."

Smadi, M. M. Bani Yasin, I. S. 2008. Behavior of high-strength fibrous concrete slab–column connections under gravity and lateral loads. Construction and Building Materials, Vol. 22, No. 8, pp. 1863-1873.

Staller, M.A., 2000, "Analytical studies and numerical analysis of punching shear failure in reinforced concrete slabs." Stockholm: Royal Institute of technology, TRITABKN, Bulletin 57.

Stein, T. Ghali, A. and Dilger, W. 2007. Distinction between Punching and Flexural Failure Modes of Flat Plates. ACI Structural Journal, Vol. 104, No. 3, pp. 357-365.

Subedi, N.K., Baglin, P.S., 2003, "Design of slab–column junctions in flat slabs" Proceedings of the ICE - Structures and Buildings, Vol. 156, No. 3, pp. 319 –331.

Sundquist H, Kinnunen S. 2004. The effect of large column section and slab thickness taper on the punching shear capacity of flat slabs. Bulletin No. 81, Dept. of Civil and

Architectural Engineering, Royal Institute of Technology, Stockholm, 42 pp. (in Swedish with summary and Figure captions in English).

Swamy, R. N. and Ali, S. A. R. 1982. "Punching Shear Behaviour of Reinforced Slab-Column Connections Made with Steel Fiber Concrete, ACI JOURNAL, Proceedings V. 79, No. 5, May, pp. 392-406.

Talbot, A.N., 1913, "Reinforced Concrete Wall Footings and Column Footings", Engineering Experiment Station, University of Illinois, Urbana, Illinois, USA, Bulletin No. 67, 114pp.

Teng, S. Cheong, H. K. Kuang, K. L. Geng, J. Z. 2004. Punching Shear Strength of Slabs with Openings and Supported on Rectangular Columns. ACI Structural Journal, Vol. 101, No. 5, Document 101-S67.

Theodorakopoulos D.D. and Swamy, R.N., 2002. Ultimate punching Strength Analysis of Slab-column Connections. Cement & Concrete Composites, Vol. 24, No.6, pp.509-521.

Theodorakopoulos D.D. and Swamy, R.N., 2003 "A Design Method for Punching Shear Strength of Steel Fiber Reinforced Concrete Slabs", ACI Special Publication,Sp 216-12, Vol. 216.

Tian, Y., 2007, "Behaviour and modelling of reinforced concrete slab-column connections" PhD Thesis, The University of Texas at Austin, UMI Number: 3268386.

Vaz, A.R.P., Gomez, R.B., Shehata, L.C.D., 2009, "Study on Minimum shear reinforcement of RC flat slabs." IBRACON Structures and Materials Journal, Vol.2, No. 1, pp. 1-24.

Yamada, T. Nanni, A. and Endo, K. 1992. Punching Shear Resistance of Flat Slabs: Influence of Reinforcement Type and Ratio. ACI Structural Journal, Vol. 88, No. 4, pp. 555-563.

Yang, J.M., Yoon, Y.S., Cook, W.D., Mitchell, D., 2010, "Punching Shear behaviour of two-way slabs reinforced with high strength steel." ACI Structural Journal, vol. 107, No. 4, pp. 468-475.

Yitzhaki, D. 1966. Punching Strength of Reinforced Concrete Slabs. Journal of American Concrete Institute, Title no. 63-25, pp. 527-542.

Appendix A

Database on slab-column connections without shear reinforcement:

Source	Specimen	*h* (mm)	*d* (mm)	*c* (mm)	Rho (%)	*fy* (Mpa)	f'c (Mpa) Cylinder	Rho bottom (%)	L (mm)	Contraflexural point	*V*test (kN)
Li (2000)	P100	135	100	200	0.98	488	39.4	0.22	925	925	330
	P150	190	150	200	0.9	465	39.4	0.11	1190	1190	583
	P200	240	200	200	0.83	465	39.4	0.14	1450	1450	904
	P300	345	300	200	0.76	468	39.4	0.1	1975	1975	1381
	P400	450	400	300	0.76	433	39.4	0.08	1975	1975	2224
	P500	550	500	300	0.76	433	39.4	0.1	1975	1975	2681
Ramadan K-E (1996): cited in Swamy and Ali (1982)	1	125	98	150	0.58	550	88.2	0	1700	1372	224
	2	125	98	150	0.58	550	56.2	0	1700	1372	212
	3	125	98	150	0.58	550	26.9	0	1700	1372	169
	4	125	98	150	0.58	550	58.7	0	1700	1372	233
	6	125	98	150	0.58	550	101.8	0	1700	1372	233
	12	125	98	150	1.28	550	60.4	0	1700	1372	319
	13	125	98	150	1.28	550	43.4	0	1700	1372	297
	14	125	98	150	1.28	550	60.8	0	1700	1372	341
	16	125	98	150	1.28	550	98.4	0	1700	1372	362
	21	125	98	150	1.28	650	41.9	0	1700	1372	286
	22	125	98	150	1.28	650	84.2	0	1700	1372	405
	23	125	100	150	0.87	650	56.4	0	1700	1372	341
	25	125	100	150	1.27	650	32.9	0	1700	1372	244
	26	125	100	150	1.27	650	37.6	0	1700	1372	294
	27	125	102	150	1.03	650	33.7	0	1700	1372	227
Marzouk and Hussein (1991)	HS1	120	95	150	0.39	490	67.0	0.42	1700	1500	178
	HS2	120	95	150	0.68	490	70.0	0.42	1700	1500	249
	HS3	120	95	150	1.17	490	69.0	0.42	1700	1500	356
	HS4	120	90	150	0.88	490	66.0	0	1700	1500	418
	HS5	150	125	150	0.52	490	68.0	0	1700	1500	365
	HS6	150	120	150	0.54	490	70.0	0	1700	1500	489
	HS7	120	95	150	0.97	490	74.0	0	1700	1500	356
	HS8	150	120	150	0.95	490	69.0	0	1700	1500	436
	HS9	150	120	150	1.47	490	74.0	0	1700	1500	543
	HS10	150	120	150	2.08	490	80.0	0	1700	1500	645
	HS11	90	70	150	0.73	490	70.0	0	1700	1500	196
	HS12	90	70	150	1.19	490	75.0	0	1700	1500	258
	HS13	90	70	150	1.58	490	68.0	0	1700	1500	267
	HS14	120	95	220	1.17	490	72.0	0	1700	1500	498
	HS15	120	95	300	1.17	490	71.0	0	1700	1500	560
	NS1	120	95	150	1.17	490	42.0	0	1700	1500	320
	NS2	150	120	150	0.54	490	30.0	0	1700	1500	396
Tolf 1998: cited in FIB bulletin 12	S2.1	240	200	250	0.8	657	24.2	0	2540	2378	603
	S2.2	240	199	250	0.8	670	22.9	0	2540	2378	600
	S2.3	240	200	250	0.45	668	25.4	0	2540	2378	489
	S2.4	240	197	250	0.45	664	24.2	0	2540	2378	444
	S1.1	120	100	125	0.8	706	28.6	0	1270	1189	216
	S1.2	120	99	125	0.8	701	22.9	0	1270	1189	194
	S1.3	120	98	125	0.4	720	26.6	0	1270	1189	145
	S1.4	120	99	125	0.4	712	25.1	0	1270	1189	148
Stein et al, 2007	V1	150	118	250	0.45	438	29.7	0.54	1900	1800	329

	V2	150	118	250	0.98	438	26.2	0.54	1900	1800	438
	V3	150	118	250	0.62	438	25.7	0.54	1900	1800	365
Guandalini *et al*., 2009	PG-1	250	210	260	1.5	573	27.6	0.2	3000	3000	1023
	PG-2B	250	210	260	0.25	552	40.5	0.2	3000	3000	440
	PG-4	250	210	260	0.25	541	32.2	0.2	3000	3000	408
	PG-5	250	210	260	0.33	555	29.3	0.2	3000	3000	550
	PG-10	250	210	260	0.33	577	28.5	0.2	3000	3000	540
	PG-11	250	210	260	0.75	570	31.5	0.2	3000	3000	763
	PG-3	500	456	520	0.33	520	32.4	0.2	6000	5700	2153
	PG-6	125	96	130	1.5	526	34.7	0	1500	1500	238
	PG-7	125	100	130	0.75	550	34.7	0	1500	1500	241
	PG-8	125	117	130	0.28	525	34.7	0	1500	1500	140
	PG-9	125	117	130	0.22	525	34.7	0	1500	1500	115
Papanikolaou *et al*., 2005	P51	100	80	150	0.54	550	33.1	0	750	750	210
	P52	100	80	150	0.54	550	34.5	0	750	750	219
	P53	100	80	150	0.54	550	31.1	0	750	750	216
	P101	100	80	150	1.08	550	33.9	0	750	750	256
	P102	100	80	150	1.08	550	31.7	0	750	750	244
	P103	100	80	150	1.08	550	32.5	0	750	750	248
	p10-5	100	80	150	0.54	550	29.1	0	750	750	164
	p10-10	100	80	150	1.08	550	32.5	0	750	750	225
	p15-5	150	130	150	0.54	550	32.1	0	750	750	310.4
	p15-10	150	130	150	1.08	550	30.6	0	750	750	355.2
	p20-5	200	180	150	0.54	550	30.3	0	750	750	459.1
	p20-10	200	180	150	1.08	550	32.1	0	750	750	501.1
	p25-5	250	230	150	0.54	550	32.5	0	750	750	578.5
	p25-10	250	230	150	1.08	550	29.4	0	750	750	635.7
Ozden *et al*., 2006	NR1E0F0	120	100	200	0.73	507	21.6	0.37	1500	1200	188
	NR2E0F0	120	100	200	1.09	507	20.0	0.52	1500	1200	202
	HR1E0F0	120	100	200	1.5	471	74.0	0.72	1500	1200	331
	HR1E0F0r	120	100	200	1.5	471	75.0	0.72	1500	1200	371
	HR2E0F0	120	100	200	2.25	471	63.7	1.13	1500	1200	405
	HR2E0F0r	120	100	200	2.25	471	74.7	1.13	1500	1200	489
	NR1E0F1	120	100	200	0.73	507	19.6	0.37	1500	1200	266
	NR2E0F1	120	100	200	1.09	507	19.3	0.52	1500	1200	245
	HR1E0F1	120	100	200	1.5	471	81.3	0.72	1500	1200	576
	HR2E0F1	120	100	200	2.25	471	79.3	1.13	1500	1200	691
Birkle and Dilger (2008)	1	160	124	250	1.54	488	36.2	0.4	1000	1000	483
	7	230	190	300	1.3	531	35.0	0.26	1500	1500	825
	10	300	260	350	1.1	524	31.4	0.19	1900	1900	1046
Regan (2004)	1	160	128	50	0.93	520	38.0	0.19	2000	1830	200
	2	160	128	75	0.93	520	43.2	0.19	2000	1830	260
	3	160	128	100	0.93	520	46.6	0.19	2000	1830	335
	4	160	128	170	0.93	520	41.7	0.19	2000	1830	380

	5	160	128	25	0.93	520	43.8	0.19	2000	1830	190
	6	160	128	50	0.93	520	30.2	0.19	2000	1830	190
	7	160	124	50	1.71	500	37.4	0.19	2000	1830	220
Regan 1986	I/1	100	77	200	1.2	500	25.8	0	2000	1830	194
	I/2	100	77	200	1.2	500	23.4	0	2000	1830	176
	I/3	100	77	200	0.92	500	27.4	0	2000	1830	194
	I/4	100	77	200	0.92	500	32.3	0	2000	1830	194
	I/5	100	79	200	0.75	480	28.2	0	2000	1830	165
	I/6	100	79	200	0.75	480	21.9	0	2000	1830	165
	I/7	100	79	200	0.8	480	30.4	0	2000	1830	186
	II/1	250	200	250	0.98	530	34.9	0	-	2745	825
	II/2	160	128	160	0.98	485	33.3	0	-	1800	390
	II/3	160	128	160	0.98	485	34.3	0	-	1800	365
	II/4	80	64	80	0.98	480	33.3	0	-	900	117
	II/5	80	64	80	0.98	480	34.3	0	-	900	105
	II/6)	80	64	80	0.98	480	36.2	0	-	900	105
	III/1	120	95	150	0.83	494	23.2	0	1500	1370	197
	III/2	120	95	150	0.83	494	9.5	0	1500	1370	123
	III/3	120	95	150	0.83	494	37.8	0	1500	1370	214
	III/4	120	93	150	1.52	464	11.9	0	1500	1370	154
	III/5	120	93	150	1.52	464	26.8	0	1500	1370	214
	III/6	120	93	150	1.52	464	42.8	0	1500	1370	248
	V/1	150	118	54	0.78	628	34.3	0	1600	1500	170
	V/2	150	118	170	0.78	628	32.2	0	1600	1500	280
	V/3	150	118	110	0.78	628	32.4	0	1600	1500	265
	V/4	150	118	102	0.78	628	36.2	0	1600	1500	285
	V/5	150	118	150	0.78	628	32.9	0	1600	1500	285
Lovrovich and McLean (1990)	F1	100	83	100	1.71	531	40.0	1.71	500	200	480
	F2	100	83	100	1.71	531	40.0	1.71	700	400	204
	F3	100	83	100	1.71	531	40.0	1.71	900	600	149
	F4	100	83	100	1.71	531	40.0	1.71	1100	800	129
	F5	100	83	100	1.71	531	40.0	1.71	1500	1200	139
Marti et al., 1977: cited in FIB bulletin 12	P2	180	143	300	1.49	558	34.6	0.46	2750	2600	628
Pralong et al., 1979: cited in FIB bulletin 12	P5	191	171	300	1.15	515	26.2	0.29	2750	2600	626
Schaefers 1978: cited in FIB bulletin 12	0	143	113	210	0.82	420	22.2	0	1960	1680	280
	3	200	170	210	0.54	450	21.3	0	1960	1680	460
Lander *et al*., (1977) : cited in FIB bulletin 12	DA6	110	80	100	1.8	550	30.0	1.8	1260	1056	183
	DA7	110	80	200	1.8	550	33.5	1.8	1260	1056	288
	DA10	110	80	240	1.8	550	32.0	1.8	1260	1056	281
	DA11	110	80	320	1.8	550	30.4	1.8	1260	1056	324
Lander *et al*., 1973 : cited in FIB bulletin 12	P1	280	240	500	1.31	544	27.9	0	2900	2650	1662
	M1	127	127	226	1.18	541	31.8	0	1400	1200	362
Corley and Hawkins (1968): cited in FIB bulletin 12	AN-1	146	111	254	1.51	404	44.4	0	2135	1820	334
	AN-2	146	111	203	1.01	444	44.4	0	2135	1820	266
Base (1966) - Bernaert and Puech (1966): all cited in FIB bulletin 12	A1/M1	140	114	203	1.1	255	16.3	0	1370	1370	322
	A1/M2	140	117	203	1.5	282	15.5	0	1370	1370	346
	A1/M3	140	121	203	1.9	282	14.2	0	1370	1370	307
	A1/M4	140	124	203	1	432	14.0	0	1370	1370	259
	A1/M5	140	117	203	1.2	432	21.0	0	1370	1370	346

	A2/M1	140	124	203	1	255	35.4	0	1370	1370	409
	A2/M2	140	117	203	1.5	282	32.8	0	1370	1370	419
	A2/M3	140	121	203	1.9	282	32.8	0	1370	1370	430
	A2/T1	140	124	203	1	432	32.5	0	1370	1370	419
	A2/T2	140	124	203	1.7	432	39.3	0	1370	1370	439
	A3/M1	140	124	203	1	255	41.4	0	1370	1370	247
	A3/M2	140	102	203	1.7	282	18.8	0	1370	1370	336
	A3/M3	140	117	203	1.9	282	19.3	0	1370	1370	298
	A3/T1	140	121	203	1	432	27.3	0	1370	1370	328
	A3/T2	140	119	203	1.2	432	20.6	0	1370	1370	298
	A4/M1	140	114	203	1.1	255	16.0	0	1370	1370	259
	A4/M2	140	119	203	1.5	282	38.3	0	1370	1370	341
	A4/M3	140	117	203	1.9	322	29.2	0	1370	1370	541
	A4/T1	140	114	203	1.1	432	32.2	0	1370	1370	384
	A4/T2	140	117	203	1.2	432	32.8	0	1370	1370	402
Manterola (1966): cited in FIB bulletin 12	P1-S1	125	107	100	1.04	304	25.6	0	3250	3000	216
	P2-S1	125	107	250	1.04	304	33.8	0	3250	3000	257
	P3-S1	125	107	450	1.04	304	29.7	0	3250	3000	301
	P1-S2	125	107	100	1.04	324	24.2	0.52	3250	3000	196
	P2-S2	125	107	250	1.04	324	33.1	0.52	3250	3000	283
	P3-S2	125	107	450	1.04	324	31.9	0.52	3250	3000	397
	P1-S3	125	107	100	1.04	324	39.7	1.04	3250	3000	184
	P2-S3	125	107	100	1.41	324	35.8	1.04	3250	3000	211
	P3-S3	125	107	100	0.52	324	39.2	1.04	3250	3000	165
	P1-S4	125	107	100	0.46	451	26.4	0	3250	3000	175
	P2-S4	125	107	250	0.46	451	31.3	0	3250	3000	246
	P3-S4	125	107	450	0.46	451	34.2	0	3250	3000	294
Moe (1961)	S1-60	152	114	254	1.05	399	23.3	0	1830	1780	389
	S2-60*	152	114	254	1.5	399	22.1	0	1830	1780	356
	S3-60*	152	114	254	2	399	22.6	0	1830	1780	364
	S4-60*	152	114	254	2.6	399	23.8	0	1830	1780	334
	S1-70	152	114	254	1.05	483	24.5	0	1830	1780	393
	S2-70*	152	114	254	2	483	25.4	0	1830	1780	378
	S3-70*	152	114	254	2.6	483	35.2	0	1830	1780	374
	S4-70A*	152	114	254	2.6	483	20.5	0	1830	1780	312
	s5-60	152	114	254	1.05	399	22.2	0	1830	1780	343
	S5-70	152	114	254	1.05	483	23.0	0	1830	1780	378
	R1	152	114	254	1.43	328	26.6	0	1830	1780	312
	R2	152	114	254	1.43	328	27.6	0	1830	1780	394
	H1	152	114	254	1.056	328	26.1	0	1830	1780	372
	M1A	152	114	254	1.51	481	20.8	0	1830	1780	433
Elstner and Hognested (1956)	I A-1a	152	118	254	1.15	332	11.3	0.56	1830	1780	303
	I A-1b	152	118	254	1.15	332	20.2	0.56	1830	1780	365
	I A-1c	152	118	254	1.15	332	23.2	0.56	1830	1780	356
	I A-1d	152	118	254	1.15	332	29.4	0.56	1830	1780	351
	I A-1e	152	118	254	1.15	332	16.2	0.56	1830	1780	356
	I A-2a	152	114	254	2.47	321	10.9	1.15	1830	1780	334
	I A-2b	152	114	254	2.47	321	15.6	1.15	1830	1780	400
	I A-2c	152	114	254	2.47	321	29.9	1.15	1830	1780	467
	I A-7b	152	114	254	2.47	321	22.3	1.15	1830	1780	512
	I A-3a	152	114	254	3.7	321	10.2	1.15	1830	1780	356
	I A-3b	152	114	254	3.7	321	18.1	1.15	1830	1780	445
	I A-3c	152	114	254	3.7	321	21.2	1.15	1830	1780	534
	I A-3d	152	114	254	3.7	321	27.6	1.15	1830	1780	547
	II A-4	152	118	356	1.15	332	20.9	0.56	1830	1780	400

	II A-5	152	114	356	2.47	321	22.2	1.15	1830	1780	534
	II A-6	152	114	356	3.7	321	20.0	1.15	1830	1780	498
	V A-9*	152	114	254	2.48	321	23.9	1.15	1830	1780	445
	V A-10*	152	114	356	2.49	321	23.8	1.15	1830	1780	489
	VII-A-13	152	121	356	0.57	294	21.0	0.28	1830	1780	236
	VIII B-1	152	114	254	0.49	324	11.4	0	1830	1780	178
	VIII B-2	152	114	254	0.49	321	38.1	0	1830	1780	200
	VIII B-4	152	114	254	0.86	303	38.2	0	1830	1780	334
	VIII B-9	152	114	254	2.04	341	35.1	0	1830	1780	505
	VIII B-11	152	114	254	2.91	409	10.8	0	1830	1780	329
	VIII B-14	152	114	254	2.91	325	40.4	0	1830	1780	578
kinnunen and Nylander (1960)	5	150	117	150	0.8	441	26.8	0	1840	1710	255
	6	150	118	150	0.79	454	26.2	0	1840	1710	275
	24	150	128	300	1.01	455	26.4	0	1840	1710	430
	25	150	124	300	1.04	451	25.1	0	1840	1710	408
	32	150	123	300	0.49	448	26.3	0	1840	1710	258
	33	150	125	300	0.48	462	26.4	0	1840	1710	258
	IA15a-5	149	117	150	0.8	441	27.9	0	1840	1710	255
	IA15a-6	151	118	150	0.8	454	25.8	0	1840	1710	275
	IA15c-11	153	121	150	1.8	436	31.4	0	1840	1710	334
	IA15c-12	154	122	150	1.7	439	28.8	0	1840	1710	332
	IA30c-30	151	120	300	2.1	436	29.5	0	1840	1710	491
	IA30c-31	151	119	300	2.1	448	29.5	0	1840	1710	540
	IA30a-24	158	128	300	1	456	25.9	0	1840	1710	430
	IA30a-25	154	124	300	1.1	451	24.6	0	1840	1710	408
	IA30d-32	155	123	300	0.5	448	25.8	0	1840	1710	258
	IA30D-33	154	125	300	0.5	462	26.2	0	1840	1710	258
	IA30e-34	150	120	300	1	461	26.9		1840	1710	332
	IA30e-35	153	122	300	1	459	24.6		1840	1710	332
Marzouk *et al*., 1996	N.H.Z.S.1.0	150	119	250	1.06	460	32.2	0.35	1900	1870	475.5
	N.N.Z.S.1.0	150	119	250	1.06	460	37.2	0.35	1900	1870	474
Marzouk *et al*., 1998	H.H.Z.S.1.0	150	119	250	1.06	460	67.2	0.35	1900	1900	511.52
Marzouk and Jiang (1997)	HS17	150	120	250	1.093	490	67.0	0.3	1950	1950	511.1
Broms (2000)	9	180	150	250	0.44	500	26.9	0.21	2600	2000	408

	9a	180	150	250	0.44	500	21.0	0.21	2600	2000	360
Alexander and Simmonds (1992)	P11S150	155	133	200	0.5	438	33.2	0.28	2750	2750	257
	P38S150	155	133	200	0.63	438	35.6	0.35	2750	2750	264
	P19S150	155	133	200	0.54	438	26.0	0.3	2750	2750	258
	P19RE	155	133	200	0.54	438	35.3	0.3	2750	2750	304
	P19S75	155	133	200	0.67	438	26.0	0.3	2750	2750	258
	P19S50	155	133	200	0.82	438	26.0	0.3	2750	2750	319
Binici and Bayrak (2003)	Control 1	152	114	304	1.76	448	28.3	0	2133	2133	494
	Control 2	152	114	304	1.76	448	28.3	0.12	2133	2133	510
Ospina et al. (Sep. 2003)	SR-1	155	120	250	0.86	430	36.8	0	2150	1794	365.1
Chen and Li (2000)	SR1-C1	100	75.2	150	0.56	482	16.9	0	1000	840	103.9
	SR1-C2	100	75.2	150	0.56	482	34.4	0	1000	840	123.88
	SR2-C1	100	75.2	150	1.23	482	16.9	0	1000	840	146.1
	SR2-C2	100	75.2	150	1.23	482	34.4	0	1000	840	225.7
McHarg et al., 2000	NU	150	110	225	1.11	434	30.0	0.36	2300	2108	306
	NB*	150	110	225	2.15	434	30.0	0.36	2300	2108	349
Swamy & Ali (1982)	S-1	125	100	150	0.52	462	38.9	0.2	1800	1690	197.7
	S-7*	125	100	150	0.72	462	38.9	0.31	1800	1690	221.7
	S-19	125	100	150	0.35	462	38.9	0.2	1800	1690	130.7
Theodorakopolus & Swamy (2003)	FS1	125	100	150	0.53	460	35.4	0.2	1800	1690	174
	FS8	125	100	100	0.53	460	36.6	0.2	1800	1690	150
	FS10	125	100	200	0.53	460	36.4	0.2	1800	1690	137
	FS19	125	100	150	0.35	460	34.5	0.2	1800	1690	191
Osman et al. 2000 ACI	NSNW0.5p	150	120	250	0.5	450	37.8	0	1900	1830	310.22
Harajli *et al*., 2006	A1	55	37	100	1	487	31.9	0	670	670	45.9
	A2	55	37	100	1	488	31.5	0	670	670	56.4
	B1	75	55	100	1.5	488	35.5	0	670	670	73.5
	B2	75	55	100	1.5	488	29.1	0	670	670	113.8
	SA1	55	37	100	1	597	26.1	0	670	670	52.9
	SA2	55	37	100	1	597	25.4	0	670	670	72.1
	SB1	75	55	100	1.5	488	28.1	0	670	670	83
	SB2	75	55	100	1.5	488	31.5	0	670	670	109.7
Mokhtar *et al*., 1985	AB1	150	108	250	1.56	516	36.0	0.38	1900	1800	408
Yamada *et al*., 1992	T1	200	160	300	1.23	811	21.6	0.62	2000	1581	441
	K1	200	156	300	1.53	568	26.0	1.53	2000	1581	658
Hallgren: cited in FIB bulletin 12	HSC0	240	200	250	0.8	643	89.2	0	2540	2400	965
	HSC1	240	200	250	0.8	627	86.7	0	2540	2400	1021
	HSC2	240	194	250	0.8	620	81.4	0	2540	2400	889
	HSC4	240	200	250	1.2	596	87.0	0	2540	2400	1041
	HSC6	240	201	250	0.6	633	103.4	0	2540	2400	960
	N/HSC8	240	198	250	0.8	631	90.2	0	2540	2400	944
	HSC9	240	202	250	0.3	634	79.9	0	2540	2400	565
Tomaszevicz (1993): cited in FIB bulletin 12	ND65-1-1	320	275	200	1.5	500	64.1	0	3000	2500	2050
	ND65-2-1	240	200	150	1.7	500	70.0	0	2600	2200	1200

	ND95-1-1	320	275	200	1.5	500	83.5	0	3000	2500	2250
	ND95-1-3	320	275	200	2.5	500	89.7	0	3000	2500	2400
	ND95-2-1	240	200	150	1.7	500	88.0	0	2600	2200	1100
	ND95-21D	240	200	150	1.7	500	86.5	0.9	2600	2200	1300
	ND95-2-3	240	200	150	2.6	500	89.3	0	2600	2200	1450
	ND95-2-3D	240	200	150	2.6	500	80.1	0.9	2600	2200	1250
	ND95-2-3D+	240	200	150	2.6	500	97.8	0.9	2600	2200	1450
	ND95-3-1	120	88	100	1.8	500	84.9	0	1500	1100	330
	ND111-1-1	320	275	200	1.5	500	111.7	0	3000	2500	2450
	ND115-2-1	240	200	150	1.7	500	118.7	0	2600	2500	1400
	ND115-2-3	240	200	150	2.6	500	107.8	0	2600	2200	1550
Mowrer and Vanderbilt (1967)	JN-1-1.7	76.2	50.8	152	1.7	352	12.4	0	914.4	914.4	113
	JN-0-2.2	76.2	50.8	152	2.2	352	15.2	0	914.4	914.4	122.78
Olivera *et al*., 2000	1-B	130	93	120	1.5	695	60.9	0	1800	1650	270
	2-B	130	97	120	1.4	695	62.9	0	1800	1650	335
	1-A	130	109	120	1.2	631	28.7	0	1800	1650	316
	2-A	130	108	120	1.2	631	28.7	0	1800	1650	255
Ghannoum (1998)	S1-U	150	110	225	1.11	445	37.2	0.36	2300	2108	301
	S1-B	150	110	225	2.15	445	37.2	0.36	2300	2108	317
	S2-U	150	110	225	1.11	445	57.1	0.36	2300	2108	363
	S2-B	150	110	225	2.15	445	27.1	0.36	2300	2108	447
	S3-U	150	110	225	1.11	445	67.1	0.36	2300	2108	443
	S3-B	150	110	225	2.15	445	67.1	0.36	2300	2108	485
Corely and Hawkins (1968)	AN-1	146	111	254	1.54	403	18.7	0	2100	1820	334.1
	BN-1	146	111	203	1.03	445	20.4	0	2100	1820	265.56
Rankins and Long (1987) [a & b]	1	51	40.5	100	0.423	530	30.7	0	700	640	36.42
	2	51	40.5	100	0.558	530	30.7	0	700	640	49.08
	3	51	40.5	100	0.691	530	30.7	0	700	640	56.55
	4	51	40.5	100	0.821	530	34.8	0	700	640	56.18
	5	51	40.5	100	0.883	530	34.8	0	700	640	57.27
	6	51	40.5	100	1.026	530	34.8	0	700	640	65.58
	7	51	40.5	100	1.163	530	29.7	0	700	640	70.94
	8	51	40.5	100	1.292	530	29.7	0	700	640	71.09
	9	51	40.5	100	1.454	530	29.7	0	700	640	78.6
	10	51	40.5	100	0.517	530	29.9	0	700	640	43.59
	11	51	40.5	100	0.802	530	29.9	0	700	640	55
	12	51	40.5	100	1.107	530	29.9	0	700	640	67.06
	13	51	40.5	100	0.601	530	34.0	0	700	640	49.39
	14	51	40.5	100	0.691	530	34.0	0	700	640	52.45
	15	51	40.5	100	1.994	530	34.0	0	700	640	84.84
	1A	57	46.5	100	0.442	530	28.8	0	700	640	45.19
	2A	57	46.5	100	0.691	530	28.8	0	700	640	66.24
	3A	57	46.5	100	1.293	530	28.8	0	700	640	89.72
	4A	57	46.5	100	1.992	530	30.9	0	700	640	97.43

	1B	45.5	35	100	0.423	530	37.7	0	700	640	28.85
	2B	45.5	35	100	0.69	530	37.7	0	700	640	37.63
	3B	45.5	35	100	1.292	530	37.7	0	700	640	56.67
	4B	45.5	35	100	1.994	530	30.9	0	700	640	72.52
	1C	64	53.5	100	0.423	530	27.8	0	700	640	62.74
	2C	64	53.5	100	0.69	530	32.4	0	700	640	87.86
	3C	64	53.5	100	1.288	530	32.4	0	700	640	124.14
	4C	64	53.5	100	1.993	530	27.8	0	700	640	125.94
Sissakis and Sheikh (2007)	Control 1	150	120	200	1.49	428	42.6	0	1500	1350	575
	Control 2	150	120	200	1.49	428	36.1	0	1500	1350	439
	Control 3	150	120	200	2.23	480	34.5	0	1500	1350	476
	Control 4	150	120	200	2.23	480	26.6	0	1500	1350	479
Beutel and Hegger (2002)	P1	230	190	400	0.806	580	21.9	0.24	2750	2400	615
Hawkins *et al*., 1974	S2075-1	165	121	254	0.79	330.6	32.4	0	2130	2030	290
	S2075-2	165	122	254	0.78	330.6	29.0	0	2130	2030	272.66
	S2150-1	165	124	254	1.54	330.6	29.6	0	2130	2030	462.6
	S2150-2	165	122	254	1.56	330.6	30.2	0	2130	2030	440.35
	S4075-1	165	127	508	0.75	330.6	26.6	0	2130	2030	342.5
	S4075-2	165	124	508	0.77	330.6	32.2	0	2130	2030	329.15
	S4150-1	165	126	508	1.52	330.6	35.4	0	2130	2030	579.13
	S4150-2	165	126	508	1.52	335.9	35.7	0	2130	2030	580.46
Li (1997)	PSS-A	175	143	200	0.703	500	25.8	0.39	2000	1700	454
Bazant and Cao (1987)	I-C	101.6	96.2	102	3.76	309	52.9	0	508	406.4	13.84
	II-C	101.6	96.2	102	3.12	309	47.9	0	508	406.4	15.56
	III-C	101.6	96.2	102	2.46	309	52.1	0	508	406.4	11.51
Graf (1938): cited in FIB bulletin 12	1362	302	271	300	1.04	270	13.9		1700	1500	1157
	1375	504	474	300	0.576	270	15.5		1700	1500	1647
Keefe (1954): cited in FIB bulletin 12	P-I	127	113	153	2.09	288	27.0	-	1090	940	315
	P-II	127	113	153	2.09	288	26.1	-	1090	940	370
Franz (1963): cited in FIB bulletin 12	1	140	129	210	1.074	457	21.4		1960	1680	343
Narasiham(1971): cited in FIB bulletin 12	L7	178	143	305	1.11	398	33.0	1.11	2280	2000	588
	L9	178	143	305	1.11	398	30.4	1.11	2280	200	687
Marti *et al*., 1977 : cited in FIB bulletin 12	P2	180	152	300	1.4	558	35.4	0.43	2750	2600	627

Muller *et al*., 1984: cited in FIB bulletin 12	P4	180	162	300	1.219	515	30.8	0.3	2750	1300	366
Broms 1990 (CEB)	1	180	150	250	0.928	681	23.4	-	2600	2000	435
Chana and Desai (1992)	1	240	200	300	0.785	500	32.2	0	3000	2400	805
	FPS1	250	210	400	0.848	500	19.3	0.85	4500	2400	1225
Lee Morley (1999): cited in FIB bulletin 12	2F22	200	160	290	1.96	500	74.2	0	2000	1500	1100
	3f22	250	230	400	1.49	500	70.2	0	2750	2250	1640
Esfahani *et al*., 2009	R0.8-C25-F0	100	73	150	0.84	490	23.0	0	1000	920	138
	R1.6-C25-F0	100	69	150	1.59	490	23.0	0	1000	920	210
Michel *et al*., 2007	R0	100	70.5	100	0.902	500	27.2	0.55	1280	1200	121.5
Regan & Samadian (2001)	1	200	160	200	1.26	670	29.0	0.21	3000	2743	560
	1A	200	160	200	1.26	670	32.9	0.21	3000	2743	587
Kim *et al*., 2009	B3-SL1	150	114	250	1.44	454	33.0	0.52	2360	2260	376
Scordelis *et al*., 1958	S-1	152.4	108	330	2.5	331	19.4	0	1828	1320	467
	S-2	152.4	108	330	2.5	331	28.0	0	1828	1320	485
Yitzhaki (1966)	II-5	102	82.3	221	0.526	471	22.8		1164	1164	151.69
	II-8	102	82.3	333	0.578	456	24.9		1164	1164	218.41
	IIS20-1	102	78.2	201	0.66	402	14.5		1706	1706	127.67
	II-1	102	82.3	221	1.21	457	14.0		1164	1164	181.05
	II-4a	102	82.3	221	0.893	558	23.8		1164	1164	244.65
	II-4b	102	82.3	201	0.893	466	13.0		1164	1164	161.47
	II-4c	102	82.3	201	0.893	510	18.5		1164	1164	215.3
	IIR20-2	102	109	201	0.93	500	19.8		1164	1164	306.5
	IIR30-1	102	80.3	300	2.02	402	23.4		1706	1706	238.86
	II-2	102	82.3	221	1.255	373	13.0		1706	1706	151.68
	II-3	102	82.3	200	1.255	490	18.0		1706	1706	244.65
	II-6	102	82.3	221	1.327	456	28.8		1706	1706	240.21
	II-9	102	79.3	201	0.85	550	12.3		1164	1164	156.58
	III-3	102	82.3	221	1.21	558	24.0		1164	1164	200.61
	7	102	82.3	119	0.736	456	13.2		1164	1164	117.45
	II-10	102	82.3	119	1.04	385	15.5		1706	1706	97.86
	8	101.6	76.2	102	2.05	450	24.2	0	1220	1117.6	129
	9	101.6	76.2	102	2.05	450	22.6	0	788	685.8	135.67
	10	101.6	76.2	102	2.05	450	24.7	0	482.6	381	129
	12	152.4	113	203	2.14	450	24.8	0	990.6	685.8	356.6
	13	152.4	122	203	0.66	450	24.8	0	990.6	685.8	271.35
	15	101.6	80.8	152	1.47	450	25.0	0	787.4	533.4	160.14
	16	101.6	85.8	152	0.45	450	23.2	0	787.4	533.4	107.38
	19	152.4	123	203	0.47	450	22.1	0	787.4	685.8	271.34
	21	152.4	122	203	0.66	450	16.1	0	990.6	685.8	230
	22	101.6	72.7	152	5.01	450	13.2	0	787.4	533.4	154.35
	23	101.6	80.8	152	1.47	450	14.6	0	787.4	533.4	107.65
	24	101.6	85.8	152	0.45	450	14.1	0	787.4	533.4	68.95
	25	152.4	122	203	0.66	450	52.1	0	990.6	685.8	306.5
	27	101.6	80.8	152	1.47	450	52.1	0	787.4	533.4	242.87

	28	101.6	85.8	152	0.45	450	52.1	0	787.4	533.4	147.68
	29	50.8	38.1	203	2.04	450	52.1	0	610	381	73.84
	30	50.8	38.1	203	2.04	450	52.1	0	610	381	70.28
Kruger *et al*., 2000	P0A	150	121	300	1	400	35.0	0	3000	2750	423
Alander (2000)	L1	197	172	200	0.464	500	26.2		1770	1570	503
	L2	201	176	200	0.454	500	26.2	0	1770	1570	537
	L3	198	173	200	0.462	500	26.2	0	1770	1570	530
	L4	197	170	400	0.675	500	26.2	0	1970	1770	686
	L5	199	172	400	0.667	500	26.2	0	1970	1770	696
	L6	202	175	400	0.656	500	26.2	0	1970	1770	799
	L8	205	174	900	1.17	500	19.3	0	2470	2270	1111
	L9	203	172	900	1.18	500	19.3	0	2470	2270	1107
	L10	204	173	900	1.17	500	19.3	0	2470	2270	1079
	L7	204	177	200	0.65	500	19.3	0	1970	1770	478
Israel (1959)	II/1	100	80	200	1.34	455.8	15.4	0	1160	1160	181.04
	II/2	100	80	200	1.32	372.3	14.3	0	1700	1700	151.68
	II/3	100	80	200*400	1.32	489.6	16.0	0	1700	1700	244.65
	II/4	100	80	200	0.98	489.6	25.1	0	1160	1160	244.65
Ozawa *et al*., 2000	LA1	85	65	100	1.05	382	39.0	0	1000	1000	120
	LA21	85	65	100	1.95	382	39.0	0	1000	1000	160
	LA22	85	65	100	1.95	382	29.1	0	1000	1000	140
	LB1	100	80	100	1.49	382	29.1	0	1000	1000	180
Matthys and Taerwe (2000)	R2	120	88	150	1.29	500	35.1	0	1000	900	294
	R3	120	86	150	1.79	500	35.1	0	1000	900	313
Sakinis and Vainiunas (2009)	1	140	112	200	0.449	400	35.5	0.47	2135	2000	331.8
	2	140	110	200	0.719	400	31.4	0.47	2135	2000	372.7
	3	140	108	200	1	400	37.3	0.47	2135	2000	402.9
	4	140	106	200	1.5	400	27.2	0.47	2135	2000	401.8
	5	140	104	200	1.9	400	2.7	0.47	2135	2000	436
Mitchel *et al*., 2007	R0	100	70.5	100	0.9	550	34.0	0.54	1200	1000	121.6
Bazant and Cao 1987 ACI	I-A	25.4	20	25.4	4.01	309	52.9	0	127	101.6	0.0668
	I-B	50.8	45.4	50.8	3.89	309	52.9	0	245	196	0.963
	I-C	101.6	96.2	102	3.76	309	52.9	0	508	406.4	13.84
	II-A	25.4	20	25.4	3.39	309	47.9	0	127	101.6	0.071
	II-B	50.8	45.4	50.8	3.23	309	47.9	0	245	196	0.989
	II-C	101.6	96.2	102	3.12	309	47.9	0	508	406.4	15.56
	III-A	25.4	20	25.4	2.76	309	52.1	0	127	101.6	0.0513
	III-B	50.8	45.4	50.8	2.55	309	52.1	0	245	196	0.762
	III-C	101.6	96.2	102	2.46	309	52.1	0	508	406.4	11.51
Yang *et al*., 2010	MU1	150	109	225	1.18	690	35.3	0.36	2300	2150	382
	MU2	150	112	225	0.64	690	35.3	0.36	2300	2150	296
	MU3	150	112	225	1.36	690	35.3	0.36	2300	2150	282
Ruiz and Muttoni (2010)	PV1	250	210	260	1.5	709	34.0	0.2	3000	2846	974
Subedi and Baglin (2003)	C	138	102	320	1.97	460	57.6	0.48	1300	1150	395
Oliveira *et al*., 2000	1	130	93	120	1.5	695	56.9	0.22	1800	1650	270
	2	130	97	120	1.4	695	58.8	0.22	1800	1650	335

Vaz *et al*., 2009	L1	130	83	150	1.56	555	39.0	0.23	1800	1650	203
	AL1	130	92	150	1.56	555	38.7	0.23	1800	1650	286
Lips and Muttoni (2010)	PL1	250	193	130	1.63	583	36.2	0	3000	3000	682
	PL3	250	197	520	1.59	583	36.5	0	3000	3000	1324
	PL4	320	267	340	1.58	550	30.5	0	3000	3000	1625
	PL5	400	354	440	1.5	580	31.9	0	3000	3000	2491
	PT21	250	214	260	1.18	552	67.5	0	3000	3000	959
	PT22	250	214	260	0.82	552	67.0	0	3000	3000	989
	PT23	250	220	260	0.55	560	66.0	0	3000	3000	591
	PT31	250	210	260	1.48	540	66.3	0	3000	3000	1433
	PT32	250	214	260	1.05	550	40.0	0	3000	3000	1157
	PT33	250	220	260	0.5	555	40.2	0	3000	3000	602
Kunz *et al*., 2008	V1	250	210	260	1.5	709	33.8	0	3000	3000	974
Pisanty (2005)	140/1	140	112	200	1.305	400	26.4	0	1700	1700	390
	140/2	140	112	200	1.305	400	22.8	0	1700	1700	355
	160/1	160	133	200	0.955	400	25.0	0	1700	1700	376
	160/2	160	133	200	0.955	400	19.0	0	1700	1700	445
	180/1	180	151	250	1.175	400	23.3	0	1700	1700	581
	180/2	180	151	250	1.175	400	25.5	0	1700	1700	606
	200/1	200	171	300	1.04	400	24.1	0	1700	1700	835
	200/2	200	171	300	1.04	400	21.8	0	1700	1700	822
Ebead and Marzouk (2005)	Ref-0.35%	150	109	250	0.35	435	30.0		1900	1830	248
	Ref-0.5%	150	109	250	0.5		34.0		1900	1830	308
	Ref'-0.5%	150	109	250	0.5		35.0		1900	1830	321
	Ref-1.0%	150	109	250	1	435	36.0		1900	1830	413
Teng *et al*., 2004	OC1	150	110	200	1.81	452	36.0	0.87	2200	1900	423
	OC13	150	110	200*600	1.71	452	35.8	0.87	2200	1900	568
	OC13-1.6	150	110	200*600	1.67	452	43.1	0.87	2200	1900	508
	OC13-0.63	150	110	200*600	1.65	452	39.7	0.87	2200	1900	455
	OC15	150	110	200*1000	1.76	452	40.2	0.87	2200	1900	649
Rizk and Marzouk (2011)	NS1	150	105	250	0.48	400	44.7	0.22	1900	1830	218.9
	HS1	150	105	250	0.48	400	78.9	0.22	1900	1830	248
	NS2	200	153	250	0.54	400	50.2	0.22	1900	1830	490.9
	HS2	200	153	250	0.54	400	81.2	0.22	1900	1830	532.5
	NS3	250	183	250	0.35	400	35.0	0.22	1900	1830	437.7
	HS3	250	183	250	0.35	400	70.0	0.22	1900	1830	573.7
	NS4	300	218	250	0.73	400	40.0	0.22	1900	1830	882.4
	HS4	300	218	250	0.73	400	64.7	0.22	1900	1830	1022.9
	HS5	300	220	250	0.43	400	75.0	0.22	1900	1830	885.5
	HS6	350	268	400	0.5	400	76.0	0.22	2650	2580	1721.8
Elshafey *et al*., 2011	NSC1	200	158	250	2.17	400	35.0	0	1900	1830	678
	HSC1	200	138	250	2.48	400	68.5	0	1900	1830	788
	HSC2	200	128	250	2.68	400	70.0	0	1900	1830	801
	HSC3	200	158	250	1.67	400	66.7	0	1900	1830	802
	HSC4	200	158	250	1.13	400	61.2	0	1900	1830	811
	HSC5	150	113	250	1.88	400	70.0	0	1900	1830	480
	NSC2	200	163	250	0.52	400	33.0	0	1900	1830	479
	NSC3	150	105	250	0.4	400	34.0	0	1900	1830	228

Sundquist and Kinnunen: cited Elshafey et al., 2011	C1	120	100	250	0.8	718	24.0				270
	C2	120	100	250	0.8	718	24.4				250
	D1	145	125	150	0.64	718	27.2				265
Smadi and Yasin (2008)	N1	150	116	250	1.06	468	28.5	0.52	1500	1470	416
	H1	150	116	250	1.06	468	58.1	0.52	1500	1470	468
Faria *et al*., 2011	Df1	100	69	200	1.91	540	24.8	0.2	2300	2000	190.7
	DF4	120	88	200	1.2	540	19.8	0.16	2300	2000	199
Cho *et al*., 2010	Control	150	125	220	0.78	440	28.4	0.3	2500	2470	297
Abgossou *et al*., 2008	R0	100	66	100	0.98	500	34.0	0.57	1280	1200	121.2
Hughes and Xiao (1995)	S1	80	60	132	0.8	450	36.8	0.22	860	800	122
	S4	65	46	132	1	450	41.6	0.29	860	800	89
	S16	50	35	132	1.5	450	39.2	0.35	860	800	66
	S21	65	46	132	1	450	36.0	0.29	860	800	116
Ramos *et al*., 2011	AR2	100	80	200	1.67	523	39.1	0.73	2300	2000	258
	BD2	125	101	100	1.28	530	39.2	1.28	1500	1300	268
	BD8	125	101	100	1.28	530	35.3	1.28	1500	1300	250
Forssel and Holmberg: cited in Oliveira *et al*., 2004	L1a	130	107	120	1.09	750	45.6		1680*2280	1500*2100	240
	L1b	130	108	120	1.08	750	47.2		1680*2280	1500*2100	322.4
	L1c	130	107	120	1.09	750	47.2		1680*2280	1500*2100	318
	L2a	130	109	120*240	1.07	750	46.4		1680*2280	1500*2100	246
	L2b	130	106	120*240	1.1	750	46.4		1680*2280	1500*2100	361
	L2c	130	107	120*240	1.09	750	45.6		1680*2280	1500*2100	330.8
	L3a	130	108	120*360	1.08	750	44.8		1680*2280	1500*2100	240.6
	L3b	130	107	120*360	1.09	750	48.0		1680*2280	1500*2100	400
	L3c	130	106	120*360	1.1	750	43.2		1680*2280	1500*2100	357.6
	L4a	130	108	120*480	1.08	750	44.8		1680*2280	1500*2100	250.8
	L4b	130	106	120*480	1.1	750	43.2		1680*2280	1500*2100	395
	L4c	130	108	120*480	1.09	750	44.8		1680*2280	1500*2100	404
	L5a	130	108	120*600	1.08	750	45.6		1680*2280	1500*2100	287.4
	L5b	130	108	120*600	1.08	750	53.6		1680*2280	1500*2100	426.4
	L5c	130	109	120*600	1.07	750	50.4		1680*2280	1500*2100	446.4
Rizk *et al*., 2011	HSS1	350	255	400	0.5	460	76.0	0.21	2650	2505	1722
	HSS3	350	245	400	1.42	460	65.0	0.22	2650	2505	2090
	NSS1	400	295	400	1.58	460	40.0	0.18	2650	2505	2234
	HSS4	400	295	400	1.58	460	60.0	0.18	2650	2505	2513

Vaz *et al*., 2009	L1	130	83	150	1.38	555	39.0	0.21	1800	1650	203
	L1-A	130	92	150	1.38	555	38.7	0.21	1800	1650	286
Guidotti *et al*., 2011	PG11	250	208	260	0.771	538	31.5		3000	2760	763
	PG19	250	206	260	0.781	510	46.2		3000	2760	860
	PG20	250	201	260	1.563	551	51.7		3000	2760	1094
Kamaraldinm (1990)	SA2	80	64	150	0.55	640	34.0	0.55	2000	2000	141
	SB1	80	62	150	1	530	27.0	1	2000	2000	133
Sistonen and Huovinen (2011)	L1	200	160	202	0.46	621	32.7	0	2300	2300	503
	L2	200	160	202	0.45	621	32.7	0	2300	2300	537
	L3	200	160	201	0.45	621	32.7	0	2300	2300	530
	L4	200	160	402	0.67	612	32.7	0	2300	2300	686
	L5	200	160	399	0.66	612	32.7	0	2300	2300	696
	L6	200	160	406	0.65	612	32.7	0	2300	2300	799
	L7	200	160	201	0.64	586	24.1	0	2300	2300	478
	L8	200	160	899	1.16	576	24.1	0	2300	2300	1111
	L9	200	160	897	1.17	576	24.1	0	2300	2300	1107
	L10	200	160	901	1.16	576	24.1	0	2300	2300	1079
Nguyen-Minh *et al*., 2011	A0	125	105	200	0.66	492	21.7	0	900	825	284
	B0	125	105	200	0.66	492	21.7	0	1200	1125	301
	C0	125	150	200	0.66	492	21.7	0	1500	1425	264
Cheng and Parra-Montesinos (2010)	S1	152	127	152	0.83	471	47.7	0	1500	1424	433
	S21	152	127	152	0.56	471	47.7	0	1500	1424	379
Alam *et al*., 2009	Slab 3	80	62	120	1	421	36.0	0	1305	1200	171.96
	Slab 14	60	42	120	0.5	421	36.0	0	1305	1200	84.73
	Slab 15	60	42	120	1	421	36.0	0	1305	1200	91.76
Erdogan *et al*., 2007	CS	150	114	250	1.226	448	32.0	0.6	2300	2000	500

Appendix B

Mill certificate for LSF pull-out test specimens

STRAIGHT BILL OF LADING-SHORT FORM
ORIGINAL-NOT NEGOTIABLE

Steel Technologies

SHIPPER'S NO. 17023592

CARRIER: YN HIGH HOPES TRANSPORTATION HIHP PAGE 1 REF#:

Received, subject to the classifications and tariffs in effect on the date of the issue of the Bill of Lading

FROM OTTAWA, OH 11/29/2007

The property described below, in apparent good order, except as noted (contents and condition of contents of package unknown), marked, consigned, and destined as indicated below, which said carrier (the word carrier being understood throughout this contract as meaning any person or corporation in possession of the property under the contract) agrees to carry to its usual place of delivery at said destination if on its route otherwise deliver to another carrier on the route to said destination. It is mutually agreed, as to each carrier of all or any of said property over all or any portion of said route to destination and as to each part at any time interested in all or any said property, that every service to be performed hereunder shall be subject to all the terms and conditions of the Uniform Domestic Straight Bill of Lading set forth (1) in Uniform Freight Classification in effect on the date hereof, if this is a rail or a rail-water shipment, or (2) in the applicable motor carrier classification or tariff if this is a motor carrier shipment.

Shipper hereby certifies that he is familiar with all the terms and conditions of the said bill of lading including those on the back thereof, set forth in the classification or tariff which governs the transportation of this shipment and the said terms and conditions are hereby agreed to by the shipper and accepted for himself and his assigns.

SHIP TO : 07528
ERICO, INC.
31700 SOLON RD.

SOLON, OH 44139
DUNS #

SOLD TO :
ERICO, INC.
34600 SOLON RD.

SOLON, OH 44139
DUNS #

F0059

NUMBER AND DESCRIPTION OF ARTICLES	* WEIGHT (Sub. to Cor.)
PO 150432 PART #HAV.063X.984 REL # ES-1239 REV B COLD ROLLED SHEET STEEL 1070/ .0610/ .0650 X .9840 ENGLISH 782 SERIAL# HEAT PCS LB 1716910001094691716910 70379 1 1760 F0059 1716910001094701716910 70379 1 1758 1716910001094721716910 70379 1 1746 1716910001094731716910 70379 1 1760 1716910001094841716910 70379 1 1764 1716910001095031716910 70739 1 1738 1716910001095051716910 70739 1 1736 1716910001095101716910 70739 1 1740 1716910001095111716910 70739 1 2460 --MATERIAL CERTIFICATION-- C MN P S AL SI YS(PSI)/(MPA) TS(PSI)/(MPA) ELG HARDNESS .740 .670 .008 .001 .040 .190 77990/537.73 84190/ 580.47 18% RB 091/092 CB CU N CR MO V NI TI CA <.008 .020 .0038 .140 < .002 .002 .020 .004 .0010 S/O 14508 TOTALS 9 16462 **********	
PO 0150434 PART #HC.0598X.75 REL # ES103.1 REV E COLD ROLLED STRIP STEEL CQ 1020/ .0578/ .0618 X .7500 171753100107928 1717531 71352 1 2308 --MATERIAL CERTIFICATION-- C MN P S AL SI HARDNESS .180 .380 .010 .011 .038 .010 RB 060/060 PREPAID CB CU N CR MO V NI TI CA <.008 .030 .0053 .020 .010 .001 .010 .002 .0002 S/O 14612 TOTALS 1 2308 **********	
PO 0150448 PART #HC.1046X.75 REL # ES103.1 REV E COLD ROLLED SHEET STEEL 1008/1010 .1026/ .1066 X .7500 171830200111612 1718302 72191 1 1742 171830200111616 1718302 72192 1 1556 171830200111626 1718302 72192 1 1758 171830200111627 1718302 72192 1 1754	

DELIVERING CARRIER

VEHICLE

IDENT

Subject to Section 7 of Conditions of applicable bill of lading, if this shipment is to be delivered to the consignee without recourse on the consignor, the consignor shall sign the following statement:
The carrier shall not make delivery of this shipment without payment of freight and all other lawful charges.

By Steel Technologies
(Signature of Consignor)

If the shipment moves between two ports by a carrier by water the law requires that the bill of lading shall state whether it is carrier's or shipper's weight. Note—Where the rate is dependent on value, shippers are required to state specifically in writing the agreed or declared value of the property. The agreed or declared value of the property is hereby specifically stated by the shipper to be not exceeding _____

Per _____
(Signature of Consignor)

If charges are to be prepaid, write or stamp "TO BE PREPAID"

Received $_____
to apply in prepayment of the charges on the property described hereon.

Per _____
(Signature of Agent)

(The signature here acknowledges only the amount prepaid)

Charges
Advanced $_____

SHIPPER: Steel Technologies
PER:

CARRIER:
PER:

Permanent Address of Shipper:

Pullout tests on L shape strips with holes (P1-h-50-3t)

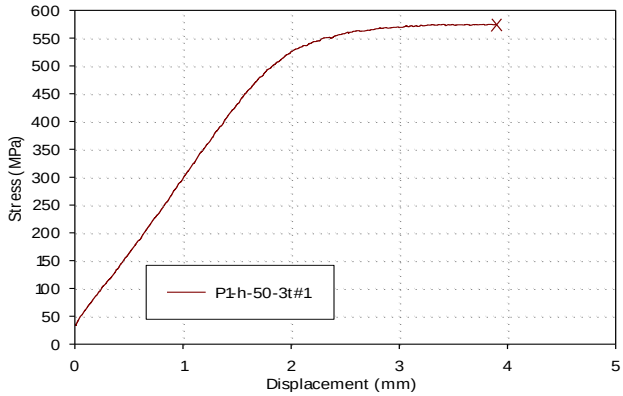

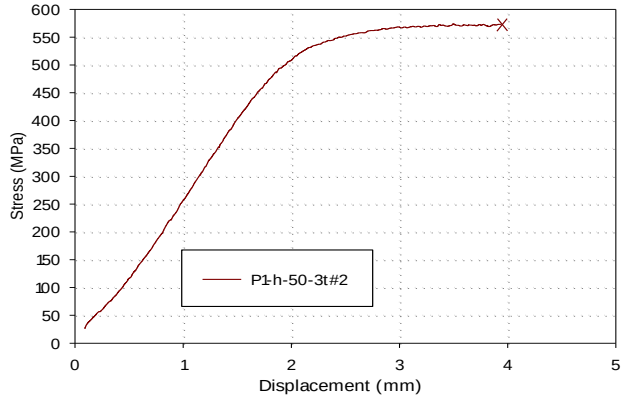

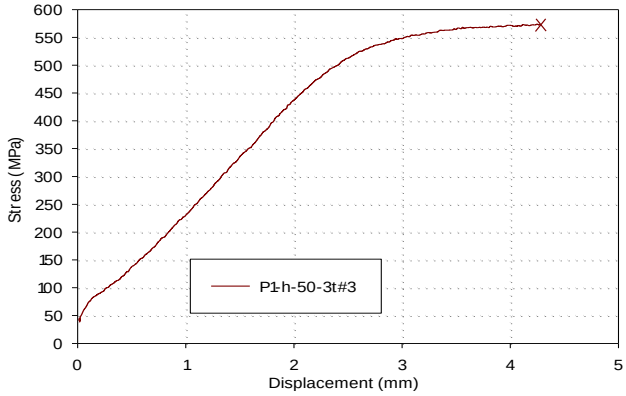

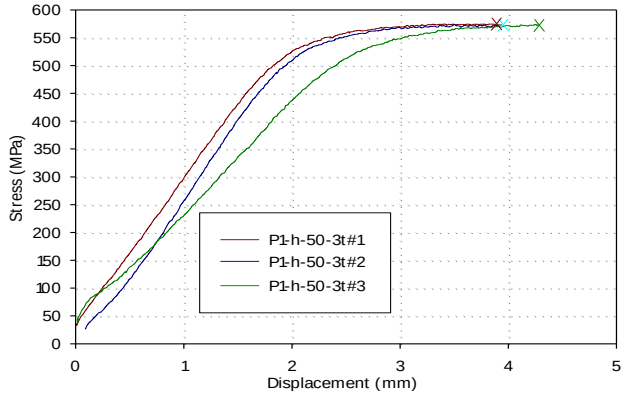

Pullout tests on L shape strips without holes (P1-w-50-3t)

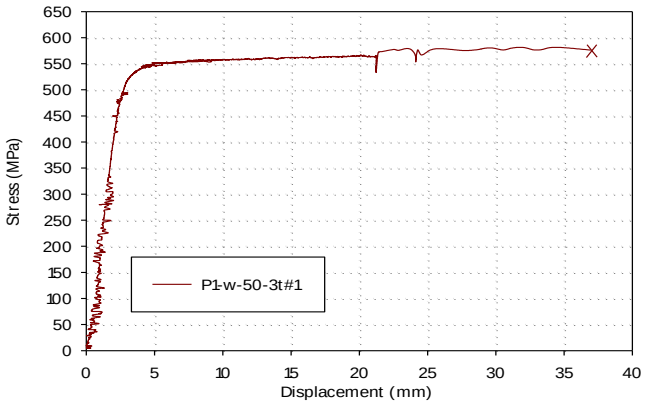

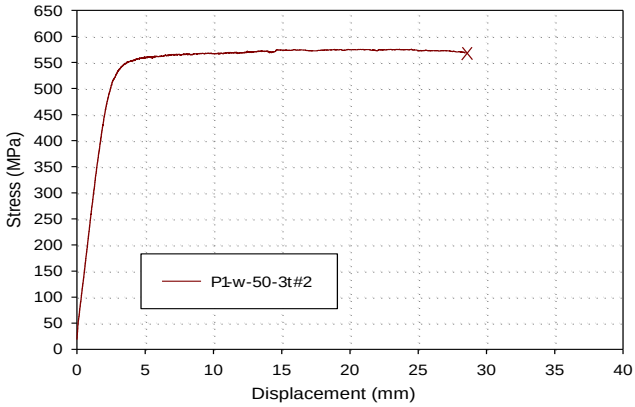

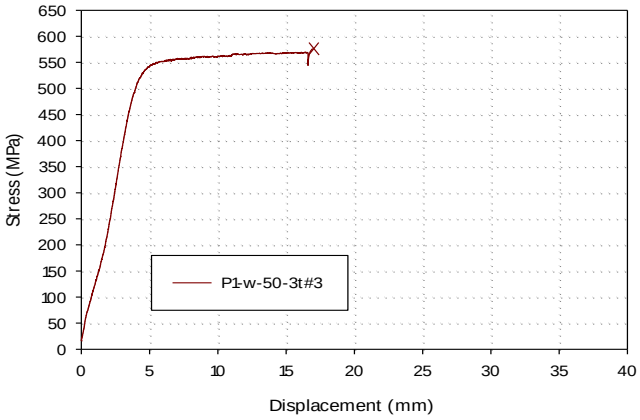

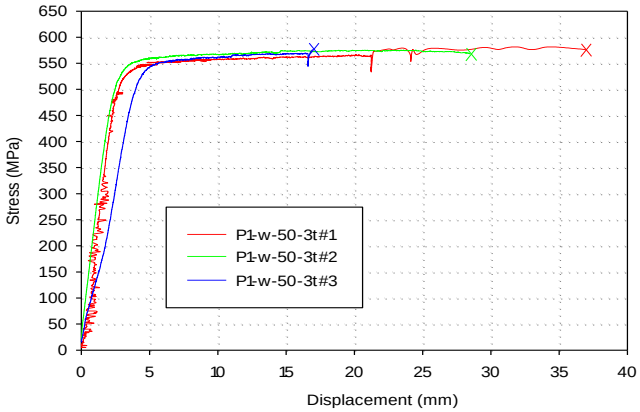

Pullout tests on L shape strips with holes (P1-h-50-5t)

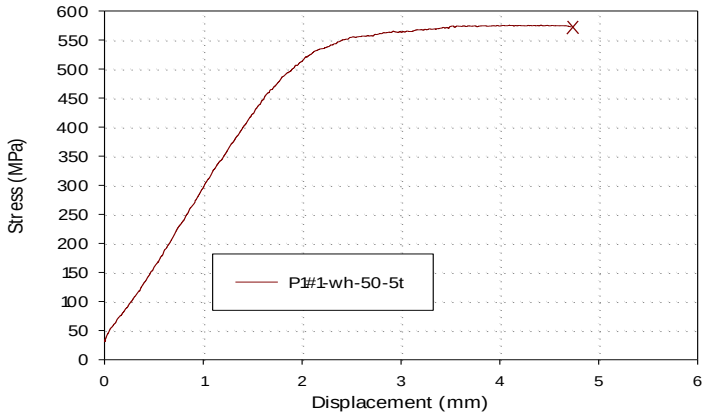

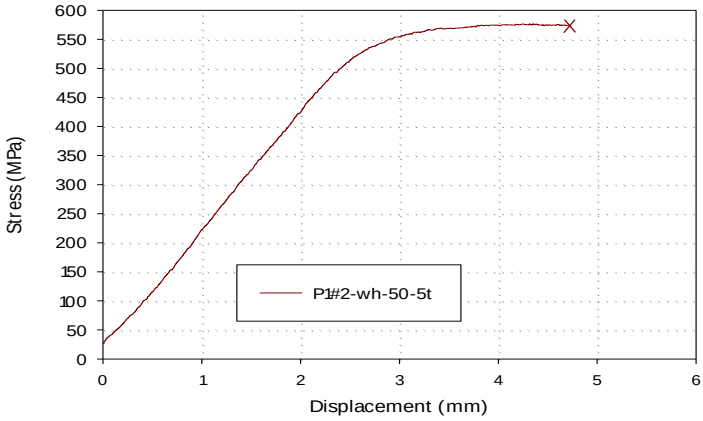

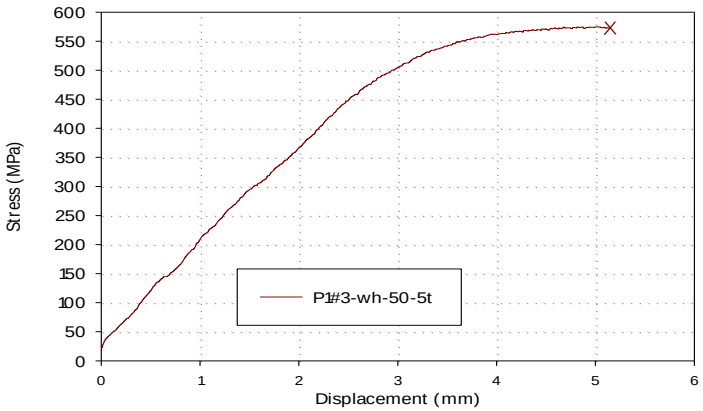

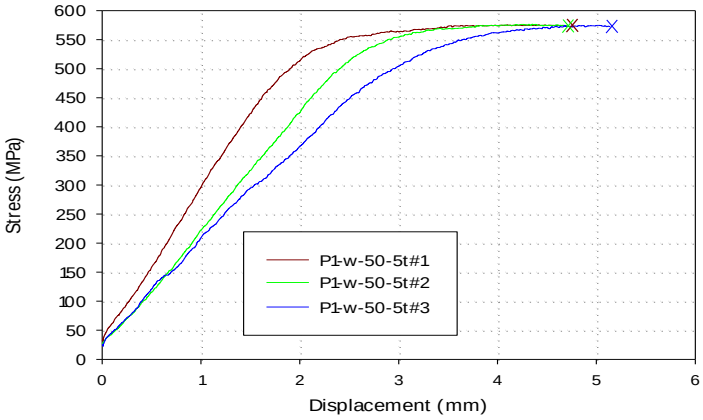

Pullout tests on L shape strips without holes (P1-w-50-5t)

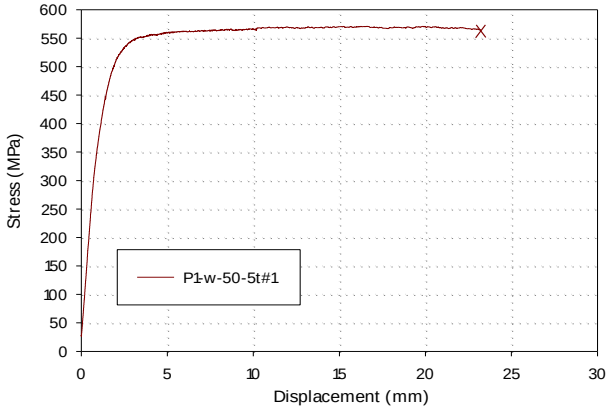

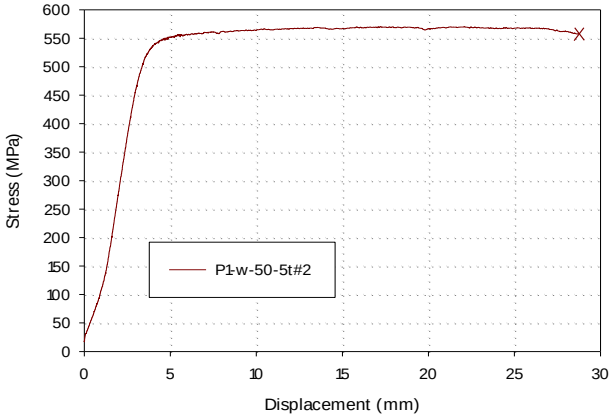

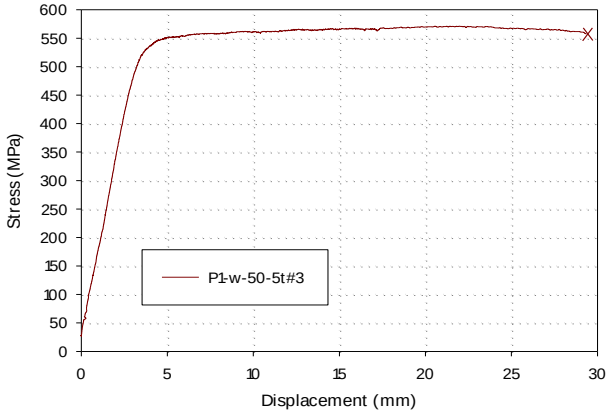

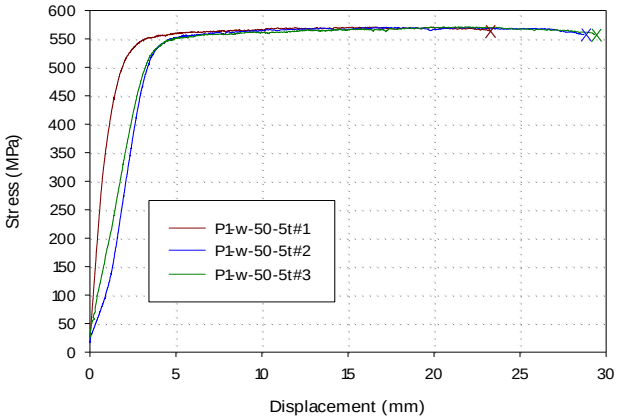

Pullout tests on L shape strips without holes (P1-w-100-3t)

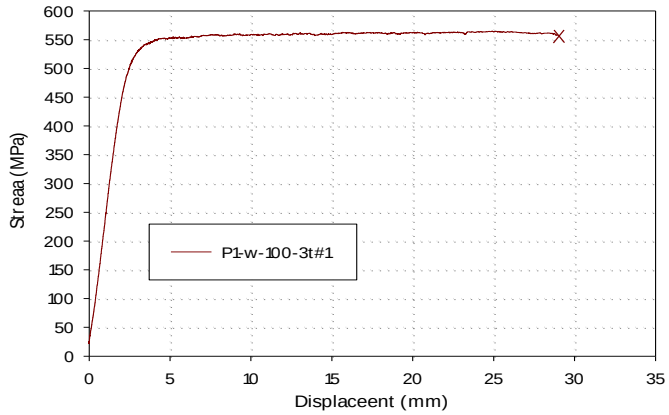

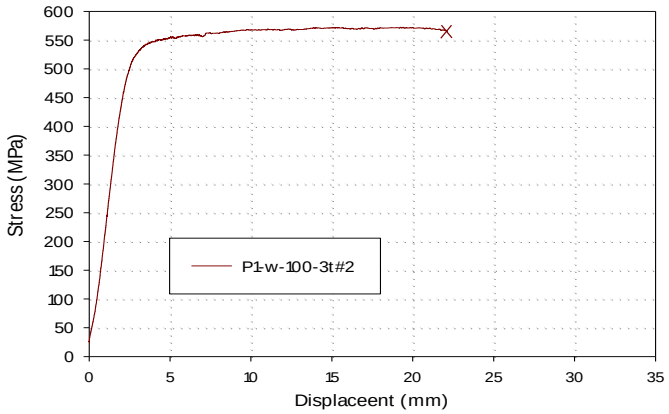

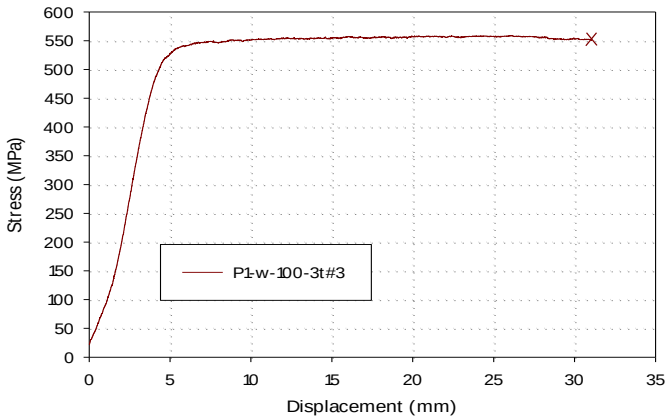

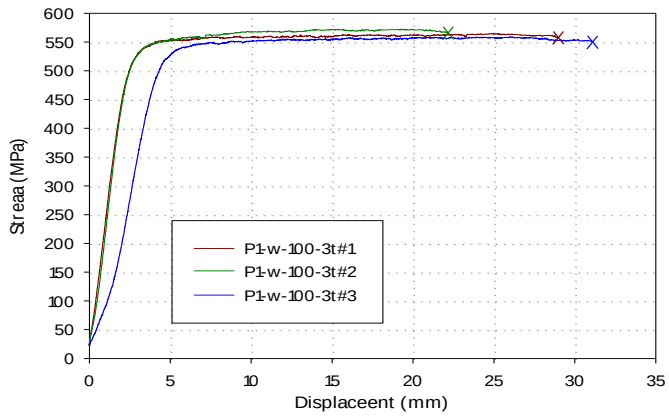

Pullout tests on L shape strips without holes (P1-w-100-5t)

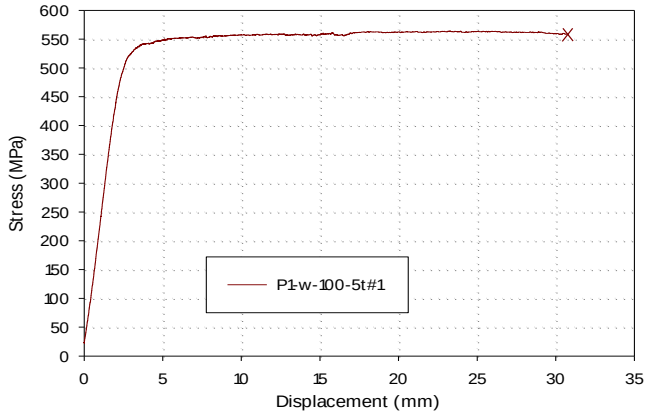

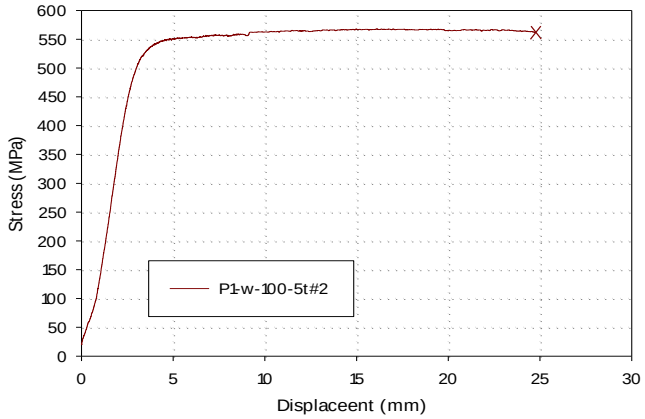

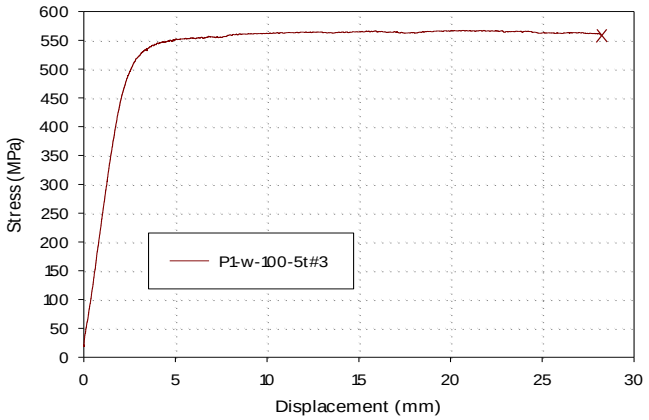

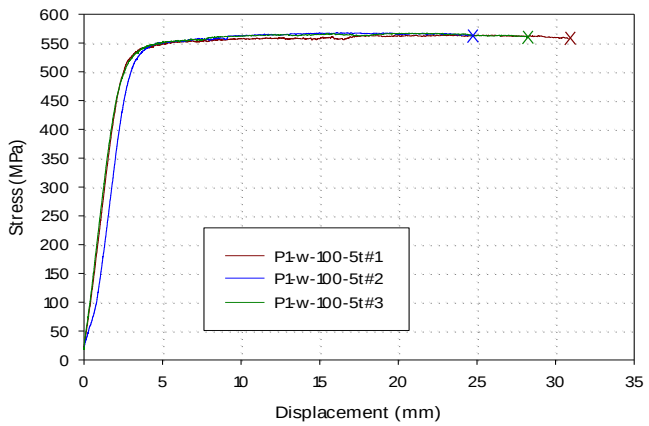

Pullout tests on L shape strips without holes (P2-w-50-5t)

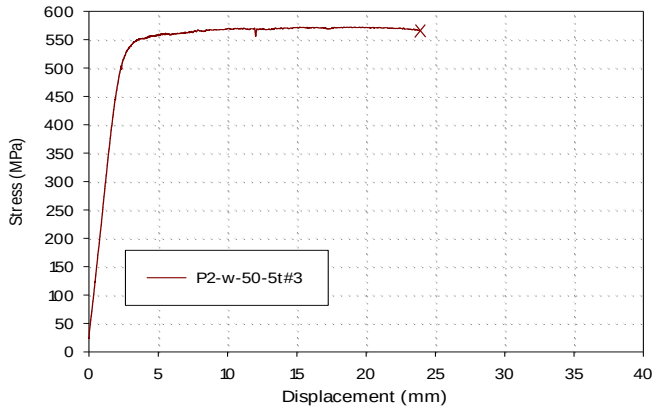

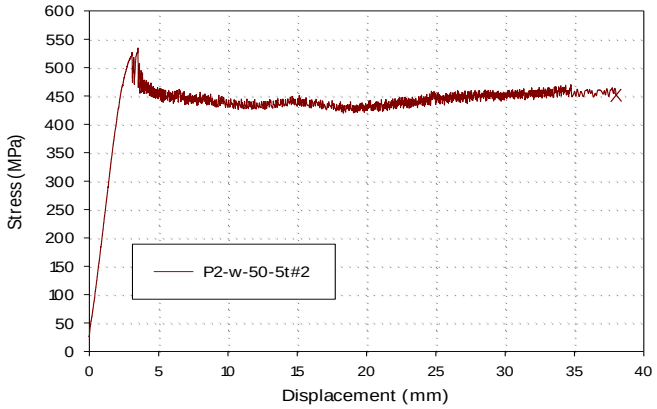

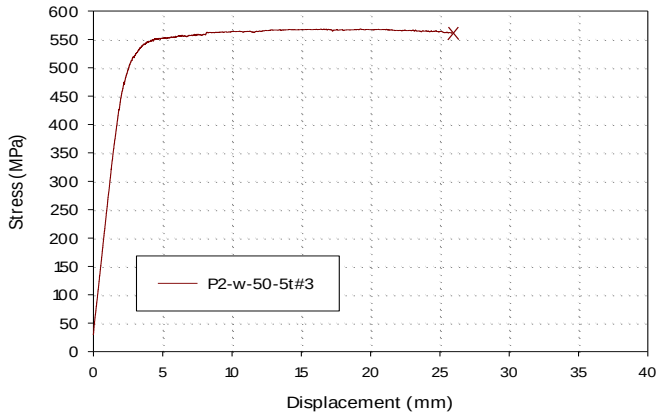

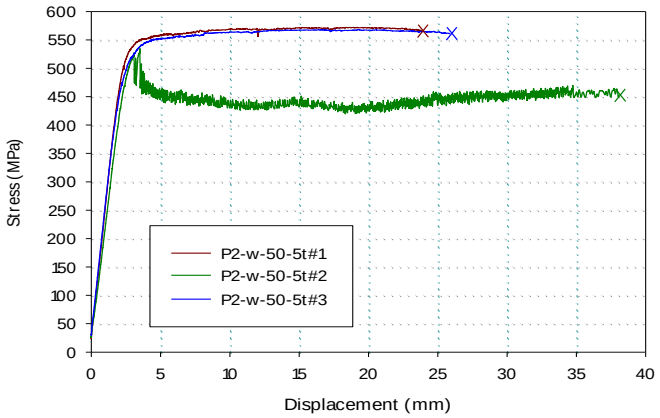

Pullout tests on L shape strips without holes (P2-w-100-5t)

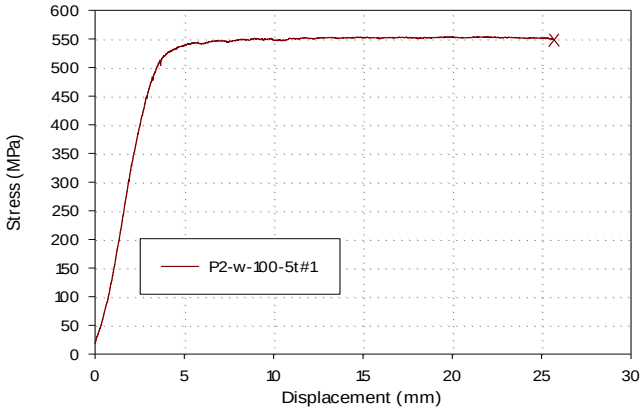

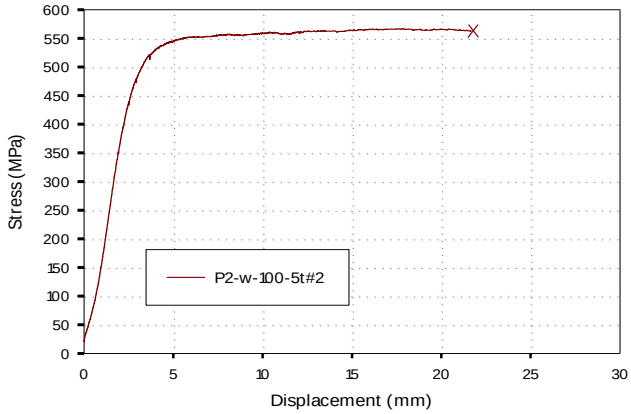

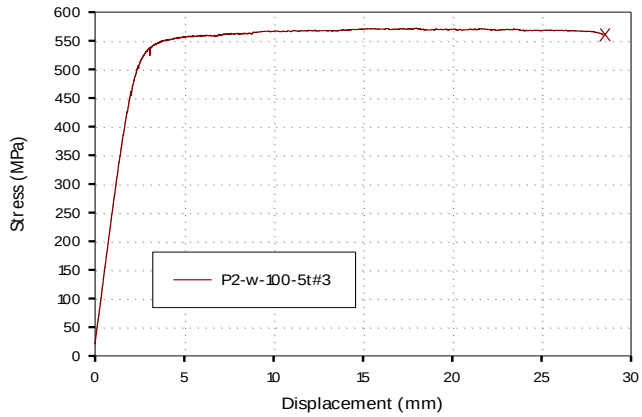

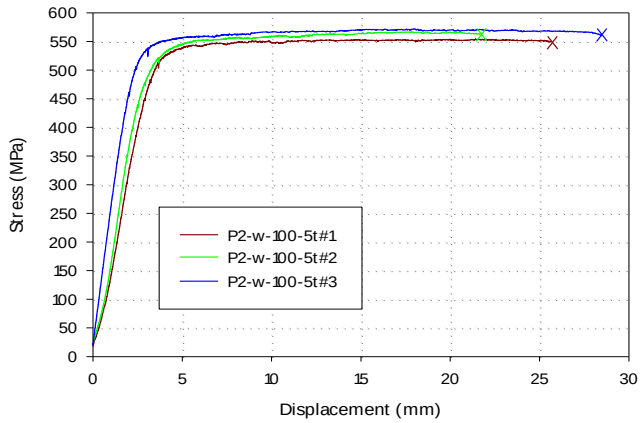

Pullout tests on U shape strips with holes (P3-w-50-3t)

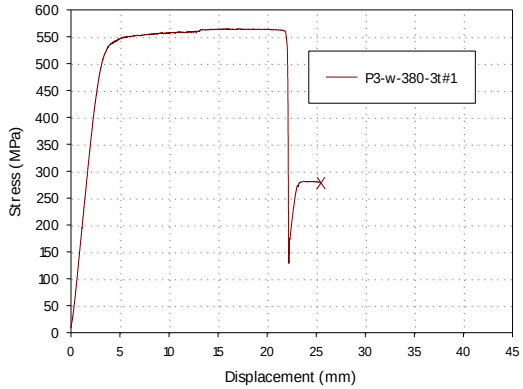

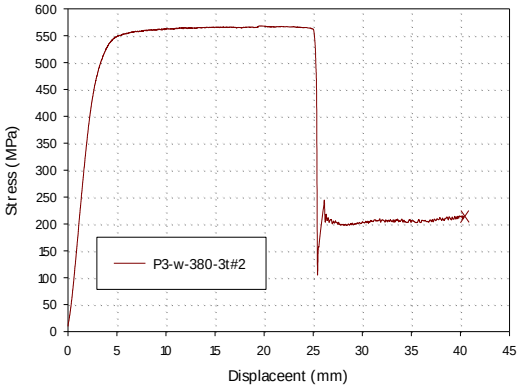

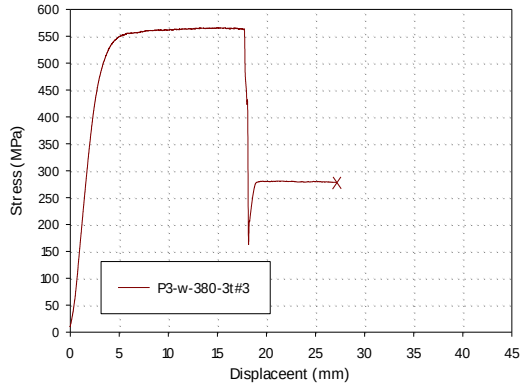

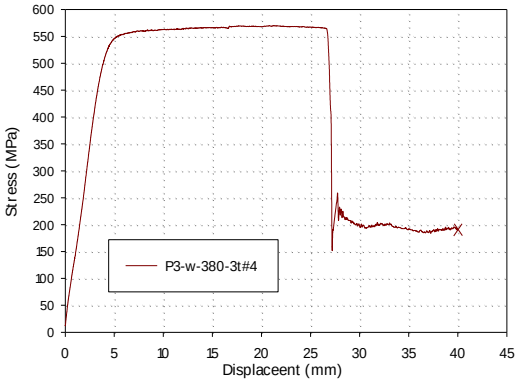

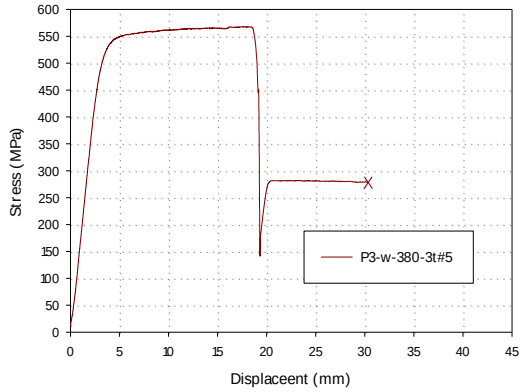

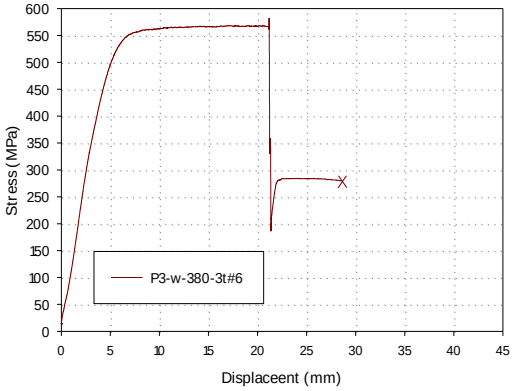

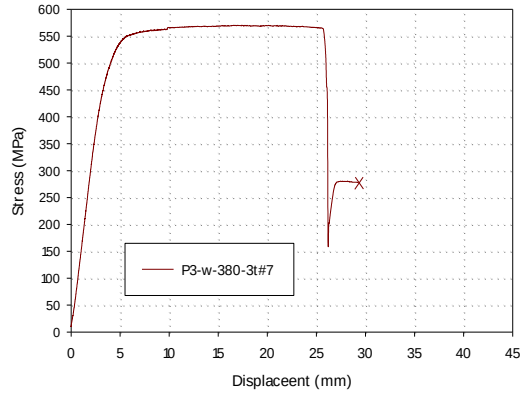

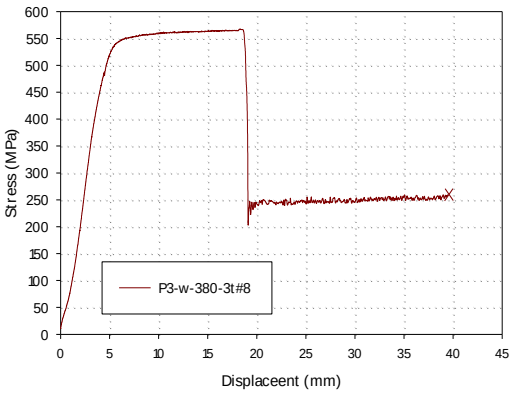

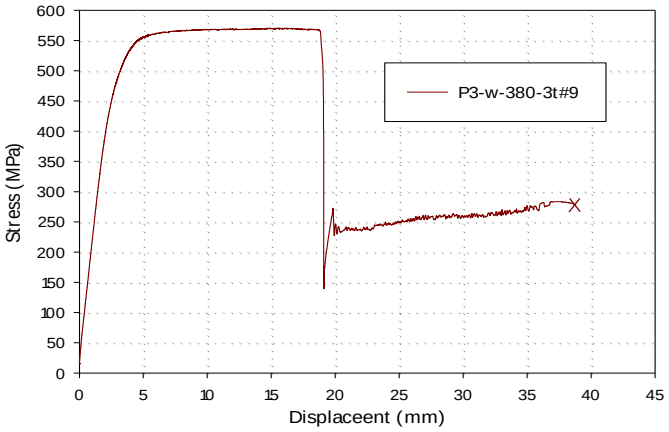
Stress (MPa)
Displaceent (mm)
P3-w-380-3t#9

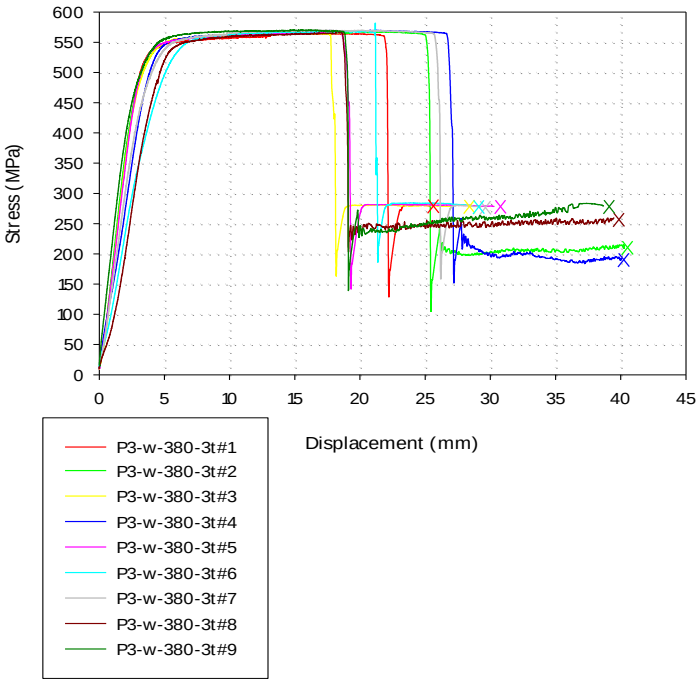
Stress (MPa)
Displacement (mm)
P3-w-380-3t#1
P3-w-380-3t#2
P3-w-380-3t#3
P3-w-380-3t#4
P3-w-380-3t#5
P3-w-380-3t#6
P3-w-380-3t#7
P3-w-380-3t#8
P3-w-380-3t#9

Pullout tests on U shape strips without holes (P3-w-380-5t)

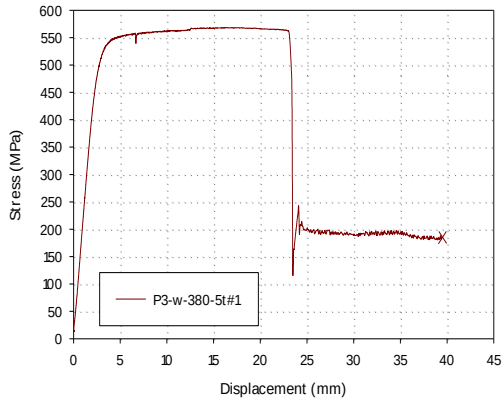

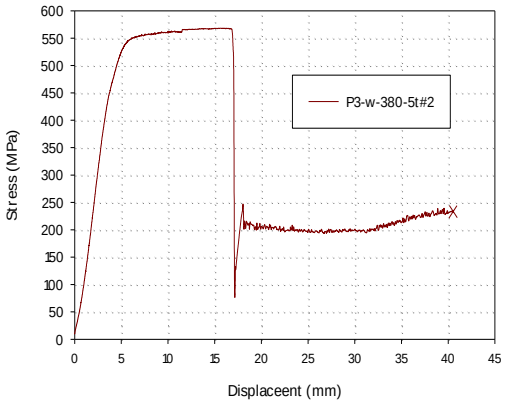

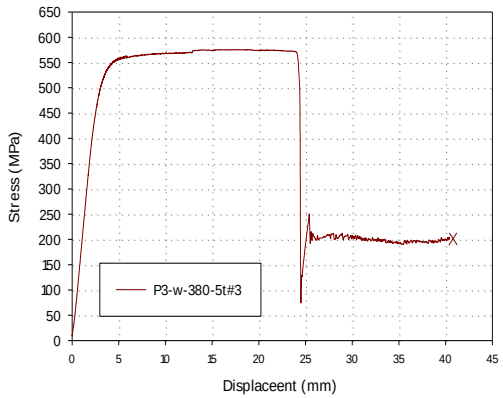

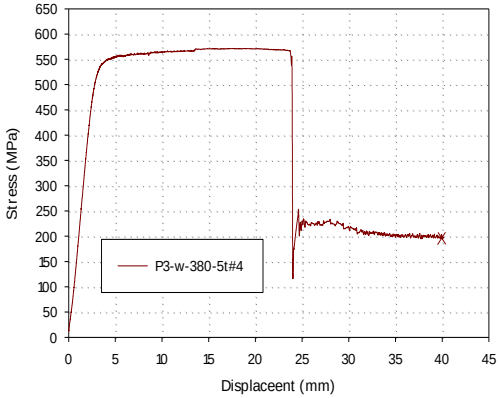

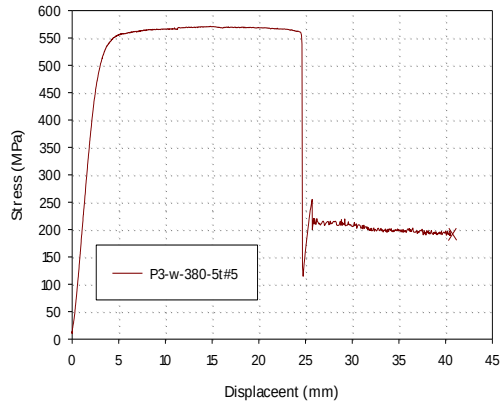

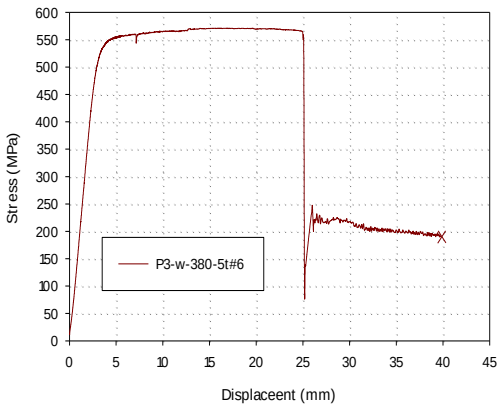

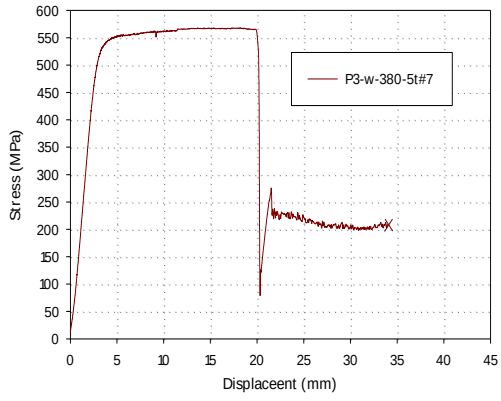

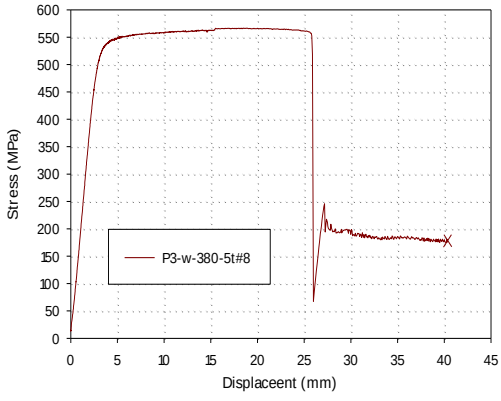

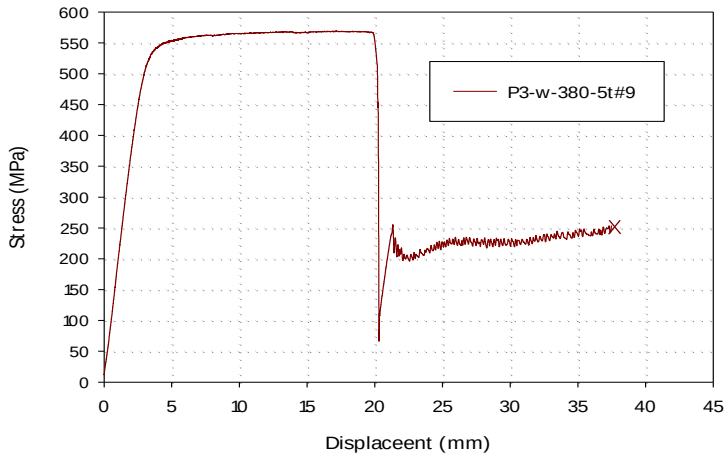
Stress (MPa)
Displaceent (mm)
P3-w-380-5t#9

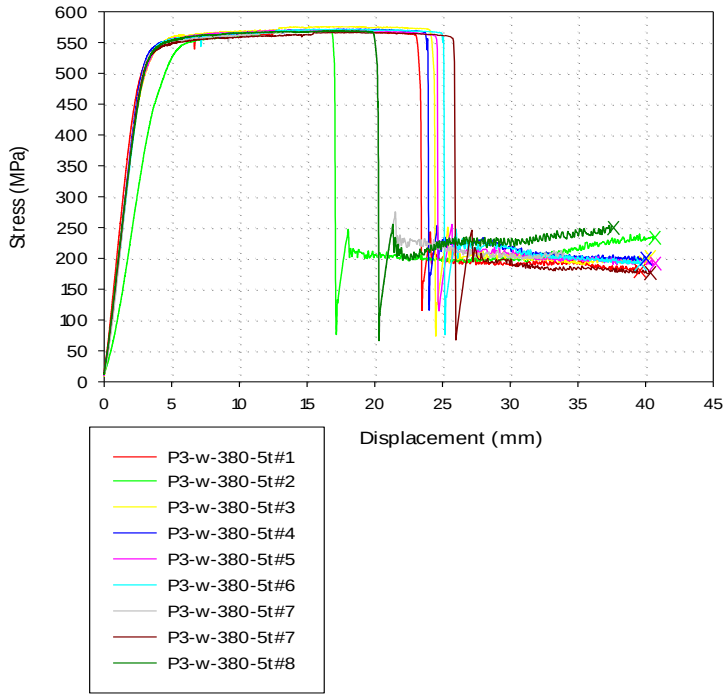
Stress (MPa)
Displacement (mm)
P3-w-380-5t#1
P3-w-380-5t#2
P3-w-380-5t#3
P3-w-380-5t#4
P3-w-380-5t#5
P3-w-380-5t#6
P3-w-380-5t#7
P3-w-380-5t#7
P3-w-380-5t#8

Appendix C

Slab 2

Measurements of Strain gauges in the first Perimeter

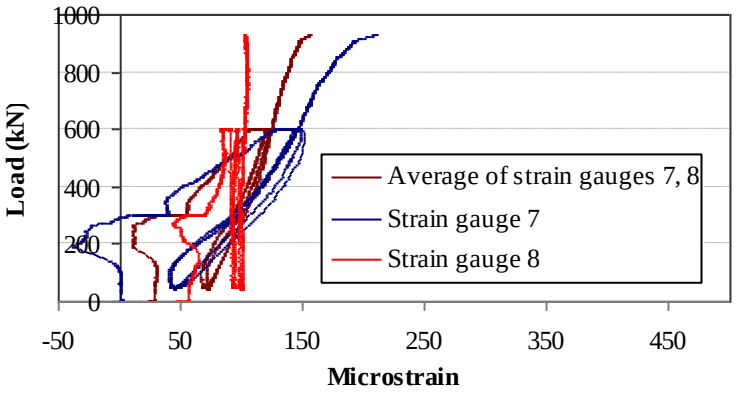

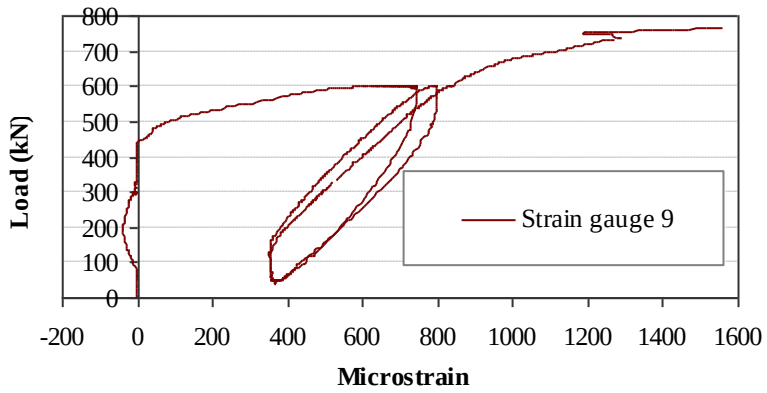

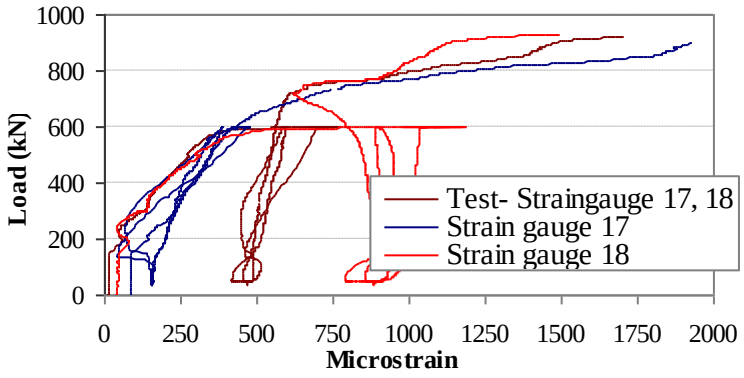

Measurements of Strain gauges in the Second Perimeter

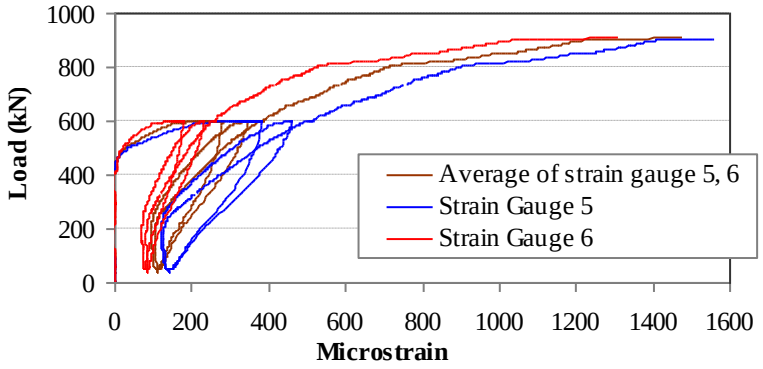

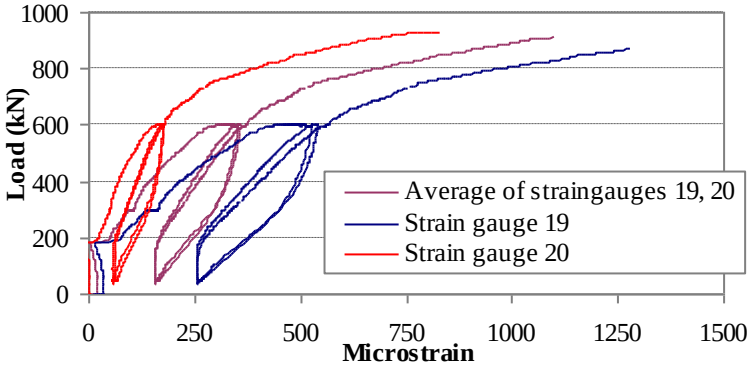

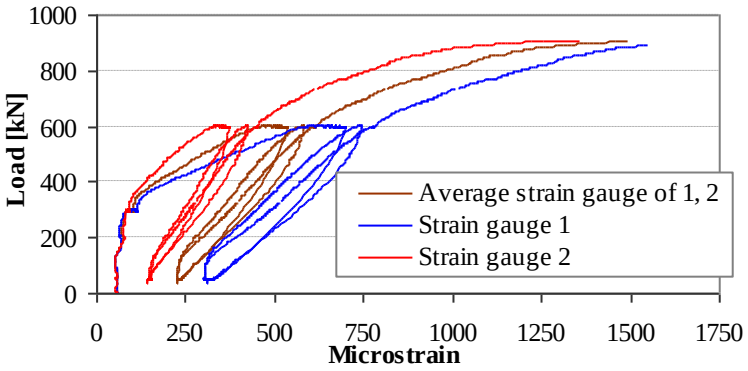

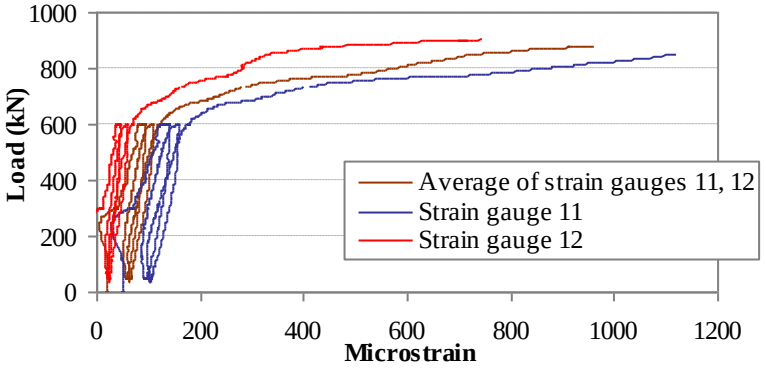

Measurements of Strain gauges in the third Perimeter

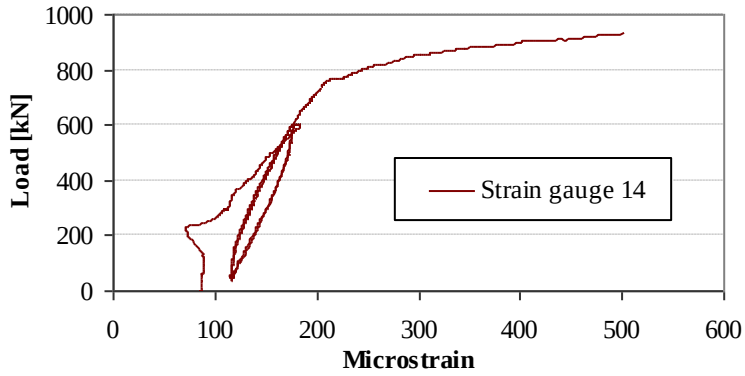

Measurement of Strain gauge in the fourth Perimeter

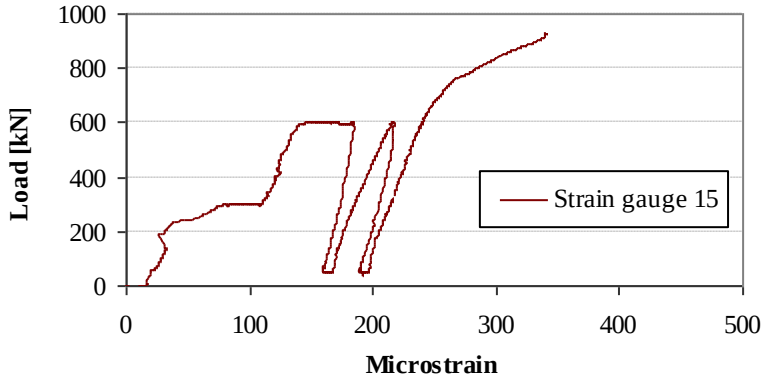

Slab 3

Measurements of strain gauges in the first perimeter

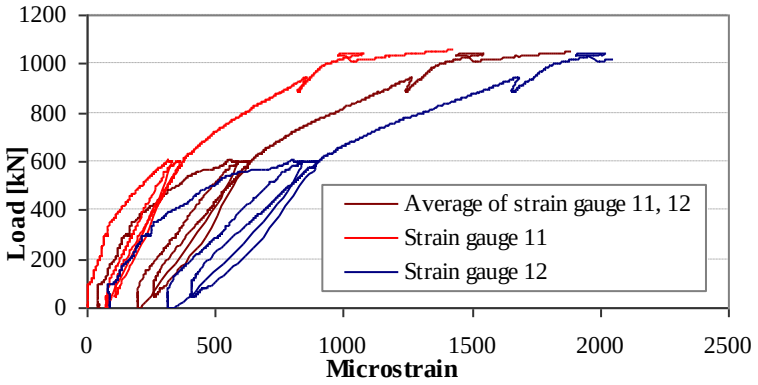

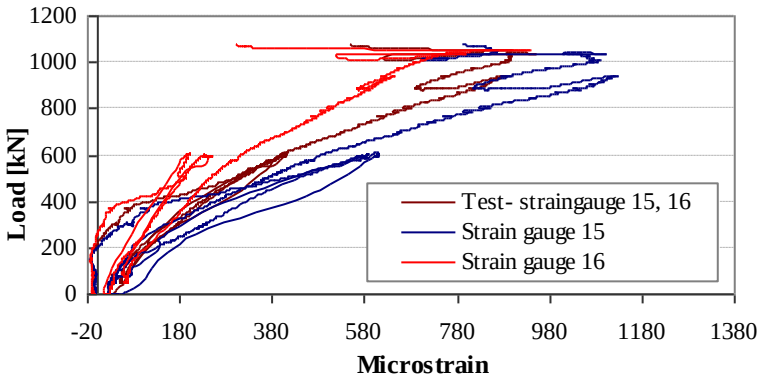

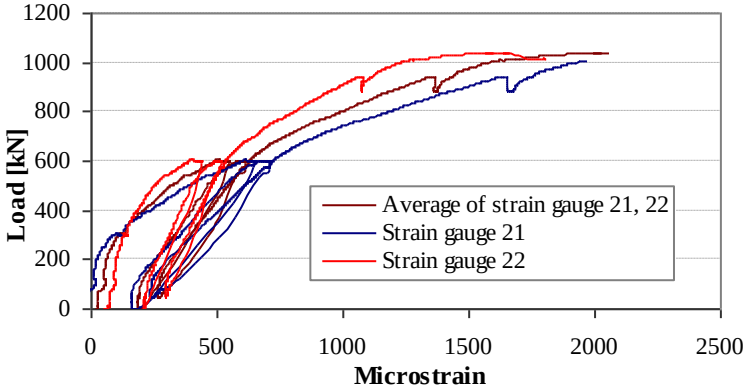

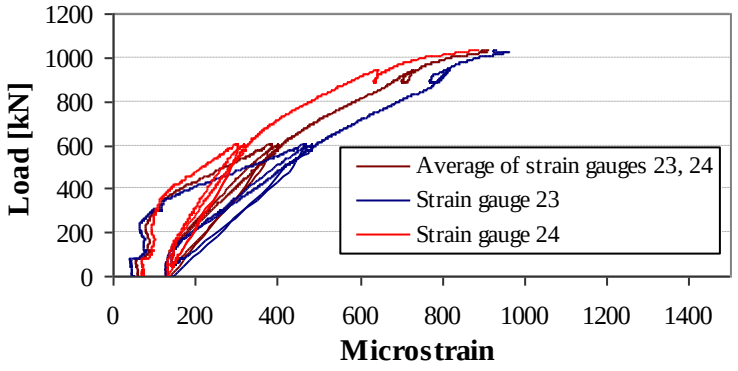

Measurements of strain gauges in the second perimeter

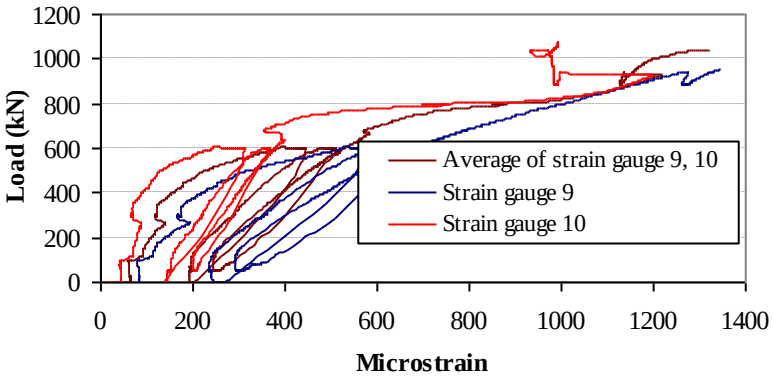

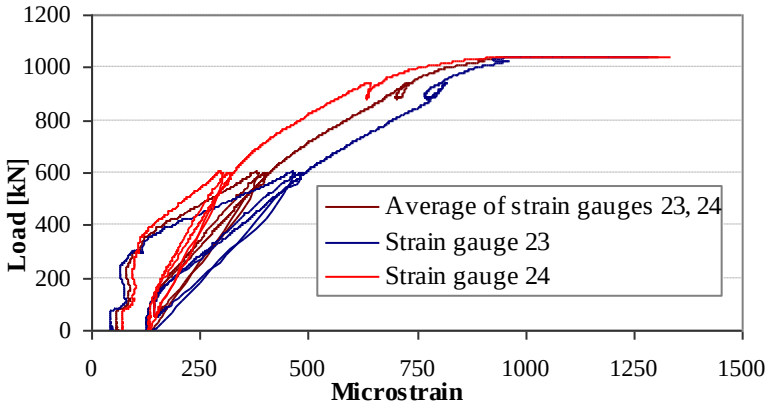

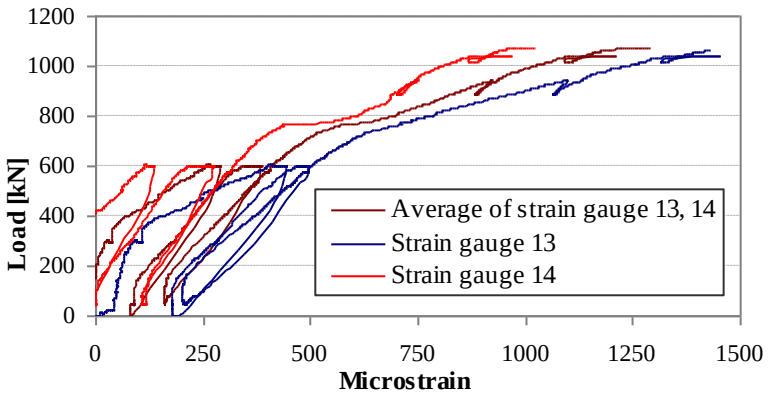

Measurements of strain gauges in the third perimeter

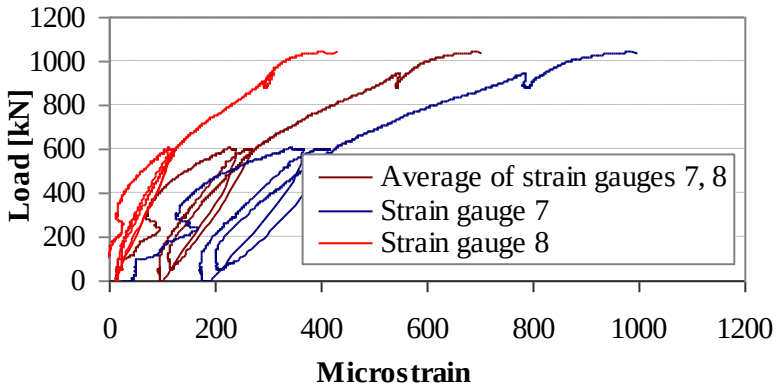

Measurements of strain gauges in the fourth perimeter

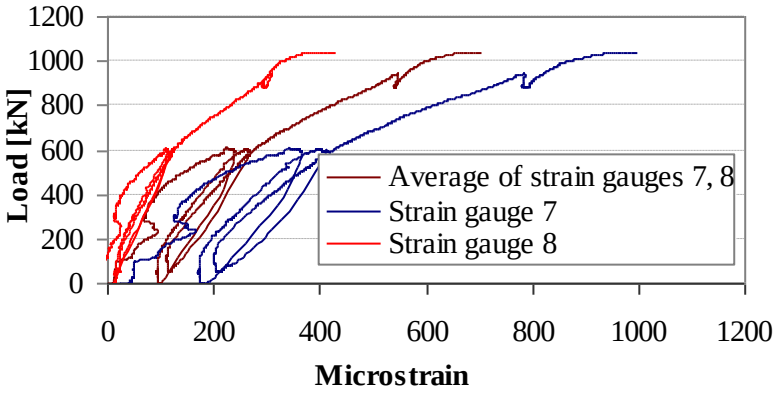

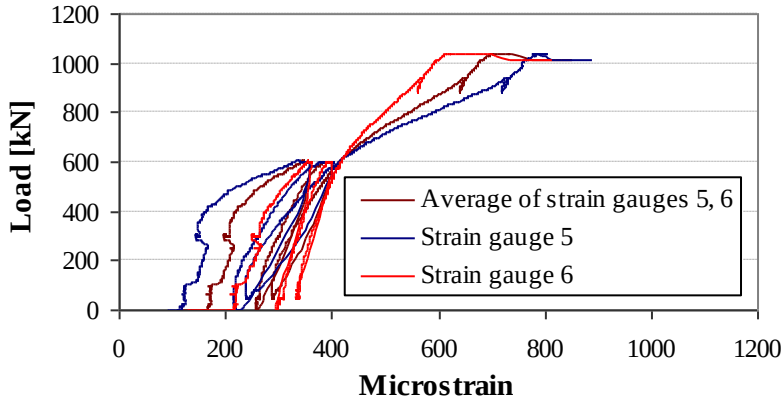

Measurements of strain gauges in the fifth perimeter

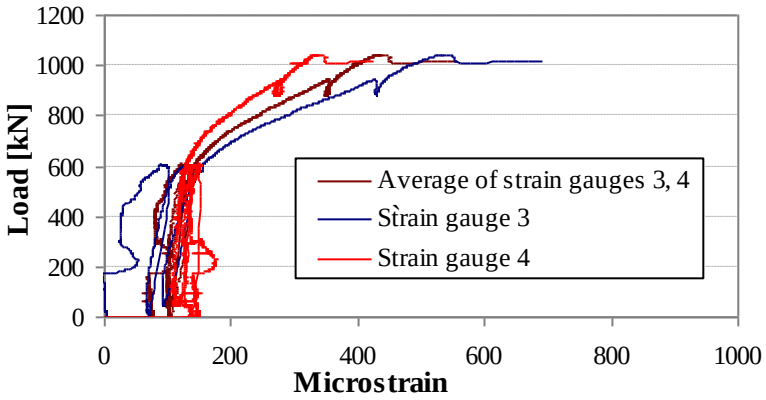

Measurements of strain gauges in the sixth perimeter

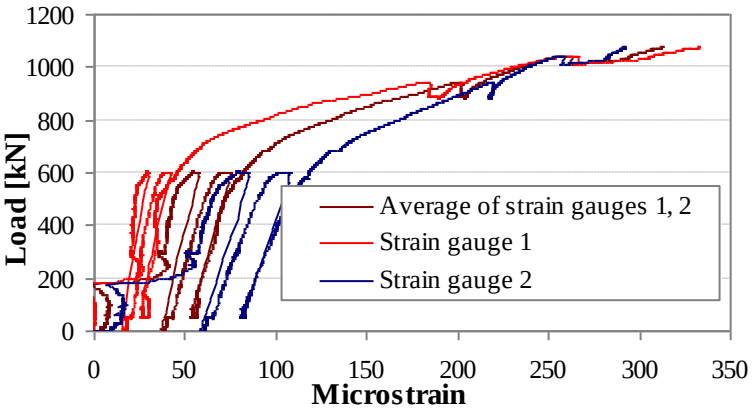

Appendix D

"Concrete smeared cracking" vs. "Concrete damage plasticity"

In smeared cracking model, the adopted yield function consists of independent surfaces; an isotropic-hardening yield surface activates when the stress is dominantly compressive and an independent "crack detection surface" that determines if a point fails by cracking. Both surfaces use linear relationship between the equivalent pressure, *p*, and the Mises equivalent deviatoric stress, *q*, which means associated flow rule assumption is used (ABAQUS material manual). Associated flow assumption overestimates the volumetric plastic strain due to simplification of the compressive behaviour. This assumption leads to inaccurate prediction due to the omission of the 3rd stress invariant dependence. Also the model uses a fixed angle crack model to detect the cracks, which results in shear stress locking problem.

This problem leads an the increase of shear stress on the crack plane due to restricting subsequent cracking to be orthogonal to the first crack since stress components associated with an open crack are not included in the definition of the failure surface used for detecting the additional cracks (ABAQUS material manual, 2008). Mesh refinement was suggested to overcome the shear stress interlocking in ABAQUS. Although, the mesh refinement method could alleviate shear stress locking problem in the finite element model as the number of elements employed is so large that cracking in any orientation can be captured, but its disadvantage is obviously the large increase in the required computational effort. Also, the smeared cracking model does not consider the damage in the elastic stiffness occurred by inelastic strain due to cyclic /unloading response. The aforementioned simplifications lead convergence problems and make the analysis stop in early loading due to numerical instability.

Concrete Damage Plasticity

Plasticity theory is a mathematical representation of the mechanical behaviour of solids. It can be used for translation of physical reality for ductile materials such as metals or a model that approximates the behaviour under certain circumstances for brittle materials such as concrete. In problems where the tension, with the crack development, plays a

significant role, such as shear failure in reinforced concrete structures, the usual procedure is to apply plasticity theory in the compression zone and treat the zones in which at least one principal stress is tensile by one of several versions of fracture mechanics (Lubliner *et al*., 1989).

Kupfer *et al*., (1969) carried out tests on biaxial loading of concrete specimens (200*200*50 mm). They found out that usually the various critical surfaces in stress space are similar. Concrete can show a significant volume change when subjected to severe inelastic loading. Figure 1 (a) shows that the increase in volume can be more than twice as large for the hydrostatic compressive stress state σ_1/σ_2= -1/-1. The points marked in stress-volumetric strain diagram (Figure 1 (a)) represents the limit of elasticity, the point of inflection in the volumetric strain, the bendover point corresponding to the onset of instability or localisation of deformation and the ultimate load. The critical stress surfaces related to these material states are shown in Figure 1 (b) (Kupfer *et al*., 1969). The same results was not found for concrete under triaxial compression test specially for the case of hydrostatic pressure; under these condition it was found that the hardening goes on indefinitely (Lubliner *et al*., 1989). This means that while the yield surface is closed, the failure surface is open in the direction of hydrostatic pressure.

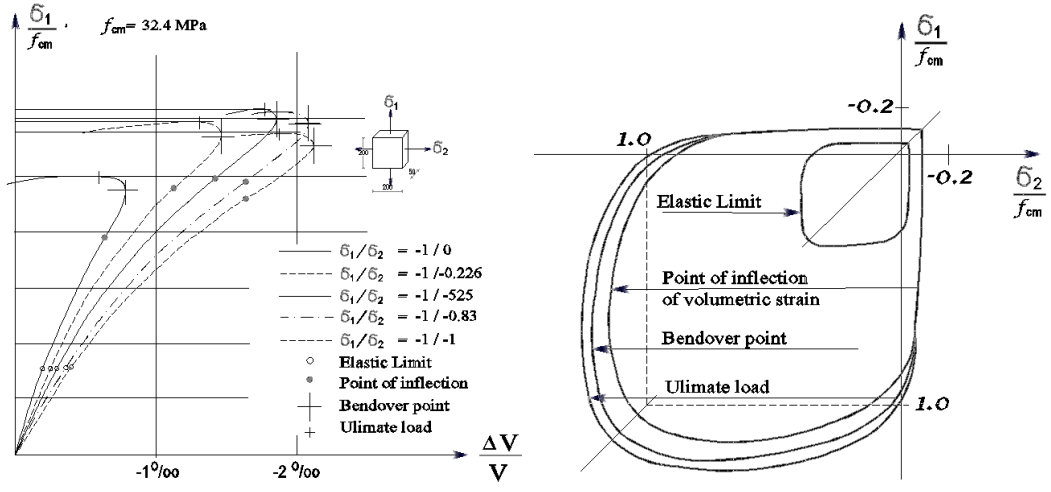

(a) (b)

Figure 1: (a) Volumetric strain of concrete under biaxial compression, (b) typical loading curves of concrete subjected to biaxial stresses. (Adopted from Kupfer *et al*., 1969)

Since the critical surfaces are similar in the biaxial behaviour of concrete, a yield function is used in plasticity based models. The size of yield function is based on the material properties defined for the uniaxial behaviour of concrete. The yield surface is defined as the material no longer acts elastic and the failure surface is based on the ultimate strengths. This means that in the biaxial tensile meridian the yield surface is equal to the failure surface. In compression, the material is usually assumed to be initially elastic up to 30-60 % of the compressive strength (Chen, 1982). There are several failure (or yield) criteria developed for concrete materials (reported by Lubliner *et al*., 1989) such as Drucker-prager and Mohr-Coulomb criteria. For steel usually the Von Mises failure criteria is used (further details can be obtained in ABAQUS user's manual, 2008). According to Lubliner *et al*., (1989), these criteria do not represent experimental results for concrete precisely otherwise they are suitably modified. For instance, one modification is to use a combination of the Mohr-Coulomb and Drucker-Prager yield functions, where the Drucker-Prager is used for biaxial compression and the Mohr-Coulomb is used otherwise. In Figure 2, the Drucker-Prager and concrete failure surfaces in three dimensions are shown schematically.

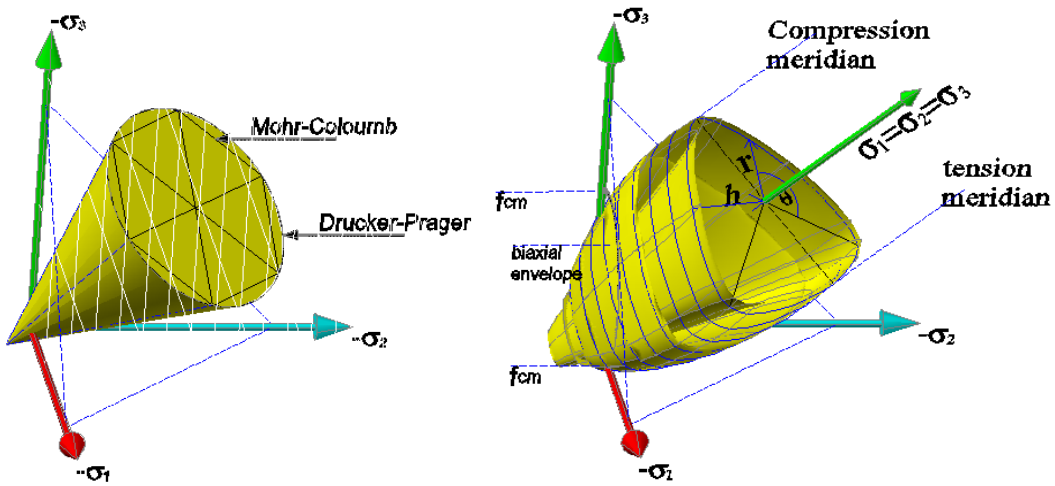

Figure 2: Drucker-prager failure surface and concrete triaxial failure space

The biaxial yield function used in concrete damage plasticity was developed by Lubliner *et al*., (1989) which also includes the modifications that was proposed by Lee and Fenves (1998) (cited in ABAQUS Manual). It is vital to understand the constitutive parameters which describe the material properties in finite element modelling to obtain authentic results. Therefore, a brief description of this is given in the next section.

Failure criteria of concrete

The connection between the yield surface and the stress-strain relationship is determined with a flow rule. Lubliner *et al*., (1989) proposed a non-associative flow rule which requires a loading surface definition. The proposed yield function given in Equation 1 is based on the loading function. Also the shape of loading surface in deviatoric plane is defined by parameter γ. According to Equation 1, cracking is assumed to occur when the triaxial stress reaches the failure surface.

$$F = \frac{1}{1-\alpha}\left(\bar{q} - 3\alpha\bar{p} + \beta(\tilde{\varepsilon}^{\mathrm{pl}})\langle\hat{\sigma}_{\max}\rangle - \gamma\langle-\hat{\sigma}_{\max}\rangle\right) - \bar{\sigma}_{\mathrm{c}}\left(\tilde{\varepsilon}_{\mathrm{c}}^{\mathrm{pl}}\right) = 0 \qquad (1)$$

where α, β and γ are dimensionless coefficients. α is explained as

$$\alpha = \frac{f_{\mathrm{b0}} - f_{\mathrm{c0}}}{2f_{\mathrm{b0}} - f_{\mathrm{c0}}} \qquad (2)$$

where $0 \le \alpha \le 0.5$, f_{bo} is the compressive strength under biaxial loading of concrete and f_{co} is the uniaxial compressive strength of concrete. β is described as

$$\beta(\tilde{\varepsilon}^{pl}) = \frac{\bar{\sigma}_c(\bar{\varepsilon}_c^p)}{\bar{\sigma}_t(\bar{\varepsilon}_t^p)}(\alpha - 1) - (\alpha + 1) \tag{3}$$

where $\bar{\sigma}_c(\bar{\varepsilon}_c^p)$ is the effective compressive cohesion stress and $\bar{\sigma}_t(\bar{\varepsilon}_t^p)$ is the effective tensile cohesion stress. γ should be defined based on the full triaxial tests on concrete, however, Lubliner *et al*., (1989) prescribed this parameter as

$$\gamma = \frac{3(1 - K_c)}{2K_c - 1} \tag{4}$$

$\bar{\sigma}_{max}$ is the algebraically maximum eigenvalue of $\bar{\sigma}$. Also the Macauley bracket $\langle . \rangle$ is described by $\langle x \rangle = \frac{1}{2}(|x| + x)$.

K_c is explained as $K_c = \frac{(\sqrt{J_2})_{TM}}{(\sqrt{J_2})_{CM}}$ at a given state of $\bar{p}$. J_2 is the second invariant of stress deviator for TM and CM subscribes. TM and CM respectively represents the "tensile meridian" ($\sigma_1 > \sigma_2 = \sigma_3$) and the "compressive meridian" ($\sigma_1 = \sigma_2 > \sigma_3$) in the yield surface. Lubliner *et al*., (1989) suggested typical values for K_c in the range of 0.64 to 0.8. ABAQUS assumes a default value of $K_c = 2/3$ which leads to γ=3. Figures 3 and 4 show the typical yield surfaces in deviatoric plane and plane stress conditions respectively.

$\bar{p}$ is the hydrostatic pressure stress, which is a function of the first stress invariant I_1, defined as

$$\bar{p} = \frac{-I_1}{3} = -(\sigma_{11} + \sigma_{22} + \sigma_{33})/3 \tag{5}$$

$\bar{q}$ is the Mises equivalent effective stress, defined as

$$\bar{q} = \sqrt{\tfrac{3}{2} S : S} = \sqrt{3J_2} \tag{6}$$

where J_2 is the second deviatoric stress invariant for biaxial loading and defines as

$$J_2 = \sigma_{11}^2 + \sigma_{22}^2 - \sigma_{11}\sigma_{22} \tag{7}$$

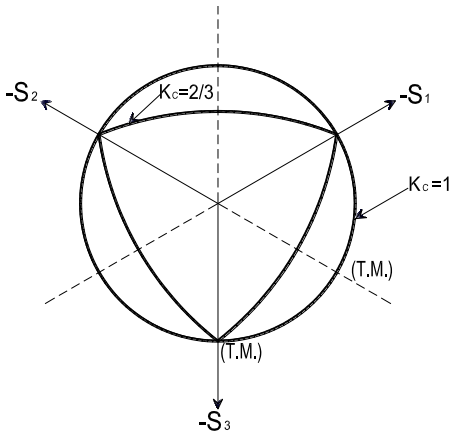

Figure 3: Yield surface in deviatoric plane with different values of K_c (from ABAQUS user's manual: Materials, 2008)

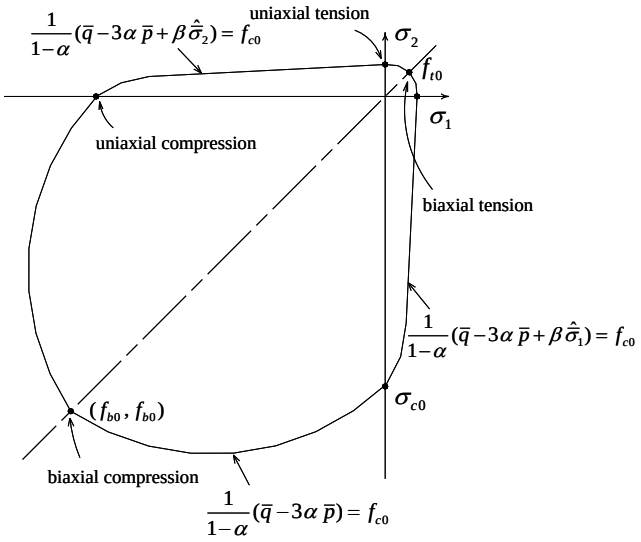

Figure 4: Biaxial yield surface in the constitutive model concrete damaged plasticity (adopted from ABAQUS manual, 2008)

Flow rule

The shape of yield surface at any given loading condition can be defined by the hardening rule. Also, the connection between the stress-strain relationship and yield surface is defined by the flow rule.

Concrete can demonstrate a significant volume change when subjected to severe inelastic states. This change in volume, known as dilation, attributable to plastic distortion, can be reproduced well by using an adequate plastic potential function *G* (Lubliner *et al*., 1989). The flow rule is expressed in Equation 8 as

$$\dot{\varepsilon}^{p} = \dot{\kappa}\frac{\partial G}{\partial \sigma} \tag{8}$$

where $\dot{\varepsilon}^{p}$ is the plastic incremental deformation, $\dot{\kappa}$ is a positive scalar hardening parameter which can change during the loading. The gradient of the potential surface $\frac{\partial G}{\partial \sigma}$ defines the direction of the plastic strain increment vector $\dot{\varepsilon}^{p}$, and the hardening parameter $\dot{\kappa}$ determines its length (Galvez *et al*., 2002).

In *associated flow,* the plastic potential function has the same shape as the yield surface. This is the simplest case, since the plastic flow is in association with the yield criterion. However; in *non-associated flow*, two separate functions are used for the plastic flow rule and the yield surface. In this case the plastic flow develops along the normal to the plastic flow potential and not to the yield surface (Galvez *et al*., 2002). Figure 5 illustrates the Drucker-Prager hyperbolic plastic function used in the material model *concrete damage plasticity* in the finite element program ABAQUS (Ver. 6.10).

The parameters in Figure 5 are given here. $\bar{p}$ is the hydrostatic pressure stress, which is a function of the first stress invariant I_1, defined as $\bar{p} = \frac{-I_1}{3} = -(\sigma_{11} + \sigma_{22} + \sigma_{33})/3$,

$\bar{q}$ is the Mises equivalent effective stress, defined as $\bar{q} = \sqrt{\frac{3}{2} S : S} = \sqrt{3J_2}$ where J_2 is the second deviatoric stress invariant for biaxial loading and defines as $J_2 = \sigma_{11}^2 + \sigma_{22}^2 - \sigma_{11}\sigma_{22}$ and ψ is the dilation angle which is measured in $\bar{p} - \bar{q}$ at high confining pressure.

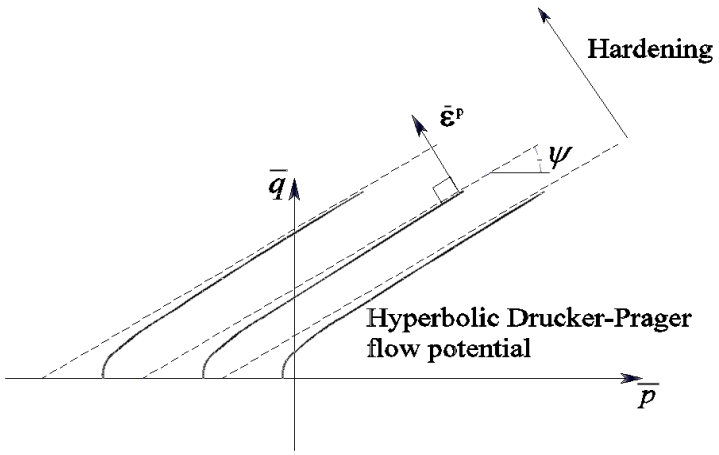

Figure 5: The Drucker-Prager hyperbolic plastic potential function in the meridional plane (adopted from ABAQUS user's Manual, 2008)

Dilatancy in the "concrete damage plasticity model"

The section presents the parametric studies for dilation angle in shear type cracking problems as well as the description of measurements and observations regarding to dilatancy.

As illustrated in Figure 5, the Drucker-Prager hyperbolic plastic potential function used for concrete damaged plasticity in ABAQUS is defined by Equation 9:

$$G = \sqrt{(\varepsilon . f_{t0} . \tan\psi)^2 + \bar{q}^2} - \bar{p} . \tan\psi \qquad (9)$$

where ε is the eccentricity that defines the rate at which the plastic potential function approaches the asymptote (the flow potential tends to a straight line as the eccentricity tends to zero), ψ is the dilation angle measured in the $\bar{p} - \bar{q}$ plane at high confining pressure.

The flow in Drucker-Prager function is non-associated, which means that the yield function and the plastic potential are coincide. The dilation angle (ψ) and the eccentricity (ε) which determines the shape of the flow potential surface are used as material parameters in ABAQUS.

The eccentricity parameter could be calculated according to the equation by Jirasek and Bazant (2002); cited in Grassl and Jirasek (2006).

However, ABAQUS suggested a default value of 0.1 for eccentricity, which means that the material has almost the same dilation angle over a wide range of confining pressure

stress values (ABAQUS user's manual, 2008). Assuming higher value of the eccentricity provides more curvature to the flow potential, indicating that the dilation angle increases more rapidly as the confining pressure (ABAQUS user's manual, 2008). To avoid convergence problems in the analysis, ABAQUS suggested not to use values less than 0.1 (default value) for eccentricity parameter.

Viscoplastic regularization

Advanced material models which develop strain softening and stiffness degradation, could have severe convergence difficulties. Viscoplastic regularization of the constitutive equations can be used to overcome some of these convergence difficulties. This can be done by regularization of plasticity damage model using viscoplasticty which permits stresses to be outside the yield surface. To improve the rate of convergence of the model in softening regions, ABAQUS suggests using the visocplastic regularization with a small value for the viscosity parameter (small compared to the characteristic time increment).

Appendix E

Newton-Raphson technique

Due to material nonlinearity, reinforced concrete structures exhibits nonlinear responses. In nonlinear analysis the external load is divided into small parts (increments) and equilibrium is checked for every increment. The nonlinear problems are solved as repeated linear problems. In this study for the FE analysis a nonlinear solving procedure, Newton-Raphson's method is adopted. This method follows equilibrium iterations until an acceptable convergence is achieved. The convergence criterion is to minimize the unbalanced force and displacement at the nodes in each load increment. Newton-Raphson approach assesses the unbalanced force vector (R_a) which is the difference between the external force (P) and the internal force (I_a):

$$R_a = P - I_a \tag{1}$$

The program checks for convergence and compares with the tolerance value, which is a default value of 0.5% of the average force in the structure, averaged over time. If the convergence criterion is not fulfilled, the unbalanced load vector will be re-evaluated until convergence is obtained.

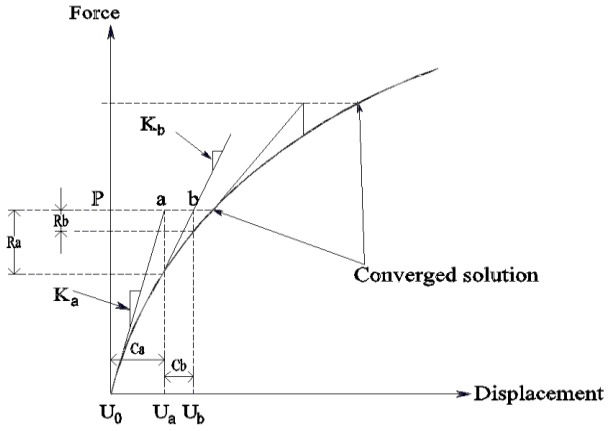

Figure 1: Newton-Raphson solution

After convergence in the unbalanced load obtained and prior to applying the next load increment, ABAQUS also performs a convergence check on the displacement correction, c_a, which should be smaller than the fraction of 1% of the total incremental

displacement assumed as a default value ($\Delta u_a = u_a - u_0$). Provided that c_a is greater than the displacement tolerance limit, ABAQUS carries out another iteration based on current structure configuration, u_a, and the new structure stiffness, K_a. Subsequently, by considering the new stiffness and the residual, R_a, a new displacement correction, c_b, is computed determining the new point *b* which is closer to the equilibrium point as shown in Figure 1. Based on the new internal force, I_b, which is related to configuration u_b, a new residue (R_b) is calculated according to Equation 2 as

$$R_b = P - I_b . \tag{2}$$

Then new convergence checks are performed for both c_b and R_b. If required, ABAQUS performs more iteration until convergence criteria are satisfied.